Assessment of inhomogeneity in gas exchange using a novel methodology

Asma O. Alamoudi

Queen’s College

University of Oxford

A thesis submitted for the degree of

Doctor of Philosophy

Hilary term 2024

Abstract

Accurate measurement of respiratory disease activity within the lung poses a significant challenge, and the inability to achieve it hampers early disease detection, effective disease management and the objective assessment of therapeutic responses. In this thesis, the utility of computed cardiopulmonography (CCP) is explored as a novel, non-invasive way to measure lung inhomogeneity across three distinct cohorts: Healthy (control) study participants, T2-high asthma patients and survivors of severe COVID-19.

Standardised normal values for CCP were established by analysis of 98 healthy people, who acted as the control group. Deviations from these baseline values were used to formulate prediction equations for each CCP parameter based on age, height, body mass index and sex. These equations were used to compute Z-scores for the asthma and post-COVID-19 cohorts. The analysis revealed that many patients exhibited abnormal Z-scores for CCP parameters. These findings highlighted deviations from the established normal ranges and demonstrated abnormalities in disease conditions.

In the T2-high asthma cohort, the effect of biological treatments on lung inhomogeneity was examined. Ninety-one patients were studied before treatment, and 65 patients were studied before and after they began biological therapies. The study was focused on $\sigma lnCL$, a metric of lung inhomogeneity, in which it correlated with the level of systemic inflammation as measured by the peripheral blood eosinophil count both at baseline and in relation to treatment effects by biologics. The use of CCP enabled differentiation between responders and non-responders based on changes in $\sigma lnCL$. Responders in terms of early change in $\sigma lnCL$ were the ones showing improvements in lung function/symptoms and increased change of having remission at one year. This finding indicates that CCP could potentially provide an early treatment response signal that might be useful to guide treatment strategies.

The COVID-19 cohort comprised 66 participants recovering from COVID-19 infection of varying clinical severity. The study aimed to assess whether CCP could identify abnormal lung function in recovered patients. Among the most severe cases, significant increases in anatomical dead space and decreases in functional residual capacity were observed. Despite the lack of pre-infection measurements, these findings highlight the potential use of CCP to assess aspects of lung function not easily measured by conventional tests.

In conclusion, the work performed for this thesis has demonstrated that CCP offers a valuable tool by which to monitor disease activity in asthma and post-COVID-19 recovery. It underscores the importance of using advanced, non-invasive techniques to enhance our understanding and management of respiratory diseases. Additionally, this thesis represents the first attempt to establish normal values for CCP parameters through the use of Z-scores.

Statement of the effect of the COVID-19 pandemic on research work

It is important to note that the course of this thesis was significantly impacted by the onset of the COVID-19 pandemic. The disruptions caused by the pandemic necessitated changes in the direction of the research, particularly in relation to the availability of human experimental subjects due to concerns surrounding the conduct of respiratory research within clinical and research settings. Despite the challenges, every effort was made to mitigate the effects of these disruptions and to maintain the quality of the research endeavour.

The timeline of the DPhil journey, which began in October 2019, included initial training on the technology and protocol development, which proceeded as planned. Recruitment for the asthma study (described in Chapter 6), which was intended to be a key component of the work that was focused on the utility of computed cardiopulmonography (CCP) in T2-high asthma, commenced in February 2020. However, the shift to remote patient appointments in March 2020 resulted in the temporary suspension of recruitment activities and the inability to conduct direct human measurements for a period of nine months. In light of these limitations, an opportunity emerged to pivot towards experimental work related to COVID-19. Recruitment for this aspect of the research, detailed in Chapter 7, began in September 2020. By the end of 2022, in consultation with my supervisors, it was determined that the remaining time should be allocated to revisiting the original aim of establishing normal controls, as outlined in Chapter 5.

Acknowledgements

Embarking on the challenging journey to a DPhil at Oxford has been an arduous yet incredibly rewarding experience, and I owe a profound debt of gratitude to the many individuals who have played pivotal roles in this academic odyssey. First and foremost, I extend my deepest appreciation to my esteemed supervisors, Prof. Peter Robbins, and Dr. Nayia Petousi. Their intellectual guidance, mentorship, and unwavering support have served as the bedrock of this thesis. The impact of their keen insights, constructive critiques, and genuine enthusiasm for my research cannot be overstated; they have been pivotal in shaping both the direction and the quality of this work. A heartfelt thank you is also extended to Prof. Grant Ritchie, Dr. Lorenzo Petralia, Dr. Nick Talbot, Dr. Nicholas Smith, Dr. Graham Richmond, future Dr. Dom Sandhu, John Couper, Dr. Jessica Luiz, Dr. Tishan Wellalagodage, and Dr. Haopeng Xu as well as everyone in the Robbins and Ritchie groups. Their collective wisdom and encouragement have been an additional source of inspiration throughout this academic journey. Beyond the confines of formalities, their support and belief in my potential have been driving forces propelling me forward.

I would like to express my heartfelt gratitude to all the volunteers and patients who generously gave their time to participate in my studies. Their involvement was invaluable to the progress of this research, and I deeply appreciate their commitment. I am also extremely grateful to the nurses and doctors in the clinics for their unwavering support. Your dedication and assistance made this research possible, and I sincerely thank you for your collaboration throughout my DPhil.

To my family and loved ones, I owe immeasurable gratitude. Your enduring patience, unwavering encouragement, and understanding have served as a constant source of strength through the highs and lows of this challenging endeavour. I deeply appreciate the sacrifices

you have made to see me through this academic pursuit. This achievement is as much yours as it is mine. A heartfelt thank you to my Mom, Dad, Maryam, and Yasmin, and a special thanks to my amazing nephew and nieces, Omar, Reem, and Deema; you were the light in my darkest moments. To my friends, thank you for believing in me. Your presence provided both respite and motivation, turning what could have been a solitary pursuit into a shared intellectual adventure. I am sincerely grateful to each and every one of you for being an integral part of this significant chapter in my academic journey.

Thesis outline

ABSTRACT **2**

STATEMENT OF THE EFFECT OF THE COVID-19 PANDEMIC ON RESEARCH WORK **4**

ACKNOWLEDGEMENTS **5**

CHAPTER 1. INTRODUCTION **11**

1.1 RESEARCH MOTIVATION **11**
1.2 RESEARCH OBJECTIVES **14**
1.2.1 HEALTHY VOLUNTEERS COHORT 14
1.2.2 ASTHMA COHORT 15
1.2.3 POST-COVID-19 COHORT 15
1.3 THESIS OUTLINE **16**

CHAPTER 2. LITERATURE REVIEW **17**

2.1 RESPIRATORY SYSTEM **18**
2.1.1 LUNG ANATOMY AND PHYSIOLOGY 18
2.1.2 LUNG VOLUMES, MECHANICS, AND GAS FLOW 19
2.1.3 DIFFUSION AND GAS EXCHANGE 21
2.1.4 VENTILATION/PERFUSION RELATIONSHIPS 22
2.2 ASTHMA **22**
2.2.1 ASTHMA OVERVIEW AND EPIDEMIOLOGY 22
2.2.2 ASTHMA BACKGROUND AND HISTORY 23
2.2.3 ASTHMA DIAGNOSIS 24
2.2.4 ASTHMA PHENOTYPES AND ENDOTYPES 26
2.2.4.1 T2-high and T2-low asthma endotypes 29
2.2.4.1.1 T2-low asthma 30
2.2.4.1.2 T2-high asthma 31
2.2.5 T2-HIGH ASTHMA PATHOPHYSIOLOGY 32
2.2.6 CLINICAL CHARACTERISTICS AND BIOMARKERS ASSOCIATED WITH T2-HIGH ASTHMA 33
2.2.7 MANAGEMENT OF T2-HIGH ASTHMA 35
2.3 CORONAVIRUS DISEASE (COVID-19) **41**
2.3.1 EPIDEMIOLOGY AND OVERVIEW 41
2.3.2 COVID-19 DIAGNOSIS 42
2.3.3 COVID-19 PATHOPHYSIOLOGY AND CLINICAL PICTURE 43
2.3.4 POST-COVID 45
2.4 LUNG FUNCTION MEASUREMENTS **47**
2.4.1 SPIROMETRY 48
2.4.1.1 Bronchodilator reversibility test 50
2.4.2 BODY PLETHYSMOGRAPHY 53
2.4.3 GAS TRANSFER 54
2.4.4 THE FORCED OSCILLATION TECHNIQUE 55
2.5 MEASUREMENTS OF INHOMOGENEITIES **56**
2.5.1 MULTIPLE INERT GAS ELIMINATION TECHNIQUE 57
2.5.2 INERT GAS WASHOUT 57
2.5.2.1 The single-breath inert gas washout (SBW) technique 58
2.5.2.2 The multiple breath washout (MBW) technique 59
2.5.2.2.1 Lung clearance index (LCI) 60
2.5.2.2.2 S_{cond} and S_{acin}: Advanced Indices of Ventilation Inhomogeneity 63
2.5.3 POSITRON EMISSION TOMOGRAPHY (PET) 66
2.5.4 HYPERPOLARISED GAS MRI 67

2.6 SUMMARY: ADVANTAGES AND DISADVANTAGES OF CURRENT TECHNIQUES USED FOR MEASURING PULMONARY FUNCTIONS AND INHOMOGENEITIES 71

CHAPTER 3. NOVEL MEASURE OF LUNG INHOMOGENEITY 73

3.1 EXISTING METHODOLOGY 73
3.1.1.1 Mass spectrometry 74
3.1.1.2 Non-dispersive infrared sensors 75
3.1.1.3 Laser absorption spectroscopy 75
3.2 COMPUTED CARDIOPULMONOGRAPHY 76
3.2.1 MOLECULAR FLOW SENSING DEVICE 77
3.2.2 COMPUTATIONAL MODEL 82
3.2.2.1 LNL 82
3.2.2.2 Model of blood CO_2 and O_2 dissociation curves 87
3.2.2.3 Model of circulatory and body gas stores 88
3.3 CCP VS. COMMERCIALLY AVAILABLE INERT GAS WASHOUT SYSTEM 93
3.4 PREVIOUS WORK ON THE MEASUREMENT OF LUNG INHOMOGENEITY THROUGH THE USE OF CCP 99

CHAPTER 4. METHODOLOGY 102

4.1 EXPERIMENTAL PROTOCOL 102
4.1.1 INCLUSION CRITERIA 102
4.1.2 EXCLUSION CRITERIA 102
4.1.3 EXPENSES AND BENEFITS 103
4.1.4 PRIOR TO THE BREATHING TEST 103
4.1.4.1 Calibration 103
4.1.4.2 Participant information sheet and informed consent 103
4.1.5 THE MFS BREATHING TEST 104
4.1.6 MODEL FITTING 108

CHAPTER 5. DETERMINATION OF NORMAL CCP PARAMETER VALUES 113

5.1 INTRODUCTION 113
5.2 METHODS 114
5.2.1 PARTICIPANTS 114
5.2.1.1 Identification of participants 114
5.2.1.2 Inclusion criteria 115
5.2.1.3 Exclusion criteria 115
5.2.2 STUDY PROTOCOL 116
5.2.2.1 Lung inhomogeneity test 116
5.2.2.2 Quality control process 117
5.2.2.3 Regression analysis 117
5.2.2.4 Outliers 119
5.3 RESULTS 119
5.3.1 PARTICIPANTS 119
5.3.2 REGRESSION ANALYSIS 120
5.3.3 NORMALITY TEST 121
5.3.4 HETEROSCEDASTICITY TEST 125
5.3.5 REGRESSION PARAMETERS 127
5.3.6 Z-SCORES 134
5.4 DISCUSSION 136
5.4.1 Z-SCORES AND PFTS 136
5.4.2 THE GLOBAL LUNG INITIATIVE APPROACH VS. THE APPROACH EMPLOYED IN THIS THESIS 138
5.4.3 COMPARISON WITH FINDINGS IN THE AVAILABLE LITERATURE AND EXPLORATION OF THE EFFECTS OF PHYSICAL CHARACTERISTICS 141
5.5 RESEARCH LIMITATIONS 144
5.6 CONCLUSION 145

.**CHAPTER 6. LUNG INHOMOGENEITY PARAMETERS IN TYPE-2 HIGH ASTHMA AND THE EFFECT OF THERAPEUTIC INTERVENTIONS....146**

6.1 INTRODUCTION....146
6.1.1 RESEARCH AIMS AND HYPOTHESISES....146
6.2 METHODS....148
6.2.1 PARTICIPANTS....148
6.2.1.1 Recruitment of participants....148
6.2.1.2 Inclusion criteria....149
Participants were required to fulfil the following requirements....149
6.2.1.3 Exclusion criteria....149
6.2.2 STUDY PROTOCOL....150
6.2.2.1 Baseline and follow up visit....151
6.2.2.2 One-year review....153
6.2.3 STATISTICAL ANALYSIS....154
6.3 RESULTS....157
6.3.1 BASELINE DATA FOR THE SEVERE ASTHMA CROSS-SECTIONAL COHORT....159
6.3.1.1 CCP parameters compared with the normal ranges identified in Chapter 5....159
6.3.1.2 Relationship among BEC and FeNO levels and ACQ-5 scores with CCP parameters....163
6.3.1.3 Exacerbations in the year before starting biologics in participants who subsequently received biologics 165
6.3.1.4 Relationship between spirometry and CCP parameters at baseline....168
6.3.1.5 Effect of BD on spirometry and CCP parameters....171
6.3.2 EFFECTS OF BIOLOGIC TREATMENTS THREE OR FOUR MONTHS AFTER THERAPY (AT THE FOURTH INJECTION)....173
6.3.3 BIOLOGICS ONE-YEAR REVIEW....184
6.4 DISCUSSION....188
6.4.1 BASELINE DATA....188
6.4.1.1 Baseline CCP parameters compared with the normal ranges....188
6.4.1.2 Relationship among BEC and FeNO levels and ACQ-5 scores with CCP parameters at baseline 189
6.4.1.3 Exacerbations one year before starting biologics in participants who subsequently received biologics 191
6.4.1.4 Relationship between spirometric and CCP parameters at baseline....192
6.4.1.5 Effect of BD on spirometric and CCP parameters....193
6.4.2 EFFECTS OF BIOLOGIC TREATMENTS THREE OR FOUR MONTHS AFTER THERAPY (AT THE FOURTH INJECTION)....194
6.4.3 BIOLOGICS ONE-YEAR REVIEW....198
6.5 RESEARCH LIMITATIONS....199
6.6 CONCLUSION....200

CHAPTER 7. THE LONG-TERM EFFECT OF COVID-19 ON RESPIRATORY PHYSIOLOGY....201

7.1 INTRODUCTION....201
7.2 METHODS....202
7.2.1 PARTICIPANTS....202
7.2.1.1 Identification of participants....202
7.2.1.2 Inclusion criteria....203
Participants were required to fulfil the following requirements....203
7.2.1.3 Exclusion criteria....203
7.2.2 STUDY PROTOCOL....204
7.2.3 STATISTICAL ANALYSIS....207
7.2.3.1 Analysis conducted on the data via linear regression....207
7.2.3.2 Analysis conducted on Z-scores for CCP parameters....209
7.3 RESULTS....210
7.3.1 CLINICAL LUNG FUNCTION PARAMETERS 3 TO 6 MONTHS POST-HOSPITAL DISCHARGE....214

7.3.1.1 Clinical lung function parameters across COVID-19 severity groups....214
7.3.1.2 Clinical lung function parameters across different CT-scores....219
7.3.2 CCP PARAMETERS 3 TO 6 MONTHS AND 12-MONTHS POST-HOSPITAL DISCHARGE....224
7.3.2.1 CCP parameters across COVID-19 severity groups....224
7.3.2.2 CCP parameters across different CT-scores....229
7.3.2.3 CCP parameters at the initial vs. follow-up visits....233
7.3.3 RELATIONSHIP BETWEEN CCP AND CLINICAL LUNG FUNCTION PARAMETERS AT THE INITIAL VISIT 235
7.3.4 ANALYSIS OF CCP PARAMETERS THROUGH THE USE OF Z-SCORES....239
7.3.4.1 Z-scores across COVID-19 severity groups....239
7.3.4.2 Z-scores across different CT-scores....244
7.4 DISCUSSION....249
7.4.1 CLINICAL LUNG FUNCTION PARAMETERS THREE-TO-SIX MONTHS AFTER HOSPITAL DISCHARGE 250
7.4.2 CCP PARAMETERS THREE-TO-SIX MONTHS AND 12-MONTHS AFTER HOSPITAL DISCHARGE .254
7.4.3 RELATIONSHIP BETWEEN CCP AND CLINICAL LUNG FUNCTION PARAMETERS AT THE INITIAL VISIT 258
7.4.4 ANALYSIS THROUGH THE USE OF Z-SCORES....260
7.5 RESEARCH LIMITATIONS....261
7.6 CONCLUSION....262

CHAPTER 8. CONCLUSION AND FUTURE RESEARCH DIRECTION....263

8.1 CHAPTER 5: DETERMINATION OF NORMAL VALUES FOR CCP PARAMETERS....264
8.2 CHAPTER 6: THE USE OF CCP TO MONITOR THE EFFECT OF THERAPEUTIC INTERVENTIONS IN T2-HIGH ASTHMA....265
8.3 CHAPTER 7: USE OF CCP TO EVALUATE THE LONG-TERM EFFECT OF COVID-19 ON RESPIRATORY PHYSIOLOGY....267
8.4 FUTURE RESEARCH DIRECTION....268

BIBLIOGRAPHY....271

Chapter 1. Introduction

1.1 Research motivation

The Global Burden of Disease study, published by *The Lancet* in 2019, revealed that chronic respiratory diseases (CRDs), such as asthma and chronic obstructive pulmonary disease (COPD), were among the leading causes of death worldwide. In 2019, CRDs ranked as the third highest cause of death, accounting for four million fatalities and affecting approximately 454.6 million individuals across the globe [1]. In Europe, respiratory diseases contributed to 15% of all deaths, leading to an annual toll of 600,000 fatalities.

Around 18% of the population in the UK has been diagnosed with asthma. Asthma imposes a significant economic burden, and there is a relationship between the severity of the disease and the corresponding economic costs [2, 3]. One study found that the annual average treatment cost of severe refractory asthma was higher than the costs of other prevalent chronic diseases such as type II diabetes and kidney diseases. The mean annual treatment cost of severe refractory asthma was reported to range from £2912 to £4217 per person [3].

By March 2023, severe acute respiratory syndrome coronavirus 2 (SARS-CoV-2), which caused the COVID-19 pandemic, had infected nearly 700 million people globally and claimed the lives of almost seven million of them [4]. Data show that approximately 50% of people who survive severe SARS-CoV-2 infection that requires hospitalisation develop a long-term multisystemic syndrome that is marked by chronic dyspnoea. Regrettably, despite the extensive efforts of numerous researchers, the root causes of these enduring respiratory symptoms have not yet been clarified definitively [5].

Despite significant advances in the diagnosis and treatment of respiratory diseases through the application of various diagnostic methods and biological therapies, the respiratory

care community continues to face challenges in early disease detection, management, classification, and the evaluation of responses to therapeutic interventions.

Most common Pulmonary function tests (PFTs), particularly in the form of spirometry and diffusion capacity measurements, are widely recognised as diagnostic of pulmonary diseases. Spirometry, which involves the measurement of exhaled volume over time, is the most commonly used lung function test for the diagnosis and monitoring of respiratory diseases, particularly in obstructive lung disease. Nevertheless, these tests have notable limitations. They rely on patient effort and provide limited insights into lung pathology and inhomogeneity. Furthermore, they exhibit low sensitivity in the detection of early-stage lung diseases and therapeutic responses [6-9].

Another lung function measure that has been gaining popularity in airway diseases is oscillometry, particularly forced oscillometry (FOT). This technique offers a valuable approach to assessing lung function by applying oscillating pressure waves during normal tidal breathing, providing insights into airway mechanics that are especially useful in diagnosing and managing obstructive lung diseases [6, 10, 11]. Despite its advantages, oscillometry has limitations that hinder its clinical adoption [6, 11]. Swallowing and upper airway artifacts can affect measurement accuracy, and while it indicates small airway dysfunction, large airway abnormalities can also influence results. The lack of universal reference ranges and the complexity of interpreting the data further complicate its use, making it less accessible to clinicians who are not specialized in respiratory physiology [6, 11].

All of the tests described above share the common characteristic of measuring a bulk property of the overall lung. Typically, these tests require a significant amount of disease before any abnormalities become apparent. An alternative approach is to use statistics that measure unevenness or inhomogeneity within the lung. Such statistics, which are essentially related to variances within the lung, should be more sensitive for early disease detection.

Of the above, the Lung clearance Index (LCI) has emerged as a valuable tool in the assessment of ventilatory inhomogeneity [12, 13], particularly through the use of the multiple breath inert gas washout (MBW) technique. The LCI is a measurement of the efficiency of gas clearance from the lungs. It involves the monitoring of the washout of inert gases during normal breathing. This approach has proven especially useful in the identification of early lung disease, particularly in patients with cystic fibrosis (CF), in which early detection and monitoring are crucial due to the progressive nature of the disease [14-18]. Despite its potential, the application of the LCI and other MBW-derived indices faces several limitations. MBW requires specialized equipment, standardized procedures, and complex software, with the equipment being prone to technical noise [14, 19, 20]. Furthermore, the derivation of LCI relies on just two points from the gas washout process, raising concerns about the robustness of the index. The requirement to perform washouts in triplicate to ensure reliability adds to the procedural burden [14, 19]. The lack of standard reference ranges complicates interpretation across populations [14, 19]. While LCI provides valuable insights into ventilation inhomogeneity, its susceptibility to external factors such as tracer gas solubility, measurement apparatus deadspace [12, 14], patient breathing patterns, and end-expiratory volume (EEV) variability [21, 22] limits its reliability and ease of use. LCI is further discussed in chapters 2 and 3 as it as it is the closest equivalent lung physiology technique to the CCP.

In the work I performed for this thesis, I aimed to investigate a novel approach to measuring variance-based statistics relating to lung function. In particular, I explored the utility of a novel, non-invasive technique (computed cardiopulmonography CCP) to measure lung inhomogeneity in the evaluation of various respiratory diseases.

To summarise, my research is driven by the global burden of chronic respiratory diseases, such as asthma and COPD, which remain leading causes of death despite advances in diagnosis and treatment. Current pulmonary function tests like spirometry and diffusion

capacity have limitations, including low sensitivity in detecting early disease or disease progression and reliance on patient effort. Emerging methods like oscillometry and LCI offer valuable insights but face challenges such as technical complexity and lack of standardized reference ranges. This thesis aims to explore the clinical utility of CCP, a novel, non-invasive technique that could provide a sensitive and comprehensive approach to assessing lung inhomogeneity and improving respiratory disease management.

1.2 Research Objectives

The hypothesis of this research is that CCP can serve as a sensitive and complementary technique to traditional lung function and physiological measures in the assessment and tracking of specific lung pathophysiological changes. To explore this hypothesis, CCP was utilised in three distinct cohorts: healthy volunteers, individuals with severe asthma, and patients who had been previously hospitalised with COVID-19 pneumonia.

1.2.1 Healthy volunteers cohort

The objective of studying the healthy control group was to describe the range of variation that occur in a healthy population. I hypothesised that physical characteristics such as age, height, BMI, and gender, will influence the normal values. I further hypothesize that regression can be used to predict the normal values and their variations, based on participants physical characteristics, and that such regression can be used to provide a method to compute the deviation of CCP parameters from normality in individuals with respiratory disease.

1.2.2 Asthma cohort

This project aimed to evaluate the utility of CCP in severe T2-high asthma and to understand how CCP parameters correlated with other markers of the disease, such as inflammatory biomarkers, symptoms, and other lung function measures. Additionally, through this project, I sought to explore the effects of therapeutic interventions in asthma on measures of lung inhomogeneity through the application of CCP. The hypothesis under investigation was that the measurement of lung physiology obtained via CCP could serve as a sensitive and complementary technique to traditional lung function measures in the assessment and tracking of specific lung pathophysiological changes. This included evaluation of correlations between CCP parameters and other disease markers in severe T2-high asthma, and assessment of the impact of therapeutic interventions on lung inhomogeneity.

1.2.3 Post-COVID-19 cohort

The primary objective of this study was to investigate the long-term effects of COVID-19 on respiratory function and lung physiology. The hypothesis is that CCP lung inhomogeneity measures can effectively detect physiological differences in the lungs of patients who have recovered from COVID-19. The specific aim was to determine whether CCP lung inhomogeneity measures can effectively detect physiological differences in the lungs of patients who have recovered from COVID-19, many months after hospital discharge, and how these differences relate to disease severity at three to six months and 12 months after discharge.

1.3 Thesis outline

Chapter 1 provides a concise overview of the research motivation, questions and objectives presented in this thesis. Chapter 2 contains an examination of the essential concepts and pertinent scholarly works that are connected to respiratory anatomy and physiology, current lung function measurements, different measurements of inhomogeneities, asthma, and COVID-19. In Chapter 3, the MFS technology and novel cardiopulmonary model are described. This serves as the foundational element for the subsequent chapters. In Chapter 4, the research methodology and protocol are described in detail, and these contents are used as references for the subsequent experimental chapters. In Chapter 5, the study on the healthy control volunteers to obtain normal ranges is described; in Chapter 6, the study on the severe T2-high asthma cohort is described; and in Chapter 7, the study on the post-COVID-19 cohort. Chapter 8 concludes this thesis with a summary of the findings, their implications, and potential directions for future research.

Chapter 2. Literature review

In this chapter, I discuss key principles and explore relevant academic literature that forms the foundation for the research presented throughout the thesis. First, I examine the anatomy and physiology of the respiratory system, including lung mechanics, gas flow, gas exchange and ventilation-perfusion ($\dot{V}/\dot{Q}$) ratios.

I then provide a summary of the respiratory diseases that are covered in this thesis. Since one of the cohorts that was investigated comprised T2-high asthma patients (Chapter 6), a concise overview of asthma pathophysiology and epidemiology is included, along with a detailed discussion of asthma phenotypes and endotypes, with a specific focus on T2-high asthma. Additionally, I offer an overview of the COVID-19 pandemic and its associated pathology, as I collaborated with the Oxford University Hospital (OUH) clinical respiratory clinic to conduct follow-ups on recovered COVID-19 patients (Chapter 7).

Next, I explain the traditional methods that are used to assess lung function, such as spirometry, body plethysmography, FOT and gas transfer. My focus is on spirometry, which is widely regarded as the standard method for the diagnosis and monitoring of respiratory diseases. I also explore methodologies that are used to measure lung inhomogeneities, particularly the inert gas washout technique and its index of ventilation inhomogeneity, the LCI, which has gained traction for the assessment of ventilation inhomogeneity. Finally, I discuss briefly the knowledge gaps and limitations of each technique. Through examination of these methods, I aim to highlight areas in which current techniques may fall short and emphasise the need for further research to improve patient outcomes in respiratory care.

2.1 Respiratory system

2.1.1 Lung anatomy and physiology

The primary function of the lung is to facilitate gas exchange. Its fundamental role is to enable the transfer of oxygen (O_2) from breathed-in air into the venous blood and the elimination of carbon dioxide (CO_2) [23]. An alveolus is a functional unit of the lung; it acts as an air sac that facilitates gas exchange and is filled with air from outside the body. The lungs contain approximately 300 million to 700 million alveoli, with the exact number varying according to body size [23, 24]. These alveoli are wrapped with very thin blood capillaries that transport CO_2 from the body to the alveoli for exhalation, and simultaneously pick up O_2 from the air during inspiration for distribution throughout the body. The movement of gases (O_2 and CO_2) across the alveolar-capillary membrane occurs through simple diffusion, in which gases move from areas of higher partial pressure to areas of lower pressure. The alveolar-capillary membrane is extremely thin, measuring as little as 0.3μm, in order to facilitate the efficient exchange of gases across the membrane [23].

The airways are constructed from a network of branching tubes that gradually narrow as they extend from the trachea to the alveoli. This complex system comprises 23 generations of airway branches that are collectively referred to as the "airway tree". These generations are further categorised into three zones according to their structure and function. The initial zone is known as the conducting zone (generations zero to 16), which is primarily responsible for transporting gases to the gas exchange unit. The conducting zone begins with the trachea, which branches into bronchi, then into multiple bronchioles and ultimately into terminal bronchioles. This conducting zone is sometimes referred to as the anatomical dead space, as it does not participate in gas exchange processes. The second zone is the transitional zone (generations 17 to 19), in which alveoli start to emerge from the respiratory bronchioles. The

third zone is the respiratory zone (generations 20 to 23), in which all gas exchange occurs. This zone consists of alveolar ducts that branch into alveolar sacs [23, 24].

2.1.2 Lung volumes, mechanics, and gas flow

When talking about gas flow from and to the lung, it is worth knowing the different lung volumes and capacities, which are explained clearly in Figure 2.1. I will also refer to some of these volumes in later chapters of this thesis.

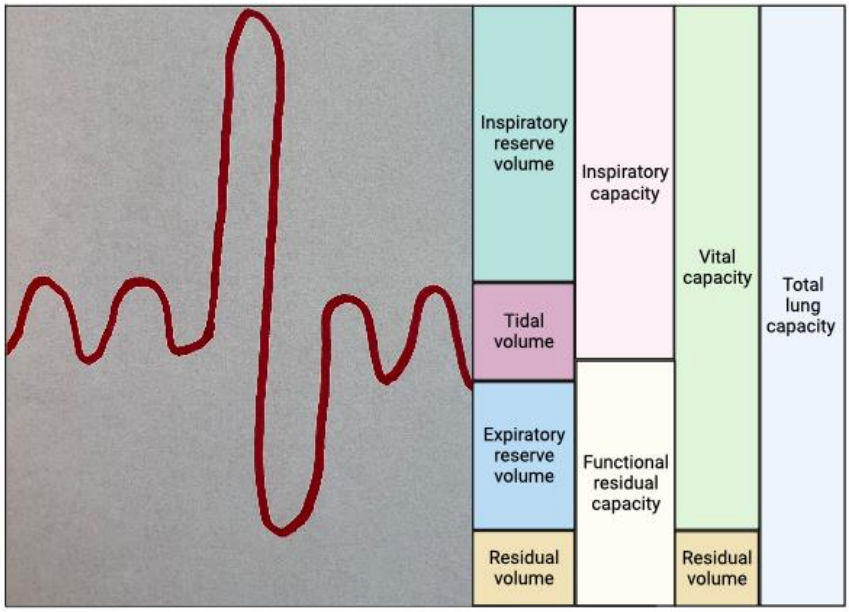


Figure 2.1. Lung volumes and capacities are measured using spirometry. The total lung capacity is the total volume of gas in the lungs at the end of a maximal inspiration. The vital capacity is the volume of gas that can be exhaled after maximum inspiration. The residual volume is the volume of gas that remains in the lung after maximum exhalation. The inspiratory capacity is the maximum volume of gas that can be inhaled after a normal tidal exhalation. The functional reserve capacity is the volume of gas that remains in the lungs after a normal tidal exhalation. The inspiratory reserve volume is the volume of gas that can be inspired at the end of inspiratory tidal breathing. The tidal volume is the volume of gas that is inspired and expired during regular breathing. The expiratory reserve volume is the volume of gas that can be expired at the end of expiratory tidal breathing. This figure was developed using BioRender and Inkscape program.

Inspiration is an active process, while expiration is passive. During normal tidal breathing, inspiration begins with the contraction of the respiratory muscles, the diaphragm and the external intercostal muscles. The contraction of the diaphragm results in the downward movement of abdominal contents, while the external intercostal muscles pull the ribs forward and upward, collectively causing the chest wall to expand. This in turn decreases intrapleural pressure, which leads to alveolar expansion and heightened elastic recoil. Consequently, the alveolar pressure decreases by around 1cmH_2O, creating a pressure gradient between the alveoli and the atmosphere. This gradient causes air to flow into the lungs until alveolar pressure equilibrates with atmospheric pressure [23, 25]. In summary, air moves into and out of the lungs due to a slight pressure difference between the air inside the alveoli and the surrounding atmosphere (approximately 1cm H_2O) [25].

Exhalation is predominantly a passive process that occurs during resting breathing. It starts with the relaxation of the lung and chest wall (contraction of the chest wall). This contraction elevates the intrapleural pressure and diminishes the force exerted on the alveoli [23, 25]. Consequently, driven by their inherent elastic recoil, the alveoli contract, and this causes the alveolar pressure to rise (by approximately 1 cmH_2O). As a result, air is exhaled from the lungs until the pressure equalises [25].

At the functional residual capacity (FRC), the elastic recoil of the alveoli, which tends to contract them, is counterbalanced by the elastic recoil of the chest wall, which tends to pull the chest wall upward. This equilibrium results in a slightly negative intrapleural pressure of around 5cmH_2O. At FRC, alveolar pressure equals atmospheric pressure, and no air flows [25].

The expansion and contraction of the lung are commonly assessed through the use of the concept of lung compliance. Lung compliance is defined as the change in lung volume divided by the change in transpulmonary pressure that is associated with volume changes. Compliance generally decreases with decreases in lung volume, and it differs between

expiration and inspiration. Lung compliance increases with age and in cases such as emphysema, and decreases in pulmonary fibrosis and pulmonary oedema [23, 25].

2.1.3 Diffusion and gas exchange

I have mentioned that the movement of gases (O_2 and CO_2) across the alveolar-capillary membrane occurs through diffusion, in which gases move from areas of higher partial pressure to areas of lower pressure. Diffusion through the alveolar-capillary membrane can be explained by Fick's law of diffusion, which states that the rate of gas exchange through a tissue is directly proportional to the surface area and pressure difference across the membrane and is inversely related to the thickness of the membrane [23].

O_2 is taken up by the blood within a pulmonary capillary. The partial pressure of O_2 (PO_2) in red blood cells as they enter the capillary is around 40mmHg. Just 0.3µm away, across the alveolar-capillary membrane, the alveolar PO_2 is 100mmHg. This large pressure gradient facilitates rapid O_2 diffusion into the red blood cell and causes the PO_2 to rise rapidly. By the time the red blood cell has travelled about one-third of the way along the capillary, its pressure nearly matches that of the alveolar gas PO_2. The partial pressure of CO_2 (PCO_2) in red blood cells as they enter the capillary is around 45mmHg and the alveolar PCO_2 is 40mmHg, and this slight pressure gradient causes CO_2 to leave the blood (Figure 2.2) [23].

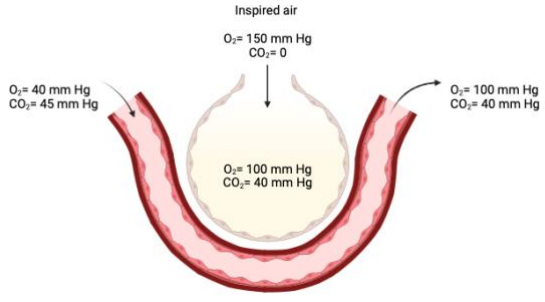


Figure 2.2. Respiratory gas exchanges and pressure gradients. Alveolar PO_2=100mmHg, alveolar PCO_2=40mmHg. Pulmonary artery PO_2=40mmHg, pulmonary artery PCO_2=45mmHg. Pulmonary vein PO_2 ~100mmHg, pulmonary vein PCO_2 ~40mmHg. This figure was developed using BioRender and Inkscape program.

2.1.4 Ventilation/perfusion relationships

The main function of the lung is to facilitate the exchange of O_2 and CO_2 between the body and the atmosphere. Central to this process is the concept of the $\dot{V}/\dot{Q}$ ratio, a fundamental physiological parameter that plays a crucial role in the maintenance of efficient gas exchange within the lungs. The $\dot{V}/\dot{Q}$ ratio provides insights into the matching of air and blood flow in the respiratory system. Any imbalance in this ratio can lead to a condition known as $\dot{V}/\dot{Q}$ mismatch, which has significant implications and may lead to hypoxaemia [23].

The $\dot{V}/\dot{Q}$ ratio is the ratio between the amount of air that reaches the alveoli (alveolar ventilation) and the amount of blood that perfuses the pulmonary capillaries surrounding those alveoli, per unit time. $\dot{V}/\dot{Q}$ mismatch, an imbalance between ventilation and perfusion, leads to inefficient gas exchange. This mismatch is most likely to occur during shunts or when alveolar deadspaces form. Shunt is the passage through the lungs of blood that does not participate in gas exchange due to ventilation impairment. Alveolar dead space occurs if ventilated alveoli lack sufficient blood supply for gases to exchange [23].

2.2 Asthma

2.2.1 Asthma overview and epidemiology

Asthma is a common chronic respiratory disease that imposes a substantial healthcare burden on a global scale [3]. The 2023 Global Initiative for Asthma (GINA) report recognised asthma as a respiratory disorder that showed heterogeneity in aetiology, pathophysiology, symptoms, and responses to treatment. In an effort to enhance comprehension and management, several distinct asthma phenotypes have been identified (which are discussed in section 2.4.4) [26-28]. The diagnosis of asthma hinges primarily on the patient's symptom history, which can range in severity and duration, as well as variable expiratory airflow

obstruction measurements, which often include the performance of a documented bronchodilator reversibility test. Common asthma symptoms are shortness of breath, wheezing, chest tightness, and coughing [29].

At present, approximately 339 million people worldwide, of different ages and genders, are affected by asthma [30]. Asthma is one among numerous chronic respiratory disorders that contribute to 15% of global non-communicable disease-related fatalities. It is ranked 23rd among the leading causes of premature mortality, 16th in terms of years lived with disability, and 28th in the list of causes of overall disease burden [29].

2.2.2 Asthma background and history

Moses ben Maimon worked as a physician in Egypt during the 12th century AD and documented certain symptoms in his patients that resembled those of the common cold, and which were aggravated during wet seasons and improved in dry seasons [31]. In 1698, *Sir John Floyer*, an English physician who himself was afflicted with asthma, published the first comprehensive account of the disease. Drawing from his personal struggles as an asthmatic, he described thoroughly several prevalent asthma symptoms. He suggested that there could be a connection between wheezing and airway narrowing, while also detailing asthma attacks and potential triggers [32].

In the late 19th and early 20th centuries, *Sir William Osler* highlighted some more detailed characteristics of asthma in his book. These included bronchoconstriction, bronchomucosal oedema, small airway inflammation, genetic involvement, and the relationship of symptoms to climate, atmosphere, and vicious emotions [33]. *Francis Rackemann* was the first to describe the heterogeneous nature of asthma and the involvement of allergies in the disease pathophysiology. He also categorised asthmatic patients as intrinsic or extrinsic. Extrinsic asthma or protein-sensitive asthma was thought to be due to external

environmental factors; intrinsic or protein-insensitive asthma was thought to be more common in older patients who had other severe diseases [34].

As modern medicine evolved, more detailed asthma descriptions were offered. In 1922, *Huber* and *Koessler* described the histopathological features of samples taken from patients who had died from asthma. Their findings included airway thickening; smooth muscle hypertrophy; submucosal oedema; and eosinophilic, lymphatic, and neutrophilic infiltration [34]. The association between asthma and expiratory airflow limitations was recognised soon after spirometry was developed as a measurement technique by John Hutchinson. In the 1940s, *Robert Tiffeneau* described the association between airflow obstruction and the ratio between a low forced expiratory volume in one second (FEV_1) and vital capacity (FVC) [35]. In the 1960s, peak flow meters were introduced to assess airway obstruction during symptomatic episodes [34].

2.2.3 Asthma diagnosis

Diagnosing asthma is a complex process that relies on multiple factors rather than a single diagnostic test. Typically, it involves a clinical assessment along with objective tests to identify variable airflow obstruction or the presence of airway inflammation. Figure 2.3 illustrates the current guidelines for the diagnosis of asthma; it highlights the complex nature of asthma diagnosis [36]. In the process of diagnosing asthma, a structured clinical assessment must be conducted. This assessment should be based on a thorough understanding of the patient's symptom history and ideally should include peak flow readings. Additionally, it is vital that information about the patient's personal and family history of atopic conditions, such as atopic eczema/dermatitis and allergic rhinitis, be collected. For adults with an intermediate probability of asthma, spirometry, including bronchodilator reversibility testing when appropriate, is the preferred initial diagnostic test [36]. On the other hand, histamine provocation or methacholine challenge is deemed the most commonly employed test for

assessing airway responsiveness and may be the most specific and categorical diagnostic test. However, it is conducted infrequently and only in specialist centres. The prevailing method by which airway responsiveness is measured involves assessment of the response in terms of the change in FEV_1 after the patient has inhaled escalating concentrations of histamine or methacholine [36, 37].

It is important to understand that both clinical assessment and objective tests have their limitations and may lead to false positive or false negative results. For instance, common asthma symptoms such as coughing, wheezing, and shortness of breath, while frequently associated with asthma, are not highly sensitive or specific indicators of the condition. Similarly, the bronchodilator reversibility test, which is used to diagnose and evaluate conditions such as asthma and COPD, measures the extent to which airflow obstruction can be reversed by bronchodilator medication. It is worth noting that in studies that involve people who are considered to have both asthma and COPD, some patients who initially test positive for reversibility may not actually have asthma. On the other hand, in cases in which the bronchodilator reversibility test yields negative results, it has been reported that one in every three individuals may indeed have asthma [36].

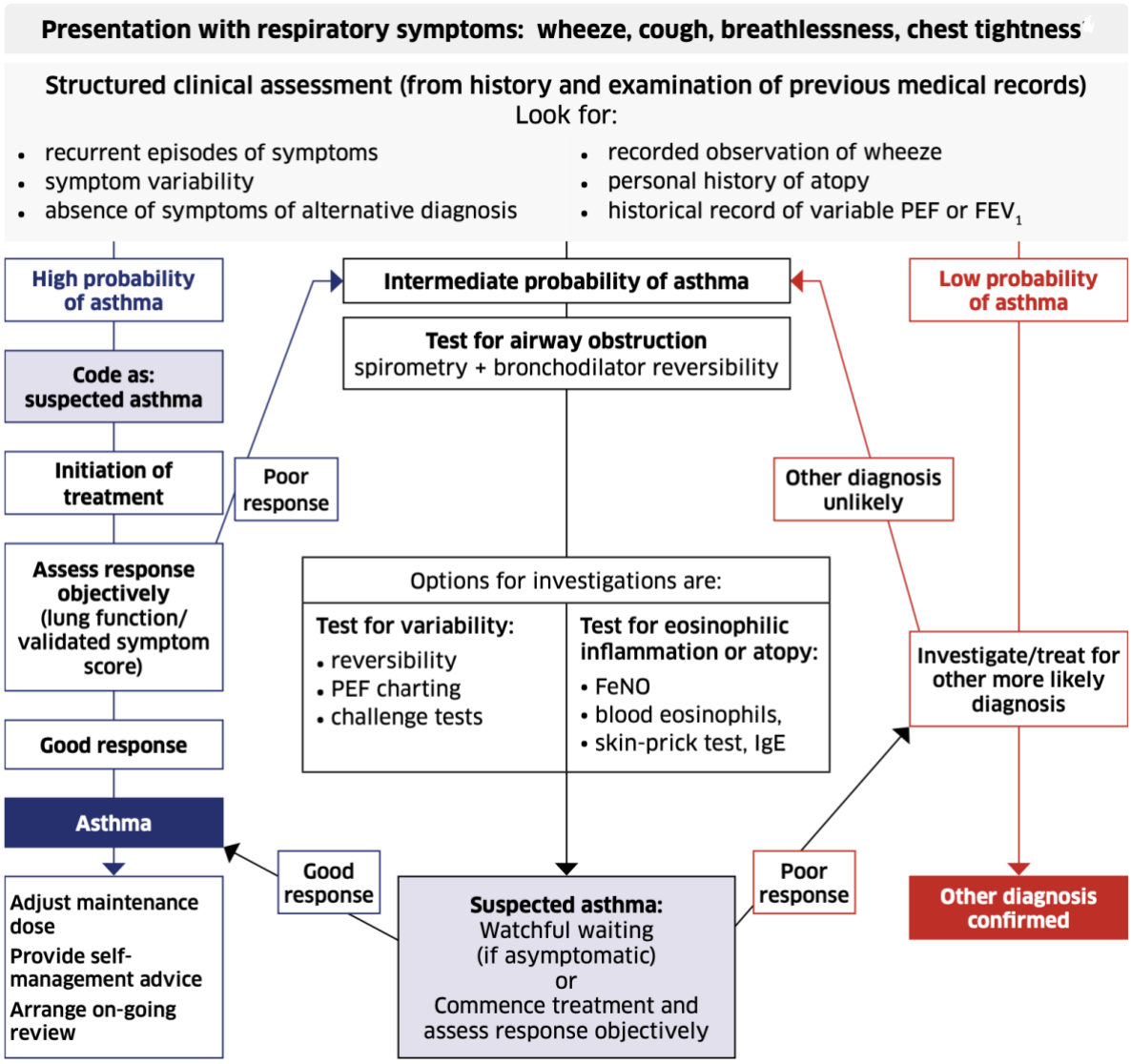


Figure 2.3. Asthma diagnosis algorithm from the Scottish Intercollegiate Guidelines Network, guideline158 2019 British guideline on the management of asthma. Peak expiratory flow rate (PEF), immunoglobin E (IgE), Forced exhaled nitric-oxide (FeNO) [36].

2.2.4 Asthma phenotypes and endotypes

Over time, the term "asthma" has evolved to encompass a spectrum of conditions that have diverse clinical manifestations and underlying pathophysiological mechanisms. This evolution has led to the recognition of asthma's heterogeneity, which manifests in variations in severity, progression, and treatment responses, all rooted in its underlying mechanisms. Various approaches have been employed to categorise asthma, which have involved the

grouping of patients based on clinical presentations, biological factors, triggers, age-related patterns, and physiological traits. These groupings, known as phenotypes, represent distinct characteristics that result from a combination of genetic and environmental influences (e.g., obesity-associated asthma, smoking-associated asthma, and late-onset asthma) [27, 38, 39]. However, the current trend is to integrate molecular mechanisms with these phenotypes, which has led to the concept of asthma endotypes that show specific pathophysiological mechanisms operating at the cellular and molecular levels (T2-high and T2-low asthma) [39].

Haldar et al. (2008) employed cluster analysis to distinguish asthma phenotypes that responded differently to treatment strategies within both primary and secondary care asthma populations (Figure 2.4) [40]. These clusters were delineated based on their different levels of symptoms and inflammation [40]. Two clusters (early-onset atopic and obese non-eosinophilic) were found in both researchers' asthma populations. These differed mainly in disease severity. Additionally, two clusters that were characterised by significant disparities between symptom expression and eosinophilic airway inflammation (early-onset symptom-predominant and late-onset inflammation-predominant) were unique to refractory asthma cases. The refractory subgroup showed higher rates of non-attendance at clinic appointments, which were associated with poor rates of therapeutic compliance, and uncontrolled eosinophilic airway inflammation. In contrast, the obese, non-eosinophilic phenotype was characterised by symptoms that were unrelated to eosinophilic inflammation. For symptom-predominant phenotypes, symptom aetiology is multifactorial and not closely linked to inflammation, which may lead to corticosteroid overuse. On the other hand, inflammation-predominant phenotypes are at risk of undertreatment, which may result in uncontrolled eosinophilic inflammation and severe asthma exacerbations [40].

Several studies have revealed a linear association between asthma and body mass index (BMI), which indicates that a higher BMI is associated with an increased risk of asthma

development [41, 42]. Three distinct traits are commonly observed in individuals with obesity-related asthma: persistent and severe symptoms despite maintained lung function, a higher prevalence among middle-aged women than among other demographic groups (late-onset), and no direct connection to atopy [39, 40]. At a molecular level, obesity-associated asthma syndrome is characterised by non-eosinophilic inflammation. In studies by *Kuruvilla et al. (2019)* and *Van Veen et al. (2008),* the relationship between airway inflammation and obesity was explored and revealed an inverse link between BMI and sputum eosinophilia, as well as levels of fractional exhaled nitric oxide (FeNO) [39, 43]. Obesity has a direct impact on the innate immune system as it promotes CD4-cell differentiation toward Th1, the presence of which has been associated with glucocorticoid-resistant asthma [39, 40]. Additionally, obesity influences Th17 pathways and the behaviour of innate lymphoid cells. Another cytokine, interleukin (IL)-6 has been linked to individuals with higher BMIs and more severe asthma symptoms [39].

Despite sharing similar clinical symptoms, individuals with asthma may respond differently to treatments due to these underlying endotypes. Recognition and understanding of these distinct asthma phenotypes and endotypes are essential if we are to comprehend the disease's origins and enhance its management. Precision medicine plays a pivotal role in the tailoring of treatments to target specific patient endotypes. For instance, the advanced understanding of the intricate type-2 inflammatory network in severe asthma has paved the way for the development of emerging targeted biological therapies [39].

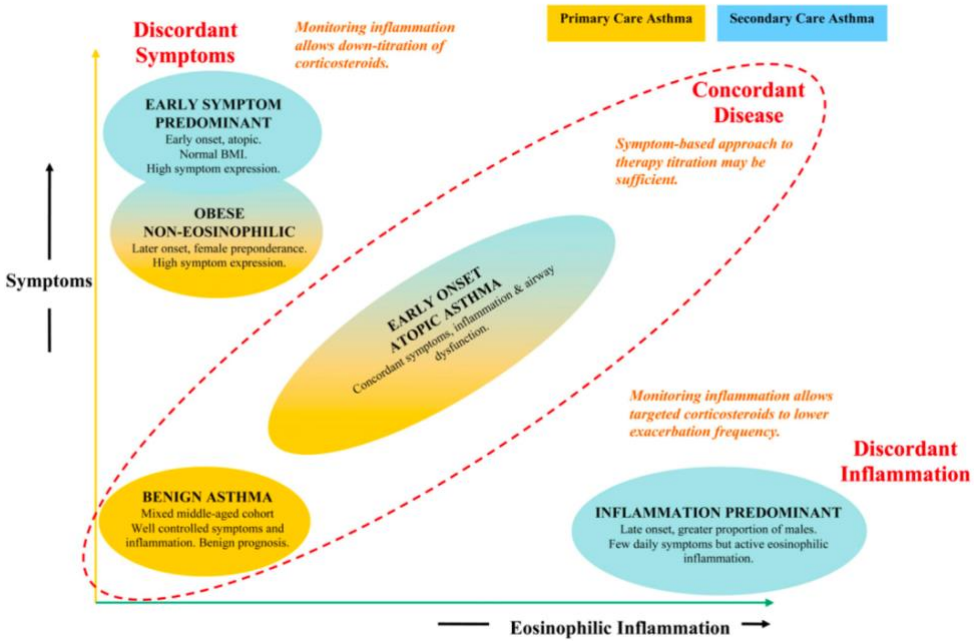


Figure 2.4. A graphical representation of asthma care, which emphasises that heightened discordance is a notable characteristic of secondary care asthma. While the precise factors behind this dissociation are unclear, it has been shown that the use of measures of airway inflammation within these subgroups is clinically valuable [40]. Body mass index (BMI).

2.2.4.1 T2-high and T2-low asthma endotypes

It is common to characterise asthma by classifying it as T2-high or T2-low. However, the condition may stem from a blend of airway inflammations, which contribute to intricate scenarios in which patients may shift between T2-high and T2-low asthma or manifest both simultaneously [44]. Given this complexity, the mechanisms of T2-high and T2-low asthma have been explored separately to gain a thorough comprehension. Please note that, although a brief overview of T2-low asthma is provided, the focus in this work was on delving into the details of T2-high asthma, which constituted the primary cohort of my asthma project.

2.2.4.1.1 T2-low asthma

Non-eosinophilic asthma, which is usually characterised by a neutrophilic component, can manifest across mild, moderate, and severe asthma cases. It is characterised by neutrophil cell counts in induced sputum samples that range from 41% to 60% of the total cell count. This type of asthma can be triggered by viral or bacterial infections, as well as exposure to air pollution. The prolonged use of inhaled corticosteroids (ICSs) has been associated with increased neutrophil survival and decreased rates of eosinophil survival [42, 45].

T2-low asthma follows a distinct pathway that is led by Th17 cells. These cells are recognised as secretors of IL-17A, IL-17F, IL-21, and IL-22, which have been identified in bronchial biopsies of individuals with severe asthma. Elevated levels of IL-17 are also observed in the blood, sputum, and bronchoalveolar lavage of individuals with asthma, and this elevation has been correlated with the severity of the condition [44, 46, 47].

IL-17 cytokines can activate epithelial cells and fibroblasts, which results in the release of neutrophil chemoattractants CXCL1/5/8 and granulocyte-macrophage colony-stimulating factor. These substances attract neutrophils to the lungs. Additionally, IL-17A has been observed to enhance the contraction, movement, and growth of airway smooth muscle, crucial factors in airway hyper-responsiveness, mucus overproduction, and bronchoconstriction [44, 46].

Common features of T2-low asthma include late-onset with a high symptom burden, but a lower exacerbation rate compared with T2-high asthma [48]. Lung function ranges from normal to showing minor obstruction characteristics. There is no allergic sensitisation. People with T2-low asthma are less responsive to corticosteroids than are those with T2-high asthma. They typically have low levels of blood and sputum eosinophils and exhaled nitric oxide [48]. While substantial progress has been made in the characterisation of T2-high asthma, T2-low

asthma remains an area with unmet research requirements and unresolved issues, as its biomarkers have not been investigated comprehensively.

2.2.4.1.2 T2-high asthma

T2-high asthma constitutes approximately 50% of mild-to-moderate asthma cases and a substantial proportion of severe asthma cases. It is primarily defined by elevated peripheral blood and sputum eosinophil counts and intraepithelial mast cells (endobronchial) [49, 50]. T2-associated inflammation typically responds to treatment with ICSs and systemic steroids at the time of exacerbation [50]. An important subset of severe T2-high asthma patients, however, displays limited response to ICSs but positive responses to systemic treatments such as steroids or biological therapies [50].

T2-high asthma can be categorised into two phenotypes: early-onset allergic asthma and late-onset eosinophilic asthma. Early-onset allergic asthma or extrinsic allergic asthma is characterised by onset during childhood, sensitivity to airborne allergens (mediated by immunoglobulin E (IgE)), and a correlation between symptom severity and eosinophil counts. In contrast, late-onset eosinophilic asthma presents in adulthood, is unrelated to atopy, displays resistance to ICSs, is strongly associated with aspirin sensitivity, chronic rhinosinusitis, and nasal polyposis, and does not exhibit a correlation between symptom severity and eosinophil counts [39, 42]. The early-onset variant is driven primarily by an allergen-dependent adaptive immune pathway, whereas the late-onset variant is influenced by an allergen-independent innate lymphoid pathway. Both late and early-onset types involve the activation of IL-5, a cytokine that is recognised for its role in eosinophil recruitment [39, 51, 52].

2.2.5 T2-high asthma pathophysiology

Type-2 cells represent a subset of $CD4^+$ T-cells that play a pivotal role in asthma pathophysiology by releasing cytokines, specifically IL-4, IL-5, and IL-13, into the airway epithelium. These cytokines contribute to key aspects of asthma, including excessive secretion, IgE production, and airway hyper-responsiveness (Figure 2.5) [46]. IL-5 and IL-13 can also be produced through the activation of type-2 innate immune cells that are triggered by IL-25, IL-33, and thymic stromal lymphopoietin (TSLP) [38, 39, 46, 50].

The immune pathway that drives type-2 inflammation in asthma begins with the prompt release of cytokines such as IL-25 and IL-33 after exposure to an insult or allergen. These cytokines activate antigen-presenting cells - dendritic cells or natural killer cells - and these stimulate a Th2 adaptive immune response. Naïve T-cells subsequently differentiate into T-helper type-1 (Th1) or T2 phenotypes, influenced by factors including antigen-related components and local cytokines such as IL-4. IL-4 plays a significant role in Th2-cell differentiation [46]. Upon antigen exposure, Th2 cytokines facilitate B-cell production of allergen-specific IgE. Consequently, repeated allergen exposure triggers IgE cross-linking, which leads to mast-cell activation and heightened recruitment of Th2-effector cells to the airways [46, 50, 53]. IL-4, IL-5, and IL-13 are pivotal cytokines that drive eosinophil influx, survival, and differentiation. This activation results in the infiltration of eosinophils into the airways, and elevated blood or sputum eosinophil levels serve as indicative markers of T2-high asthma [38].

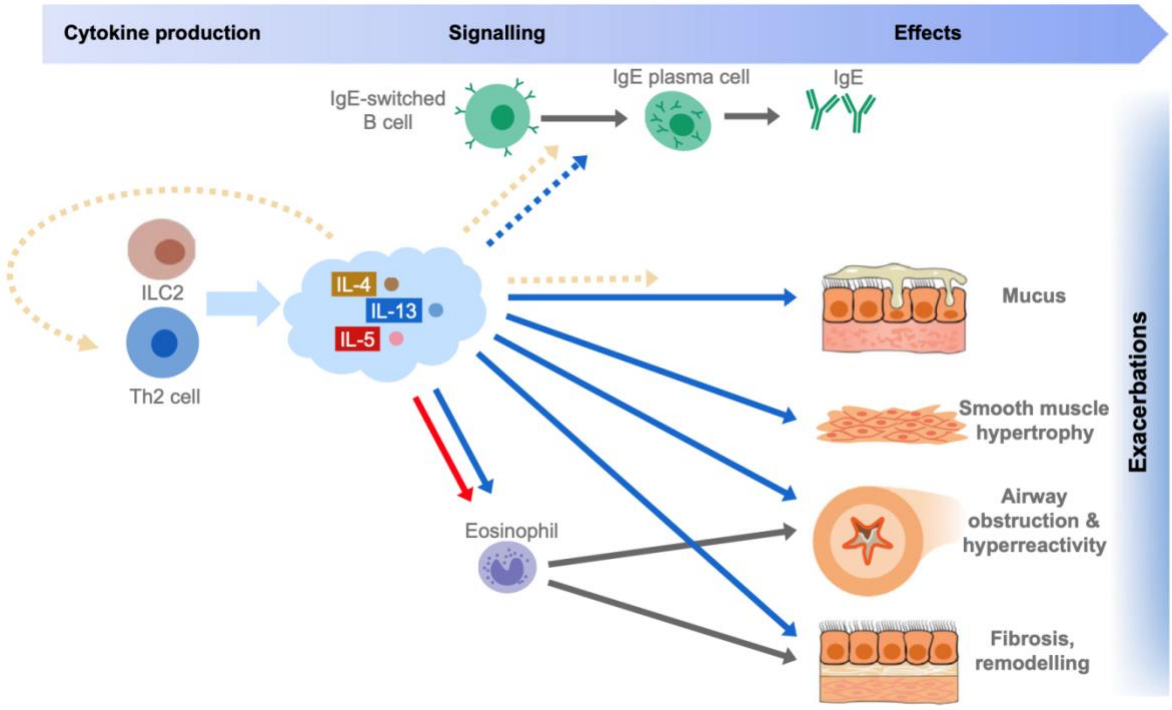


Figure 2.5. An overview produced by *Robinson et al.* of the type-2 inflammatory response in T2-high asthma. The process starts with the activation of IL-13 and IL-5 cytokines via type-2 cells, eventually causing excessive mucus production, airway hyper-responsiveness and airway remodelling [46].

2.2.6 Clinical characteristics and biomarkers associated with T2-high asthma

Several biomarkers of inflammation have been adopted in clinical practice to aid the management and treatment of T2-high asthma. Examples are FeNO, blood or sputum eosinophils, serum IgE, and periostin levels [46].

FeNO measurement is an accurate, simple, reproducible, and non-invasive technique that is used as an indicator of corticosteroid-sensitive airway inflammation in severe asthma and IL-13-mediated eosinophilic inflammation [44, 54]. Airway epithelial cells produce nitric oxide through the up-regulation of nitric oxide synthase, which is induced by IL-13. As a result, nitric oxide has been considered a precise indicator of T2 airway inflammation. Several factors, such as demographics, smoking, diet, atopic status, and the presence of nasal polyps, can affect FeNO levels, and act as potential sources of error or bias. While most patients with elevated FeNO levels show positive responses to corticosteroid treatment, a subset of patients does not

respond as expected. These patients exhibit persistently high FeNO levels and have elevated levels of Th2 cytokines and chemokines in their sputum [44]. Although a positive FeNO test indicates the presence of eosinophilic inflammation, it is not conclusive, as there is an overlap in FeNO levels between normal, non-asthmatic individuals and those with atopic asthma. More importantly, several factors can influence FeNO levels, including allergic rhinitis, rhinovirus infection, gender, height, high intake of dietary nitrates, age, smoking, and steroid use (in steroid-naïve adults, a FeNO level of 40ppb or higher is considered positive). Therefore, a positive FeNO test increases the likelihood of asthma but does not confirm it definitively, and conversely, a negative test does not rule out asthma. These findings are based primarily on studies from secondary care; there are few data from primary-care populations [36].

Eosinophils are essential cellular mediators in the type-2 inflammation pathway and are believed to have a significant impact on the persistence of inflammation in asthma over an extended period. They play a crucial role in asthma pathogenesis as they influence immune response modulation and contribute to the development of airway hyper-responsiveness and remodelling, which are key features of the disease. Severe asthma patients with elevated levels of eosinophils in blood or sputum have been found to have fixed airway obstruction. Additionally, studies have shown that a high eosinophilic blood count may be a marker of an increased risk of mortality [46]. Sputum eosinophil levels above 2-3% or a blood eosinophil count (BEC) of greater than 300 cells/µl are considered the standard level in eosinophilic inflammation [46, 55].

The presence of allergen-specific IgE antibodies is a valuable diagnostic tool in the evaluation of inflammation in people with atopic asthma. Elevated levels of IgE are commonly observed in individuals with asthma. Studies have demonstrated a correlation between IgE levels, skin testing, and lung function in people with asthma. Notably, an inverse relationship between IgE levels and the FEV_1/FVC ratio has been observed [44].

Associations have been noted between serum periostin levels and multiple pathological processes in asthma, including airway remodelling, subepithelial fibrosis, eosinophil recruitment, and regulation of mucus production. However, further research is required to understand the serum periostin levels in healthy individuals and patients with asthma and other diseases [46].

2.2.7 Management of T2-high asthma

The main long-term goals of asthma management are to control symptoms, improve quality of life, and decrease the likelihood of exacerbations, all while minimising any potential treatment side effects. The GINA guidelines [28] present a comprehensive and evidence-based approach to treating asthma in general. Key elements of the guidelines involve a stepwise treatment approach, which customises therapy according to symptom severity and asthma control (Figure 2.6). In terms of medications, the GINA guidelines stress the preference for ICSs as the initial controller medication for most asthma patients. If necessary, long-acting beta-agonists can be added to ICSs, while short-acting beta-agonists are recommended as quick relievers of acute symptoms. The guidelines also highlight the importance of add-on therapies for patients who require additional treatments to achieve optimal control [28].

According to the British Thoracic Society and GINA guidelines, difficult-to-treat asthma is characterised by persistent symptoms and/or frequent asthma exacerbations despite treatment with high-dose ICSs and LABAs or anti-leukotrienes [28, 36]. For T2-high asthma, the guidelines suggest the use of biological therapies that target particular pathways. Patients who suffer from severe asthma, reaching GINA Step 4 or above, fail to respond to various controller treatments and suffer multiple exacerbations that require steroids, may be eligible for the latest biological therapies (Figure 2.6) [28]. Step 4 involves the use of medium- or high-dose ICSs combined with a LABA. This treatment is recommended for patients who experience frequent asthma symptoms and are at risk of exacerbations despite their use of lower-dose ICS-

LABA therapy. In addition to ICS-LABA, other controller options at this stage include leukotriene receptor antagonists, long-acting muscarinic antagonists or theophylline. Step 5 is reserved for patients with severe asthma that remains uncontrolled despite adherence to step 4 treatments and the use of high-dose ICS-LABA therapy. This step involves the addition of biological therapies that target specific pathways involved in asthma inflammation (Figure 2.6) [28].

In terms of managing exacerbations, the guidelines offer a clear strategy. Early intervention involves short courses of oral corticosteroids (OCSs) and increased use of short-acting beta-agonist inhalers. Biologics serve to reduce exacerbations and minimize the long-term use of OCS. This proactive approach aims to regain control quickly and prevent further deterioration and airway remodeling [28].

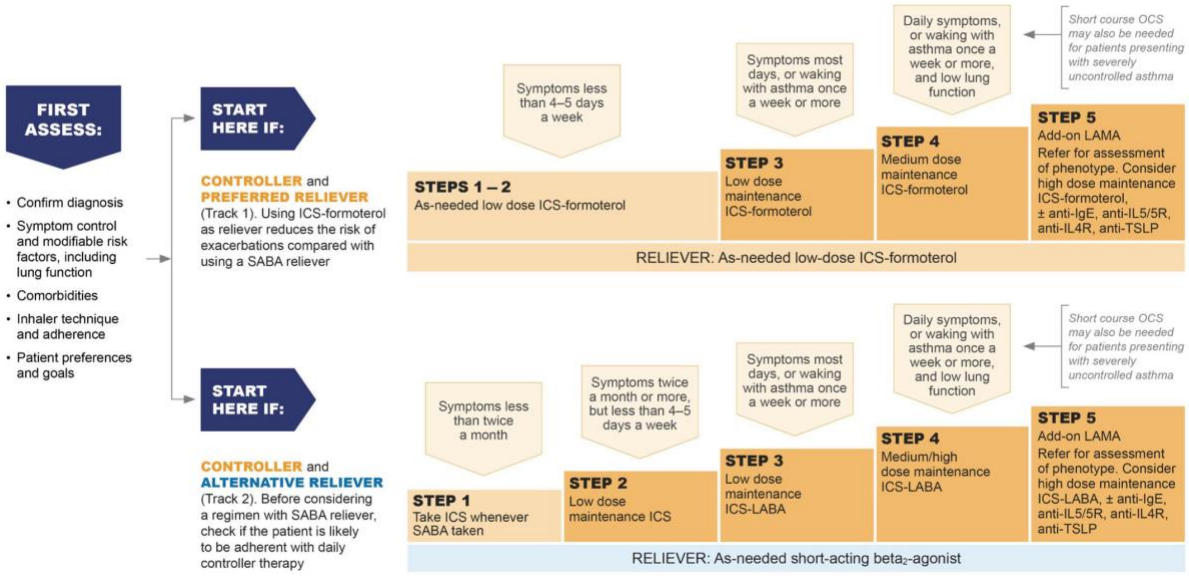


Figure 2.6: GINA steps [28]. Diagram showing the various GINA steps for Initial medications for adults and adolescents diagnosed with asthma. It outlines initial treatment options for asthma, providing guidance on medication levels for each treatment track based on symptoms and, where applicable, lung function. ICS (inhaled corticosteroid), LABA (long-acting beta2 agonist), LAMA (long-acting muscarinic antagonist), MART (maintenance and reliever therapy with ICS-formoterol), OCS (oral corticosteroids), and SABA (short-acting beta2 agonist) [28].

It is crucial that asthma therapy be customised and that the "treatable traits" approach be employed to manage asthma. It is known that the T2-high asthma phenotype responds to various types of therapeutic management including ICSs, systemic steroids, and biologics. The crucial role of type-2 cytokines in the development of asthma has led to the exploration of various targeted treatments such as antibodies that focus on IL-4, IL-5, or IL-13 pathways. Like type-2 cytokines, some type-2 biomarkers such as elevated levels of blood eosinophils or FeNO may suggest the likelihood of a corticosteroid response in individuals with asthma. Treatment with corticosteroids is effective in people with T2-high asthma, but in many cases, high doses are required to manage the symptoms. Therefore, these people must be cautious to reduce their dependence on corticosteroids and to mitigate the risk of dose-dependent side effects [46].

Haldar et al. (2008) revealed that the tailoring of treatment based on inflammation levels yielded better results than blanket corticosteroid treatment [40]. This approach led to a decrease in exacerbation frequency in the inflammation-predominant cluster and a reduction in the required ICS dose in the symptom-predominant cluster [40]. In patients with persistent eosinophilia who do not respond well to corticosteroid treatment, the use of type-2-targeted treatments may be beneficial [50]. *Couillard et al.* (2022) proposed an intriguing method to sub-stratify T2-high asthma for better and more tailored therapeutic decision-making, which they referred to as the “bomb” (BEC) “magnet” (FeNO) approach [56]. In their study, the researchers underscored the importance of incorporating both BEC and FeNO levels alongside traditional markers for the enhanced management of severe T2-high asthma. This dual-marker strategy enabled more precise treatment planning, potentially enhancing patient outcomes by aligning therapies more closely with the specific inflammatory profiles of individuals. Their study also highlighted the critical role of multi-dimensional biomarkers in the management of complex diseases such as severe asthma, in which the degree and nature of inflammation can differ markedly between patients. If patient stratification is improved through the combined

use of the "bomb" (BEC) and "magnet" (FeNO), clinicians can optimise the effectiveness of biological therapies and other targeted treatments.

Currently, there are four known strategies for monoclonal antibody targeting (biological drug therapy), each of which inhibits different aspects of the immune response that is responsible for triggering asthma attacks [57]. Figure 2.7 shows *Couillard et al.*'s 2022 illustrative summary of T2-inflammation pathways, which clearly explains the pathways that are inhibited by the relevant biological therapies [57].

Omalizumab was the first targeted biological treatment for severe asthma. It was approved by the US Food and Drug Administration (FDA) in 2003 [58]. This monoclonal antibody targets the distal effector of allergic reactions, anti-IgE, with minimal impact on the type-2 immune response. By binding to IgE, it reduces blood IgE levels by up to 99%. It also diminishes the expression of the high affinity IgE receptor FCRI on inflammatory cells such as mast cells and basophils. This dual action weakens the allergic responses and enhances the antiviral immune response, ultimately preventing asthma exacerbations [58, 59]. Omalizumab is approved for use in individuals, including children aged six and above, who have moderate-to-severe persistent allergic asthma that is driven by IgE. It can be prescribed to those in whom asthma remains uncontrolled despite treatment at GINA steps 4/5, and who have elevated blood IgE levels and confirmed sensitisation to a perennial allergen [28].

Biological drugs that target IL-5 have gained significant popularity in recent years. The most commonly used biologics that are licensed against IL-5 pathways are mepolizumab and benralizumab [58]. Mepolizumab is effective in the management and treatment of severe eosinophilic asthma. It is a monoclonal antibody that blocks IL-5 and therefore inhibits eosinophilic inflammation [60]. Mepolizumab is recommended for use under specific conditions as an add-on therapy for severe refractory eosinophilic asthma. The conditions include the requirement that adult patients must have adhered to an optimised standard

treatment plan that involves high doses of ICSs and long-acting beta-agonists, which has proved ineffective (as discussed earlier), and they must meet specific criteria related to BECs and exacerbation history. To qualify to be prescribed mepolizumab, patients' BECs should be 300 cells/µl or more, and they should have experienced at least four exacerbations that have required treatment with systemic corticosteroids in the previous 12 months or have been on continuous OCSs equivalent to at least 5mg of prednisolone per day for the past six months. They are also eligible if their BEC is 400 cells/µl or more, and they have had at least three exacerbations that required treatment with systemic corticosteroids in the previous 12 months (making them also eligible for benralizumab). Treatment response is assessed typically after 12 months, and mepolizumab should be discontinued if the patient has not responded adequately. Conversely, it should be continued if the patient has had an adequate response, which is defined as a meaningful reduction in severe exacerbations that require systemic corticosteroids or a significant reduction in continuous OCS use while they have maintained or improved their asthma control [61].

Benralizumab is another common biological drug that has been recommended as an additional therapy option to treat severe eosinophilic asthma in adults for whom standard treatments have proven ineffective. It has also demonstrated its effectiveness in reducing the frequency of exacerbations. It works by targeting IL-5 alpha receptors and inhibiting eosinophilic inflammation [60, 62-68]. To be eligible for benralizumab, the patient must have adhered to the optimised standard treatment plan, their BEC should be 300 cells/µl or more, and they require a history of four or more exacerbations that have required systemic corticosteroids in the previous 12 months or continuous OCSs equivalent to at least 5mg of prednisolone per day over the past six months (making them eligible also for mepolizumab), or they must have a BEC of 400 cells/µl or more and have faced three or more exacerbations that have required systemic corticosteroids in the past 12 months. Benralizumab treatment

should be initiated if it is the most cost-effective option, taking into account both drug and administration costs. At the 12-month mark, the treatment with benralizumab should be discontinued if the response has been inadequate. Conversely, it should be continued if there has been a satisfactory response [68].

Another common biological drug that has been approved by the FDA recently as an add-on therapy in the treatment of severe asthma is dupilumab. It is a monoclonal antibody that targets and binds to IL-4 and IL-13 receptors and inhibits both IL-4 and IL-13 pathways [58]. According to *Rabe et al.* (2018), patients with severe asthma who have been on long-term use of glucocorticoids have experienced a reduction in oral glucocorticoid usage, a decrease in the rate of severe exacerbations, and an increase in FEV_1 with dupilumab treatment [69].

Tezepelumab is a monoclonal antibody that is designed to bind specifically to TSLP, and this binding prevents the interaction of TSLP with its heterodimeric receptor. TSLP is a cytokine that is derived from epithelial cells. It is implicated in various downstream processes that are associated with asthma pathophysiology. In people with asthma, high TSLP levels are associated with airway obstruction, disease severity, and resistance to glucocorticoids [70].

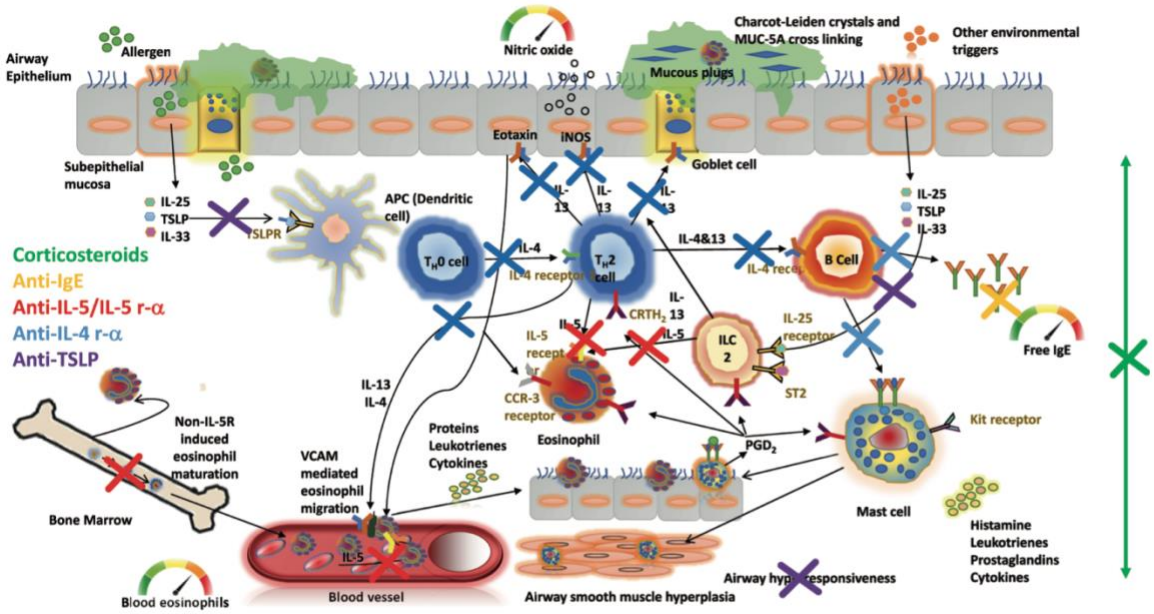


Figure 2.7. *Couillard et al.*'s 2022 overview of type-2 inflammatory responses in asthma. The diagram illustrates key cellular players, cytokines, chemokines, and effector mediators along with their receptors. Coloured crosses indicate the pathways that are inhibited by the relevant biological therapy (depicted in the same colour). It is worth noting that corticosteroids inhibit most pathways, albeit with associated toxicity [57].

2.3 Coronavirus disease (COVID-19)

2.3.1 Epidemiology and overview

In late 2019, a new type of coronavirus, SARS-CoV-2, which was associated with pneumonia, emerged in Wuhan in central China. Just a few months later, on March 11, 2020, the World Health Organisation officially declared the outbreak a global pandemic and named the disease the virus caused COVID-19 (coronavirus disease 2019) [71, 72]. As of March 2023, the number of confirmed cases of COVID-19 worldwide has reached nearly 700 million, resulting in a loss of nearly seven million lives [46]. COVID-19 can be transmitted through various means, including the inhalation of respiratory droplets (within a distance of two metres), direct contact with the mucosal secretions of an infected individual, or contact with

contaminated surfaces or objects. The incubation period for the virus ranges from three days to two weeks [71, 72].

SARS-CoV-2 belongs to the beta coronavirus group within the coronavirinae family. It is the most recent addition to the coronavirus family, following the discovery of severe acute respiratory syndrome coronavirus (SARS-CoV) and Middle East respiratory syndrome coronavirus (MERS-CoV) over the past two decades. Researchers who analysed the complete genome sequences of SARS-CoV-2 observed that it had a closer resemblance to SARS-CoV than to MERS-CoV. SARS-CoV-2 is a large, single-stranded ribonucleic acid (RNA) virus enclosed in a protein envelope. It is transmitted rapidly among humans. A significant contributor to its swift transmission, which distinguishes it from MERS-CoV and SARS-CoV, is its strong affinity for the angiotensin-converting enzyme 2 (ACE2) receptor [72, 73]. ACE2 is a transmembrane metalloprotein receptor that is present primarily in the respiratory system, gastrointestinal tract, kidneys and blood vessels. SARS-CoV-2 exploits ACE2 as its functional receptor to invade and infect host cells, and this accounts for numerous COVID-19 symptoms [74].

The emergence of SARS-CoV-2 caused substantial economic challenges and placed immense strain on global healthcare systems due to its novelty, widespread prevalence, genetic diversity, and mutation capabilities. Since the onset of the outbreak, researchers have made extensive efforts to understand the disease and to devise effective therapeutic and pharmacological strategies to curtail its spread, enhance patient outcomes, and reduce mortality rates.

2.3.2 COVID-19 diagnosis

Due to the vague nature of COVID-19 symptoms, doctors cannot rely solely on symptoms to diagnose it. Current diagnostic criteria emphasise the importance of laboratory examinations, particularly swab tests, as a crucial approach to confirming COVID-19 infection.

Among these methods, quantitative polymerase chain reaction (qPCR) is the most reliable way to identify SARS-CoV-2 [75, 76]. Despite its dependability, there have been cases in which radiographic signs of COVID-19 were evident in patients with negative qPCR test results [77]. The qPCR technique quantifies viral transcripts in the sampled material relative to a standard control RNA and determines the number of amplification cycles required for virus detection. An alternative measure of viral load is the threshold cycle at which viral transcripts become detectable [75, 76].

2.3.3 COVID-19 pathophysiology and clinical picture

There is a wide spectrum of clinical responses to the disease, which vary significantly from one individual to another. These responses span from being asymptomatic or experiencing mild viral infection, which typically necessitates only supportive care, to severe and fatal instances of COVID-19 pneumonia. Among survivors of the latter, many people develop acute respiratory distress syndrome (ARDS) and other critical complications such as pulmonary and vascular thromboses. Some of these severe cases require interventions such as mechanical ventilation and extracorporeal membrane oxygenation. Common symptoms encompass fever, shortness of breath, dry cough, general discomfort, myalgia, muscle pain and headaches. Less common symptoms involve loss of taste, diarrhoea and nausea [71, 72].

A clear pathophysiological mechanism of COVID-19-induced lung injuries and the disease's various phenotypes and stages have yet to be described, as to confirm such information, a large number of biopsies and autopsies is required. Despite the numerous unknowns, several hypotheses have been proposed, and ongoing research is dedicated to comprehending the pathophysiological mechanism of COVID-19.

In a review of the pathological findings of COVID-19, *Polak et al.* (2020) described the clinical manifestation of COVID-19 as three successive and possibly overlapping stages of disease severity [78]. Stage one is the infection stage, characterised by mild, flu-like symptoms

that in some people might develop into viral pneumonia that requires hospital admission and respiratory support. Stage two is the inflammatory stage, which is characterised by pulmonary inflammation (ARDS) and coagulopathy. This stage can be distinguished by high levels of inflammation biomarkers (C-reactive protein (CRP), IL-6, IL-1, d-dimer). Stage three is the final stage of the disease and is characterised by fibrotic changes [78].

COVID-19 pneumonitis exhibits distinct and notable histopathological alterations in comparison with other viral pneumonia types (MERS-CoV and SARS-CoV) as well as conventional ARDS. SARS-CoV-2 affects both epithelial and vascular tissues and may progress to induce fibrotic changes approximately three weeks after symptom onset. It is noteworthy that viral presence is observed in both pulmonary epithelium and vascular endothelium, and alterations in both these components can manifest at all stages, even in the early phases of the disease [78]. Epithelial transformations encompass diffuse alveolar damage, deposition of alveolar fibrin, and infiltration of perivascular T-lymphocytes. Vascular modifications are characterised by distorted pulmonary vascularity, endothelial microvascular injuries, diffuse vascular thrombosis and angiogenesis [79].

COVID-19 can impact people of all ages and genders, yet research indicates that older males with underlying health conditions that might compromise their immune systems are more vulnerable than other demographic groups to infection [78, 80, 81]. *Zhang et al.* (2020) identified several risk factors that were associated with disease severity, as well as the likelihood of intensive care unit (ICU) admission and mortality. The most common comorbidity was hypertension, followed by diabetes, high BMI, and cardiovascular disease [81, 82]. The risk of ICU admission was greater in cases that showed elevated levels of five noteworthy factors: leukocytes, alanine aminotransferase (ALT), aspartate transaminase (AST), procalcitonin, and lactic acid dehydrogenase (LDH). Elevated ALT and AST levels in severe COVID-19 cases could be attributable to hepatic damage due to direct binding of SARS-

CoV-2 to ACE2 receptors. A high LDH level indicates tissue damage, since LDH is secreted when the cytoplasmic membrane is injured. Additionally, an elevated LDH level in severe COVID-19 cases has been associated with predictions of ARDS development and a higher mortality rate [82]. In a retrospective study conducted by *Zhou et al.* (2020) on hospitalised COVID-19 patients in Wuhan, three common risk factors emerged for fatal and severe cases: a high sequential organ failure assessment (SOFA) score upon admission, advanced age, and a d-dimer level that exceeded 1μg/ml. The SOFA score is used to assess for sepsis and multi-organ failure. Many people of advanced age have compromised adaptive immune systems (T-cells and B-cells), and this reduces the immune system's ability to control viral spread and increases the rate of secretion of type-2 cytokines, which prolong proinflammatory responses and exacerbate damage. Elevation in d-dimer levels is a consequence of systemic proinflammatory responses or may indicate direct cardiac involvement, given that ACE2 is also expressed in cardiovascular endothelial cells [81].

2.3.4 Post-COVID

The long-term effects of COVID-19 on respiratory physiology and function are under investigation. Some COVID-19 survivors have reported persistent symptoms and impairments that have lasted beyond the active infection period. This situation suggests that there are some long-term effects of this novel virus on the respiratory system. In most bodily organs, injury typically leads to tissue fibrosis. An infection such as that caused by SARS-CoV-2 can trigger systemic inflammatory responses that may result in fibrosis of the pulmonary, cardiac and vascular systems [83].

Fatigue and dyspnoea have been commonly reported in patient follow-up visits within the first three months after their recovery from COVID-19. Interestingly, some studies have found that the level of fatigue that patients experience is not associated with the severity of their disease or the presence of abnormal radiological changes [84, 85]. In a multicentre UK

study that involved 370 individuals who had been hospitalised with COVID-19, many patients continued to experience breathlessness, fatigue and other respiratory symptoms months after hospitalisation [86].The prevalence of these symptoms was notably higher in those with more pronounced lung abnormalities on high-resolution computed tomography (HRCT) scans [86]. Reductions in functional capacity and health-related quality of life have also been observed in COVID-19 infection survivors [85].

Post-COVID-19 lung function impairments have also been observed. Reductions in the diffusion capacity of the lungs for carbon monoxide (DLCO) are the most common lung function changes, followed by some reported cases of restrictive lung function patterns. According to *Zhao et al. (2020)* and *Sanchez-Ramirez et al. (2021),* COVID-19 survivors, particularly those who were hospitalised, often show impaired lung function, with a reduction in DLCO being the most common finding [84, 85]. This reduction is especially prevalent in individuals who have experienced severe COVID-19 and is indicative of damage to the alveolar-capillary membrane, which is a characteristic that is commonly associated with interstitial lung diseases and pulmonary fibrosis [84, 85]. Other findings point to abnormalities in lung volumes, with reductions in total lung capacity (TLC) and FVC that are indicative of restrictive lung disease, especially in patients who have had severe COVID-19 [85]. Another significant issue is $\dot{V}/\dot{Q}$ mismatch. Studies such as those by *Ackermann et al. (2020)* indicate that inflammatory and thrombotic damage to the pulmonary vasculature leads to impaired perfusion, which results in regions of the lung that are ventilated but not adequately perfused [79]. This mismatch contributes to the breathlessness and reduced oxygenation levels that are seen in many patients post-COVID-19 [79].

Persistent radiological changes have also been observed in the three months after COVID-19 recovery. The most common abnormality that has been observed on computed tomography (CT) scans is persistent ground-glass opacity, followed by interstitial thickening

[84-87]. Imaging studies have provided essential insights into structural lung changes that have followed COVID-19 infection. CT scans are widely used during the acute phase of the disease, revealing persistent ground-glass opacities and fibrotic changes in a significant number of patients months after recovery. These residual parenchymal changes are especially common among patients who have required hospitalisation for severe COVID-19 [5, 86]. *Grist et al. (2022)* used hyperpolarised ^{129}Xe magnetic resonance imaging (MRI) to study patients with post-COVID-19 symptoms and found ventilation defects even in individuals who had suffered mild or moderate disease and who had not required hospitalisation [88]. These defects were heterogeneous, with some areas of the lung showing poor gas exchange while others remained relatively unaffected [88].

In conclusion, lung function tests and imaging in COVID-19 survivors reveal a range of abnormalities, including impaired gas exchange, $\dot{V}/\dot{Q}$ mismatch, and structural changes such as fibrosis. A more detailed discussion of the effects of COVID-19 are presented in Chapter 7.

2.4 Lung function measurements

Pulmonary function tests (PFTs) serve as well-established diagnostic tools for pulmonary diseases. These tests offer precise and consistent evaluation of the functional status of the respiratory system. It must be emphasised that although these tests are valuable, they do not provide specific disease diagnoses [89]. In this section of my thesis, I delve into various routine PFTs that are commonly used to assess airway diseases. However, my primary focus will be on spirometry and gas transfer. These two tests are particularly pertinent to Chapter 6 (as they were used to evaluate the T2-high asthma cohort) and Chapter 7 (as they were applied to assess the post-COVID-19 infection survival cohort).

2.4.1 Spirometry

Spirometry is the most commonly used lung function test, both to diagnose and to monitor airway diseases. This physiological assessment explores the functional dimensions of the lungs. It utilises an objective measure to quantify a patient's inhalation and exhalation capacities at maximum effort. During a spirometry test, three critical variables are measured: FVC, forced expiratory volume in one second (FEV_1), and the ratio between these two volumes (FEV_1/FVC). This ratio is of clinical significance in the diagnosis of obstructive pulmonary diseases, such as asthma and COPD. Furthermore, FEV_1, expressed as a percentage of its predicted value, indicates the extent of airflow obstruction. The configuration of flow-volume curves can also yield information regarding the functionality of small airways. Many individuals who have obstructive pulmonary diseases and airflow limitations exhibit a concave expiratory limb within their flow-volume curves (Figure 2.8) [89-91].

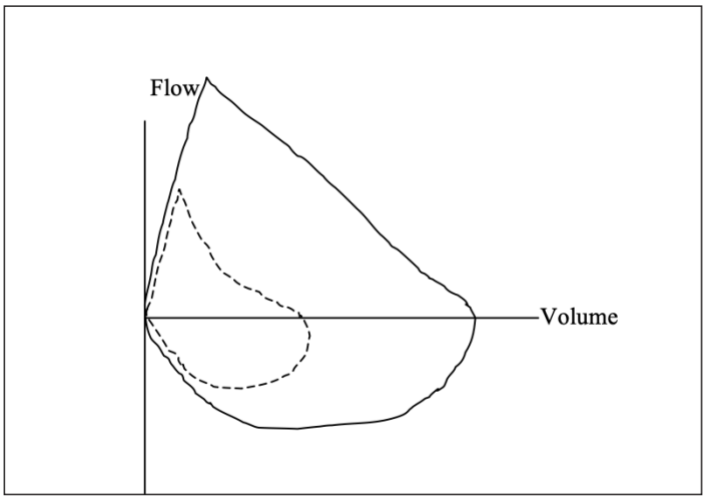


Figure 2.8. Curves showing flow and volume of air through the lungs of healthy people and of those with lung disease. The solid line shows the shape of a flow-volume curve in a healthy individual, while the dotted line represents the concave appearance that is seen in individuals with obstructive lung disease [90].

Spirometry has widely been regarded as the cornerstone for the diagnosis and monitoring of airway diseases, yet it has notable limitations that constrain its effectiveness in

capturing the full spectrum of lung pathology [6-9, 90]. One significant limitation of spirometry lies in its focus on the detection of airflow obstruction, which may not occur in the early stages of certain lung diseases or patients with small airway involvement. Spirometry often fails to detect early or peripheral airway abnormalities, and this drawback leads to potential under-diagnosis or misclassification of diseases such as asthma and COPD [6]. *Gustafsson et al. (2008)* illustrated the limitations of spirometry in the context of CF [7]. Their study compared the use of spirometry with that of an MBW technique and found that spirometry often led to underestimations of the extent of structural lung disease when compared with MBW-derived indices [7]. This finding is supported by *Sanders et al. (2011)*, who demonstrated that spirometry might not correlate well with the severity of structural lung damage that might be observed in chest CT scans of children with CF [8]. *Brody et al. (2014)* also highlighted a critical limitation in relying solely on spirometry to assess lung function in children with CF [92]. They found that it was common for these patients to have normal PFT results (with FEV_1, FVC, and forced expiratory flow between 25% and 75% of vital capacity (FEF_{25-75}) values >85% of predicted) while simultaneously exhibiting abnormal findings on HRCT, including evidence of bronchiectasis [92]. Moreover, *Subbarao et al. (2015)* highlighted the inadequacy of spirometry in the detection of ventilation inhomogeneities, which would be better assessed through the use of techniques such as MBW [9].

In addition to its diagnostic limitations, spirometry is also less sensitive than other techniques to peripheral inflammation, which can be present even when spirometry results are normal. *Lehtimäki et al. (2005)* demonstrated that patients with symptomatic asthma and significant peripheral airway inflammation had normal spirometry measures [93]. These studies suggest that although spirometry is useful to monitor disease progression, it may not provide a comprehensive assessment of lung function, particularly in diseases that are characterised by heterogeneous or peripheral airway involvement.

Spirometry, as mentioned earlier, utilises an objective measure to quantify a patient's inhalation and exhalation capacities at maximum effort. Hence it is inherently effort-dependent [91, 94, 95]. Due to the effort- and instruction-dependent nature of the technique, one of its primary challenges is that the quality of test results relies heavily on the skill and training of the operator [95-97]. Inaccurate test results can lead to misdiagnosis or inappropriate management of respiratory conditions. To address this, the UK has implemented recommendations for "quality-assured" spirometry to ensure that the results are reliable and that the interpretations are accurate [95-97]. Training programmes are offered by regulatory bodies or governing organisations. The Association for Respiratory Technology & Physiology (ARTP) is the professional examination body in the UK that provides a benchmark for competency standards. Healthcare professionals who conduct PFTs are required to be registered with an appropriate professional body, such as the Registration Council for Clinical Physiologists, the Academy for Healthcare Science, or the Health and Care Professions Council. All individuals who perform spirometry in the UK must hold the ARTP Spirometry Certificate or an equivalent qualification and be listed on the Register of Spirometry Practitioners. Revalidation is required every three years [95]. Achieving this level of quality assurance presents significant challenges in practice. Passage through the training pathways that must be completed to equip primary care and respiratory clinic staff with the necessary skills to carry out and interpret spirometry measurements is extensive and time-consuming [96, 97]. As a result, many healthcare providers find it difficult to fund the required training, and this has led to a shortage of qualified personnel who can perform spirometry to the required standard.

2.4.1.1 Bronchodilator reversibility test

The bronchodilator reversibility test is an integral component of the spirometry examination. The aim is to assess the impact of a short-acting β2-bronchodilator on

measurements of volume and flow. This test is administered in cases in which signs of obstructive ventilatory impairment are evident. It serves as a diagnostic and evaluative tool for conditions such as asthma and COPD, as it quantifies the reversal of airflow obstruction that is induced by bronchodilator medication [91].

Typically, the test is conducted by first asking the patient to perform a baseline spirometry test, and then administering a bronchodilator (usually 4 x 100mcg salbutamol via a spacer). Another spirometry test is then performed, usually 20 to 30 minutes after administration of the bronchodilator [91, 94, 95].

Prior to the test, the subject must not have taken certain respiratory medicines that they may be prescribed. This is a critical limitation of the test, as its utility is reduced in individuals who are already on long-acting bronchodilators such as long-acting beta-agonists (LABAs) or long-acting muscarinic antagonists (LAMAs). These medications can augment bronchodilation and therefore blunt the response that is caused by the short-acting bronchodilator used in the test [95, 98, 99]. As a result, the test may not show significant reversibility even in patients with reversible airway obstruction, so it may produce false negatives or underestimations of disease severity. This is particularly relevant in clinical settings, where patients are often tested while on maintenance therapy. Figure 2.9 shows a table taken from *Sylvester et al. (2020),* in which they summarise the recommended period for which each medication should be withheld before the measurement [95]. However, it is a challenge to determine a uniform duration of activity that applies to all patients due to various confounding factors. These include the number of available receptors in the airways, the individual's size, and the mechanism, route and efficiency of action of previous drug doses. For example, with salbutamol, pharmacokinetic studies have shown that it typically takes four to six hours for lung function to return to its pre-medication state. Currently, the generally

accepted medication-withhold periods are four hours for short-acting beta-agonists (SABAs) and 12 hours for LABAs [95, 98-100].

The effectiveness of the bronchodilator reversibility test is limited in cases of variable disease activity. For instance, in patients with asthma, the degree of airway obstruction may fluctuate significantly, as it is influenced by factors such as allergen exposure, infections or medication use [95, 98, 100]. This variability may result in inconsistent test outcomes, making it challenging to obtain a clear diagnosis or to monitor disease progression accurately. The test's utility is further limited in individuals whose lung function is close to the lower limit of normal but still within normal ranges. In such cases, even if there is a response to the bronchodilator, it may not be sufficient to meet the standard criteria for reversibility, and this may lead to under-diagnosis or misinterpretation of disease severity [95, 98, 100]. Additionally, it is important to note that in cases that involve individuals who have been diagnosed with both asthma and COPD, some patients who initially test positive for bronchodilator reversibility may not actually have asthma. Conversely, in cases in which the reversibility test yields negative results, research suggests that one in three individuals have asthma [36].

There is also considerable variability in the guidelines and literature regarding how bronchodilator reversibility should be calculated. Different guidelines recommend different thresholds for what constitutes significant reversibility, typically based on percentage changes in FEV_1 or absolute improvements in millilitres. For example, some guidelines suggest that an increase in FEV_1 of 12% and 200ml from baseline represents significant reversibility, while others propose different cutoffs. This inconsistency can lead to confusion in clinical practice and variability in diagnosis, depending on which criteria are applied [95, 98, 100].

Drug type	Example	Washout interval
Muscarinic antagonists	SAMA (eg, ipratropium)	12 hours
	LAMA (eg, tiotropium)	7 days
Beta-agonists	SABA (eg, salbutamol)	6 hours
	LABA (eg, salmeterol)	24 hours
	uLABA (eg, olodaterol)	48 hours
Xanthines	Theophylline	Not necessary
Inhaled glucocorticosteroid	Single dose (eg, budesonide)	Not necessary
	Stable dose (eg, budesonide)	Unknown
Leukotriene receptor antagonists	Single dose or up to 1 week (eg, montelukast)	Not necessary
	Stable dose	Unknown
Antihistamines	(eg, diphenhydramine, desloratadine)	Not necessary
Combination therapies (limited or no data)	ICS/LABA (eg, fluticasone/formoterol)	24 hours
	ICS/uLABA (eg, fluticasone/vilanterol)	48 hours
	LAMA/LABA (eg, glycopyrronium/indacaterol)	7 days

Figure 2.9. Table taken from *Sylvester et al. (2020)* shows recommended periods for which medications should be withheld prior to the bronchodilator reversibility test [95]. ICS, inhaled corticosteroids; LABA, long-acting beta-agonist; LAMA, long-acting muscarinic antagonist; SABA, short-acting beta-agonist; SAMA, short-acting muscarinic antagonist; uLABA, ultra-long-acting beta-agonist.

2.4.2 Body plethysmography

Body plethysmography is another well-established technique for the measurement of lung function. The test is performed inside an airtight, glass-walled chamber, which enables the measurement of static lung volumes. It measures TLC, residual volume (RV), RV/TLC, FRC and airway resistance (Raw). The RV and RV/TLC measures are useful for the detection and determination of the degree of hyperinflation; hence, the technique is used routinely to guide volume reduction surgery [6, 101].

Body plethysmography offers a comprehensive assessment of lung function as it captures a range of functional and structural attributes. Although spirometry is widely regarded as the gold standard by which to evaluate lung function, it falls short in terms of the delivery of information regarding specific parameters such as RV and TLC. The use of body plethysmography also enables the determination of additional features such as Raw and

intrathoracic gas volume. Usually, a full plethysmography test includes a spirometry test as well [101].

2.4.3 Gas transfer

Gas transfer, also known as the measurement of the DLCO, plays an important role in the assessment of the integrity and size of the alveolar blood membrane. This evaluation quantifies the diffusion of carbon monoxide (CO) across the alveolar-capillary membrane, which is a process that is dependent on the surface area and soundness of the alveolar membrane and of the pulmonary vascular bed. The resulting value is typically corrected for the patient's haemoglobin levels (DLCOc). The assessment involves the use of CO gas, which has a high affinity to haemoglobin and undergoes diffusion-limited uptake. The measurement technique involves a single-breath procedure, in which the patient rapidly inspires a gas mixture of 10% helium and 0.3% CO, holds their breath for 10 seconds and then exhales. The CO that remains in the exhaled breath is measured. A comparison of the fractions of inspired and expired CO enables the calculation of DLCOc. Since the DLCOc relies on the alveolar membrane's surface area, it is compromised in conditions that cause surface area reduction, such as pulmonary fibrosis, emphysema or a pulmonary embolism (PE).

During the 10-second breath hold, the transfer coefficient (KCO), which measures the rate of CO uptake from the alveolar gas into the capillary blood, is determined. The lung volume (V_A) is estimated through helium dilution. The correction of DLCO to produce DLCOc through the use of KCO factors in the alveolar volume. In cases of pneumonectomy, DLCOc is decreased due to the substantial reduction in surface area of the alveolar membrane. Yet, KCO remains unaffected or may even be higher than normal, as the functional integrity of the alveolar-blood membrane is maintained in the remaining lung. The transfer factor for CO (TLCO) is computed by multiplication of KCO by V_A. It serves as an indicator of overall lung

CO transfer from gas to blood. The TLCO is linked directly to the alveolar-capillary membrane surface area relative to lung volume.

The TLCO has proved valuable to distinguish conditions that are characterised by alveolar damage, such as emphysematous COPD, from those that preserve alveolar tissues, such as asthma. In asthma, CF and similar conditions, the TLCO and KCO usually remain the same or may even be elevated. This is attributable to increased pulmonary blood flow (which increases TLCO and KCO) or reduced apparent V_A (which disproportionately raises KCO) [6, 90].

2.4.4 The forced oscillation technique

The FOT is a non-invasive measure of lung function. It involves the application of different oscillation frequencies (3-30Hz) to the respiratory system during normal breathing [6]. This enables measurement of the system's impedance, which encompasses both resistance (Rrs) and reactance (Xrs), across a range of oscillatory frequencies. Knowledge of these properties provides a comprehensive evaluation of the mechanical properties of the respiratory system, from the central airways to the peripheral lung regions. The Rrs is a measure of friction in the airways, which opposes airflow. The Xrs primarily reflects the elasticity of the peripheral lung parenchyma and chest wall, which also impacts Rrs [102, 103]. Low frequencies (5Hz) penetrate deep into the lung, while high frequencies (20Hz) are absorbed before they reach the smaller peripheral airways. Thus, R5 represents total-airway resistance, R20 central-airway resistance, and R5 minus R20 denotes small airway resistance [6, 102, 103]. Oscillometry offers the ability to measure both total- and small airway resistance, and to differentiate between central and peripheral airway involvement, and therefore offers clinicians a detailed picture of airway dynamics [6, 10, 11].

Compared with spirometry, the FOT is relatively simple to apply and does not require any coordination or breathing manoeuvres. The FOT has been shown to be reliable in the assessment of airway hyper-responsiveness in both adult and paediatric patients [6, 103]. It is also a sensitive measure of bronchodilator responsiveness in asthma and COPD. Yet the FOT is not widely adopted in clinical lung function laboratories, despite being commercially available. This may be because there is no standardised reference range and interpretation of the results is complex. Additionally, data have shown that the FOT cannot be used to differentiate effectively between obstructive and restrictive respiratory disorders [6, 103].

PFTs, specifically spirometry and diffusion capacity measures, are well-established diagnostic tests for pulmonary diseases; however, as stated earlier, they have significant limitations. They are effort-dependent, provide little information about lung pathology or inhomogeneity, and are insensitive to early-stage lung disease or therapeutic responses [6-9].

2.5 Measurements of inhomogeneities

Lung inhomogeneities may provide early signs of pulmonary disease, and their measurement can be used to monitor the progression of the disease [104]. In COPD patients, alveolar $\dot{V}/\dot{Q}$ mismatch is the most common cause of arterial hypoxaemia. In the early stages of COPD, pulmonary gas exchange abnormalities are observable before FEV_1 declines [105]. Abnormalities in ventilation distribution that occur in obstructive lung disease may not show up in spirometry and lung function tests, and this finding underscores the potential benefits of inhomogeneity tests [106].

Yet despite such benefits, no simple, precise and non-invasive inhomogeneity measures have been incorporated into standard lung function tests. In this section, I discuss various approaches that are available to explore lung inhomogeneity. In Chapter 3, I explain CCP,

which is the technique I used in the work for this thesis, as a novel measure of pulmonary inhomogeneity.

2.5.1 Multiple inert gas elimination technique

During the early 1970s, a novel method called the multiple inert gas elimination technique (MIGET) was developed to study the pulmonary exchange of six different inert gases. These gases were dissolved in a saline solution and simultaneously infused intravenously into the bloodstream, after which their concentrations were measured in both mixed expired gas and arterial blood through the use of gas chromatography [107]. Through the application of a mathematical model of the lung, the MIGET was used to calculate the distribution of $\dot{V}/\dot{Q}$ ratios, and these shed light on how gases were exchanged throughout the lung [6, 107].

The use of this technique enabled researchers to quantify disturbances in $\dot{V}/\dot{Q}$ ratios and to identify cases of pulmonary shunting. The findings that were obtained from its use significantly enhanced comprehension of pulmonary pathophysiology [6, 107]. It has demonstrated sensitivity in the detection of early COPD, even in patients with mild spirometric disease [108]. In asymptomatic asthmatics who had mild airway obstruction, MIGET exhibited extensive $\dot{V}/\dot{Q}$ mismatch [109]. However, MIGET is seldom used clinically due to its complexity and invasive nature.

2.5.2 Inert gas washout

More than six decades ago, the concept of inert gas washout was introduced to the assessment of ventilation inhomogeneity. With subsequent rapid advances in gas analysers and compact computers, it is possible to use the technique not only to evaluate pulmonary ventilation inhomogeneity, but also in some cases to gain valuable insights into the underlying pathological abnormalities [12, 110]. Inert gas washout can be performed in a single breath or

several breaths [106]. As the test name indicates, inhalation or exhalation of an inert gas is measured during a breathing test. The gas must be inhalation-safe, a non-participant in gas exchange, and exhibit minimal solubility in blood or other tissues. The available choices are either naturally occurring gases such as N_2 or externally introduced gases such as sulphur hexafluoride (SF_6), helium (He) or methane (CH_4) [12].

2.5.2.1 The single-breath inert gas washout (SBW) technique

The SBW test is used to assess ventilation inhomogeneity, particularly in the peripheral airways. During the test, the subject sits upright and breathes through a mouthpiece with a nose clip attached. The procedure involves exhalation of RV, inhalation of 100% oxygen or a gas mixture such as SF_6 and He to TLC, and then exhalation from TLC to RV at a steady flow. The test produces an expirogram that shows four phases: phase I (dead space), phase II (bronchial phase), phase III (alveolar phase) and Phase IV, which indicates airway closure as RV is approached. The phase III slope is particularly important, as it reflects ventilation inhomogeneity across lung volumes, which is influenced by both large- and small-scale factors (Figure 2.10). A modified approach, in which the patient inhales from FRC to TLC or to just above FRC, better represents normal tidal breathing and may be more sensitive to peripheral airway issues. Pathological airway obstructions increase the phase III slope, and this indicates greater ventilation inhomogeneity. The phase IV portion, which marks the start of airway closure, produces the "closing volume". However, this is not visible in all subjects, so the phase III slope is the preferred measure. The SBW test requires significant patient cooperation and is therefore only feasible in older children (aged 10 years and above) and adults. Despite its complexity, the SBW test is a valuable tool for the detection of early or subtle airway abnormalities, especially in peripheral airway diseases [12, 106].

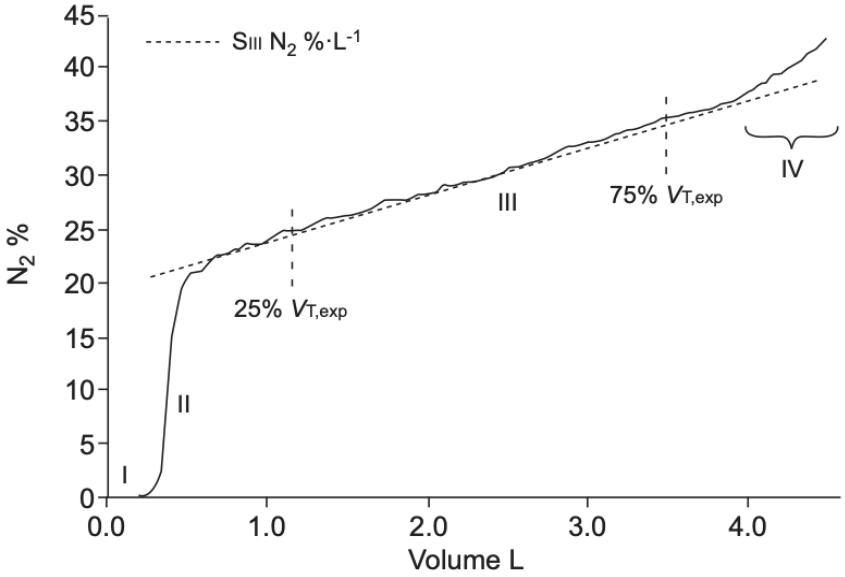


Figure 2.10. A typical SBW expirogram [106]. It shows a nitrogen (N_2) trace that illustrates the calculation of the phase III slope (S_{III}) in a vital capacity SBW test performed by a 60-year-old smoker. The S_{III} is calculated between 25% and 75% of the expired volume to exclude the influence of phase IV. The expirogram demonstrates the four phases: phase I (absolute dead space), phase II (bronchial phase), phase III (alveolar phase) and phase IV (the rapid rise at the end of expiration). The closing volume is the expired volume, which is measured from the point at which phase IV begins (upward deflection) to the end of the breath. $V_{T,exp}$ is the expired tidal volume [106].

2.5.2.2 The multiple breath washout (MBW) technique

The MBW technique is more informative than the SBW, and it offers greater feasibility across a wide age range. The MBW test requires minimal cooperation and coordination from the patient, aside from maintaining an adequate seal and ensuring a regular breathing pattern [12]. The MBW test involves switching the patient either out of a 100% O_2 supply (in the case of nitrogen MBW) or out of an inert gas mixture (such as 4% SF_6, 4% He, 21% O_2 and balance N_2) into room air. The test continues until the end-tidal inert gas concentration drops to one-fortieth of its starting concentration, which corresponds to approximately 2% for nitrogen MBW and 0.1% for SF_6/He MBW (Figure 2.11) [6, 12, 14, 106].

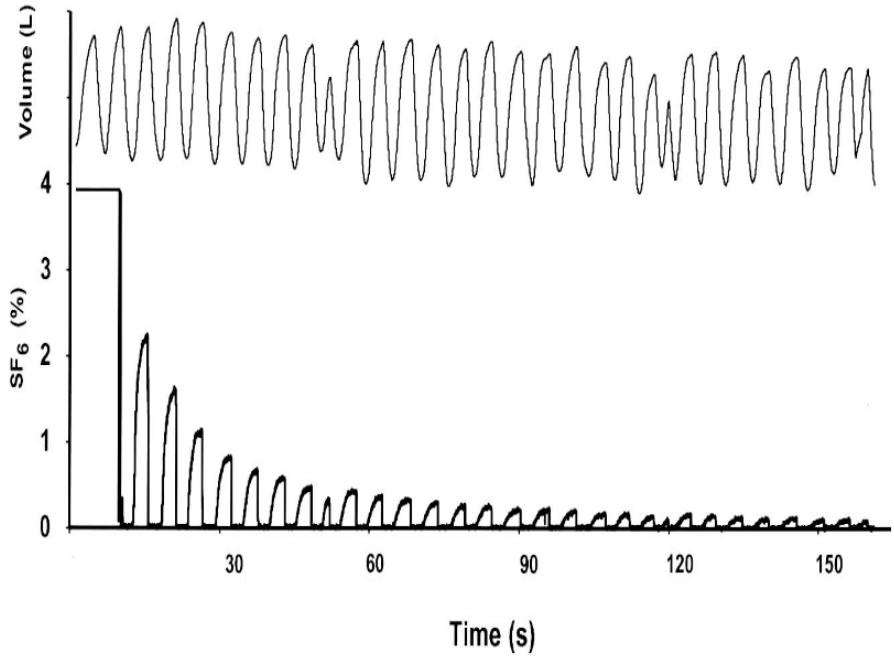


Figure 2.11. SF_6 MBW tracings [12], showing tidal volume (upper) and inert gas SF_6 concentration (lower). The MBW test begins with an SF_6 concentration of approximately 4% and continues until the SF_6 concentration drops below 0.1% [12].

2.5.2.2.1 Lung clearance index (LCI)

LCI was conceptualised in the 1950s as an index driven by MBW, but it has gained prominence only in recent decades with advances in gas analysers and computational methods [6]. LCI is a very useful measure of ventilation inhomogeneity that can be calculated from the MBW curve. LCI shows the efficiency of gas clearance from the lungs as it is measured from the washout of inert gases, such as N_2 or SF_6, during normal breathing [13, 106]. To calculate the LCI, the washout procedure starts at the FRC and continues until the exhaled N_2 level has decreased to 2.5% of its starting level; this is why it is sometimes reported as $LCI_{2.5}$. The LCI is quantified as the number of FRC lung turnovers that are required to achieve this decline in tracer gas concentration [6, 12].

$$LCI = \frac{CEV}{\mathrm{FRC}} \qquad \text{(Equation 2.1)}$$

in which *CEV* represents the total volume of air exhaled during the washout phase, and *FRC* is calculated from the MBW test.

$$FRC = \frac{V(tracer)}{\mathrm{Ci} - \mathrm{Ce}} \qquad \text{(Equation 2.2)}$$

In this equation, *V(tracer)* is the total volume of tracer gas exhaled at the end of the washout, *Ci* is the starting or initial fractional concentration of the tracer gas, and *Ce* is the final or end fractional concentration of the tracer gas.

The higher the LCI value, the greater the ventilation inhomogeneity [12-14, 16]. Ventilation inhomogeneity is common in conditions such as CF, asthma and COPD. Throughout the MBW test, a consistent tidal volume must be maintained to minimise variations in the dead-space-to-tidal-volume ratio, which could influence the LCI results independently of inhomogeneity [6, 106, 111].

This approach has proved especially useful in the identification of early lung disease, particularly in patients with CF, for whom early detection and monitoring are crucial due to the progressive nature of the disease. It gained popularity as a sensitive marker of early lung disease in children and in adults with CF [6, 7, 13, 112]. *Gustafsson et al. (2008)* highlighted the advantage of LCI over spirometry in the detection of subtle lung disease in CF patients [7]. They demonstrated that LCI was a more sensitive indicator of lung disease in CF patients than were traditional spirometry measures such as FEV_1 or FEF_{25-75} [7]. An interesting finding in their study was that LCI compared with the traditional measures was better for the detection of structural lung damage, as confirmed by HRCT, and they observed that a normal LCI result meant that abnormalities would almost certainly not be visible on HRCT [7]. *Aurora et al. (2005)* also demonstrated that LCI could be used to identify early lung abnormalities in preschool children with CF, even when traditional spirometry indicated that the lungs were

normal [16]. This suggests that LCI shows superior sensitivity in the identification of early lung pathology in CF and can indicate such pathology even when spirometry results are within normal limits. *Stanojevic et al. (2017)* supported the use of LCI to monitor disease activity in CF patients as they showed its effectiveness in tracking the disease progression in the lungs of preschool-aged CF patients; their study offered valuable insights into early disease development [17]. Additionally, *Davies et al. (2013)* found that LCI was more sensitive than spirometry in the detection of lung function improvements in CF patients who had been treated with ivacaftor, particularly in those who carried the G551D-CFTR mutation and showed normal spirometry results [18]. Collectively, these studies underscore the importance of LCI as a sensitive and informative measure of ventilation inhomogeneity that offers usefulness in both early detection and monitoring of lung disease progression and treatment response.

LCI usage in asthma has also been explored by researchers [112-116]. *Gustafsson et al. (2007)* provided an important insight into the role of LCI as a significant measure of peripheral airway function in asthma, which was additional to its well-established use as a sensitive marker in the detection of ventilation inhomogeneity and early lung disease in CF [113]. The researchers found that LCI could be used to differentiate effectively between the degree of peripheral airway involvement in CF and asthma, with asthma patients exhibiting less pronounced but still significant ventilation inhomogeneity compared with those with CF [113].

Zwitserloot et al. (2014) studied the clinical application of LCI during the use of the MBW technique in children and adolescents with asthma [114]. Their research cohort included paediatric patients with varying degrees of asthma severity, through mild, moderate and well-controlled asthma. Their study found that LCI was a highly sensitive indicator of ventilation inhomogeneity in children and teenagers with asthma. Importantly, the use of LCI enabled the detection of abnormalities in lung function that were not detected through the use of traditional spirometry measures, even in cases of mild or well-controlled asthma [114].

Nuttall et al. (2019) also provided valuable perceptions regarding the utility of LCI in the assessment of lung function in children with asthma. Their research demonstrated that LCI was a sensitive tool that could be used to identify subtle abnormalities in the children's lung function that did not show up in the spirometry results. This is a particularly significant result for cases in which asthma affects primarily the peripheral airways, for which conventional spirometry often does not provide adequate assessment [112].

In the study by *Svenningsen et al. (2016),* the relationship was explored between LCI and asthma control in adult asthmatics [115]. They demonstrated that higher LCI values were strongly associated with poorly controlled or uncontrolled asthma, which was characterised by frequent symptoms and exacerbations [115]. *Farah et al. (2012)* studied the relationship between LCI and levels of asthma control, particularly in regard to ICS dose titration in adults with asthma [116]. They demonstrated that LCI was a significant predictor of the level of asthma control after ICS dose adjustments. The study found that patients with higher baseline LCI values (greater ventilation inhomogeneity) were less likely to achieve well-controlled asthma even after they increased their ICS doses [116]. Their findings suggest that LCI can be used to identify underlying ventilation inhomogeneities that contribute to poor asthma control and that may not be detected through the use of standard lung function tests such as spirometry.

2.5.2.2.2 S_{cond} and S_{acin}: Advanced Indices of Ventilation Inhomogeneity

The MBW test can be used to generate indices other than LCI that provide more detailed information about the location and nature of ventilation inhomogeneities. Two such indices are the conductive airways ventilation inhomogeneity index (S_{cond}) and the acinar airways ventilation inhomogeneity index (S_{acin}), both of which are derived from the slope of the phase III portion of the nitrogen washout curve. The phase III slope represents the relationship between the concentration of the tracer gas and the volume of air that is exhaled during the washout phase [12, 112, 113].

S_{cond} reflects ventilation inhomogeneity in the conducting airways, which include the larger airways such as the bronchi and bronchioles. S_{cond} is calculated from the normalised slope of the nitrogen phase III curve over multiple breaths during the washout phase. A steeper slope indicates greater inhomogeneity in the conductive airways. S_{cond} is particularly sensitive to early changes in the larger airways, such as those that are caused by mucus obstruction or bronchoconstriction [12, 112, 113].

S_{acin} reflects ventilation inhomogeneity in the peripheral or acinar airways, which include the alveolar ducts and alveoli. S_{acin} is calculated from the initial portion of the phase III slope after the first breath of the washout phase. It provides information regarding the distribution of ventilation within the small airways and alveolar regions [12, 112, 113]. *Gonem et al. (2015)* conducted a comprehensive study that involved 37 patients with asthma and 17 age-matched healthy control subjects [117]. Their cohort underwent a range of assessments, including spirometry, body plethysmography, MBW with the tracer gas SF_6, and hyperpolarised ^{3}He diffusion MRI. Their study offers significant perceptions of the role of the acinar regions in asthmatic patients, which is a relatively underexplored area in asthma research. They leveraged both MBW and advanced imaging techniques to investigate the structural and functional changes that occurred in the acinar airways, with a particular focus on ventilation heterogeneity as measured by S_{acin}. The study's findings revealed that higher S_{acin} values were strongly associated with more severe asthma, as indicated by the observation that nearly all patients with elevated S_{acin} indices required GINA Step 4 or 5 asthma treatment. Moreover, the study found that the apparent diffusion coefficient of ^{3}He after one second was significantly higher in patients with elevated S_{acin} indices, which suggested that these patients had more pronounced structural alterations in the acinar airways compared with those with lower values of S_{acin} [117].

The MBW ventilation inhomogeneity indices LCI, S_{cond} and S_{acin} are highly valuable in

clinical settings, particularly for the early detection and monitoring of lung diseases. One of the key advantages of LCI is the ability to use it to detect subtle, early changes in lung function before they become apparent during the use of spirometry. This is particularly important in diseases such as CF, in which early intervention can significantly improve patient outcomes. LCI is non-invasive and can be used across a wide age range, so it is particularly useful in paediatric populations, including very young children. Additionally, LCI is repeatable and can be performed without the need for forced breathing manoeuvres, which can be challenging for young children or severely ill patients [13, 14, 118].

Despite its advantages, LCI has limitations. One of the main challenges is the technical complexity of the MBW test, which requires careful equipment calibration and strict adherence to standardised protocols [21]. The accuracy of LCI can be affected by factors beyond the intrinsic properties of the lung, and this problem complicates its interpretation and reliability. For instance, the solubility of the tracer gas in the blood and the dead space of the measurement apparatus can impact the accuracy of the LCI readings. Additionally, the patient's breathing pattern plays a crucial role. Deep, slow breaths can reduce the fraction of each tidal volume that is dedicated to ventilating the dead space, and this leads to variations in the LCI measurements [22, 119].

Another challenge arises from the variability in EEV in spontaneously breathing patients. Since LCI calculations often rely on the single EEV immediately preceding the washout phase, any breath-to-breath variation in EEV can introduce significant variability into the LCI results. This variability is particularly problematic in awake patients, in whom EEV can fluctuate considerably from one breath to the next. To mitigate these issues, a practical approach often employed is to repeat the LCI test multiple times and to accept a result only when two of the values fall within a certain percentage of each other. Although the use of this method can improve the consistency of the results, it also increases the complexity and duration

of the testing process, and this may limit the feasibility of LCI as a routine clinical tool [12, 14, 118]. Moreover, the variability in software algorithms and equipment settings that are used to analyse MBW data can lead to inconsistencies in LCI results across different centres [19, 20]. This variability makes it difficult to compare LCI values between studies or to establish universal reference ranges for LCI and related indices such as S_{cond} and S_{acin}. Another limitation is that LCI, while sensitive to ventilation inhomogeneity, does not provide specific information about the underlying pathology. For example, a high LCI value may indicate a range of conditions from small airway disease (SAD) to more severe structural changes, without differentiating between them [14].

2.5.3 Positron emission tomography (PET)

Positron emission tomography (PET) was introduced to clinical medicine in the mid-1960s, and it has gained significant popularity in research related to PE [120]. In this method of lung analysis, a radiotracer, such as the radioisotope nitrogen-13 ($^{13}N_2$), is introduced through either intravenous injection or inhalation into the lungs. A PET scanner then maps the regional radiotracer activity to estimate lung ventilation, perfusion, or ventilation-perfusion distributions [120-123]. *Ament et al. (2013)* explored the use of PET imaging in lung $\dot{V}/\dot{Q}$ studies that used gallium-68 (^{68}Ga) aerosol (galligas) and ^{68}Ga-labelled macro-aggregated albumin (MAA). This method enables the simultaneous visualisation of ventilation and perfusion, and therefore offers a clearer picture of regional lung function and the possible detection of mismatches between the two. The ability to assess these factors is particularly useful in diseases such as PE, COPD and other conditions in which $\dot{V}/\dot{Q}$ mismatch plays a crucial role [120]. It is reported that PET offers high accuracy and a potential radiation reduction of almost 50% [121]. Figure 2.12 illustrates PET lung ventilation and perfusion imaging through the use of a ^{68}Ga aerosol and ^{68}Ga-labelled MAA in a 70-year-old female with

a PE [120]. The images show inhomogeneous nuclide accumulation, with hypoperfusion in the right lower lobe and preserved ventilation in the same region, all of which indicates a $\dot{V}/\dot{Q}$ mismatch that is consistent with PE [120].

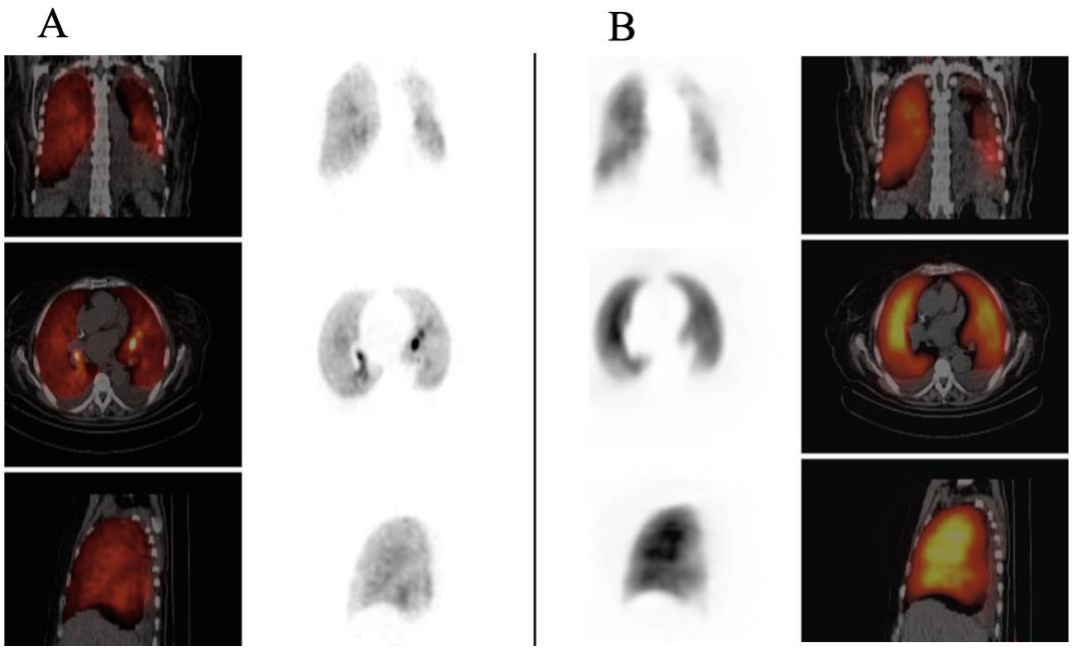


Figure 2.12. PET lung ventilation and perfusion imaging through the use of a ^{68}Ga aerosol and ^{68}Ga-labelled MAA in a 70-year-old female A)-ventilation and B)-perfusion images show hypoperfusion in the right lower lobe and preserved ventilation in the same region, which indicate a $\dot{V}/\dot{Q}$ mismatch defect that is consistent with PE [120].

2.5.4 Hyperpolarised gas MRI

In standard MR images of the lungs, the air spaces are not clearly visible because they contain low numbers of protons, and the clarity of each image is affected by the surrounding lung tissue. However, this limitation can be overcome through the incorporation of a blend of inhaled, hyperpolarised, noble gases such as ^{3}He or xenon-129 (^{129}Xe) during the MRI examination. These hyperpolarised gases possess stronger magnetic characteristics than the water in the surrounding tissue, and this effect enables improved differentiation in the images between the airways and lung tissue. This enhancement improves the signal that is shown by the lung air space [124-126].

Hyperpolarised gas MRI is a valuable method by which lung conditions can be evaluated through analysis of the intensity of signals from the gases within the lung tissue during a short breath hold. The patient inhales a mixture of hyperpolarised gases such as ^{3}He or ^{129}Xe. This technique provides two crucial measurements of lung function: the percentage of ventilated volume, which identifies ventilation abnormalities that are linked to bronchoconstriction or inflammation; and the apparent diffusion coefficient, which serves as an indicator of tissue damage, as seen in emphysema cases [126]. The use of ^{129}Xe is advantageous because the gas dissolves in lung tissue and blood, so detailed assessments of gas exchange are enabled [126].

Hyperpolarised ^{3}He MRI has demonstrated its sensitivity and potential in the measurement of ventilation heterogeneity, as well as in the monitoring of the response to therapeutic interventions in individuals with asthma [127, 128]. Recent investigations that utilised hyperpolarised ^{129}Xe MRI revealed definitive gas transfer impairment within the lungs of non-hospitalised dyspnoeic people with post-COVID-19 conditions whose CT scan results showed no such issues [88]. This highlights the potential of hyperpolarised gas MRI to detect initial signs of lung abnormalities that might go unnoticed during use of traditional imaging methods.

Altes et al. (2001) provided preliminary findings on the use of hyperpolarised ^{3}He MRI to show lung ventilation in asthmatic patients [127]. The study found that this technique was effective in the detection of ventilation defects in these patients and offered a detailed understanding of the heterogeneous nature of asthma [127]. *Aysola et al. (2010)* reinforced these findings as they used both CT and hyperpolarised ^{3}He MRI to demonstrate the heterogeneous distribution of asthma in the lungs [128]. Their study showed that asthma affects lung regions unevenly, and that hyperpolarised gas MRI could highlight these differences more effectively than traditional imaging methods. By combining hyperpolarised gas MRI with CT,

the researchers provided a more comprehensive picture of lung function and structure than would have been possible through one technique alone, and they stated that this method could be used to guide more targeted interventions for asthma patients [128].

Fain et al. (2007) explored the broad applications of hyperpolarised gas MRI, particularly with ^{3}He and ^{129}Xe, to image functional lungs [125]. They demonstrated the sensitivity of hyperpolarised gas MRI to detect early-stage lung diseases (asthma, CF and COPD) and abnormalities in lung ventilation, even when other conventional modalities, such as CT scans or spirometry, show normal results [125]. Most recently, *Grist et al. (2022)* explored the utility of hyperpolarised ^{129}Xe MRI in the detection of lung abnormalities in patients with long COVID [88]. The study found that through the use of hyperpolarised ^{129}Xe MRI, researchers were able to detect ventilation and gas exchange impairments in patients with long COVID, even when their CTs appeared normal [88].

Figure 2.13 presents ^{129}Xe MRI 3D renderings that visualise ventilation patterns in study participants with post-COVID-19 conditions who had or had not been hospitalised during acute COVID-19 infections. The images show subtle yet heterogeneous ventilation defects. These abnormalities were more pronounced in post-hospitalised participants (Figure 2.13.B) compared with those who had not been hospitalised (Figure 2.13.A) [88].

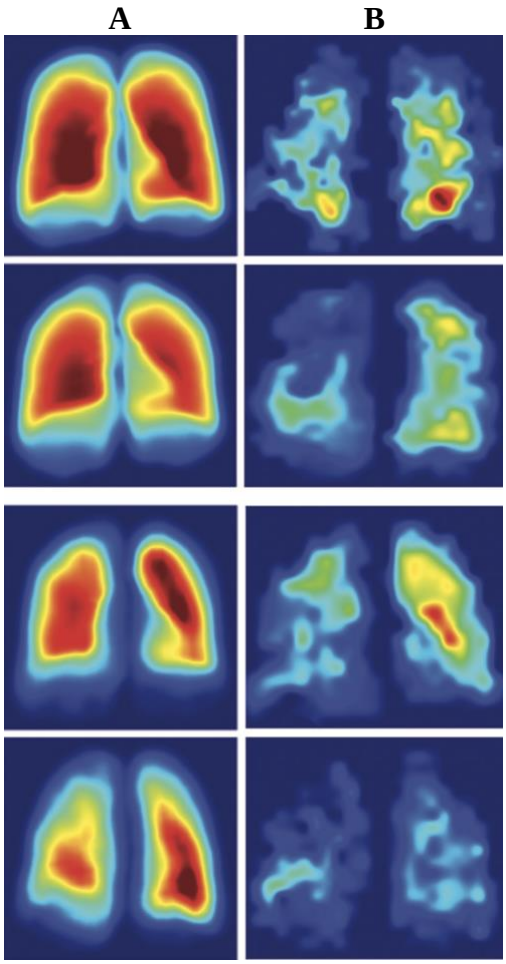


Figure 2.13. 3D ^{129}Xe MRI of the lungs of non-hospitalised **(A)** and post-hospitalised **(B)** study participants with post-COVID-19 conditions [88].

Although hyperpolarised gas MRI has revolutionised the field of respiratory medicine as its use has provided details regarding lung ventilation, perfusion and gas exchange, several limitations hinder its widespread clinical application. One of the key limitations is the availability and cost of hyperpolarised gases, particularly ^{3}He. *Ebner et al. (2017)* noted that the limited supply of ^{3}He had led to high costs, which meant its routine clinical use was less feasible than it had been previously [124]. Additionally, ^{129}Xe is not readily available in certain regions [124]. The specialist equipment that is required for gas polarisation and MRI scanning adds to the overall cost so that it is not accessible to many healthcare facilities [124, 125]. The complexity of the imaging procedure itself is a major limitation to the use of the technique, as those who apply it require specialised expertise in both MRI technology and respiratory

physiology. Also, the need for patient cooperation and carefully achieved breath-hold sequences make it difficult to apply in populations such as young children, the elderly, or those with severe respiratory conditions who may struggle with breath control [125]. In terms of technical limitations, hyperpolarised gas MRI provides excellent spatial resolution by which ventilation defects can be imaged, but it is not as effective for the visualisation of structural lung abnormalities, such as airway remodelling or fibrosis, when compared with traditional CT [127, 128].

2.6 Summary: Advantages and disadvantages of current techniques used for measuring pulmonary functions and inhomogeneities

In the preceding sections of this chapter, I have explored various techniques that are used to measure lung function and inhomogeneity and have introduced the supporting literature that discusses their advantages and limitations when used to investigate respiratory disease. Table 2.1 provides a summary of most of these techniques and lists their respective advantages and limitations. Each method that is currently used to assess pulmonary function and to detect ventilation inhomogeneities has its strengths and weaknesses.

The diverse methods that have been explored in this section highlight the potential advantages of the study of lung inhomogeneity and the value of the ongoing pursuit of a practical and widely applicable approach to its quantification. Unfortunately, none of the methods that have been explained in this section has been adopted widely for various reasons, such as complexity and cost. Among the presented techniques, N_2 washout stands out as a relatively straightforward, non-invasive method. In Chapter 3 of this thesis, a new technical advance in the measurement and analysis of N_2 washout data is discussed. This method may provide a more accessible way to assess lung inhomogeneity.

Table 2.1. Advantages and disadvantages of current techniques that are used to measure pulmonary function and inhomogeneity.

Technique	Advantages	Limitations
Spirometry	• Widely recognised. • Established standardised criteria. • Is relatively reproducible. • Sensitive measure of bronchodilator responsiveness.	• Effort- and technique-dependent. • Lacks sensitivity to detect early-stage and small airway dysfunction. • Bronchodilator reversibility testing has limited sensitivity for asthma diagnosis.
Oscillometry	• Simple to perform and does not require any coordination or breathing manoeuvres. • Sensitive to airway hyper-responsiveness. • Sensitive measure of bronchodilator responsiveness.	• No standardised reference range. • Interpretation of the results is complex. • Does not differentiate between obstructive and restrictive respiratory disorders. • Can be affected by artefacts, such as swallowing or upper-airway interference.
LCI	• Valuable in the detection of ventilation inhomogeneity in diseases such as CF and early-stage lung disease. • Fairly simple for patients to perform.	• Technically complex. • Requires specialist equipment and expertise. • Procedural burdens such as the need for washouts to be performed in triplicate to ensure reliability.
Hyperpolarised gas MRI	• Provides unique insights into ventilation, perfusion and gas exchange at the alveolar level. • Highly sensitive. • Can be used to detect subtle ventilation defects.	• High cost. • Limited availability of hyperpolarised gases. • Need for specialist equipment and expertise.

LCI, lung clearance index; MRI, magnetic resonance imaging.

Chapter 3. Novel measure of lung inhomogeneity

In this chapter, I build on the discussion of available techniques for the measurement of lung function and inhomogeneity, which was included in the previous chapter, with the introduction and exploration of computed cardiopulmonography (CCP) as a way to assess lung inhomogeneity. The assessment of lung inhomogeneity employed in the work performed for this thesis was established based on the development of a molecular flow sensor (MFS) [129] and of a computational model of an inhomogeneous lung with a set of parameters that were derived from the fitting of non-invasive MFS data [104].

This technique formed the basis for the experimental work that is explained in subsequent chapters: Chapter 5 (healthy control cohort), Chapter 6 (asthma cohort) and Chapter 7 (post-COVID-19 infection cohort). In all three cohorts, the same methodology and breathing test protocol were applied, so as to ensure consistency in the assessment across different groups. Additionally, a comparison was made between existing MBW systems with the CCP to highlight the strengths and limitations of both approaches in the assessment of lung function and inhomogeneity.

3.1 Existing methodology

Gas analysis in breath diagnostic tests commonly employs mass spectrometry and non-dispersive infrared sensors. Breath is analysed through the use of side- or main-stream (in-line) methods. In side-stream systems, a portion of breath is sampled from the primary gas flow and is analysed remotely. In contrast, in main-stream devices, the sensor is placed directly in the gas flow path. Side-stream sensors are robust and sensitive, but the need to transport the gas

means that there is a time delay between the measured breath and the analysis. Mixing of samples, changes in water vapour pressure and pressure drops along the sampling tube can affect accuracy. Different pressure, temperature and humidity at the sensor compared with those of the body (or even the primary gas flow) can lead to incorrect measurements. Moreover, it is difficult to obtain accurate flux measurements through the use of side-stream analysis, whereas this is not a problem in well-designed main-stream devices [130].

3.1.1.1 Mass spectrometry

Mass spectrometry is widely used in breath concentration analysis. In this technique, the breath sample is ionised, and the ions are separated according to their mass-to-charge ratios. A mass spectrum is produced from which ions can be identified and quantified [131]. Mass spectrometry is useful for detecting trace gases, particularly volatile organic compounds (VOCs), and therefore its use facilitates the detection of exhaled biomarkers of certain diseases [132]. Ions may fragment, but this can be mitigated if proton transfer reaction mass spectrometry or chemical ionisation mass spectrometry is used [133]. Field asymmetric ion mobility spectrometry has also shown potential in the measurement of VOCs. In this method, an electric field is created to separate ionised species based on their mobility rather than their mass [134]. Mass spectrometry is employed exclusively in side-stream gas analysis, due to the necessary alteration of the sample. Aside from the drawbacks that are associated with side-stream analysis, there are challenges with the use of mass spectrometry; these encompass high power consumption, substantial cost, the need for a relatively bulky machine (although the latest versions are more compact), susceptibility to mechanical vibration and shock, and the need for frequent recalibration of the machine [133, 135].

3.1.1.2 Non-dispersive infrared sensors

Non-dispersive infrared (NDIR) sensors utilise infrared lamps and an optical filter to detect gas absorption at specific wavelengths. Concentrations are determined by subtracting thermal background signals, which are calibrated through the use of a mechanical chopper. NDIR sensors are used primarily in side-stream devices due to mechanical part vulnerability [130].

3.1.1.3 Laser absorption spectroscopy

Absorption spectroscopy involves analysis of the attenuation in radiation intensity as the radiation passes through an absorbing medium. The extent of intensity reduction reveals the absolute concentration of the absorber within the sample (expressed as molecules per unit volume) [136]. The light intensity at the optical frequency ν, observed while scanning across an absorption feature, depends on several factors, which include the optical path length within the sample, the absorption probability (represented by the absorption cross-section), and the concentration of absorbing species. These relationships are described by the Beer-Lambert law:

$$I\ (\nu) = I_0(\nu) e^{-\sigma(\nu)[N]l} \qquad \text{(Equation 3.1)}$$

Here, $I(\nu)$ represents the light intensity that is detected through the absorber medium and $I_0(\nu)$ is the incident light intensity. The parameter $\sigma(\nu)$ is the absorption cross-section for a molecular transition at frequency ν, while N indicates the concentration of the absorbing species and l is the path length across the sample.

Although absorption spectroscopy is advantageous because it provides an absolute number of densities, it is somewhat limited in sensitivity due to its reliance on the detection of

a small change in a significant background, which can be influenced by fluctuations in laser intensity and detector noise [137].

Cavity-enhanced absorption spectroscopy (CEAS) is used to improve the sensitivity of absorption spectroscopy. This increased sensitivity is achieved by effectively elongating the path length within the absorbing medium through the containment of light between two mirrors with high reflectivity, forming an optical cavity. In the case of CEAS, the value of I(ν) is determined by measuring the light transmitted through the exit mirror while the laser wavelength sweeps over an absorption feature. Consequently, the concentration of the absorber can be calculated by a modified version of Equation (3.1):

$$\frac{I_0(\nu) - I(\nu)}{I(\nu)} = \frac{\sigma(\nu)[N]l}{1-R} \qquad \text{(Equation 3.2)}$$

Here, R is the geometric mean of the reflectivity that is attributed to the mirrors of the cavity. It is clear that in CEAS, the term $(1-R)^{-1}$ contributes to an effective elongation of the path length. For instance, when the reflectivity is $R=0.9999$, the enhancement factor is around 10^4.

To obtain an absolute value of the absorber's concentration from Equation 3.2, the value of R must be known, and this can be accomplished by calibrating the system with a gas sample that contains a known concentration of O_2. Typically, multiple scans over the absorption feature are necessary to improve the signal-to-noise ratio [136].

3.2 Computed cardiopulmonography

CCP, which was the method used to assess lung inhomogeneity in the work performed for this thesis, was established based on the development of an MFS [129] and of a computational model of an inhomogeneous lung with a set of parameters that were derived

from the fitting of non-invasive MFS data [104]. The hypothesis behind the development of this novel measure of lung inhomogeneity was that if the data acquired through precise measurements taken with the MFS were combined with the computational model of the lung and body gas stores, an innovative, non-invasive technique for evaluation of lung function through quantification of inhomogeneity could be established. The underlying principle was that sufficient information to achieve this evaluation was encoded within the profiles of gases expired from the lungs during steady air breathing and a subsequent N_2 washout. This information could be exploited to reveal insights into the nature and extent of inhomogeneity within the lung.

3.2.1 Molecular flow sensing device

The MFS was a novel instrument that employed laser absorption spectroscopy to measure respiratory gas concentrations with exceptional sensitivity. This main-stream gas analyser was integrated into a highly precise flow meter, which enabled more accurate measurements of respiratory gas flux than was previously possible. For the purposes of this thesis, a brief overview of the MFS is provided; a comprehensive discussion is offered by *Ciaffoni et al.(2016)* [129].

Participants breathe in and out through a mouthpiece and bacterial filter, which are attached to the device's measurement head, as shown in Figure 3.1. The measurement head is attached to an electronics module via hybrid cables. The device is controlled by a laptop that is connected to the electronics module via a USB cable. During operation, the gathered data are streamed to the laptop, and the use of bespoke analysis software enables real-time reporting of gas concentrations.

The MFS features a highly accurate, in-airway, laser absorption spectrometer as the gas analysis (gas-measuring-cell) component and a very precise flow meter to measure the flow rate (Figure 3.2). The laser absorption spectroscope measures the concentration of O_2, CO_2 and

water vapour every 10ms within the airway. Fast, linear measurements are produced. There is no time delay, and measurements are taken at the same temperature and pressure as those of the airway flow. This enables accurate alignment with measurements of the subject's respiratory flow. The balance gas (assigned as N_2) is calculated by subtraction.

The development of any device that involves human participation should prioritise participant comfort during usage. The size of the MFS measurement cell, known as the "device dead space", must be restricted to prevent the rebreathing of exhaled gas. However, minimisation of the dead space may increase resistance to respiratory flow, and this would affect breathing patterns and mechanics. Addressing these crucial considerations has led to the creation of a compact device that introduces only 50ml of dead space to the airway compared with 80ml formerly [129, 138]. This design maintains relatively low resistance and accommodates a flow axis bore size that is suitable for standard respiratory tubing.

As mentioned above, the MFS is used to measure the respiratory gas concentrations directly in the main airway. Concentrations of CO_2 and water vapour within the measurement cell are determined through the use of direct laser absorption spectroscopy. To determine gas concentrations, the Beer-Lambert law is employed with a known path length and an absorption cross-section that is specific to the absorption feature of interest. A dual-pass configuration is employed to extend the path length while the dead space is kept to a minimum (shown in Figure 3.2.B, in yellow).

Simultaneously, the O_2 concentration is assessed through the use of the CEAS technique (see section 3.1.1.3). Since the absorption cross-section of O_2 is considerably smaller (two to three orders of magnitude) than that of CO_2 or water vapour, the optical cavity is introduced to amplify the effective path length and thus achieve the required sensitivity [129]. The effective enhancement of the path length is calculated by passing pure (N5 grade) O_2 through the cavity to establish a known concentration. Measurements of total pressure and gas

temperature are conducted within the device, facilitating the application of the ideal gas law to calculate the total gas concentration of all molecular species. By subtracting the calculated concentrations of O_2, CO_2, and water vapour from the overall gas concentration, the N_2 concentration (including argon in air) is determined (Figure 3.3) [129].

The flow sensor consists of a custom-made pneumotachograph that is formed of two meshes that enclose the lasers' optical paths within the gas. The error in the gas flow measurement is <0.2%. This error is much better than that of a normal pneumotachograph. It is achievable because the flow measurement takes into consideration the gas temperature (temperature probe), pressure (pressure port) and composition, all of which are measured every 10ms and are included in the flow calculation. The measurements of temperature, pressure and gas composition enable the calculations of gas density and viscosity within the measurement cell. This enables the accurate calculation of flow and cumulative volume [129]. By combining the converted laser spectra (gas fractions) with accurate flow measurements, real-time molar flux data are obtained (Figure 3.3). These indicate the number of molecules of each gas that are inhaled and exhaled.

As this technology offers highly accurate flow measurements and accurate readings of O_2, CO_2 and water vapour concentrations, it holds great promise to improve the monitoring of gas exchange in various clinical settings. It has been piloted and proved to be well-tolerated by various groups of participants [119, 129, 139, 140].

Non-invasive respiratory gas exchange measurement is a valuable tool by which to gain physiological insights. Over a century ago, gas exchange was measured through the collection of expired gas in Douglas bags; these experiments provided estimates of lung function and capacity over long periods [141]. Modern instruments can be used to measure the respiratory gas flows of specific gases over short intervals with high accuracy under stable conditions [142]. Nevertheless, it is a challenge to track accurately the dynamic changes in gas

composition and flow on a breath-to-breath basis, due to delays that are caused by the sampling catheter [130, 142]. The measurement of O_2 is particularly sensitive to these delays, given the low net exchange of this gas during each breath. Even small temporal errors can result in significant inaccuracies in measurements of pulmonary gas exchange [143]. The unstable nature of the environment of respiratory gases, which includes variations in temperature, pressure, amounts of water vapour, density and viscosity, further complicates the achievement of accurate measurements. Many commercial devices are not made to take into account these dynamic factors, and none can be used currently to measure rapidly changing water vapour content during the respiratory cycle. The MFS, first described by *Ciaffoni et al.* (2016) [129], was designed specifically to address these challenges. This innovative in-airway device serves as a prototype that enables the measurement of gas composition at high resolution at 10ms intervals. This enhanced resolution results from improvements in both flow and composition estimation, marking a significant advance compared with readings obtained from existing, commercial, side-stream gas analysers.

The most notable enhancement in the gas exchange measurements is attributable to the use of spectroscopy. An independent laser is employed for the analysis of each gas species in the primary gas stream. This approach ensures precise temporal alignment between gas composition measurements and respiratory flow measurements. The MFS can be used to measure O_2, water and CO_2 flux, and to measure additional tracer gases such as acetylene and methane [129, 138].



Figure 3.1. A healthy participant breathes through a mouthpiece and a heat-moisture exchanger attached directly to the MFS.

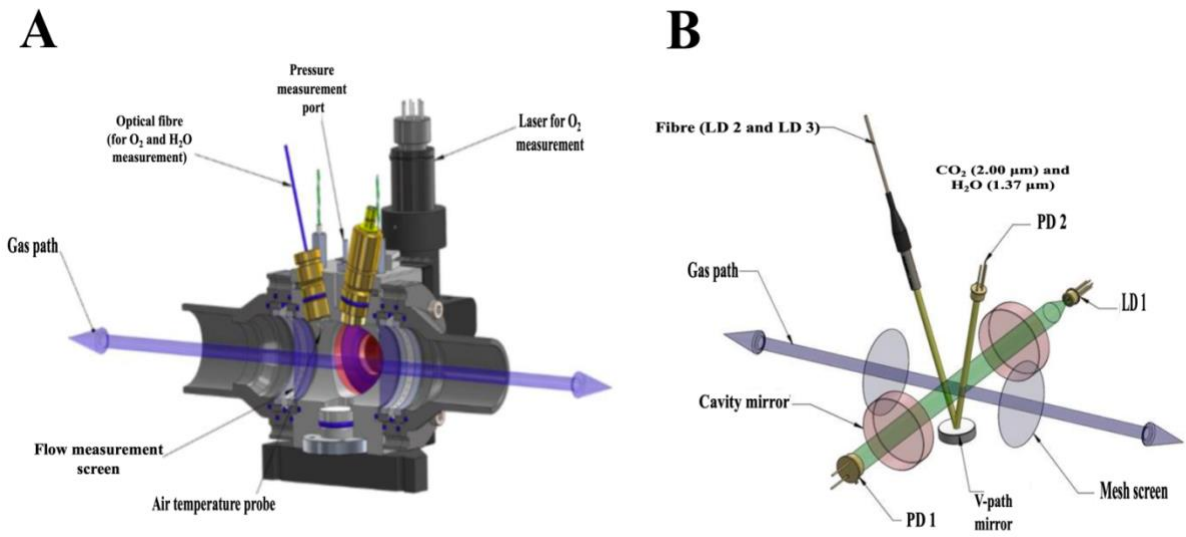


Figure 3.2A. The cell assembly of an MFS. The concentrations of O_2, CO_2 and water vapour are measured within the cell through the use of laser absorption spectroscopy, with different optical wavelengths tuned to each specific absorption line for each gas. The concentration of N_2 is not measured directly as it can be calculated from the other measurements. **B.** A simplified schematic of the device set-up. It shows the multichannel absorption spectrometer and a pneumotachograph within the measurement cell. The pressure drops are measured across two mesh screens (shown in grey) along the two-way gas path (shown in blue). For O_2 probing, radiation is introduced into an optical cavity that is formed by reflective mirrors (shown in red) and detected through the use of a photodiode (PD 1), which is positioned along the optical axis (shown in green). Radiation that probes the CO_2 and water vapour is directed into the V path (yellow), reflected by a concave mirror and captured by the photodiode PD 2 [138]

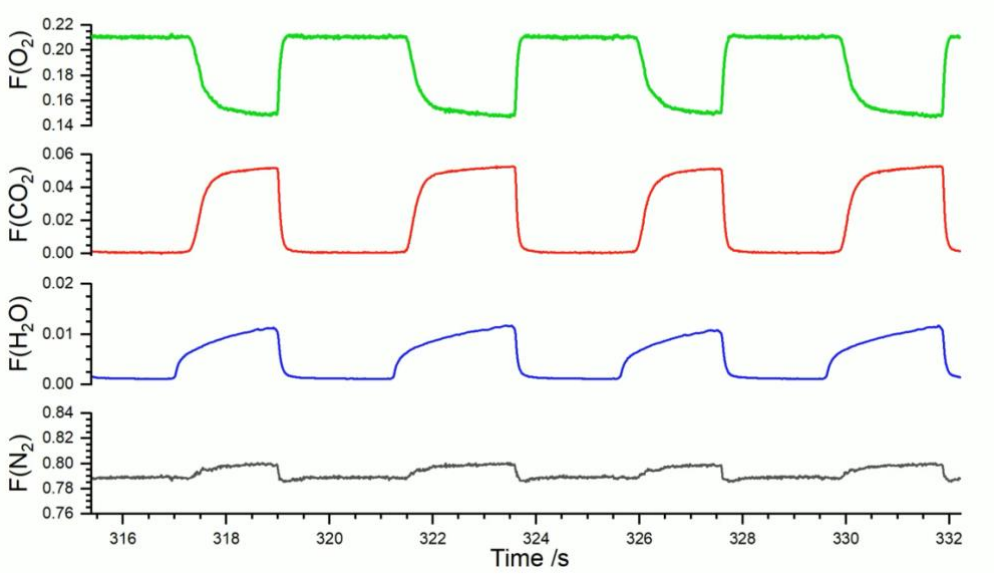


Figure 3.3. MFS measurements of gas fractions during the breathing test. The laser spectra are translated into gas fractions. The changes from inspiration, when the O_2 level is high and the levels of the other gases are low, to expiration, when the opposite is the case, are clearly visible. The fraction of oxygen **($F(O_2)$)** is shown in green, the fraction of CO_2 **($F(CO_2)$)** in red, the fraction of water vapour **($F(H_2O)$)** in blue, and the fraction of N_2 **($F(N_2)$)** in black.

3.2.2 Computational model

The computational model used in this project was formed by combining three existing models. The first was a lung model designed to simulate lung inhomogeneity known as the log-normal lung. The second was a model of blood CO_2 and O_2 dissociation curves that includes physiological effects such as Bohr and Haldane effects. The third model was focused on the circulatory system and the body's gas storage.

3.2.2.1 LNL

In an ideal lung, each unit volume receives an equal amount of air (ventilation) and blood flow (perfusion). Lung inhomogeneity is the term usually used to describe a discrepancy between ventilation and perfusion or between ventilation and alveolar volume. Healthy lungs naturally exhibit some level of inhomogeneity that stems from inherent variations in the regional distribution of ventilation and blood perfusion across the respiratory system [144]. The LNL model is designed to mirror underlying lung physiology. *Mountain et al.* (2018)

described the LNL model of gas exchange inhomogeneity, which took into consideration three important physiological aspects that represented lung inhomogeneity. These were: standardised compliance, which signifies the distribution of lung expansion capacity during ventilation; standardised conductance, which represents the distribution of perfusion across the lungs; and standardised dead space, which is a measure of the distribution of conducting airways in relation to gas-exchanging units [104]. Alongside these inhomogeneities, the model estimated lung alveolar and anatomical dead-space volumes [104, 145].

The lung of the LNL model consists of multiple alveolar compartments. It is assumed that all gas exchange occurs within the lung in the alveolar compartments. Each alveolar compartment is ventilated via a personal dead-space volume (VD_P), which represents the airway volume in which gas is not exchanged. This dead space reduces the amount of fresh gas that reaches the compartment during inspiration. These individual dead-space compartments are ventilated and connected via a shared dead-space compartment (VD_C). The VD_C represents the known dead-space volume that is introduced by the measurement apparatus (the MFS, the mouthpiece and the bacterial filter). The total volume of the alveolar compartments at FRC, which is equivalent to the lung volume (V_A), and the volume of the personal dead-space compartments (VD_P) are parameters that must be determined for each participant. Initial estimates for these model parameters are made according to each person's height and sex (Figure 3.4) [104].

Consequently, in order to represent inhomogeneity, the LNL model assumes a lung of total alveolar volume ($V_{A\,tot}$) that is constructed from 125 lung units. Each lung unit has the same resting and fractional alveolar volumes (FV_A) at FRC but differs in the fractional share (F_{CL}) of the total lung compliance (CL_{tot}), the fractional share (F_{Cd}) of total vascular conductance of the lung (Cd_{tot}), which is the fraction of total blood flow that a compartment receives (the perfusion), and the fractional share (FV_D) of the total dead space (VD_{tot}). These

three properties (F_{CL}, F_{Cd} and FV_D) are distributed unequally throughout the lung. They represent the underlying respiratory physiology. The widths of these distributions define the efficiency of the lung and constitute our model's parameter set. In this way, measures of pulmonary inhomogeneity take into consideration the inhomogeneities that are shown in real physiological properties of the lung. Total ventilation and perfusion can then be introduced into the model [104].

To simplify the model, each fractional share is not treated as a separate parameter. Instead, it is assumed that the dead space has a continuous normal distribution and that both the fractional compliance and perfusion are described by a bivariate log-normal distribution. This distribution is defined by three parameters that are estimated for each participant: (i) σlnC_L, which tells us the width of the compliance distribution; (ii) σlnC_d, which tells us the width of the perfusion distribution; and (iii) ρ, which shows how compliance and perfusion distributions are correlated. Employment of this method means that the model estimates the variance in these parameters, rather than calculates the individual values for each compartment [145].

The model is aligned with the collected data through a process that adheres to the principle of mass balance, in which O_2 consumption and CO_2 production in the tissue compartments drive the model. The model's cardiac output, which supplies venous blood to the lungs (described briefly in upcoming section 3.1.3), is largely influenced by metabolism. The model employs MFS-measured gas composition throughout inspiration and simulates the gas composition during expiration. Parameter estimation involves the adjustment of model parameters to match the simulated expired gas fractions with the MFS-recorded values. Prior to simulation (in which the model is aligned with the collected data), the 125-compartment model lung is built based on specified parameters (described above), which include end-expiratory alveolar volume, dead-space volume, the widths of the standardised compliance and

conductance distributions and the width of the fractional dead-space distribution. Parameter sources may be direct measurements from patients, data from the literature, or those that are fitted to the individual, in which patient-individualised data for height, weight, age and sex are used to calculate the sizes of the body's gas stores (section 3.1.3). For certain parameters such as blood haemoglobin and ion concentrations, literature values are employed [145].

The original LNL model relied on nine parameters, which were described in detail elsewhere [104, 145]. They were: the total alveolar volume when the lungs are at FRC (V_A); the CO_2 equivalent tissue volume (V_t); cardiac output (Q_T); the width of the compliance distribution (σ_x); the width of the perfusion distribution (σ_y); the correlation of compliance and perfusion (ρ); the apparatus dead-space volume (V_{DC}); the total personal dead-space volume (V_{DP}); and the width of the dead-space distribution (σ_z) [145].

In the current model, five of these parameters are related to lung characteristics. These parameters (using updated notation) are:

- VD (V_{DC}), which represents the dead-space volume at FRC (at end-expiration);
- CDS, which represents the fractional expansion of dead space relative to the fractional expansion of alveolar space (and used to be called δsVD [139]);
- VA, which is the alveolar volume at FRC;
- σVD (σ_z), which describes the standard deviation (SD) of the normal distribution for (normalised) dead space across lung volume. It essentially informs us about the variability in the length of the dead space relative to the lung unit, and serves as the SD of the length of those pipes; and
- σlnCL (σ_x), which is the SD of log-normal distributions for (normalised) alveolar compliance. This parameter serves as an indicator of the variability in lung inflation and deflation throughout the breathing cycle. It is an intrinsic marker of ventilation inhomogeneity.

In this thesis, I chose to work with two volumes which were functions of the model parameters, as volumes that would be most familiar to physiologists and clinicians. They were:

- V_{DI}, which is the end-inspiratory dead space (C_{DS} is used to calculate V_{DI} from V_D). It was preferable in this study because it is the inspired volume that does not take part in gas exchange, and it corresponds with the Fowler dead space [146]; and
- FRC (V_A+V_D). It was preferable to work with FRC because it is a well-recognised lung volume and can be converted to FRC % predicted through the application of a standard formula, if desired.

In general, in the following chapters, but with exceptions, the four variables that are used are V_D (now used to refer to end-inspiratory dead space), FRC, σV_D and $\sigma \ln C_L$ (Table 3.1).

Table 3.1. Lung inhomogeneity parameters discussed in this thesis

FRC / l (BTPS)	Functional residual capacity
V_D / l (BTPS)	Dead space at end-inspiration
σV_D	The SD of the normal distribution for (normalised) dead space across lung volume
$\sigma \ln C_L$	The SD of log-normal distributions for (normalised) alveolar compliance

BTPS, body temperature (37°C), ambient pressure and gas saturated with water vapour.

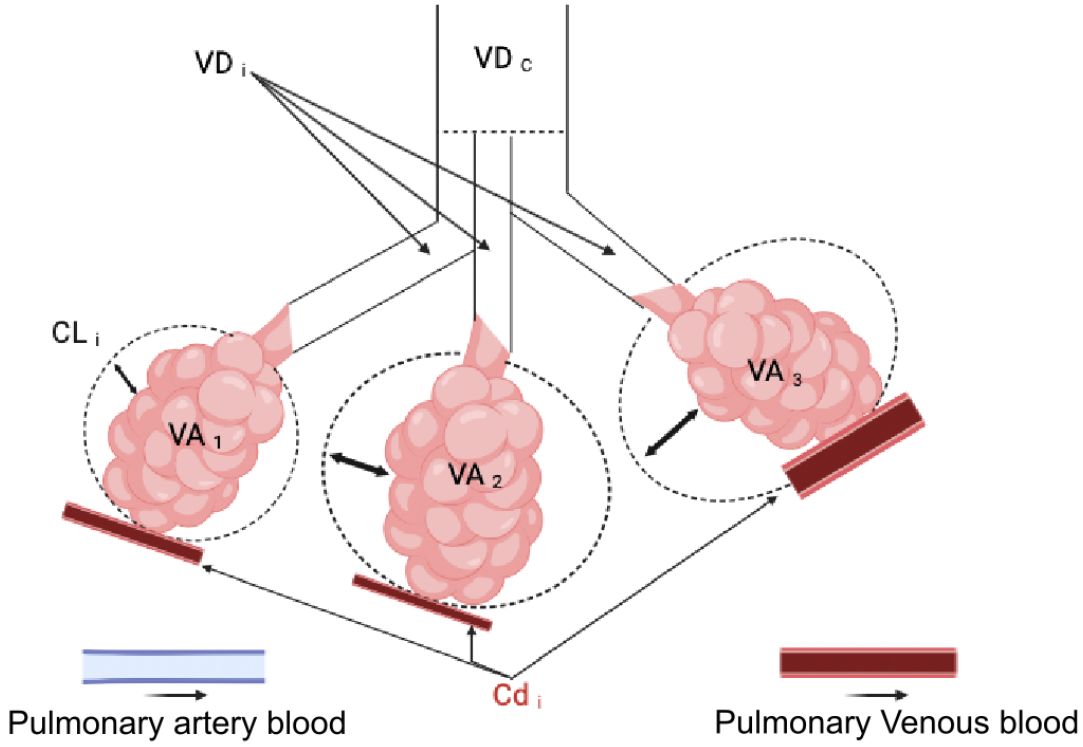


Figure 3.4. A diagram of the LNL model. Three simplified lung sections are shown, each with a share of total perfusion (Cd_i), dead space (VD_i) and compliance (CL_i), while they have the same volume at FRC (VA_i). VD_C represents the common dead space introduced by the device (MFS), VA_i stands for mixed alveolar compartments, and VD_i refers to their connected personal dead-space compartments. Only the alveolar compartments support gas exchange, and the gas within each compartment is assumed to be completely mixed. This figure was developed using BioRender and Inkscape programmes.

3.2.2.2 Model of blood CO_2 and O_2 dissociation curves

As mentioned earlier in this chapter, one of the three models that was employed in the CCP measurement was a physicochemical representation of blood, as described by *O'Neill et al. (2017)* [147]. This model effectively generates dissociation curves for CO_2 and O_2, with consideration of the Bohr and Haldane effects [147].

This blood CO_2 and O_2 model demonstrates that, with current knowledge of blood's major components, it is possible to predict accurately the CO_2-carrying properties of whole blood. This has been achieved through the creation of a detailed mechanistic model that considers chemical equilibria in both plasma and red blood cells, and the exchange of permeant

species across cell membranes, based on physicochemical principles. The use of this model enables the exploration of the carriage of CO_2 through the body in ways not possible with simpler models [147].

This model introduces a physicochemical framework for the transportation of CO_2 by blood, coupled with an accepted phenomenological model for O_2 transportation. The core of the model revolves around the interaction of protons and CO_2 with different blood components, as well as anionic exchange across the membranes of red blood cells. The model provides an accurate prediction of blood-borne CO_2 transportation in a general sense, illustrating the Haldane effect.

3.2.2.3 Model of circulatory and body gas stores

To represent human physiology as accurately as possible, a model of the circulation and body gas stores (CBGS) has also been developed. The purpose of this model is to simulate accurately the pulmonary arterial blood that flows to the LNL model (Figure 3.5). The CBGS model is designed to be comprehensive and grounded in anatomy and physiology. It includes circulatory delays and gas storage and can be applied to both respiratory and other tissue-soluble gases. Beyond this work, *Magor-Elliott et al. (2021)* aimed to develop a scalable model that could accommodate individuals of different sizes and body compositions [148]. The CBGS model incorporates independent body compartments, each of which is connected to the lung through parallel circulatory pathways. The liver and gastrointestinal tract are exceptions, as the model instead includes the portal system's anatomy [148].

The model compartments for a standard male (1.8m tall, of 70kg mass, and 25 years old) are derived from data gathered by the International Commission for Radiological Protection (ICRP) [149, 150]. The organ and relative weights are obtained from the ICRP as summarised in *Brown et al.'s (1997)* review [151]. In this model, smaller organs such as the adrenals, pancreas and thyroid are condensed into a "rest of body" compartment. This

simplification results in the use of 11 compartments (Figure 3.5), as described by *Magor-Elliott et al. (2021)* [148]. Volumes for each compartment are calculated based on mass divided by tissue density. Values of perfusion and blood volume come from ICRP recommendations and other references. The systemic capillary volume accounts for 5% of the total blood volume and is distributed based on relative perfusion. Additional blood volumes in large arteries and veins outside organs are incorporated. In the model, compartments are categorised as discrete tissues (e.g., heart and lungs) or dispersed tissues (e.g., muscle or skin). Blood flows to compartments are apportioned, and venous blood volume is allocated according to arterial blood volume. The model includes metabolic rates for tissues [148].

The model for the body gas stores, as described by *Magor-Elliott et al. (2021)*, also includes the exchange of inert gases such as N_2 between body tissues and the circulatory system [148]. Body N_2 is stored in different tissues, with significant amounts in adipose tissue due to the high solubility of N_2 in fat. The model accounts for circulatory transport delays and gas stores in various compartments; N_2 exchange is determined according to tissue-specific solubilities. The exchange for inert gases such as N_2 between blood and tissues follows a conservation-of-matter equation, in which the rate of N_2 exchange depends on its rate of perfusion through tissue and its solubility in each tissue compartment. This allows for the dynamic simulation of N_2 washout during the MBW tests [148].

Cardiac output (CO) directly affects the rates of gas exchange, including that of N_2. Increased CO results in faster transport of gases between the lungs and body tissues, and this leads to accelerated equilibration of gases. In the case of impaired CO, as might occur in conditions such as heart failure or after infection with COVID-19, gas transport is slowed, and this prolongs the equilibration of N_2 and could potentially alter the results of tests such as MBW. However, for N_2, there is only around 12.5ml of gas per liter of blood. If the CO were 5 L/min, then the maximum possible release of N_2 from the blood would be 60ml/min. As such,

dissolved N_2 is not likely to be very important in washout studies of short duration. The CBGS model is likely to be more important for the more soluble gases like CO_2 [148].

Figure 3.6, by *Sandhu et al. (2023)*, summarises the process of combining the measured breathing test (through the MFS) with computational models to produce the CCP inhomogeneity parameters [119]. The 125 lung model compartments are treated collectively in terms of blood flow and ventilation, which are distributed according to a bivariate log-normal distribution of standardised vascular resistance and compliance. Before the model is run, the 125-compartment lung must be built through the application of parameters that specify end-expiratory alveolar volume, dead-space volume, and the SDs for lung compliance, vascular resistance and dead space. The size of the gas stores is initialised through adjustment of the tidal volume until the ideal PCO_2 matches the parameter value at the start of the simulation. For this project, patient-specific values such as height, weight, mass, age and sex were used to calculate body gas stores. These characteristics were also used to calculate the initial values for a number of other parameters that were subsequently estimated through the model fitting process. For other parameters, such as haemoglobin and ion concentrations, literature values were used. Ventilation during both inspiration and expiration was generated to match precisely the individual's total respiratory flow, which had been recorded in the use of the MFS during the breathing test. The model used the inspired gas composition as measured during the use of the MFS to calculate gas fractions during expiration. The model parameters were adjusted to ensure that the calculated expired gas fractions closely matched those recorded through the use of the MFS [119].

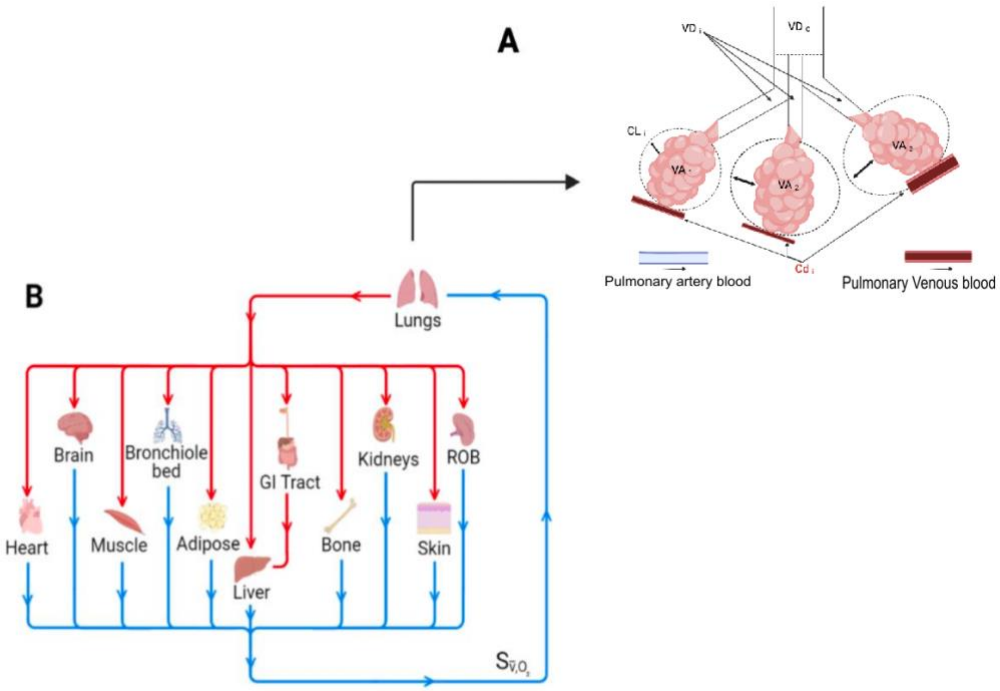


Figure 3.5. A diagram of the CBGS model and its supply of blood flow through the pulmonary arteries to the LNL model. **A.** Simplified lung section of the LNL model. **B.** Graphic representation of the CBGS model showing the 11 compartments. Each compartment represents a distinct tissue or group of tissues with similar properties. Allocation of blood flow and metabolism to each tissue is determined from data in published literature. The model is personalised by scaling it according to an individual's characteristics (height, age, weight, and sex). Arterial blood (shown in red) circulates throughout the body within the circulatory system and engages with the body's gas reservoirs. Subsequently, the venous blood (shown in blue), high in CO_2 and low in O_2, returns to the lungs to undergo the cyclic process once more. GI, gastrointestinal; ROB, rest of body; venous blood SvO_2.

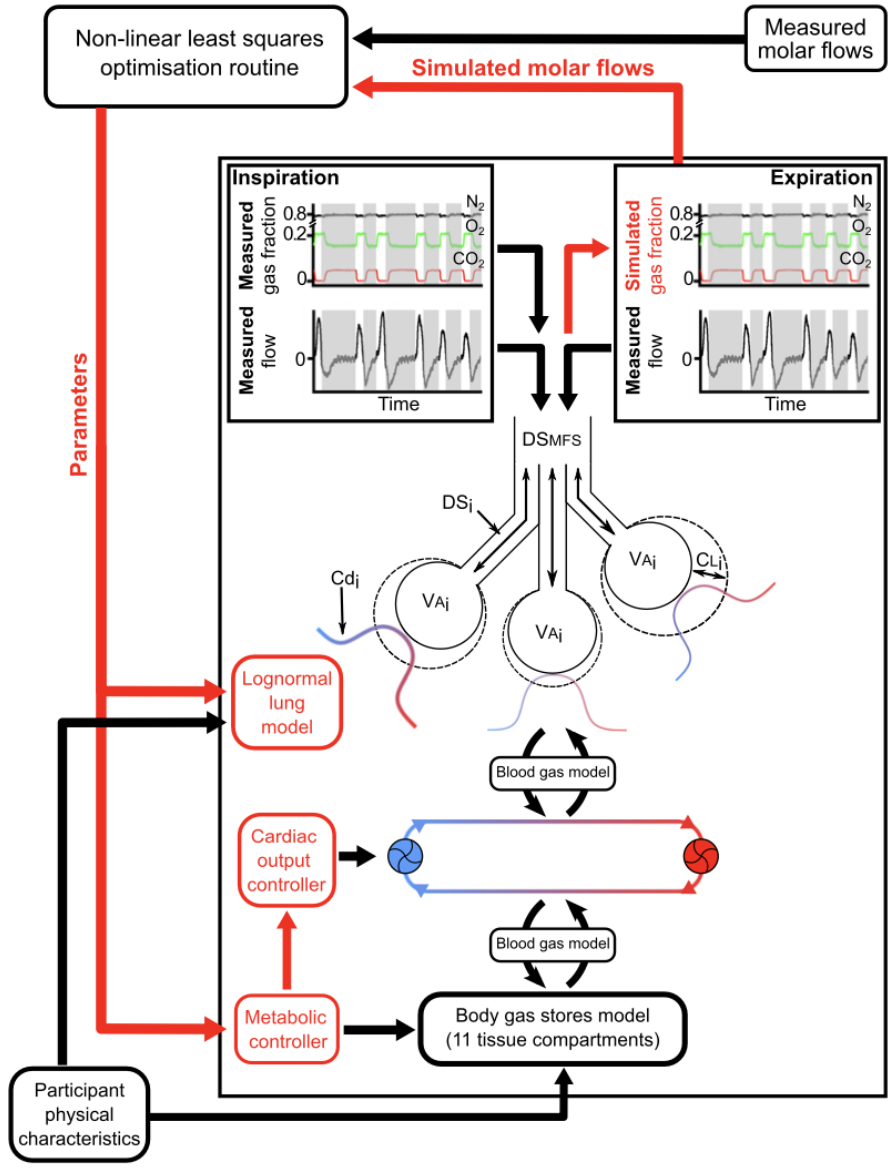


Figure 3.6. A schematic illustration of the computational model and parameter estimation technique, including the three sub-models: one for O_2 and CO_2 dissociation curves, another for circulation and body gas stores (CBGS) and a third for the log-normal lung (LNL), which accounts for inhomogeneity [119]. The size of the body gas stores and the initial parameter predictions are based on the individual's physical characteristics. The model is driven by the metabolic consumption of O_2 and production of CO_2, which, along with body size, determine cardiac output. Ventilation of the lungs is controlled by the respiratory flows that are recorded by the MFS, and the inspiratory gas composition is set to match the readings from the sensor. The model calculates simulated expiratory compositions, and these calculations lead to simulated molar flows for each gas species during expiration, which are then compared with those measured by the MFS. A non-linear optimisation routine is used to adjust parameters between successive model runs to minimise the errors between simulated and experimentally recorded molar flows during expiration. Cd_i represents the vascular conductance for the i^{th} lung unit, CL_i the compliance, DS_i the dead space, DSMFS the apparatus dead space for the MFS, and VA_i the alveolar volume for the i^{th} lung unit. O_2, oxygen; CO_2, carbon dioxide, N_2, nitrogen [119].

3.3 CCP vs. commercially available inert gas washout system

In Chapter 2, I provided an in-depth exploration of MBW technology, which was focused on its application in respiratory function assessment and the supporting literature. Here, I explore the devices that are available to measure LCI and evaluate their methodologies and effectiveness, with particular emphasis on the Exhalyzer. This focus is relevant because MBW tests from which indices such as LCI, S_{acin}, and S_{cond} are derived are the most commonly available breathing tests that physiologically measure and represent lung inhomogeneity, much like CCP. Both methods utilise a similar inert gas washout technique, so it is critical to understand their roles in the assessment of lung function and disease.

Several commercially available devices are designed to measure the LCI with the use of MBW technology. *Nuttall et al. (2019)* summarised the most widely available devices in a table (Figure 3.7) [112]. These devices employ different techniques and offer different capabilities, particularly in their handling of tracer gases and analyses of washout data.

The Innocor system from Innovision employs SF_6 as the tracer gas and uses a closed-circuit wash-in design. This system is particularly advantageous because it prevents the rebreathing of CO_2 through the use of a CO_2 scrubber. The use of SF_6 allows for a different sensitivity in the detection of small airway dysfunction and a shorter test time than the others. However, SF_6 is a potent greenhouse gas, which raises environmental concerns. This system is portable and self-contained, and therefore of practical utility for clinical and research settings [112].

The EasyOne Pro Lab system from ndd Medical Technologies measures LCI through the use of N_2 washout with medical air and 100% O_2. The system is portable, but it does not routinely implement the analysis of S_{cond} and S_{acin} in its standard software [112].

The Exhalyzer system, produced by Eco Medics (AG, Duernten, Switzerland) and which uses MBW, is widely used. This device has gained considerable prominence, especially

in CF clinical trials, for its ability to measure ventilation inhomogeneity. It operates based on N_2 washout and indirectly measures N_2 by calculating residual O_2 and CO_2 [19, 112, 152, 153]. The use of this method makes it particularly sensitive to errors in O_2 signal measurement, especially in the later phases of the washout, in which small errors can cause significant deviations in the N_2 signal. This leads to an overestimation of N_2, prolongation of the washout and therefore an overestimation of the FRC and LCI [19, 112, 152, 153]. Recent studies have revealed substantial and clinically relevant errors in the Exhalyzer system, particularly in its early software versions [154]. For example, in these versions, the effect of expired CO_2 on the O_2 signal reduced the O_2 reading and thus increased the calculated N_2, which prolonged the washout time and resulted in inflated LCI and FRC values [19, 152-154]. To correct these errors, an updated version of the software was introduced [154]. This software mitigated the cross-sensitivity error and hence significantly reduced the overestimation of LCI values. This correction led to a decrease in LCI by 10-15% [152, 154]. Although software updates have addressed these errors, historical data remain affected. Table 3.2 provides a comparison between the CCP and the Exhalyzer.

Sandhu et al. (2023) compared the Exhalyzer D (ExD) and CCP measurements for FRC and $LCI_{2.5}$. Their study revealed several differences in methodology and accuracy [119]. Figure 3.8 demonstrates the researchers' comparison of both techniques across their two cohorts of healthy control individuals (n=14) and patients with CF (n=11) [119]. For FRC, the techniques showed very similar values (Figure 3.8 A and C).

CCP does not measure the LCI directly. Rather, the idealised lung clearance index ($iLCI_{2.5}$) is a simulated value of $LCI_{2.5}$ that is calculated through the use of a cardiopulmonary model (discussed in section 3.2.2, 'Computational model') that standardises all extra-pulmonary influences that might influence the LCI measurement. The parameters of an individual's lung function are estimated through the use of CCP, while other parameters such

as O_2 consumption ($\dot{V}O_2$), cardiac output and CO_2 production ($\dot{V}CO_2$) are standardised based on the individual's height, mass, sex and age. A respiratory quotient of 0.8 and a fixed ideal PCO_2 of 5.3kPa are assumed. The respiratory rate is chosen iteratively with the tidal volume to match the ideal PCO_2. Additionally, the dead space of the apparatus is removed, a hypothetical insoluble tracer gas replaces N_2, and the pulmonary arterial blood composition is held constant. The $iLCI_{2.5}$ is calculated by simulating a washout phase in which the tracer gas concentration falls to 2.5% of its starting value, and the elapsed time is converted into the number of lung turnovers by dividing the total expired gas volume during the washout by the FRC [119].

In terms of $LCI_{2.5}$, *Sandhu et al. (2023)* found that both techniques were able to distinguish between healthy controls and people with CF, but they produced significantly different values of LCI; the Exhalyzer D produced higher measurements than did the CCP (Figure 3.8B and D). The likely reason behind this difference is that the standardised breathing pattern that *Sandhu et al.* used was relatively slow and deep [119]. An interesting aspect of the study by *Sandhu et al.* was the finding that the Exhalyzer D value for $LCI_{2.5}$ was best predicted by a combination of ventilation inhomogeneity ($\sigma lnCL$) and deadspace to FRC ratio (V_D/FRC). This suggest that multiple aspects of the pathology associated with CF, which can be separated by CCP, are all combined into the value for $LCI_{2.5}$ [119].

	Eco Medics AG Exhalyzer D	Innovision Innocor	Ndd EasyOne Pro Lab
Measurement principle	Ultrasonic transit in time	Photoacoustic spectroscopy	Ultrasonic transit in time
Overall design of set-up	Open circuit wash-in and washout design using bias flow	Closed, re-breathing circuit wash-in designed with CO_2 scrubber to prevent CO_2 accumulation Open circuit washout design	Open circuit washout design using bias flow
Inert gas assessed	N_2 and SF_6 MBW options available	SF_6	N_2
Bias flow gas mixture used	Medical air and 100% O_2 required for N_2-based MBW Wash-in $SF_6/O_2/N_2$ mixture for SF_6-based MBW sourced by individual user from local supplier	Wash-in gas available as licensed SF_6 gas mixture supplied by Innovision	Medical air and 100% O_2 required for N_2-based MBW
Application	Adults, children and infants >3 kg	Anyone capable of following instructions from the operator	Adults and children aged >4 years and >18 kg
Additional comments	Semiportable Operator interface through linked laptop Phase III slope analysis for S_{cond} and S_{acin} is integral to the software	Self-contained, portable User interface, LCD touch screen Phase III slope analysis not available	Self-contained, portable Operator interface, LCD touch screen Phase III slope analysis not routinely implemented; research software available

Figure 3.7. A summary produced by *Nuttall et al. (2019)* of the commercially available MBW devices [112]. SF_6: sulphur hexafluoride; S_{cond}: usual index of ventilatory inhomogeneity in the conducting airways; S_{acin}: index of ventilatory inhomogeneity within the acinar airways; O_2, oxygen; CO_2, carbon dioxide, N_2, nitrogen; LCD, liquid crystal display [112].

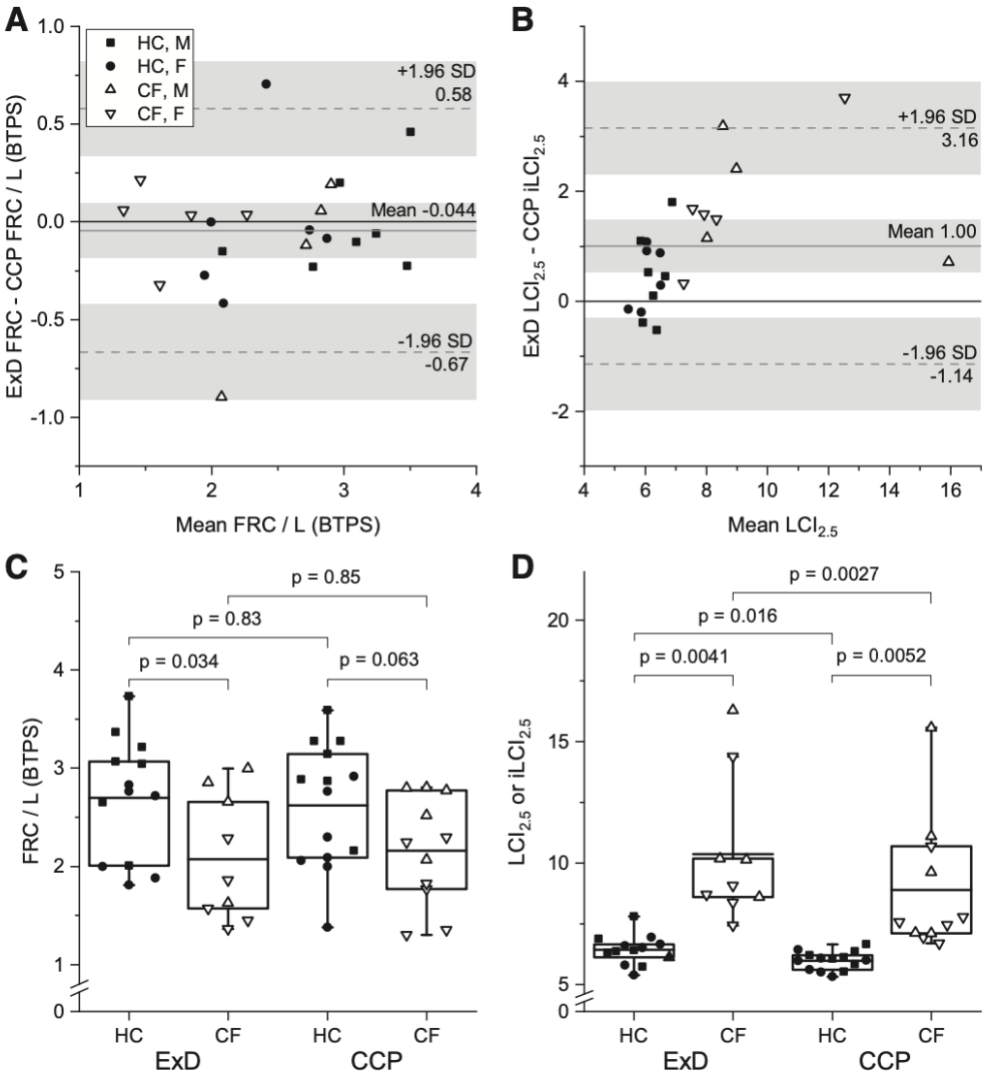


Figure 3.8. Comparison of the Exhalyzer D (ExD) and CCP measurements for FRC and $LCI_{2.5}$ produced by *Sandhu et al. (2023)*, [119]. **A.**comparison of FRC values between the two techniques. **B.** comparison of $iLCI_{2.5}$ with $LCI_{2.5.}$ **C.**box and whisker plots comparing FRC values for healthy control and CF groups produced through the use of ExD and CCP. **D.** box and whisker plots comparing values for ExD $LCI_{2.5}$ with those for CCP $iLCI_{2.5}$ for healthy controls and CF patients. CCP, computed cardiopulmonography; HC, healthy controls; CF, cystic fibrosis; ExD, Ecomedics Exhalyzer D; FRC, functional residual capacity; $iLCI_{2.5}$, idealised lung clearance index; $LCI_{2.5}$, lung clearance index [119].

Table 3.2. CCP vs. the Exhalyzer system.

	CCP	Exhalyzer
Technology basis and gas analysis	• Gas composition measured by laser absorption spectroscopy. • Gas analysis include water vapor measurement. • No crosstalk between gas signals. • Flow measurement fully compensated for variations in viscosity and density [104, 119].	• Gas composition measured by infra-red CO_2 sensor and paramagnetic O_2 sensor. • Gas analysis does not include water vapor measurement. • Crosstalk present between CO_2 and O_2. • Flow measurement not fully compensated for variations in viscosity and density [152, 154].
Clinical applications	• Not a medical device. • It has been used primarily in adults with asthma, COPD and CF, after COVID-19 infection, and critical care settings. • In critical care it offers continuous, non-invasive monitoring of O_2 consumption [119, 129, 139, 140, 155].	• Approved as medical device. • Widely used for CF studies and to study airway disease. • Widely and successfully used for paediatric patients [6, 7, 13, 112].
Advantages	• The use of 100% O_2 as a washout gas, which is easy to source in clinical settings. • Overall, easy and quick to perform and is not effort dependent. • Results virtually independent of the breathing pattern [104, 119, 139].	• The use of 100% O_2 as a washout gas, which is easy to source in clinical settings. • Overall, test is easy to perform and is not effort dependent. • Portable and more established in respiratory disease [112].
Limitations	• Novel device that requires validation and standardisation. • Bulky. • Results only available after fitting of the model to the data. • Requires a practitioner with specific knowledge and training [104, 119, 139].	• The test requires the participant to repeat the procedure multiple times, with the LCI result only being accepted when two of the values fall within a specified percentage of each other. • Susceptible to signal errors and prolonged measurement times. • Results partly dependent of the breathing pattern. • Requires a practitioner with specific knowledge and training [14, 152].

O_2, oxygen; CO_2, carbon dioxide; N_2, nitrogen; COPD, chronic obstructive pulmonary disease; CF, cystic fibrosis; LCI, lung clearance index.

3.4 Previous work on the measurement of lung inhomogeneity through the use of CCP

Previous studies have employed MFS and CCP in various participant groups [104, 119, 129, 139, 140, 155, 156]. *Ciaffoni et al. (2016)* addressed the challenge of monitoring O_2 consumption in critical care settings by using an MFS to provide real-time measurements of O_2, CO_2 and water vapour within the airway (main-stream measurement) [129]. This demonstrated the clinical usefulness of this system as O_2 consumption was accurately recorded during aortic aneurysm repair in a critically ill, intubated patient [129].

Mountain et al. (2018) utilised CCP in three distinct participant groups: young adults (aged 20-30 years), older adults (aged 70-80 years), and patients diagnosed with mild-to-moderate COPD. The primary objective was to determine whether CCP could provide reliable and reproducible estimates of lung inhomogeneity, a key marker of early lung dysfunction. The results from this study offer promising insights into the utility of CCP in both healthy and diseased populations. The authors demonstrated that CCP measurements of gas exchange are highly precise and reproducible, which is critical for establishing any novel diagnostic tool. The ability to consistently detect inhomogeneity across different participant groups, including healthy individuals and those with COPD, suggests that CCP can reliably differentiate between normal and abnormal lung function. A key finding of this study was the significant variation in CCP parameters between the three participant groups. Participants with COPD exhibited higher CCP values, reflecting greater lung inhomogeneity compared to the healthy young adults. These differences were statistically significant ($p < 0.001$) for all parameters related to lung inhomogeneity, underscoring the sensitivity of CCP in detecting early and subtle variations in lung function. Additionally, the study highlighted CCP's ability to provide detailed data on gas exchange, which could be valuable for assessing treatment responses in chronic respiratory conditions. Another important observation from this research is the reproducibility of the CCP method across diverse subject groups and conditions. The

consistency of the technique in detecting lung inhomogeneity, regardless of whether the lungs were healthy or diseased, is a crucial step towards its potential clinical application. [104].

Smith et al. (2020) were the first to investigate whether σlnCL, a CCP parameter that measures lung inhomogeneity (uneven inflation/deflation), could assess disease activity in asthma [140]. They also explored whether CCP could provide a better measure of disease activity in asthmatic patients' lungs than standard spirometry. This was done by comparing σlnCL with the commonly used FEV_1 % predicted. While σlnCL showed a modest correlation with FEV_1 % predicted, it was distinct and not a mere substitute. Notably, σlnCL appeared to more reliably reflect disease control in asthma compared to FEV_1 [140].

Smith et al. (2022) employed CCP to assess gas exchange inhomogeneities in COPD patients (n=26) who showed different levels of disease severity, and they compared their results with those of age-matched healthy controls (n=10) [155]. Their results demonstrated the reliability and sensitivity of the CCP parameters to distinguish between healthy people and those with mild-to-moderate COPD and to distinguish between mild-to-moderate and severe cases [155].

Sandhu et al. (2023) assessed the application of CCP in the evaluation of lung function in patients with early-stage CF who had preserved lung function [119]. This research aimed to determine whether CCP, in combination with the idealized lung clearance index ($iLCI_{2.5}$), could provide more detailed insights into the lung physiology of CF patients compared to traditional lung clearance index ($LCI_{2.5}$) measurements. The study showed that participants with early-stage CF exhibited greater lung inhomogeneity compared to healthy controls, as reflected in CCP-derived parameters such as σlnCL, $iLCI_{2.5}$, and increased variability in the size of anatomical dead spaces relative to their predicted FRCs (DS/FRC). These findings indicate that CCP can detect subtle changes in lung ventilation that occur early in the progression of CF, even when conventional spirometry results are normal [119].

Redmond et al. (2024) explored the utility of CCP in identifying early changes in the lungs of young smokers before traditional diagnostic methods revealed lung damage. The study found that CCP is particularly effective in detecting subtle ventilation inhomogeneity, a hallmark of early lung impairment caused by smoking. These findings suggest that CCP could be a sensitive tool for early intervention and prevention of long-term respiratory conditions [156].

In summary, this chapter has introduced the MFS and CCP and has highlighted the potential of these novel techniques. It shows particularly the role of CCP in the provision of insights into the physiological characteristics of individuals with various respiratory diseases. Its findings underscore the necessity for further investigation of the use of the MFS and CCP through large clinical research studies.

Chapter 4. Methodology

4.1 Experimental protocol

The experimental approach to the measurements of lung inhomogeneity explained here was applied to all the cohorts that were studied for the work described in this thesis. The inclusion and exclusion criteria mentioned below are the general criteria for the inclusion of a participant in a CCP-related study. These criteria vary according to the cohort and are detailed independently in each cohort chapter. More detailed criteria were applied depending on the project. For example, for the study of the healthy control volunteers, participants were excluded if they had an established diagnosis of respiratory disease, in order to gain the most appropriate control data. Other inclusion/exclusion criteria still apply.

4.1.1 Inclusion criteria

- Male or female, aged 18 years or over.
- Willing and able to provide informed consent for participation in the study.

4.1.2 Exclusion criteria

- Inability to tolerate mouthpiece/nose clip
- Major abdominal surgery in the previous three weeks
- Pregnancy
- Significant cardiac disease

4.1.3 Expenses and benefits

The work for this thesis included one cohort of healthy volunteers as a control group (Chapter 5) and two patient cohorts: the asthma cohort (Chapter 6), members of which were recruited from the special airway clinic, and the post-COVID-19 cohort (Chapter 7), members of which were recruited from the OUH. Patients were not reimbursed for their involvement in this study, but reasonable travel expenses were paid for any visits that were additional to patients' normal clinical care. Healthy volunteers were offered a payment of £10 per hour for their time, in addition to reimbursement for travel expenses.

4.1.4 Prior to the breathing test

4.1.4.1 Calibration

The instructions for the MFS required that it should be turned on for at least 30 minutes before the calibration process could begin. This was done to allow the device to heat up to a steady temperature before calibration. Calibration was performed at the start of the day or if the MFS was moved from the original location where calibration had been conducted. The calibration procedure took three minutes. Initially, pure N_2 was passed through the measurement cell at a flow rate of approximately 5 $l.min^{-1}$. This step identified the baselines for O_2, CO_2 and H_2O. An additional calibration step was necessary to assess the reflectivity of the optical cavity for the O_2 measurement. This was accomplished by switching the gas supply from pure N_2 to pure O_2 (laboratory grade 99.995%) at a flow rate of 5 $l.min^{-1}$.

4.1.4.2 Participant information sheet and informed consent

Each participant was offered a participant information sheet, which contained written details about the study, either at their clinical visit or through email or text message. Each potential participant had the opportunity to discuss their involvement before consenting. Before

they provided consent, participants were briefed both verbally and in writing about the study's objectives, their potential role, and the associated risks and benefits. They were explicitly informed of their right to withdraw at any time without compromising their future care or legal rights and without any need to justify their decision. Participants were given sufficient time to deliberate on their involvement.

Written, informed consent was acquired from all participants. I obtained consent personally from nearly all the participants who were involved in this work, except for the younger control cohort (which is described in Chapter 5). To achieve this, I completed training in Good Clinical Practice, and this was endorsed by the chief investigator. Each participant was offered a copy of the signed consent form, with the original forms securely stored at the research site (the Department of Physiology, Anatomy, and Genetics).

Each participant's height, age, and weight were taken on the day of the test. Additionally, a brief summary of their cardiopulmonary and smoking history was recorded.

4.1.5 The MFS breathing test

It was crucial to ensure that the participant was in a steady, resting state and sitting in a comfortable position before the test was initiated. Additionally, it was important to allow participants time to become accustomed to the mouthpiece and nose clip (Figure 3.1). This was typically achieved by having participants breathe through the MFS for a few minutes before the test. Participants were also offered the option to watch something on an iPad or to listen to their chosen music to help ease the test, pass time, and distract them from focusing solely on the breathing test. They were instructed while attached to the machine to breathe as normally and in as relaxed a manner as possible. Ideally, participants were placed so that they could not view their breathing test screen so that they could not attempt to control their breath to match the curves.

During the test, participants were asked to breathe normal tidal breaths (steady tidal breathing) through the MFS mouthpiece for a total of 12 minutes. During this period, respired gases were measured during a steady air-breathing period (seven minutes) and a subsequent 100% medical O_2-breathing period (five minutes) (Figure 4.1). Throughout the breathing test, the nose was sealed with a nose clip to create a closed system between the MFS and the participant's airway, in order to ensure that all the gas passed through the MFS. A pulse oximeter was used to measure O_2 saturation and heart rate, and these data were sent to the MFS. Also, throughout the test, I examined the expirograms to check for any possible leaks, which typically occurred around the mouthpiece. Any identified leaks could be addressed easily by ensuring the participant maintained a good seal.

The advantage of this breathing manoeuvre lies in its simplicity; it does not require coordination or forceful breathing manoeuvres such as those needed for spirometry and is effort-independent, making it suitable for individuals with lung disease or breathing problems. A small project was conducted within our research group as part of a Final Honours School project (student Thomas Grill), in which we surveyed a small number of healthy participants (n=11) who had undergone both the CCP breathing test and the spirometry-forced vital capacity (FVC) measurement. When participants were asked how comfortable they found it to breathe through the MFS for 12 minutes, nearly half (36.4%) of the participants responded that it was comfortable, while only 9.1% found it uncomfortable. Furthermore, 63.6% of the participants reported that the MFS breathing test was easier to perform than the spirometry test (Figure 4.2). These findings suggest that a majority of participants found the MFS breathing test more comfortable and easier to perform than the spirometry test. This was particularly important for patients with respiratory conditions, as use of this test would improve the feasibility of pulmonary function assessments in clinical settings.

To explore the reproducibility of parameters that were collected through use of the MFS, *Mountain et al.* (2018) [104] studied six young (20-30-year-old) healthy participants, six older (70-80-year-old) healthy participants, and six participants with mild or moderate COPD. For each participant, the breathing test was performed three times with the same measurement protocol on each of two days. An important feature of the results was that the within-participant standard deviations and coefficients of variation for the parameters were generally small, and the intra-class correlation coefficients were high (young vs. old, healthy vs. COPD) [104]. The findings demonstrated that the results were highly repeatable from test to test for a given participant.

The experimental protocol that was chosen in this study involved an N_2 washout during the final five minutes of the breathing test, which ensured that sufficient information would be encoded for the model-fitting process. It was utilised to estimate lung volume based on the volume of expired N_2; also, the rate at which the lung volume equilibrated with O_2 offered insights into the ventilation-volume ratio distribution. Additionally, the pattern of the N_2 washout provided insights into the distribution of ventilation. For example, a perfect exponential decay would suggest ideal ventilation/perfusion matching and uniform distribution of alveolar ventilation. To run the model, it was necessary to obtain total gas flow and inspiratory gas composition profiles. The model's outputs were the compositions of exhaled gas.

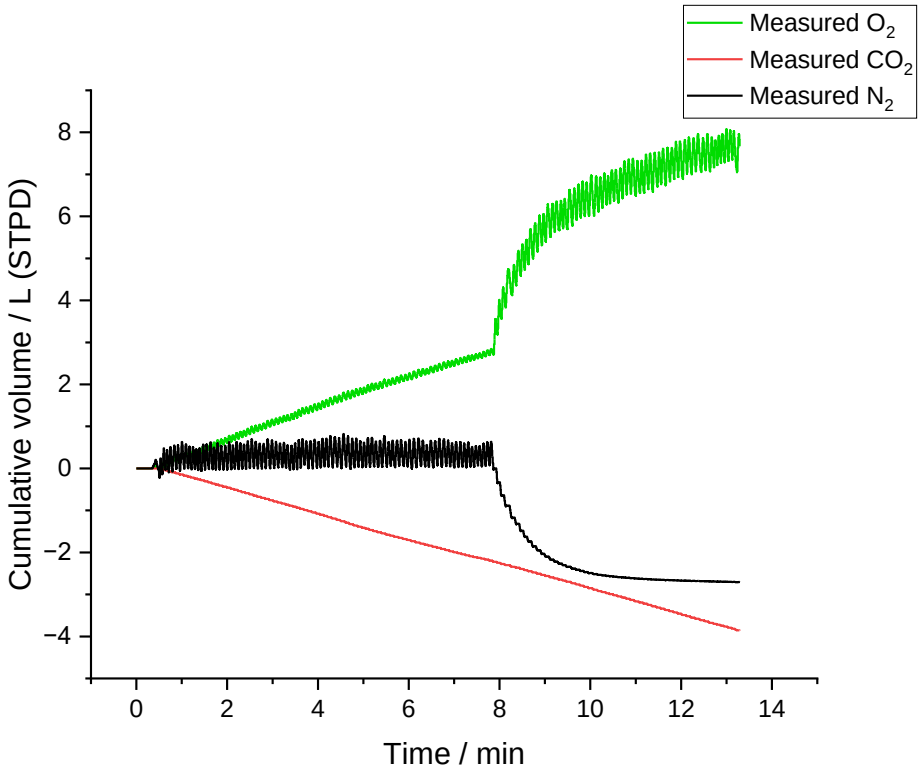


Figure 4.1. Graph of gas respiration during a 12-minute breathing test. Breathing followed a normal tidal breathing pattern for 12 mins. In the first seven minutes, the participant breathed air, followed by O_2 in the last five-minute period (N_2 washout). In this plot, the cumulative volume uptake of N_2 (black), O_2 (green) and CO_2 (red) were measured. The O_2 profile displays a positive slope as it is consumed by the body, while the CO_2 profile has a negative slope as it is produced by and released from the body. An important observation is that the N_2 profile remains nearly flat during air-breathing, indicating that it is neither produced nor consumed. This consistent gradient for N_2 signifies the accuracy of the measurement. STPD, standard temperature pressure dry.

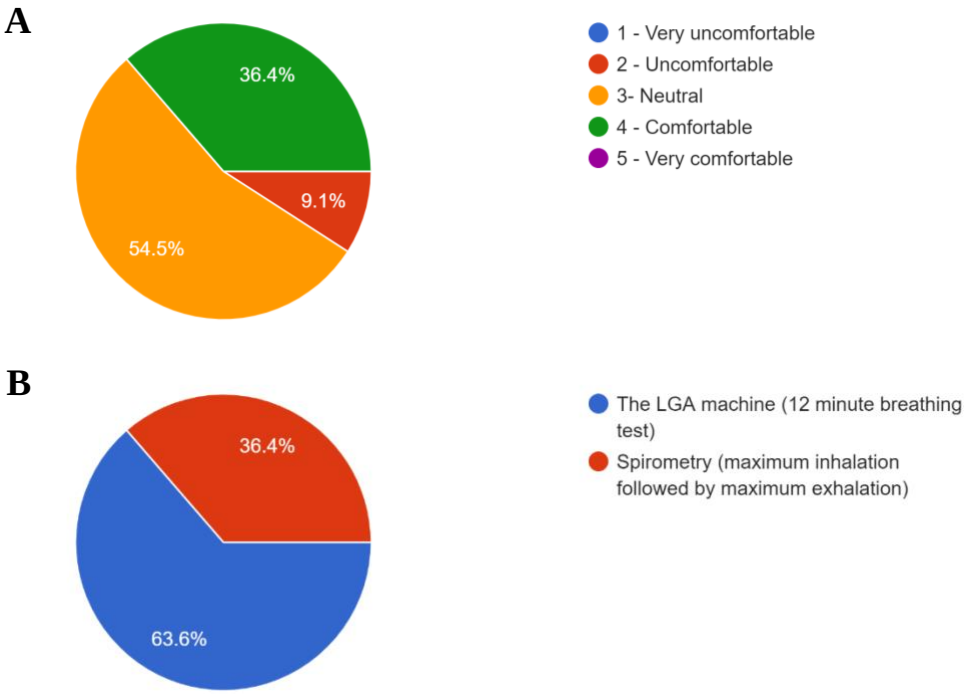


Figure 4.2. Pie charts illustrate the responses to two survey questions. A. How comfortable did you find the apparatus for the 12-minute breathing test (referred to as the laser gas analyser (LGA) test)? B. Which of the two breathing tests was easier to complete? The survey received 11 responses. The term LGA was used to refer to the MFS in participant communications and the survey. Thus, LGA and MFS were used interchangeably in this context. (Figure credit: Thomas Grill).

4.1.6 Model fitting

The fitting process was performed through the application of a non-linear least squares optimisation (NLSQ) algorithm. Before this was completed, patient demographics and MFS data (from the 12-minute breathing test) were entered into a graphical user interface. After fitting, various parameters that reflected different aspects of lung inhomogeneity (as discussed in section 3.1.1) were returned by the model. Figures 4.3 and 4.4 illustrate a portion of the fitting software's report.

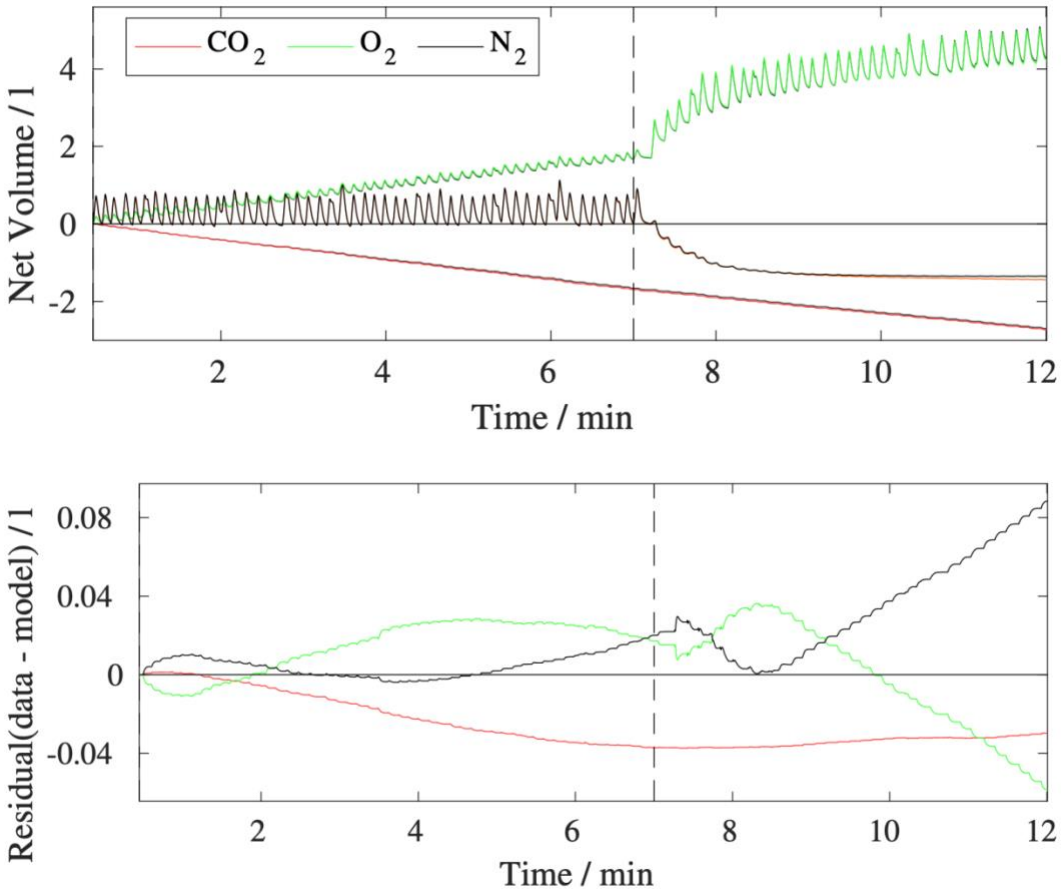


Figure 4.3. Graphs show results from the fitting routine. **Upper:** the cumulative volume of each gas that was recorded throughout the experiment. The data traces (coloured as in key) are superimposed on the model fit traces (encoded in black or red for N_2). The close mirroring of the simulated and measured data shows the quality of the fit. **Lower:** the fitted cumulative gas volume residuals. Throughout the protocol at all points the residual was low.

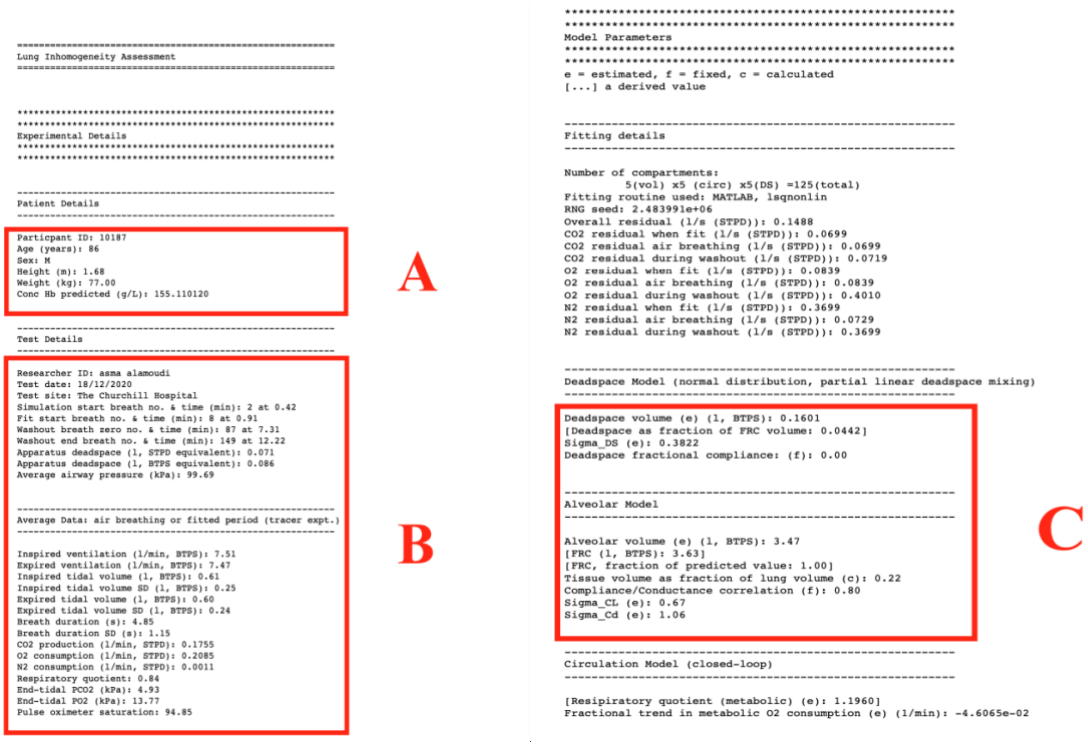


Figure 4.4. Lung inhomogeneity assessment report. A. Patient research ID and demographics. **B**. Measured values: O_2 saturation, gas volumes, compositions, and pressures at the mouth. **C.** Lung inhomogeneity parameters: sigma CL: standard deviation (SD) for the log distribution in lung compliance to alveolar volume; sigma Cd: SD for the log distribution in vascular conductance to alveolar volume; sigma DS: SD for the distribution in dead space to alveolar volume.

The governing equations were based on the principle of mass conservation. Solving the forward problem was relatively straightforward; the inspired gas content measured by the MFS was input into a model lung, which set a subset of parameters to physiologically reasonable values and assigned values to the parameters that govern lung function. However, it is important to note that these lung parameters were not measured directly by the MFS. Therefore, to obtain representative parameter values, the inverse problem had to be tackled. Unlike the forward problem, the resolution of the inverse problem required more intensive computation. To estimate the parameter set from experimental data, a recovery procedure was performed, which involved an optimisation routine that minimised the squared differences between the model's simulated gas fractions and the experimental data through the use of an NLSQ algorithm. This process continuously adjusted the model parameters to minimise the squared

difference between the model's expiratory molar gas flows and the experimental values found during the 12-minute breathing test.

The profile of expired partial pressures of O_2 and CO_2 during a single breath offered insights into the distribution of anatomical dead space and compliance. If all personal dead space volumes to each alveolus were identical in length/volume, and all compliances were the same across compartments, there would be a distinct point at which gas fractions would shift from being close to air (from conducting zones) to those equilibrated with blood (from alveolar zones). Physiological lung inhomogeneity, however, blurs this profile. The extent of smearing and sigmoidal change in partial pressures indicated the breadth of distribution in alveolar compliance or dead space volumes that supplied alveolar units.

The main coding for the model was performed using MATLAB (R2022a, MathWorks Inc, Natick, MA), supplemented by two smaller, numerically intensive routines in C++. The University of Oxford's ARCUS high-performance computer system was used to run the model and estimate parameters. Typically, the fitting process took less than an hour. To ensure reliability, the fitting procedure was repeated three times with different randomised starting points to verify consistent convergence to the same minimum residual.

To summarise, this chapter has provided detailed descriptions of the CCP experimental protocol (Figure 4.5) and breathing test. These remained consistent across all experimental procedures, which are described in the experimental chapters. Chapter 5 is focused on the investigation of inhomogeneity parameters in healthy control participants with the goal of establishing standardised normal values for lung inhomogeneity parameters. Chapter 6 contains an explanation of the investigation of inhomogeneity parameters in patients with T2-high asthma, which was aimed at evaluating the effects of therapeutic interventions on measures of lung inhomogeneity that had been obtained through the use of the novel technique. Chapter 7 explains the study of the long-term effects of COVID-19, the main objective of

which was to explore the enduring impacts of COVID-19 on respiratory function and lung physiology over an extended period.

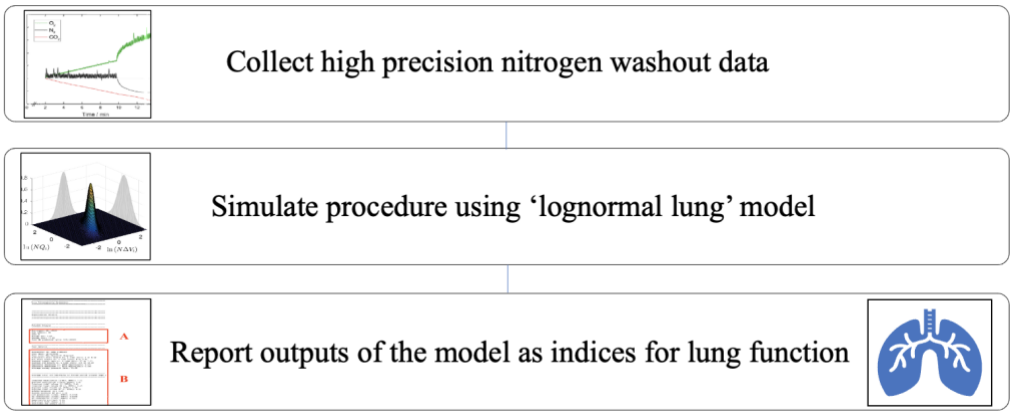


Figure 4.5. Outline of the CCP experimental protocol.

Chapter 5. Determination of normal CCP parameter values

5.1 Introduction

The original objective of this thesis was to collect a comprehensive dataset from a diverse group of healthy volunteers with various demographic characteristics. This would have enabled the establishment of standardized normal values from healthy control participants, which could be used as comparison data for testing a novel technique aimed at measuring lung inhomogeneity. However, the COVID-19 pandemic significantly impacted the progression of this work, causing a substantial shift in my research direction. The suspension of human experimental work required a reassessment of my approach. During the pandemic, only research related to COVID-19 was possible, which provided the opportunity to focus on the work described in Chapter 7. Once restrictions eased, patient appointments at the asthma clinic, which had been suspended for nine months, were able to resume. Fortunately, as my final year began, I had the opportunity to partially revisit the original objective of my DPhil. As a result, the work described in Chapter 7 (post-COVID-19 cohort) and Chapter 6 (asthma cohort) took place before the completion of the healthy control project.

In the work described in this chapter, standardised normal values for CCP, the novel way to measure inhomogeneity, were established through the examination of healthy control participants. This enabled the quantification of the deviation of an individual's CCP parameters from the anticipated normal values, which were determined by their physical characteristics. A regression analysis model was used to construct and establish normal ranges for the novel inhomogeneity parameters. The provision of normal ranges for these parameters would

facilitate future clinical investigation studies, by providing straightforward measures of lung abnormality and removing the requirement for an additional control cohort.

5.2 Methods

5.2.1 Participants

5.2.1.1 Identification of participants

Participants were studied as healthy volunteers and then were recruited under ethical approval reference 17/SC/0172. They were recruited through various advertisement channels. Physical notices were placed around the departments of the University of Oxford and electronic notices were posted on social media platforms to draw the attention of potential participants. Some of the older control participants, who were recruited at a later stage, were reached through more targeted efforts. Brochures were distributed in the University Park, and a brief presentation about the project, the CCP and its potential benefits was given to a community forum called the Café Scientifique. This forum is a public space where scientific ideas are discussed informally among scientists and non-scientists alike, with the aim of informing, entertaining, and provoking debate. Most attendees are in their late 50s to 80s. Other volunteers were members of the research group and their families, and friends.

I examined the datasets of a possible 216 participants that were recruited as healthy controls. After careful screening for histories of excessive smoking or respiratory diseases, including having had COVID-19 (first wave before vaccination), and whether or not they had completed the required breathing test protocol (using the MFS described in Chapter 4), 112 participants were included in this project (Figure 5.1), that fulfilled the below inclusion and exclusion criteria. Among these were 78 healthy controls, who had been examined previously by members of our research group, and another 34 older healthy controls that I recruited. These

latter participants were recruited because a significant portion of the existing data pertained to individuals aged 40 years and under.

5.2.1.2 Inclusion criteria

Participants were required to fulfil the following requirements.

- Male or female aged 18 years or over.
- Willing and able to provide informed consent for participation in the study.
- No previous diagnosis of respiratory diseases (including childhood asthma) and no history of contraction of COVID-19 (during the first wave of COVID-19, prior to vaccination, and pre-Omicron).
- No smoking history, or limited smoking history of fewer than five pack-years.

5.2.1.3 Exclusion criteria

- Inability to tolerate mouthpiece/nose clip
- Major abdominal surgery in the previous three weeks
- Pregnancy
- Significant cardiac disease
- History of respiratory disease

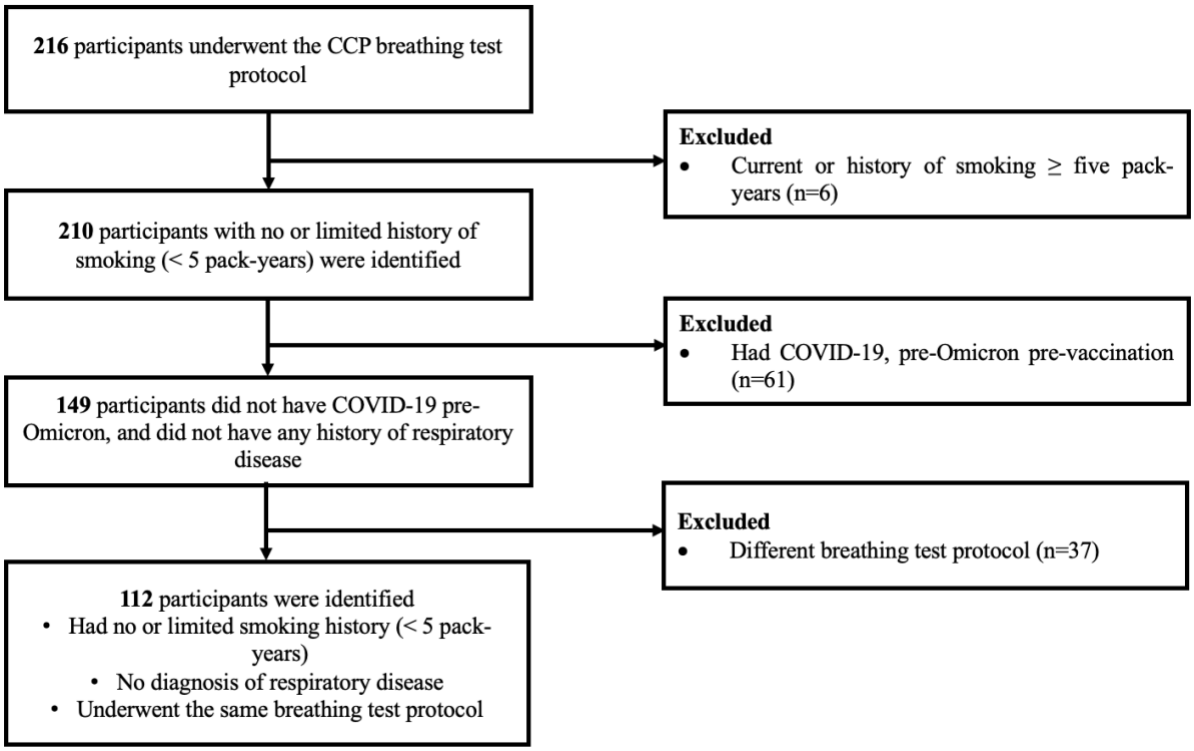


Figure 5.1. Diagram illustrating the healthy control data allocation.

5.2.2 Study protocol

5.2.2.1 Lung inhomogeneity test

All 112 participants underwent or had previously undergone the same breathing test protocol that involved the use of the MFS (described in chapter 4 of this thesis). All lung inhomogeneity breathing test data were processed using the cardiopulmonary model, described in section 3.2.2 of this thesis, and the output parameters are detailed in Table 5.1.

Table 5.1. Lung model parameters.

FRC / l (BTPS)	Functional residual capacity
V_D / l (BTPS)	Dead space volume at end-inspiration
σV_D	The SD of the normal distribution for (normalised) dead space across lung volume
$\sigma \ln C_L$	The SD of log-normal distributions for (normalised) alveolar compliance

BTPS, body temperature (37°C), ambient pressure and gas saturated with water vapour. SD, standard deviation.

5.2.2.2 Quality control process

The collected data and the quality of the model fit were examined. Any data with N_2 production greater than or equal to an absolute value of 60 ml/min during the air-breathing phase were excluded, as high N_2 production indicated that there may have been a leak during the breathing test.

5.2.2.3 Regression analysis

Most statistical analyses were conducted with the use of SPSS [157]. Each of the CCP parameters (Table 5.1) was fitted through the use of a regression model. Regression analysis is the simplest and most frequently employed method to quantify relationships between continuous variables. It is widely utilised in modelling as it captures efficiently the relationship between a singular dependent variable and one or more predictors. The application of linear regression is underpinned by four fundamental assumptions:

- linearity: i.e. that the model accurately represents the underlying associations;
- homoscedasticity: that the spread of the residuals does not systematically change across the range of predictor values;
- independence: that each data point contributes unique information (an assumption crucial to the avoidance of biases in the analysis); and,
- normality: errors are normally distributed (an assumption that facilitates the interpretation of statistical tests and confidence intervals associated with the regression coefficients).

Adherence to these assumptions is essential to ensure the reliability and validity of insights that are derived from linear regression analysis [158, 159].

In the work described in this chapter, linear regression was employed to assess the impact of various factors such as log(age), log(height), log(BMI), and sex on the CCP parameters. The principles that guided the construction of the regression models were that the:

- dependent variables were the CCP parameters;
- use of dependent variables both as their absolute values and log transforms would be explored; and
- independent predictors were the logarithms of age, BMI and height, and sex.

Predictors were sequentially excluded via a stepwise regression analysis starting with the least significant until only those with $p<0.1$ remained.

Subsequently, I tested the validity of the linear regression assumptions, primarily the normality of the residuals, and the homoscedasticity. Residuals from the regression model were inspected for normality through the application of the *Shapiro-Wilk* and *Kolmogorov* tests. These tests are commonly employed to examine whether the data follows a normal distribution. The *Shapiro-Wilk* test is considered more suitable for smaller cohorts (n<50), whereas the *Kolmogorov–Smirnov* test is preferred for cohort sizes that are greater than or equal to 50. In each of these tests, the null hypothesis posits that the data are derived from a normally distributed population. If the *p-value* is greater than *0.05*, the null hypothesis is accepted, indicating that the data is considered normally distributed [160]. These tests were undertaken for both the natural logarithm and absolute values of the CCP parameters (Table 5.1) to determine which residuals showed the more normal distributions.

Finally, I examined the data for heteroscedasticity through the use of the modified and original *Breusch-Pagan* tests. Heteroscedasticity refers to the deviation of data from the statistical assumption of homoscedasticity; violation of this assumption would mean that the variance of the dependent variable could not be treated as a constant, and depended on predictors [161].

5.2.2.4 Outliers

I examined the CCP modelling results for participants who were outliers in terms of their parameter values (discussed in section 5.3.3).

5.3 Results

5.3.1 Participants

All the breathing test data for the 112 participants were passed through the quality control process, which involved screening for the N_2 balance. This process led to the exclusion of 12 participant datasets, leaving 100 participants. Table 5.2 shows the basic demographic characteristics of these 100 participants and Figure 5.2 shows the frequency distribution of their ages. All were healthy volunteers, aged 18 and above, with an average age of 40 years (SD±19 years). The mean BMI was 24kgm^{-2} (SD±4kgm^{-2}). The group comprised 30 females and 70 males.

Table 5.2. Characteristics of the participants in the healthy control group

Characteristics	**Healthy control cohort**
Number of participants	100
Number of females (/ %)	30 (30)
History of respiratory disease (/ %)	0
Smoking (/ %)	6 (6)
Age±SD / yr	40±19
Height±SD / m	1.75±0.09
Weight±SD / kg	74±14
BMI±SD / kg.m^{-2}	24±4
Spirometry	n=31
FEV_1±SD / % predicted	105±14
FVC±SD / % predicted	109±14
FEV_1/FVC±SD	0.80±0.05

BMI, body mass index; FEV_1, forced expiratory volume in 1s; FVC, forced vital capacity. Values are means ± SD.

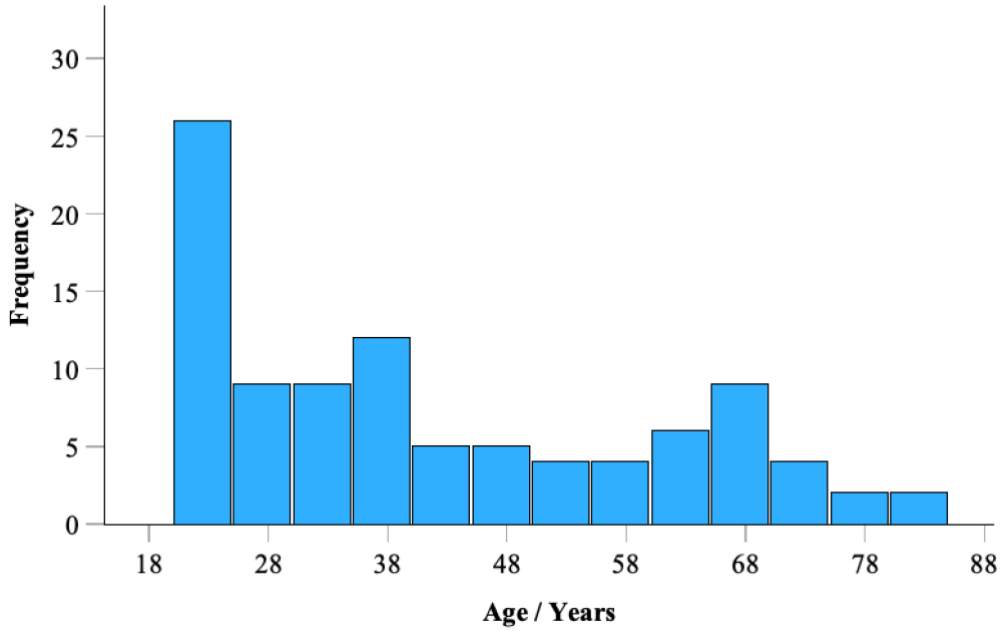


Figure 5.2. Histogram illustrating the age profile of the 100 healthy volunteers.

5.3.2 Regression analysis

A single equation (Equation 5.1) was created for both males and females by incorporating "isFemale" as a factor:

$$P_i = \alpha*log(age)_i+\beta*log(height)_i+\gamma*log(BMI)_i+\delta*isFemale_i+\varepsilon+error_i \quad \text{(Equation 5.1)}$$

in which P_i was the CCP parameter to be modelled and i represented a participant. The factor $error_i$ was the residual between the value predicted according to the model and the measured value. The characters α, β, γ, δ, and ε were coefficients to be estimated via linear regression. The term *isFemale* accounted for sex; it took a value of 1 if the participant was female, and 0 if male.

To establish conclusive linear regression models for each output parameter, I applied the linear regression model shown in Equation 5.1 to the 100-member control dataset in order

to calculate the coefficient for each independent variable and to progressively remove any terms that were not significant as predictors *(p>0.1)*.

5.3.3 Normality test

Initially, the *Shapiro-Wilk* and *Kolmogorov–Smirnov* normality tests were performed to determine whether, for each CCP parameter, the residuals exhibited more normal distributions when either the actual parameter value or the log-transformed parameter value was considered. Specifically, log(FRC) vs. FRC, log(V_D) vs. V_D, log(σV_D) vs. σV_D, and log($\sigma \ln C_L$) vs. $\sigma \ln C_L$ were examined (as shown in Table 5.3). Based on the results shown in Table 5.3, log(FRC), log(V_D), σV_D, and $\sigma \ln C_L$ were selected for further analysis.

Table 5.3. Normality test results for the 100 participants

Parameters		Shapiro-Wilk test	Kolmogorov test
log(FRC)	Statistic	0.983	0.047
	p-value	0.210	0.200
FRC / l	Statistic	0.960	0.053
	p-value	0.004	0.200
log(V_D)	Statistic	0.961	0.053
	p-value	0.005	0.200
V_D / l	Statistic	0.930	0.098
	p-value	<0.001	0.019
log(σV_D)	Statistic	0.962	0.072
	p-value	0.006	0.200
σV_D	Statistic	0.985	0.051
	p-value	0.303	0.200
log($\sigma \ln C_L$)	Statistic	0.975	0.081
	p-value	0.056	0.105
$\sigma \ln C_L$	Statistic	0.980	0.072
	p-value	0.141	0.200

Log(FRC), natural logarithm of the functional residual capacity; log(V_D), natural logarithm of deadspace volume (end-inspiratory); σV_D, the SD for the standardised dead space; $\sigma \ln C_L$, SD for the natural logarithm for the standardised lung compliance.

While checking for normality of the data through the inspection of the residuals of the regression analysis for each CCP parameter, I identified some outlier datasets (Figure 5.3). One of these outliers exhibited the highest N_2 production among all the datasets, indicating that the outlier value was probably caused by a leak during the breathing test. This outlier was excluded.

Another outlier was excluded because the lung inhomogeneity data for this participant (all CCP parameters σlnCL, VD, σVD) suggested that they may have had an underlying respiratory pathology. Their lung inhomogeneity parameters were higher than the average parameters of the healthy cohort group and resembled what had previously been observed in people with COPD or asthma [140, 155]. A third outlier was examined thoroughly by reviewing the full CCP report, the breathing test, and the participant's history. There was no reason to exclude this participant.

There was no reason to exclude any other parameter sets, so 98 healthy control participants were retained. Figure 5.4 illustrates a summary diagram of the recruitment screening process for the final participants included in this study. Table 5.4 shows the basic demographic characteristics of the 98 participants, which were comparable with those shown in Table 5.2. All were healthy volunteers, aged 18 and above, with an average age of 40 years (*SD ±19 years*). The mean BMI was 24kgm^{-2} (*SD ±4kgm*$^{-2}$). The group comprised 29 females and 69 males. The average values that were obtained from the 98 participants for the four CCP parameters, for which normal ranges were established based on participants' physical characteristics, were: FRC *3.30±0.77*, VD *0.150±0.049l*, σVD *0.35±0.06*, and σlnCL *0.51±0.09*.

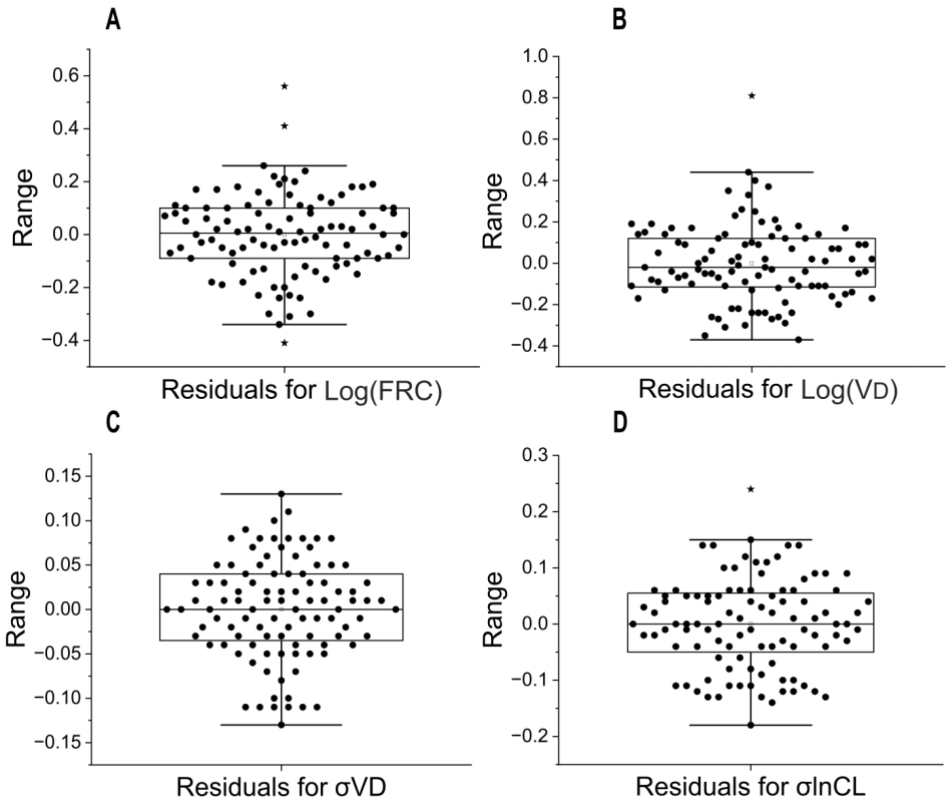


Figure 5.3. Box and whisker plots illustrate the residuals of the regression model for each CCP parameter for the datasets of the 100 participants. For box and whisker plots, the median line is shown with the interquartile range as the box. The whiskers show the maximum and minimum values that still remain within 1.5 times the interquartile range beyond the box. Outliers are shown as points beyond the whisker plots (stars). **A.** Residuals for log(FRC), showing three outliers. **B.** Residuals for log(VD), showing one outlier. **C.** Residuals for σVD, showing no outliers. **D.** Residuals for σlnCL, showing one outlier.

Table 5.4. Participants characteristics of the final healthy control data.

Characteristics	Healthy control
Number of participants	98
Number of females (/ %)	29 (29.6)
History of respiratory disease (/ %)	0
Smoking (/ %)	6 (6)
Age±SD / yr	40±19
Height±SD / m	1.75±0.09
Weight±SD / kg	74±14
BMI±SD / kg.m^{-2}	24±4

BMI, body mass index. Values are means ± SD.

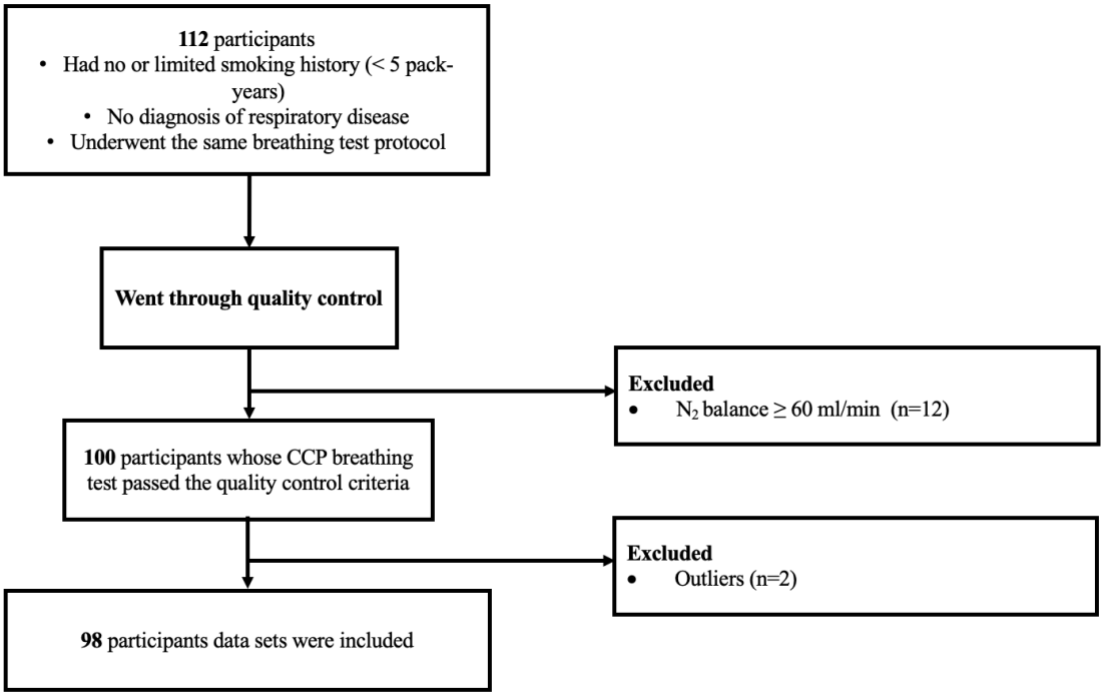


Figure 5.4. Diagram illustrating the healthy control data allocation and screening process.

I then repeated the regression analysis on the selected CCP parameters (log(FRC), log(VD), σVD, σlnCL) for the 98 participants and re-tested the normality of the residuals. As indicated in Table 5.5, after the data had been inspected and the two outliers removed, the test of normality for log(VD) significantly improved. The *Shapiro-Wilk test p-value* changed from *0.005* (when all participants were included before the outliers were removed) to *0.577*.

The *Shapiro-Wilk* test for σlnCL was significant (*p value=0.038*). Upon inspection of the data, this was attributed to the fact that σlnCL did not change substantially for participants between the ages of 20 and 30 years old (Figure 5.10). Therefore, the decision was made to refit the regression with the addition of the term $(log(age))^2$. With this adjustment, the residuals exhibited a more normal distribution, and the *Shapiro-Wilk* test *p-value* became insignificant (*p=0.510*). Most importantly, the *Akaike information criterion (AIC)* was more negative (*-209.2 vs. -207*) when the $(log(age))^2$ term was included, which indicated that the addition of

this term created a significantly better fit (Table 5.5). In contrast with σlnCL, the inclusion of the $(log(age))^2$ term did not improve the fit for the other CCP parameters.

5.3.4 Heteroscedasticity test

I explored whether there were significant variations in the size of the residuals with the predictors for the remaining 98 participants. To do this, I performed the *Breusch-Pagan* and *modified Breusch-Pagan* tests of heteroscedasticity. Table 5.5 presents the combined results of the normality and heteroscedasticity tests for the 98 participants.

The modified *Breusch-Pagan* test for log(FRC) was found to be significant ($p=0.040$), as indicated in Table 5.5, although the *Breusch-Pagan* test was not significant ($p=0.057$). The plot for measured log(FRC) against the predicted log(FRC) was examined (Figure 5.5), and it was observed that there might be some reduction in variance at the higher values. However, when the *SD* was fitted as a function of log(FRC) (the log(FRC) was added as a random effect + intercept in the model, introducing a variable SD), the plot for the 5% and 95% confidence intervals revealed that too many points fell outside this range (Figure 5.5, in blue). Therefore, the more conservative fixed variance was retained, which involved use of the square root of the mean squared error from the regression analysis (Figure 5.5, in green).

For σlnCL, the addition of the $(log(age))^2$ term not only improved the normality test, but also improved the *modified Breusch-Pagan* test (Table 5.5).

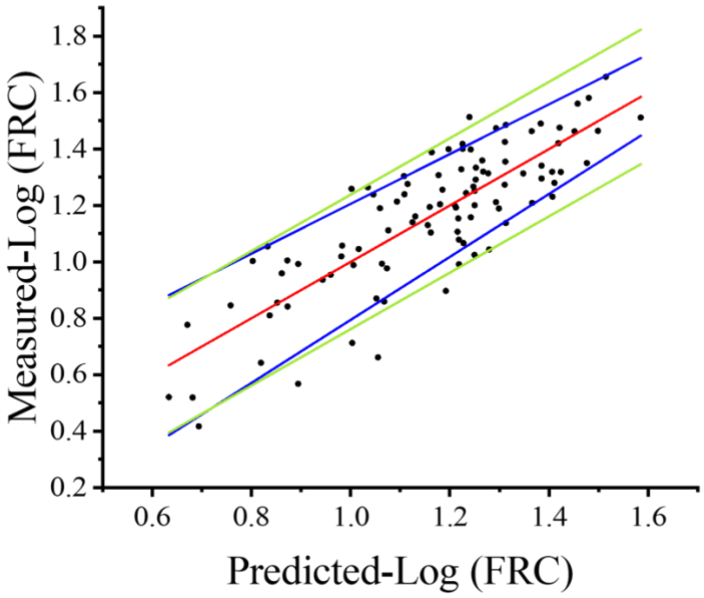


Figure 5.5. Measured log(FRC) against predicted log(FRC): the blue line represents the fitting of the SD as a function of log(FRC)(variable SD), while the green line depicts the more conservative method of SD calculation (square root of the mean squared error from the regression analysis, hence a fixed SD). The red line corresponds to the predicted log(FRC). The plot represents a 95% confidence interval for both approaches.

Table 5.5. Normality and heteroscedasticity tests of the data for the 98 participants.

Parameters		Shapiro-Wilk	Kolmogorov	Modified Breusch-Pagan	Breusch-Pagan
log(FRC)	Statistic	0.984	0.600	4.208	3.616
	p-value	0.260	0.200	0.040	0.057
log(V_D)	Statistic	0.989	0.050	1.181	1.026
	p-value	0.577	0.200	0.277	0.311
σV_D	Statistic	0.985	0.052	3.726	3.071
	p-value	0.316	0.200	0.054	0.080
σlnC_L	Statistic	0.973	0.076	4.989	3.183
	p-value	0.038	0.194	0.026	0.074
σlnC_L^*	Statistic	0.988	0.047	2.234	1.607
	p-value	0.510	0.200	0.135	0.205

log(FRC), natural logarithm of the functional residual capacity; log(V_D), natural logarithm of dead space volume (end-inspiratory); σV_D, SD for the standardised dead space; σlnC_L, SD for the natural logarithm for the standardised lung compliance; σlnC_L^*, refitted σlnC_L with addition of the $(\log(age))^2$ term.

5.3.5 Regression parameters

Table 5.6 lists the regression parameters for the 98 participants. For log(FRC) and log(VD), all independent predictors were significant and remained in the model:

$$log(FRC)_i = 1.460 + 0.133 * log(age)_i + (-0.107) * isFemale + 2.979 * log(height)_i + (-0.759) log(BMI)_i \quad \text{(Equation 5.2)}$$

$$log(VD)_i = (-1.808) + 0.259 * log(age)_i + (-0.276) * isFemale + 1.379 * log(height)_i + (-0.550) log(BMI)_i \quad \text{(Equation 5.3)}$$

in which *i* represents a participant.

It was observed that log(FRC) exhibited a linear increase with log(age) and log(height), and a linear decrease with log(BMI) and isFemale. Figure 5.6 shows the relationship between the FRC and its predictors (age, height, sex, BMI). It illustrates the linear regression models after the exponentiation of both sides of the equation. To visualise this dependency, all independent predictors were adjusted to those of a "standard man", except for the predictor parameter of interest. The “standard man” used was derived from data for a hypothetical man according to the International Commission for Radiological Protection (ICRP): a 25-year-old male, 1.8m tall, with a BMI of 21.6 $kg.m^{-2}$ [149, 150]. The shapes of the curves were determined by the α, β and γ coefficients in the linear model. For example, if the effect of age on log(FRC) was under study, the equation would look like:

$$log(FRC) = 1.460 + 0.133 * log(age)_i + 2.979 * log(1.8) + (-0.759) * log(21.6) \quad \text{(Equation 5.4)}$$

in which $log(age)_i$ represents the participant’s age.

Figure 5.7 shows my exploration of the relationship between FRC and BMI after removal of the two participants with the greatest BMIs (34 and 40 $kg.m^{-2}$) from the cohort. This adjustment was made because the relationship depicted in Figure 5.6.C (log(BMI) and log(FRC)) seemed to be heavily skewed by these two outliers with very high BMIs and this may have obscured the true relationship. However, after re-exploration of the regression analysis without these outliers, a linear decrease with log(BMI) was still evident. This indicated that the observed relationship between log(BMI) and log(FRC) was robust and persisted even after removal of the extreme BMI values. Below is the equation that was used for the adjusted regression analysis:

$$log(FRC)_i = 1.4685 + 0.126 * log(age)_i + (-0.106) * isFemale + 2.952 * log(height)_i + (-0.754) * log(BMI)_i \quad \text{(Equation 5.5)}$$

Log(V_D) was found to vary with all the independent variables in the same way as log(FRC). Figure 5.8 illustrates the relationship of V_D with all its independent predictors (age, height, sex, BMI). To visualise this dependency, all independent predictors were fixed to those of the standard man, except for the predictor parameter of interest.

For σV_D, each independent predictor was significant except for log(height):

$$\sigma VD_i = 0.254 + (-0.052) * log(age)_i + 0.030 * isFemale + 0.087 * log(BMI)_i \quad \text{(Equation 5.6)}$$

For $\sigma \ln C_L$, the only significant predictor was age:

$$\sigma lnCL_i = 1.684 + (-0.750 * log(age)_i) + (0.116 * (log(age))_i^2) \quad \text{(Equation 5.7)}$$

It was found that σVD exhibited a linear decrease with log(age) and an increase with log(BMI) and with isFemale. Figure 5.9 illustrates the relationship of σVD with its predictors (age, sex, BMI). To visualise this dependency, all independent predictors were fixed to those of the standard man, except for the predictor parameter of interest.

On the other hand, σlnCL displayed a positive curvilinear relationship with an overall function of age. Figure 5.10 illustrates the relationship of σlnCL with its only independent predictor, age.

Table 5.6. Regression model output parameters

Parameters		Constant	log (age)	$(\log(age))^2$	log (height)	log (BMI)	isFemale	Sqrt (MSE)
log(FRC)	coefficient	1.460	0.133	-	2.979	-0.759	-0.107	0.1449
	p- value	0.002	< 0.001	-	< 0.001	< 0.001	0.02	
log(VD)	coefficient	-1.808	0.259	-	1.379	-0.550	-0.276	0.1788
	p- value	0.001	< 0.001	-	0.004	< 0.001	< 0.001	
σVD	coefficient	0.254	-0.052	-	-	0.087	0.030	0.0547
	p- value	0.054	< 0.001	-	-	0.046	0.032	
σlnCL	coefficient	1.684	-0.750	0.116	-	-	-	0.0774
	p- value	0.004	0.023	0.011	-	-	-	

BMI, body mass index; sqrt (MSE), square root of the mean squared error; log(FRC), natural logarithm of the functional residual capacity; log(VD), natural logarithm of dead space volume (end-inspiratory); σVD, SD for the standardised dead space; σlnCL, SD for the natural logarithm for the standardised lung compliance.

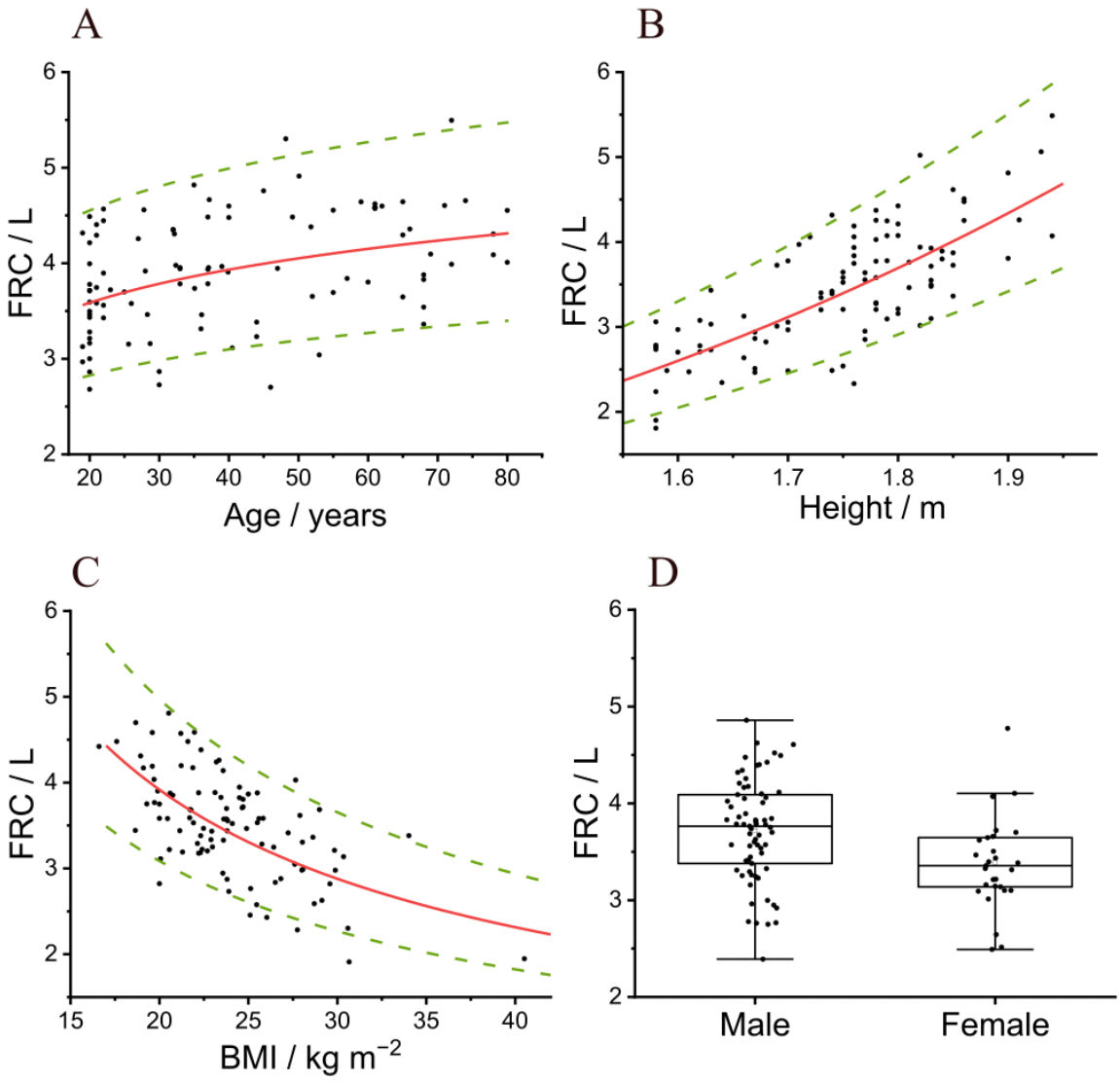


Figure 5.6. Linear regression model results for variation of FRC with age, BMI, height and sex. Where exemplar variation is not plotted, age, BMI and height are for a 25-year-old male with a BMI of 21.6 kg.m^{-2}, who is 1.8m tall. The red line represents the prediction equation from the regression analysis. The dotted lines on either side of the solid red line represent a 95% confidence interval of the model. A: the linear relationship between age and FRC. B: the linear relationship between height and FRC. C: the inverse relationship between BMI and FRC. D: the relationship with sex and FRC, which is at lower values in females.

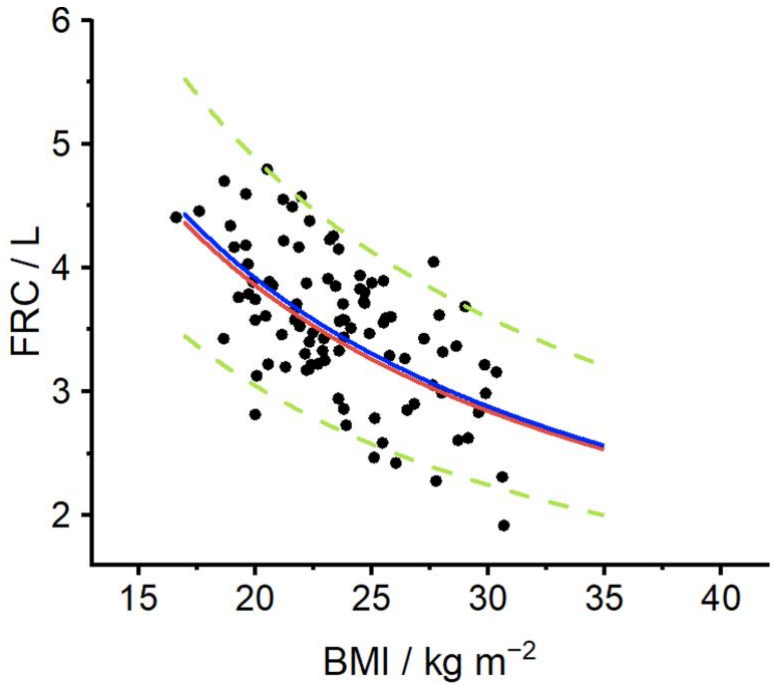


Figure 5.7. Linear regression model results for variation of FRC with BMI after removal of the two highest BMIs. Where exemplar variation is not plotted, age and height are for a 25-year-old male, who is 1.8m tall. The red line represents the prediction equation from the regression analysis after removal of the two highest BMIs. The blue line represents the prediction equation from the original regression analysis, which included all BMI values. The dotted lines either side of the solid red line represent a 95% confidence interval of the model. The figure shows a clear inverse relationship between BMI and FRC. Additionally, it shows that the prediction equations are almost identical, regardless of whether the two highest BMI values are included in or removed from the analysis.

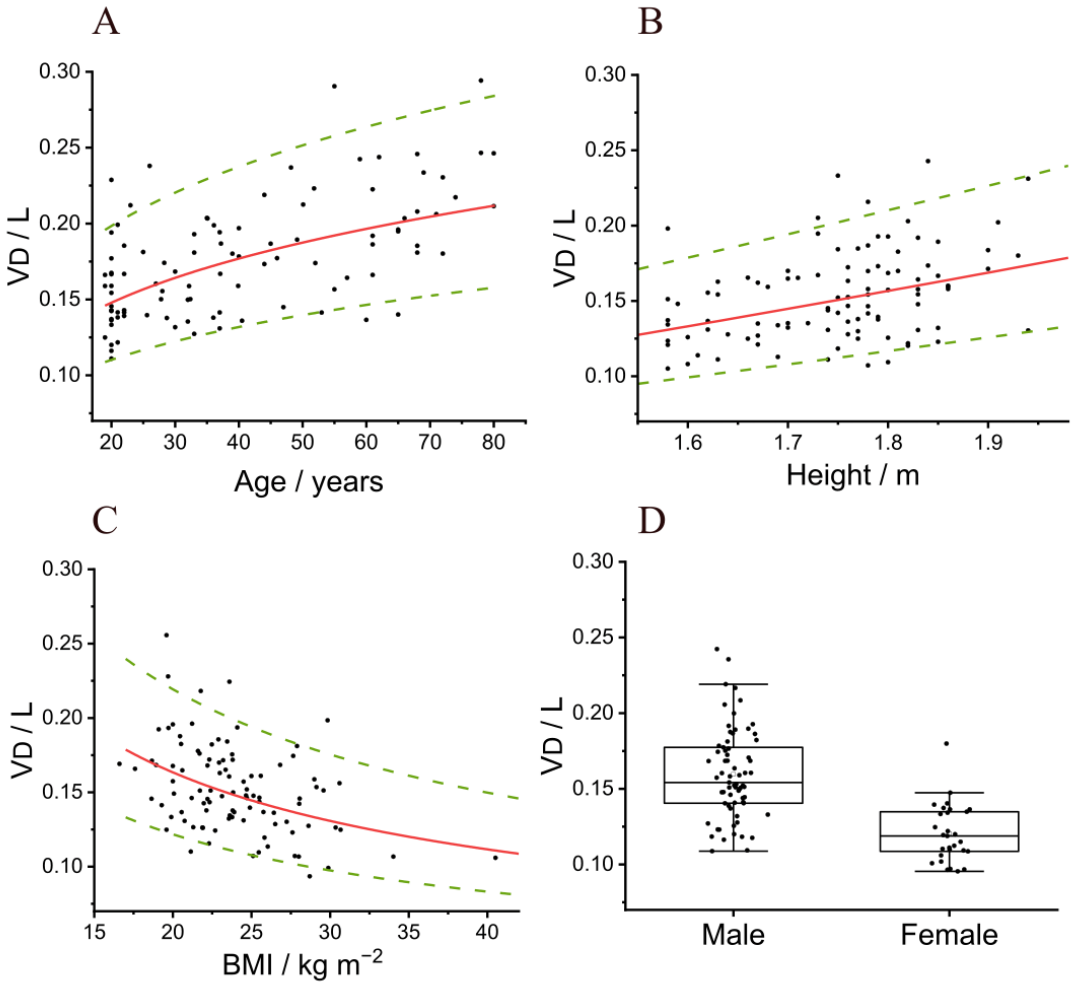


Figure 5.8. Linear regression model results for variation of VD with age, BMI, height and sex. Where exemplar variation is not plotted, age, BMI and height are for a 25-year-old male with a BMI of 21.60525 kg.m^{-2}, who is 1.8m tall. The red line represents the prediction equation from the regression analysis. The dotted lines on either side of the solid red line represent a 95% confidence interval of the model. A: the linear relationship between age and VD. B: the linear relationship between height and VD. C: the inverse relationship between BMI and VD. D: the relationship between sex and VD, which is at lower values in females.

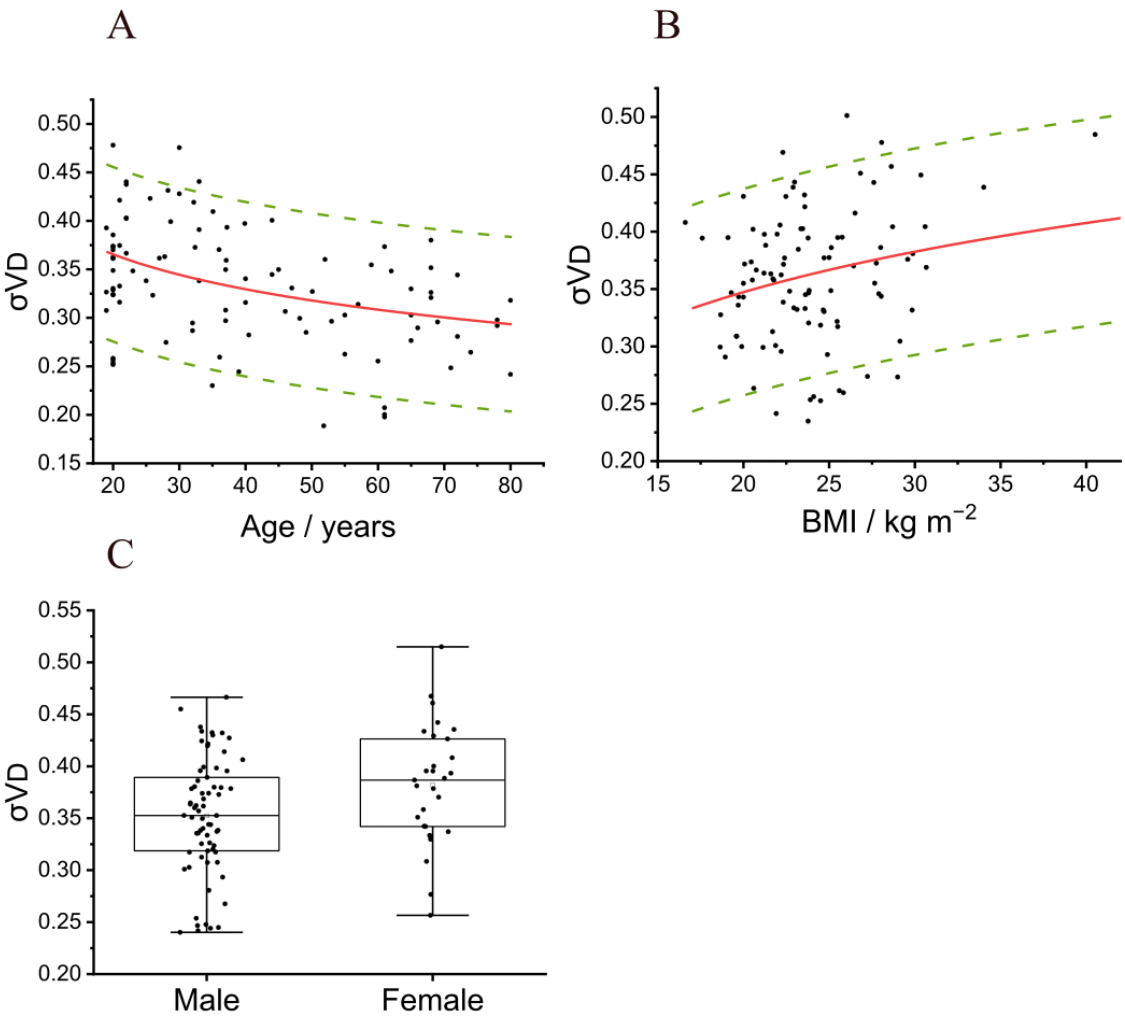


Figure 5.9. Linear regression model results for variation of σVD with age, BMI and sex. Where exemplar variation is not plotted, age and BMI are for a 25-year-old male with a BMI of 21.60525 kg.m^{-2}. The red line represents the prediction equation from the regression analysis. The dotted lines on either side of the solid red line represent a 95% confidence interval of the model. A: the inverse relationship between age and σVD. B: the linear relationship between BMI and σVD. C: the relationship between sex and σVD, which is at higher values in females.

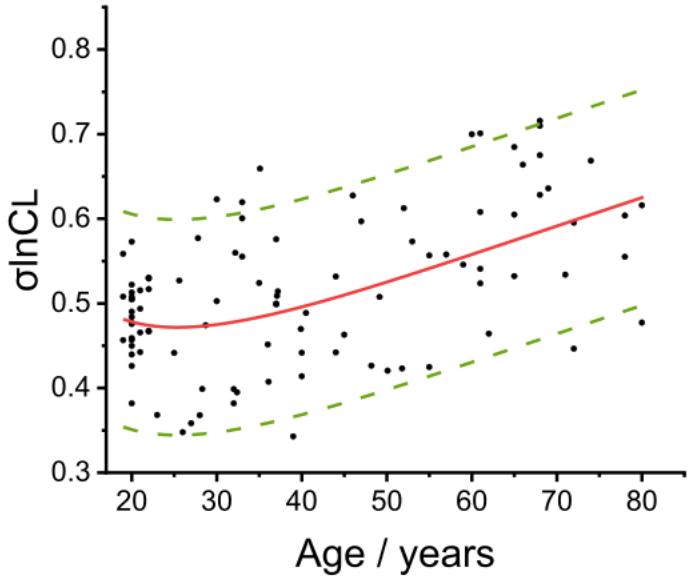


Figure 5.10. Linear regression model results for variation of σlnCL with age. The solid red line represents the prediction equation from the regression analysis. The dotted lines on either side of the solid red line represent a 95% confidence interval of the model.

5.3.6 Z-scores

The development of the regression equations enabled us to derive predicted parameter values for individual cases, with consideration of the factors age, BMI, height and sex. The homoscedastic errors (the constant variance of the errors) that were associated with the equations enabled the use of the square root of the mean squared error as a variance. To convert these data into a metric for the assessment of abnormality in lung inhomogeneity, Z-scores for each parameter were computed for any participant through the use of the following formula:

$$Z = \frac{x-\mu}{\sigma} \qquad \text{(Equation 5.8)}$$

in which Z was the standard score, x the observed participant value, μ the predicted value from the regression model for a given participant (the prediction equation for each CCP parameter), and σ was the SD of the output parameter distribution (square root of the mean squared error).

Figure 5.11 shows the Z-scores for the healthy cohort (n=98). The goal was to describe the airways solely in terms of a series of Z-scores. These scores indicated by how many SDs a value deviated from the mean, thereby normalising data to a distribution with a mean of 0 and an SD of 1. In Figure 5.12, the Z-scores of the healthy cohort CCP parameters are shown. They display an approximately normal distribution, with mean (μ) values centred on 0. All observations fell within 3σ of μ (confidence interval of 99.7%).

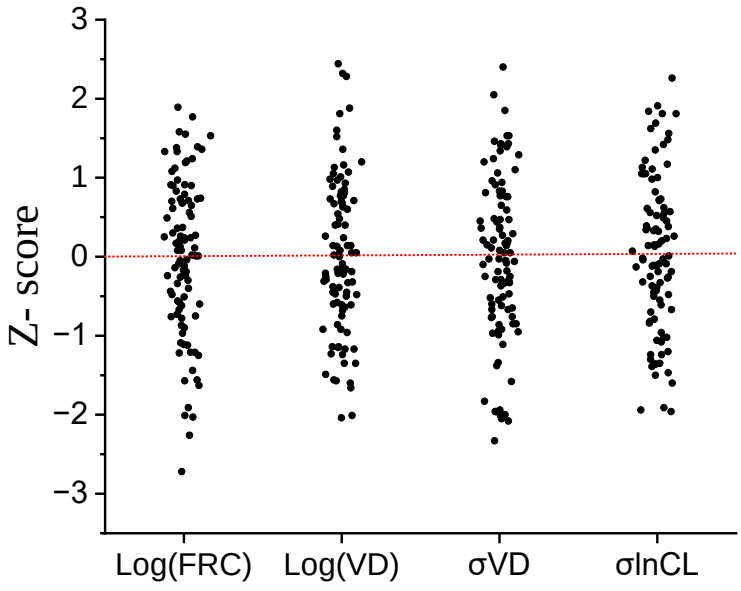


Figure 5.11. Z-scores for each CCP parameter for the healthy controls cohort (n=98).

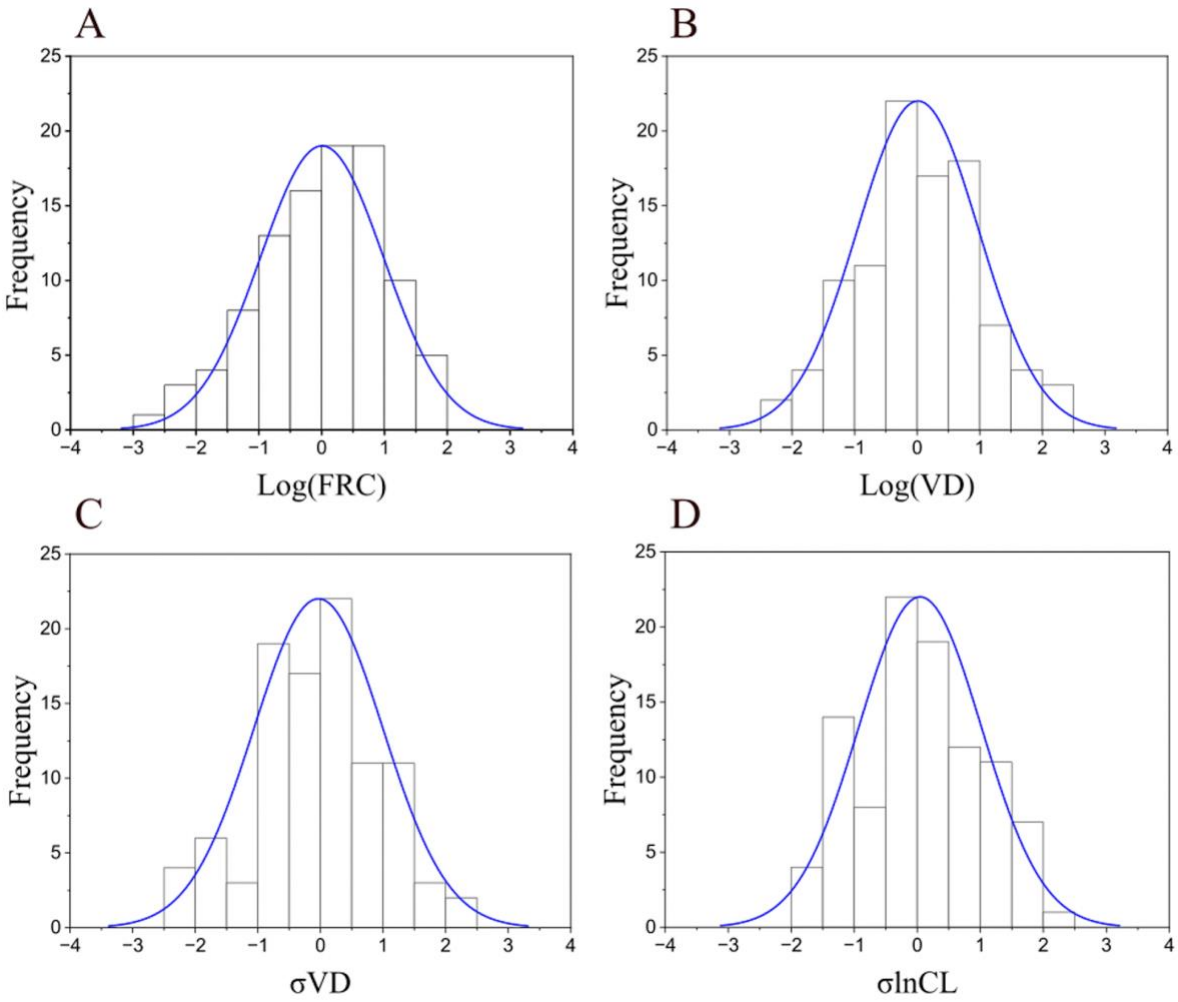


Figure 5.12. Plotted histograms for the calculated Z-scores for A: log(FRC); B: log(VD); C: σVD; and D: σlnCL. The curves represent normal distributions.

5.4 Discussion

5.4.1 Z-scores and PFTs

In PFTs, Z-scores are used to standardise different measurements to make them comparable regardless of the original units or scales used. A Z-score is a statistical measurement that describes a value's relationship to the mean of a group of values, measured in terms of SDs from the mean (Equation 5.8). Z-scores indicate by how much an observed value deviates from the predicted value, taking into consideration factors such as an individual's age, sex, height and ethnicity, and are expressed in terms of SDs. Z-scores are

particularly useful in clinical practice to simplify the interpretation of test results relative to a normal population. This tailored standardisation helps to better identify any deviations from the expected normal values, and therefore to facility the diagnosis and the monitoring of respiratory diseases. For instance, a Z-score of below -1.645 indicates that a patient's lung function is below the fifth percentile of the healthy population, which is taken as clinically significant [100, 162, 163].

While Z-scores are commonly used in respiratory medicine, other methods for standardizing test result interpretations exist. For example, T-scores are primarily used in the context of bone density measurements, such as those obtained from dual-energy X-ray absorptiometry (DEXA) scans. T-scores offer the same advantage as the Z-scores but differ in how the *SD* in the formula is calculated. For a Z-score, the *SD* is calculated from the reference data, whereas for a T-score, the *SD* is derived from a small set of repeated measurements on an individual. In a DEXA scan, the clinician compares the individual's average and SD with those of a young, healthy population. With T-scores, an individual's bone density is compared with the average peak bone density of a healthy young adult population, rather than an age-matched population. This comparison is useful for the diagnosis of conditions such as osteoporosis, in which a T-score of -2.5 or lower indicates osteoporosis [162-165]. In contrast, for lung function tests, the individual's measurements are compared with predicted values based on people of similar sex, age and height.

A Z-score of -1.645 corresponds to the fifth percentile, meaning that 95% of healthy individuals will have values above this threshold. This Z-score is set as the lower limit of normal (LLN). Defining the LLN as -1.645 SD helps with the identification of individuals who may have clinically significant deviations from normal lung function. Similarly, a Z-score of +1.645 corresponds to the 95^{th} percentile, which is set such that 95% of healthy individuals will have values below this threshold. This Z-score is set as the upper limit of normal (ULN).

The use of Z-scores in CCP parameters, such as σVD and σlnCL, is usually focused on the ULN, +1.645SD, rather than -1.645SD, the LLN. For σVD and σlnCL, which represent the SD of the normal distribution for (normalised) dead space across lung volume and the SD of log-normal distributions for (normalised) alveolar compliance, respectively, the higher the value, the more variation there is. Greater variation in dead space across lung volume (σVD) or alveolar compliance (σlnCL) indicates a sicker, more inhomogeneous lung. In contrast to σVD and σlnCL, parameters such as FRC and VD utilise both the LLN and ULN as they are actual, measured values. For example, FRC increases with age, typically in obstructive lung and small-airway diseases, and decreases in restrictive lung diseases. This observation is further discussed in Chapter 7 in the context of post-COVID-19 survivors.

The application of Z-scores to set thresholds in PFTs enables effective interpretations of CCP parameters, which ensure that clinically significant deviations are identified while a robust framework is maintained for the assessment of lung health across different patient populations.

5.4.2 The global lung initiative approach vs. the approach employed in this thesis

The small number of members of the healthy cohort in this study limited what was possible for the determination of normal ranges. In response, I opted for transforms of the CCP parameters, to ensure that the residuals were normally distributed. This approach enabled us to define the Z-scores under the assumption of normal distribution. In situations with a larger number of observations, it would be feasible to employ more sophisticated non-parametric approaches, such as the global lung function initiative (GLI) [166].

To derive GLI reference equations, the lambda-mu-sigma method and the generalised additive models of location, shape and scale programmes were used in the software program R (the lambda-mu-sigma method is an extension of regression analysis). Data from 17 centres were submitted and reference equations were derived from 7190 observations that had been

taken from participants of European ancestry who were between the ages of five and 80 years. For example, for FRC, the derivation involved two reference equations, one for males and another for females.

The FRC reference equation for males was:

$$FRC\ predicted = exp(-13.4898+0.1111*log(age)+2.7634*log(height)+Mspline)$$ [166]

The FRC reference equation for females was:

$$FRC\ predicted = exp(-12.7674+0.1251*log(age)+2.6049*log(height)+Mspline)$$ [166]

If these equations were logarithmically transformed, they would assume a linear relationship except for *Mspline*, which is a factor that displays some fluctuation but consistently remains below 5% for participants aged between 6.5 and 70 years. Given that the majority of the control cohort fell within the age range of 19 to 80 years, with an average age of 40 and an SD of 19 years, the *Mspline* factor was omitted. Consequently, the GLI reference equations would be expressed as:

for males:

$$log(FRC) = 0.1111*log(age)+2.7634*log(height)+(-13.4898)$$ (Equation 5.9)

and for females:

$$log(FRC) = 0.1251*log(age)+2.6049*log(height)+(-12.7674)$$ (Equation 5.10)

Notably, the derivers of the GLI equations did not incorporate BMI as a predictor in their equations [166]. However, numerous other studies have examined the impact of BMI on lung function, specifically on FRC [146, 167], have consistently reported a significant curvilinear relationship between BMI and FRC. Therefore, BMI was included as a predictor in this equation (Equation 5.1). This decision was supported by my review of the examined healthy cohort data (Figure 5.6C). Figure 5.13, which is taken from *Jones et al.* (2006) [168], clearly shows a curvilinear decline in FRC with BMI. For this reason, I opted for the natural logarithm of BMI. I also used the natural logarithms of height and age, following the approach of GLI prediction equations [166].

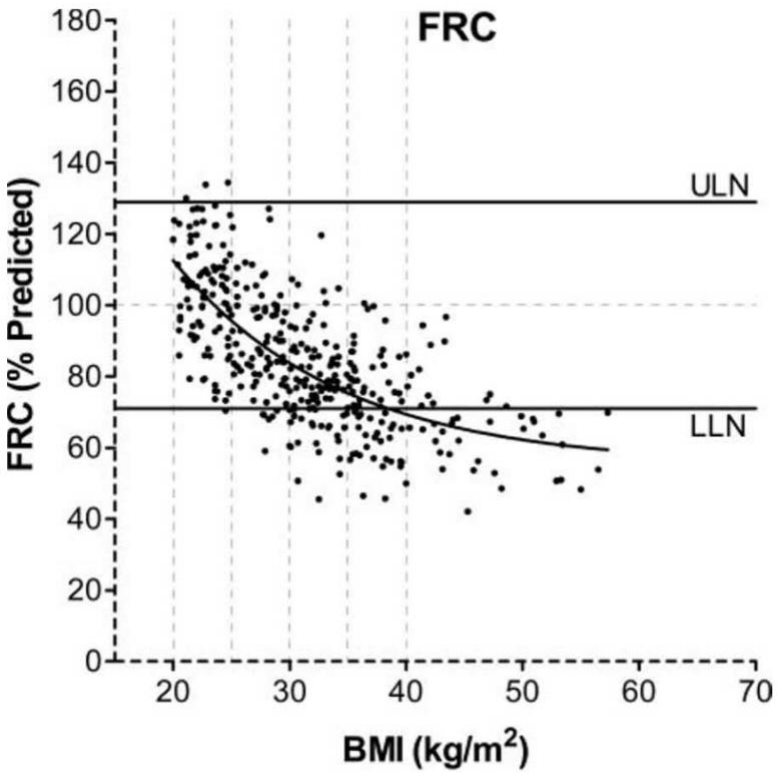


Figure 5.13. *Jones et al.* (2006) [168] showed the curvilinear decline in FRC with increased BMI (showing a less steep change with BMI >30 $kg.m^{-2}$) [168]. ULN; upper limit of normal; LLN; lower limit of normal.

5.4.3 Comparison with findings in the available literature and exploration of the effects of physical characteristics

A comparison of the outcomes of my regression analysis concerning FRC showed that my findings aligned with those in the literature. In this cohort, FRC demonstrated an increase with age (Figure 5.6A). Senile hyperinflation or emphysema is a physiological phenomenon that involves age-related deterioration of the lung parenchyma or the loss of supportive structures within the parenchyma itself [169]. The changes in lung structure are predominantly attributable to an enlargement of the alveolar space, which occurs without any accompanying inflammation or destruction of the alveolar walls. This degeneration contributes to the enlargement of airspaces. The decrease in amounts of supporting tissue results in the premature closure of small airways during normal breathing, which leads to air trapping and hyperinflation, which in turn increases FRC [169, 170]. Previous studies have reported that lung volume increases with the cube of height [171]; this finding aligns with the observation that FRC increases with height (Figure 5.6B). Increased amounts of body fat have been linked with reductions in lung volumes [167, 168, 172, 173], and these reports are consistent with the finding in my study that FRC decreases with increasing BMI (Figure 5.6C).

In obesity, the mechanical properties of the lungs and chest wall change significantly due to the accumulation of fat in the mediastinum and abdominal cavities. These alterations lead to elevated intra-abdominal pressure, which subsequently results in a rise in intra-thoracic pressure that affects the breathing pattern and causes a substantial reduction in FRC [172, 173]. According to *Jones et al.* (2006) [168], the severity of FRC reduction is not linear with the degree of obesity, and the greatest effect occurs at BMI values $<30 kgm^{-2}$ (Figure 5.12) [168]. In some cases of obesity, the decrease in FRC is clinically significant and reaches a point at which FRC approaches residual volume (RV) [167]. RV is the volume of air that is retained in the lungs after a maximum exhalation. It signifies the portion of air that cannot be intentionally

expelled [89]. In this cohort, FRC was lower in females than males (Figure 5.6D). This might be attributable to the volume and configuration of the female ribcage, the size of which is proportionally smaller than that of males and causes females to have smaller lung volumes than males [174].

FRC is a common lung function parameter that falls between the CCP and the GLI study of static lung volumes. Through the use of the GLI equation to calculate predicted FRC values for the 98 participants included in this project, I found that the average predicted volume was only 1% (30ml) smaller than the measured volume. The SD for the difference between predicted and measured volumes was 0.53l and led to the calculation of a coefficient of variation of 16.1%. In comparison, using my equation, which was developed using this dataset, the SD for the difference between predicted and measured volumes was lower at 0.44l, which corresponded to a coefficient of variation of 13.3%. One key difference between the two approaches was that the GLI did not include BMI as a predictor. When I recalculated my equation to predict FRC without the inclusion of BMI, the SD for the difference between predicted and measured values increased to 0.52l, which yielded a coefficient of variation of 15.7%. Thus, the omission of BMI as a predictor in the GLI equation seems to be the primary cause of the higher coefficient of variation in the *Jones et al.* (2006) results compared with mine. This finding aligned with the well-recognised influence of BMI on FRC [168].

Sandhu et al. (2023) [119] compared the FRC that they obtained through the use of the same novel technology that was used in the work for this thesis (CCP) to a known measure, Exhalyzer D [152], by measuring the FRC in two different cohorts: 13 healthy controls and nine participants with CF. Their results illustrated that the application of the two techniques gave very similar results, with a very small mean difference of 40 ml [119].

Unlike FRC, there are no large-scale datasets available for V_D, the dead space volume at end-inspiration. However, it is noteworthy that the predictors (age, height, BMI and sex)

produced similar effects in this study on both VD and FRC, which indicated comparable influences on these two volumes. Regarding VD, my data concur with those of Fowler's classic study [146] on dead space, which reported average values of 0.156l for 45 males and 0.104l for four females [146]. These values aligned closely with our predictions of 0.155l for males and 0.102l for females when the average age, height and weight of *Fowler's* participants were applied. My data are consistent with findings in the literature regarding dead space, which tends to increase with height [146] (Figure 5.8A). For instance, *Tusman et al.* (2013) [175] conducted a study in which non-invasive volumetric capnography was applied to 66 participants. They reported that physiological dead space increased with height (Figure 5.14). Similar trends were observed in my results. These trends indicate a direct relationship between VD and height (Figure 5.8B). Additionally, my findings showed that VD was comparatively smaller in females (Figure 5.8 D). Sexual dimorphism in the human skull has implications for the upper airway structure. On average, males have larger skeletal cranial airways than females. In terms of the pharynx, there are sex-related differences in size and resistance, with males having a larger cross-sectional area than females. The tracheal cross-sectional area is also 29% larger in males than in females [174, 176].

In alignment with a previous study that employed the same technology [104], my observations reveal a notable increase in σlnCL, an intrinsic marker of ventilation inhomogeneity, with advancing age (Figure 5.10). This outcome underscores the significance of age as the primary parameter that influences σlnCL. This discovery holds particular value for an index that is characterised as having the capacity to define an individual in relation to both "lung age" and the "presence of airway disease" [139, 140, 155]. The identification of age as a significant factor that affects σlnCL enhances the understanding of its implications for the assessment of the presence of airway disease and provides a foundation for further research in this domain.

Conversely, σVD, the SD of the normal distribution for (normalised) dead space to alveolar volume at FRC, exhibited a linear decrease with age (Figure 5.9A) [104].

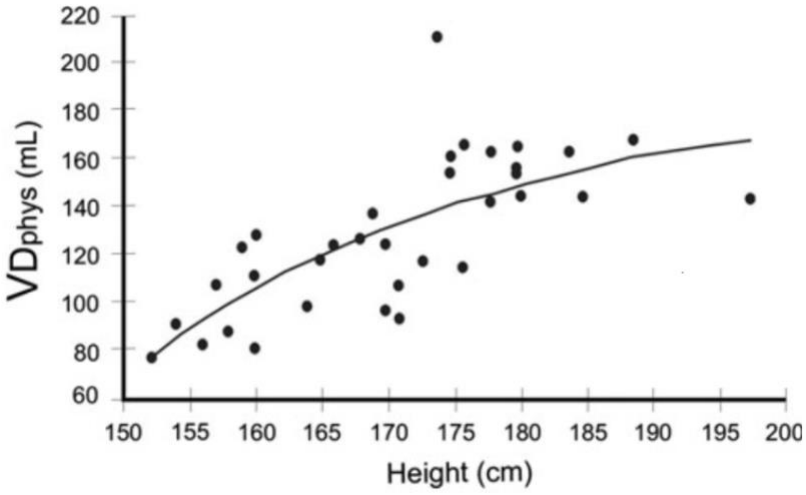


Figure 5.14. *Tusman et al*. (2013) [175] demonstrated the relationship between physiological dead space (VDphys) and height. The functional association between VDphys and height was established through regression analysis.

5.5 Research limitations

One limitation of the use of regression models in this study stems from the sample size. We expect to refine this model as more data from healthy volunteers are gathered. It is hoped that this will lead to a progressive improvement of the normal range and increased confidence in the regression model.

Notably, all volunteers who were included in the study fell within the age range of 18 to 80 years, which is typical for individuals who participate in clinical trials. Furthermore, the majority of the cohort was white Caucasian and predominantly Oxford residents with semi-active lifestyles. Additionally, lung function measurements were available for only 31 of the

98 participants; having spirometry measures for all participants would have strengthened the data. In future investigations, the inclusion of controls below the age of 18 years would facilitate the exploration of normal values and Z-scores and would particularly benefit studies that involved paediatric patients. The concentration of healthy volunteers around the modal age of 20 was due to the substantial student population in Oxford. Expansion of recruitment to include more volunteers who were older than 20 years would enhance the reliability of age-dependent trends that were identified in the regression models.

5.6 Conclusion

The behaviour exhibited by the regression models aligned closely with patterns documented in the literature concerning the general population. These models are expected to serve as valuable tools in forthcoming studies, as their use will enable the quick evaluation of CCP lung inhomogeneity parameters and facilitate potential diagnostic applications. Their reliability and consistency make them promising assets in the efficient assessment and diagnosis of conditions related to lung function.

Future work should aim also to diversify the demographic profile of the cohort to include a broad range of ethnic backgrounds and lifestyle variations. This would help to generalise the findings and enhance the applicability of the regression models across different populations. Additionally, the integration of comprehensive lung function tests for all participants would provide a more robust dataset and therefore support the development of more accurate and reliable predictive models.

Chapter 6. Lung inhomogeneity parameters in type-2 high asthma and the effect of therapeutic interventions

6.1 Introduction

The work described in this chapter focuses on data collected from T2-high asthma patients at the severe asthma clinic. T2-high asthma, which is discussed in more detail in Chapter 2, accounts for approximately 50% of all asthma patients and likely represents an even higher proportion of those with severe asthma. This subtype is characterized by elevated levels of type-2 inflammation biomarkers, such as FeNO and BEC. These biomarkers are useful for tracking disease activity and treatment response. Indeed, T2-high asthma, has clearly defined, targeted treatments, such as corticosteroids and biologics, to which patients typically respond well. These patients also represent the highest percentage of those seen in the severe asthma clinic, making them a good focus for further clinical research.

Despite the effectiveness of targeting type-2 inflammation with treatments like corticosteroids and biologics, there remains a lack of precise physiological measures that consistently track disease activity and treatment response within the lungs.

6.1.1 Research aims and hypothesises

This study was designed to evaluate the utility of CCP in severe T2-high asthma and to understand how CCP parameters correlated with other disease markers, such as levels of inflammatory biomarkers, symptoms or other lung function measures. Additionally, I sought

to explore the effects of therapeutic interventions in asthma on measures of lung inhomogeneity through the application of CCP.

More specifically, this project sought to test the following key hypotheses related to T2-high asthma:

- some or all of the parameters identified by CCP in severe asthma fall outside the normal ranges that were identified in Chapter 5;
- the values that can be calculated through consideration of some or all of the parameters identified by CCP correlate with symptoms, exacerbations and other biomarkers of T2-high asthma;
- the values of some or all of the parameters identified by CCP correlate with those found in spirometry; and,
- the values of some or all of the parameters identified by CCP are affected by bronchodilation.

For a sub-cohort of patients with T2-high asthma who were starting biological therapy, this project sought to investigate the following additional considerations, such as whether:

- CCP parameters changed after biological therapy that lasted over three or four months (i.e. early changes in CCP parameters post-biologics);
- changes in CCP parameters after biological therapy were related to changes observed through the use of spirometry and changes in recognised markers of T2-high inflammation. It was hypothesised that any early signal identified by CCP would correlate with the magnitude of responses observed in spirometry and changes in levels of markers of T2-high inflammation; and,
- there might be some relationship between any early response signal in CCP parameters and the clinical response at one year, even though the study was not powered to examine clinical outcomes.

6.2 Methods

6.2.1 Participants

6.2.1.1 Recruitment of participants

This was an observational study performed at a specialist asthma outpatient clinic of a hospital. Participants were studied under ethical approval reference 17/SC/0172. This approval allowed for the study of patients with airway diseases, including access to their clinical notes and data obtained for clinical purposes, which were used for research. This study was undertaken alongside the clinical care pathway of the Oxford Special Airway Clinic at the John Radcliffe Hospital.

Typically, this clinic handles patients with difficult and uncontrolled airway problems. Patients are initially characterised/phenotyped according to whether they have T2-high asthma (typically shown in the form of FeNO levels >50ppb and BECs >300/µl) or T2-low asthma.

For the purpose of this study, T2-high asthma patients who were being treated according to GINA 4 or 5 treatment guidelines (but had not yet started biological therapy) [28] were identified and recruited from the clinic for this work and studied at baseline. A subset of these patients proceeded to receive biological therapy if they met National Institute for Health and Care Excellence (NICE) criteria for anti-interleukin (IL)-5 therapy (benralizumab or mepolizumab) [61, 68]. These participants attended the clinic at two-time points: the baseline visit, at which they received their first biological drug injection, and three or four months later for follow-up, when they received their fourth biological drug injection. The timing of the follow-up depended on which biological drug they were on, either mepolizumab (three months) or benralizumab (four months).

These participants also underwent clinical reviews one year after they had started biologics to evaluate their response to the therapy.

6.2.1.2 Inclusion criteria

Participants were required to fulfil the following requirements.

- Male or female aged 18 years or over.
- Willing and able to provide informed consent for participation in the study.
- Established diagnosis of asthma, identified from the clinic as having severe type-2 high asthma on GINA Step 4 or 5.

6.2.1.3 Exclusion criteria

- Inability to tolerate mouthpiece/nose clip
- Major abdominal surgery in the previous three weeks
- Pregnancy
- Significant cardiac disease
- Current exacerbation of respiratory disease

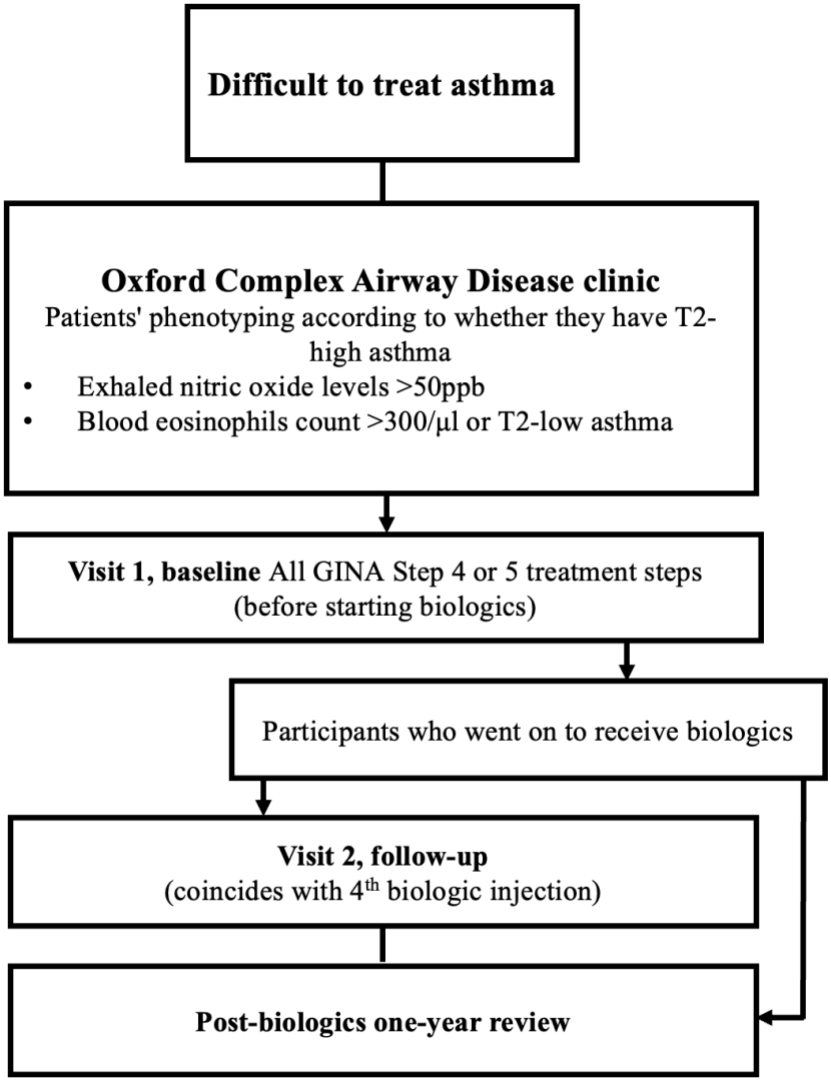


Figure 6.1. CCP research pathway for T2-high asthma patients. This research pathway followed the clinical care pathway of T2-high asthma patients who underwent biological therapy (mepolizumab or benralizumab) at Oxford's clinic for complex airway diseases.

6.2.2 Study protocol

All patients gave informed consent to the primary researcher, before they participated in the study. In the clinic, all the spirometry measurements are quality-assured and of sufficient calibre to be utilised for this study. All the complex airway nurse practitioners have undergone training by the ARTP. Additionally, I hold the Registered Pulmonary Function Technologist (RPFT) credentials from the National Board for Respiratory Care (NBRC). To maintain accuracy and reliability, the spirometers are subject to annual checks by clinical engineers and

are calibrated before each use through the use of a 3-liter syringe, in line with ARTP guidelines [95]. The clinic has developed a standard practice procedure for spirometry based on ARTP guidelines.

6.2.2.1 Baseline and follow up visit.

At each visit, the participant undertook (Figure 6.2):

- a FeNO measurement (discussed in Chapter 2), using the NIOX-VERO machine;
- blood tests to obtain complete blood counts, from which the blood eosinophil count (BEC) was obtained (discussed in Chapter 2);
- completion of the ACQ-5, a score for which is determined by averaging the responses to five questions, which cover issues such as symptoms that occur during the day or night, activity limitations and the use of rescue medication [177-179]. Figure 6.3 [180] shows the five symptom questions that were asked during the visits. Each question has a score from 0 to 6. This is the standard questionnaire used in the Oxford Special Airway clinic to assess symptoms;
- a spirometry test (covered in Chapter 2) according to standard practice, i.e. FEV_1 and FVC are measured and the FEV_1/FVC ratio is calculated. In accordance with the British Thoracic Society standard-of-practice, quality-assured diagnostic spirometry protocols [94], the spirometry test involved the completion of three technically acceptable and two repeatable forced manoeuvres; and
- lung inhomogeneity tests (covered in detail in Chapter 4) to measure multiple lung inhomogeneity parameters.

At each visit, two measurements of lung inhomogeneity and spirometry are made, one prior to the administration of salbutamol (400μg) inhaled through a spacer and one 20 minutes after. This approach enables assessment of the effect of salbutamol administration (i.e. bronchodilation) on the inhomogeneity parameters.

Spirometry, FeNO and the ACQ-5 scoring were performed primarily by the clinical research nurse practitioner or myself. I performed all the CCP experiments. Data that were collected during the research visits were recorded on case report forms and immediately transcribed to the data collection spreadsheet, which was used later for data analysis.

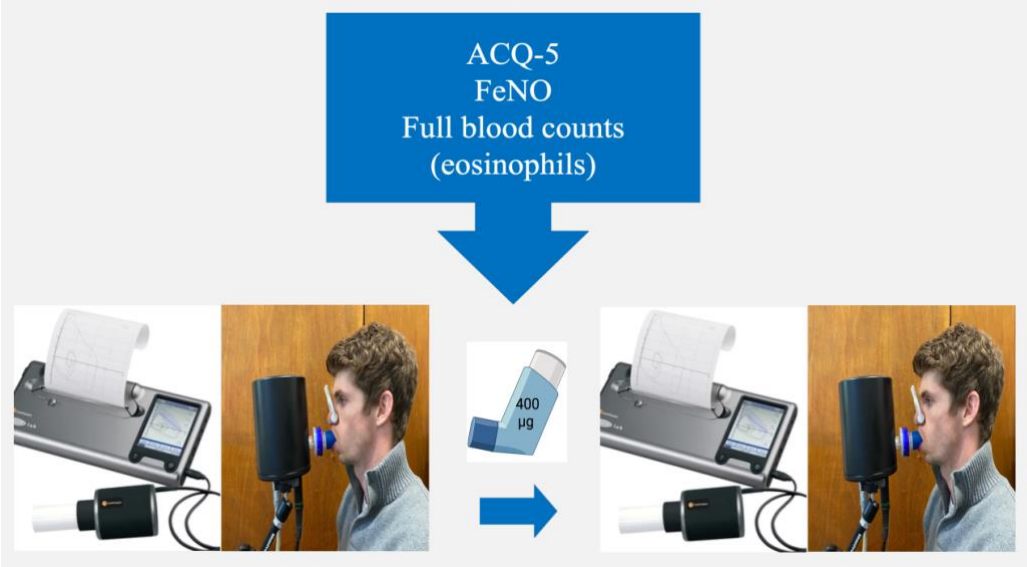


Figure 6.2. Diagram showing protocol and experimental approach at each visit to the airway clinic. The ACQ-5 was completed and measurements of FeNO and complete blood counts were performed at each visit. The participant underwent two measurements of lung inhomogeneity and spirometry, one before and one after the administration of a BD.

Circle the number of the response that best describes how you have been during the past week		
1.On average, during the past week, how often were you woken by your asthma during the night?		
0. Never 1. Hardly ever 2. A few times	3. Several times 4. Many times	5. A great many times 6. Unable to sleep because of asthma
2. On average, during the past week, how bad were your asthma symptoms when you woke up in the morning?		
0. No symptoms 1. Very mild symptoms 2. Mild symptoms	3. Moderate symptoms 4. Quite severe symptoms	5. Severe symptoms 6. Very severe symptoms
3. In general, during the past week, how limited were you in your activities because of your asthma?		
0. Not limited at all 1. Very slightly limited 2. Slightly limited	3. Moderately limited 4. Very limited	5. Extremely limited 6. Totally limited
4. In general, during the past week, how much shortness of breath did you experience because of your asthma?		
0. None 1. Very little 2. A little	3. A moderate amount 4. Quite a lot	5. A great deal 6. A very great deal
5. In general, during the past week, how much of the time did you wheeze?		
0. Not at all 1. Hardly any of the time 2. A little of the time	3. A moderate amount of the time 4. A lot of the time	5. Most of the time 6. All the time

Figure 6.3. The five questions that were used from the ACQ-5 for this study [180].

6.2.2.2 One-year review

All participants who underwent biological therapy were reviewed after one year to assess reductions in exacerbation frequency and OCS use. Medical records were reviewed to gather this information, and participants were contacted directly if data were missing. Exacerbations were defined as any emergency visit or hospital admission due to worsening symptoms, and/or an appointment with a general practitioner that resulted in a prescription for a course of OCS due to symptoms. Exacerbation rates and OCS use were recorded for the year prior to biologics treatment and the subsequent year.

6.2.3 Statistical analysis

All statistical tests were conducted through the use of SPSS software [157] and the results were assumed to be statistically significant at $p<0.05$. CCP parameter Z-scores were calculated using the methods described in Chapter 5. A *Student's t-test* was employed to compare the CCP parameter Z-scores with zero, in order to assess how they differed from the expected values. Additionally, a *chi-square* (X^2) goodness-of-fit test was conducted to examine whether the number of abnormal Z-scores for each CCP parameter differed significantly from the number of observations that would be expected to arise by chance.

To compare two groups of values, *a Mann-Whitney U-test* (for unpaired data) or a *Wilcoxon signed-rank* test (for paired data) was employed if the distribution was determined to be non-normal based on a *Shapiro-Wilk* test. Otherwise, for normally distributed data, either a *Student's* or a *Welch's t-test* was used, depending on whether or not the two groups exhibited similar variances, as determined by an *F-ratio* test. For the comparison of frequencies, to assess the significance of associations between two categorical variables, *Fisher's exact* test was utilised.

To assess the impact of various factors on spirometric and CCP variables, either linear or linear mixed-effects (LME) regression was employed, depending on whether or not repeated observations for one person were being assessed. LME models offer greater flexibility than linear alone as they incorporate all available data while excluding irrelevant sources of variation within a single model. Furthermore, LME models can consider simultaneously the variance associated with multiple independent factors. Their use enables the modelling of both fixed and random effects, in which fixed effects are consistent across populations, and random effects vary from one subject to another [181]. The principles that guided the construction of the LME models are listed below.

A) The dependent parameters were derived from spirometry and CCP and comprised the following variables: FEV_1 / % predicted, FVC / % predicted, FEV_1/FVC, FRC, V_D, σV_D, and $\sigma \ln C_L$ (see Table 3.1, for lung inhomogeneity parameters).

B) The independent factors were whether the measures had been taken pre- or post-BD, baseline BEC, and baseline FeNO and ACQ-5 scores.

C) Random effects factors were incorporated for situations in which the sample did not encompass all possible outcomes and for which a random influence on the data was expected (in this case, participant ID). It allowed for repeated measures taken from one person at both visits to be accounted for in the model.

Several different models were deployed based on the specific analysis requirements (mentioned below). Models that were used to evaluate effects on baseline spirometric or CCP parameters considered binary fixed effects, such as pre- or post-bronchodilation, along with continuous variables such as FeNO, BEC and ACQ-5 scores. Models that were used to assess the impact of biologics on spirometric or CCP parameters also featured binary fixed effects for the visits (before or after biological therapy), the type of biologic, and the interaction term "visit*type of biologic".

The first LME model that was adopted was designed to analyse baseline data in T2-high asthmatics. The independent variables were pre- or post-BD status, baseline BEC, FeNO level and ACQ-5 score. These variables were selected as they represent key indicators of T2-high asthma. The dependent variables were FEV_1/% predicted, FVC/% predicted, FEV_1/FVC, V_D, σV_D, FRC and $\sigma \ln C_L$. In almost all of the analyses presented throughout this chapter, the data included both spirometric and CCP measures, as spirometry is considered the standard practice in asthma assessment. This dual approach ensured a comprehensive evaluation of lung function that would capture both central and peripheral airway abnormalities. The participant

number was added as a random effects factor, for the reasons mentioned before. Therefore, the formulation for the LME model concerning variable x was as follows:

$$\times\sim \text{pre- or post-BD+ BEC+FeNO+ACQ-5+(1|participant ID)} \qquad \text{(Model 6.1)}$$

The second LME model was designed to investigate the effects of biologics. The dependent variables were the same as those used in Models 6.1. The independent variables were pre- or post-BD status, visit type (baseline or follow-up), type of biologic used (mepolizumab or benralizumab) and visit by type of biologics. The participant number was added as a random effects factor. The structure of this LME model was:

$$\times\sim \text{pre- or post-BD+visit+visit*type of biologic+visit*pre- or post-BD+(1|participant ID)} \qquad \text{(Model 6.2)}$$

To investigate how the effects of changes induced by the use of biological therapy on the spirometric and CCP parameters were affected by parameters such as, the BEC, FeNO, and ACQ-5 scores, BEC and ACQ-5 (as well as FeNO) were incorporated into the LME model, to assess their association with physiological parameters measured before and after biologics (as in Model 6.1).

Finally, a comparison for goodness-of-fit among the various models was assessed through the application of the AIC [182].

6.3 Results

This study involved 91 individuals who had been diagnosed with severe T2-high asthma (the cross-sectional cohort), of whom 67 were later initiated on biologics (the biologics cohort). The plan was that all participants (that commenced biologics) would undergo CCP assessments during their second visits, which were scheduled for three or four months after the first dose of biologics. However, due to the COVID-19 pandemic, only 54 of these second visits took place. Per the Oxford Complex Airway Clinical Care Pathway for T2-high asthma, patients who had been prescribed biological therapy were required to undergo a clinical review after one year. This review was intended to assess their response to the biologics, which was measured in terms of reductions in the number of exacerbations and OCS use after the biologic regimen had begun. Of the initial 67 patients who had been started on biologics, 65 patients had one-year data. One patient was missing due to the clinic's inability to contact them, and another did not complete their one-year post-biologic follow-up at the time of this study (Figure 6.4).

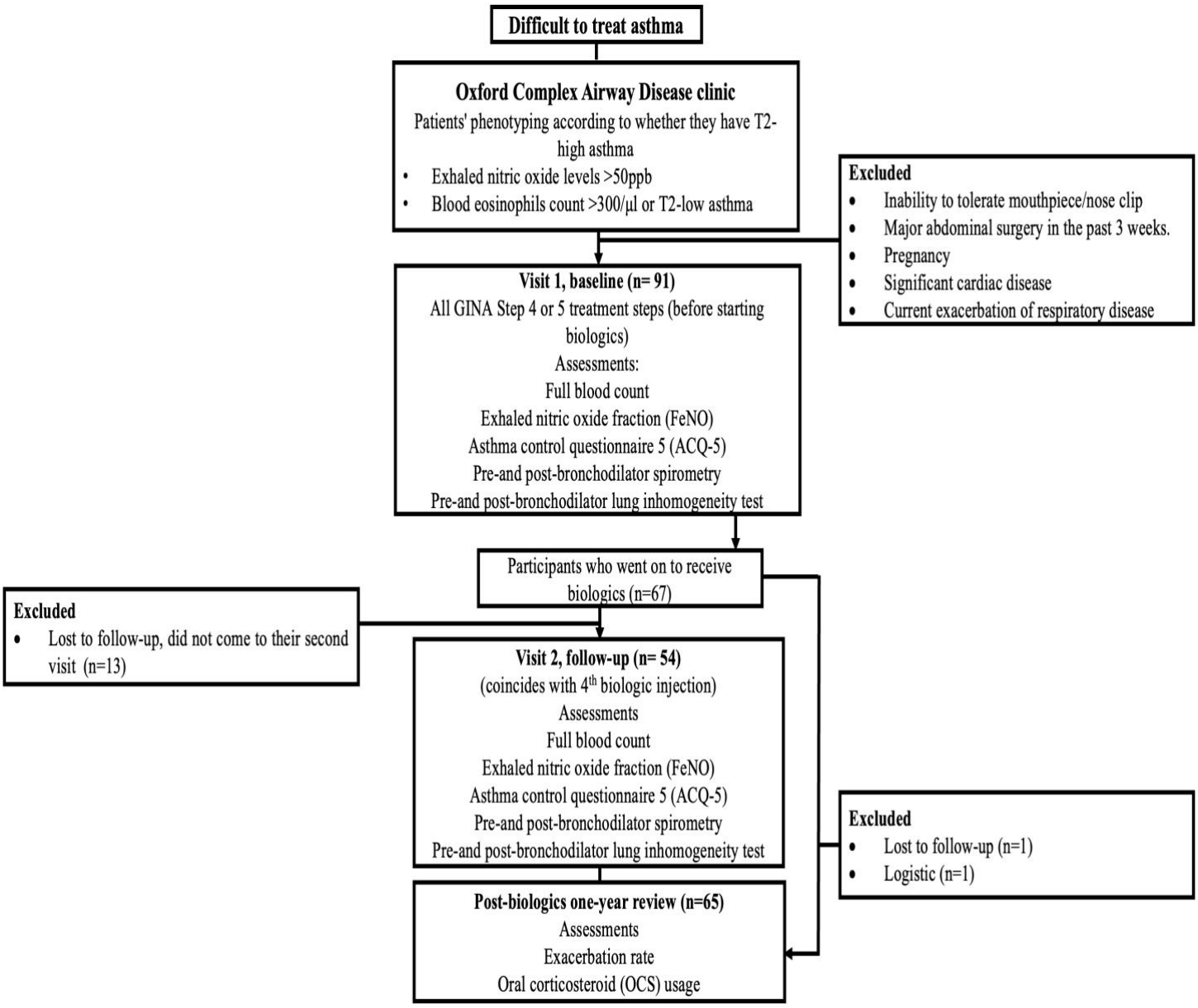


Figure 6.4. Flow diagram showing treatment journey for the study participants within the clinical care pathway for T2-high asthma. Each participant underwent a baseline visit before treatment, followed by a follow-up visit (three or four months after biological treatment). Finally, they underwent a clinical review one year after the initiation of their biological treatment. OCS, oral corticosteroids; FeNO, fractional concentration of exhaled nitric oxide; ACQ-5, asthma control questionnaire-5.

Table 6.1 shows the basic demographic and phenotypic characteristics of the 91 severe asthma patients who were recruited at their first visits, 67 of whom were placed on biologics. The remaining 24 patients did not receive biologics because they did not meet the NICE criteria at that point in time, and they were not included in the biologics three- or four-month follow-ups and one-year review visits. At each visit, all participants underwent the study protocol explained in Section 6.2.4.1 and illustrated in Figure 6.2. Unfortunately, baseline exacerbation data were available for only the severe asthma cohort who subsequently underwent biologics.

Table 6.1. Patient characteristics.

Characteristics	**SA-All**	**SA-biologics**	**SA-not on biologics**
Numbers of participants	91	67	24
Number of females (/ %)	45 (50)	36 (54)	9 (37.5)
Age±SD / yr	57±12	59±11	52±16
Height±SD / m	1.69±0.09	1.68±0.09	1.72±0.07
Weight±SD / kg	81±17	82±18	77±14
BMI±SD / $kg.m^{-2}$	28.3±6.3	30±6.5	26±5
Exacerbations±SD / yr^{-1}	NA	5±3	NA
OCS (% of patients on maintenance)	25 (27)	25 (37)	0
Eosinophils±SD /$x10^9$ l^{-1}	0.46±0.40	0.43±0.40	0.57±0.40
FeNO±SD / ppb	67±62	54±54	103±70
ACQ-5 score±SD	2.3±1.2	2.4±1.3	2.2±1.0

SA, severe asthma patients; SA-biologics, subset of SA patients prescribed biologics; SA- not on biologics, subset of SA patients who did not go on biologics; BMI, body mass index; NA, not applicable as the assessment of baseline exacerbations was done only on patients who received biologics; OCS, oral corticosteroids; FeNO, fractional concentration of exhaled nitric oxide; ACQ-5, asthma control questionnaire-5. Values are means ± SD.

6.3.1 Baseline data for the severe asthma cross-sectional cohort

6.3.1.1 CCP parameters compared with the normal ranges identified in Chapter 5.

Table 6.2 and Figure 6.5 present the Z-scores that were calculated for each lung inhomogeneity parameter, pre-and post-BD, within this cohort, taking into consideration each participant's age, height, BMI and sex, using the prediction equation that was developed for this work and is shown in Chapter 5.

A *Student's t-test* was employed to compare the CCP parameter Z-scores with zero (Table 6.3). The results revealed that the pre-BD ZFRC values showed statistically significant differences from the expected values ($p<0.01$). The post-BD ZFRC values showed a trend toward significance but did not reach statistical significance ($p>0.05$). The pre-BD ZσVD value was highly significantly different from the expected ($p<0.001$), and the post-BD ZσVD value remained significantly different from the expected, although the *p-values* were higher ($p<0.05$), which indicated some reduction in variability post-BD but still a significant level of abnormality in deadspace inhomogeneity. The ZσlnCL values were extremely significantly different from the expected values in both pre- and post-BD ($p<0.001$), which indicated severe and consistent abnormalities in ventilation inhomogeneity. The data showed significant levels of abnormality in lung inhomogeneity parameters (ZFRC, ZVD, ZσVD, and ZσlnCL) in severe asthma patients, both before and after BD use. The most pronounced levels of abnormality were seen in the ZσlnCL parameter. These findings highlight the extent of respiratory impairment in these T2-high asthma patients.

Additionally, *a chi-square (X^2)* goodness-of-fit test was conducted to examine whether the number of abnormal Z-scores for each CCP parameter differed significantly from the number of such observations that would be expected to arise by chance (Table 6.4). The data indicated that a significant number of participants demonstrated CCP parameters (ZFRC, ZVD, ZσVD and ZσlnCL) outside the normal range. The significant X^2 values and the frequency of occurrence of *p-values* < 0.001 across all parameters underscored the extent of respiratory impairment. The most pronounced differences were seen in ZσlnCL, which highlighted the severe effect of severe asthma in terms of inhomogeneity in total lung compliance.

Table 6.2. Calculated Z-scores for each CCP parameter in all of the severe asthma cohort at baseline

Variables	All-SA cohort	
CCP	**Pre-BD**	**Post-BD**
ZFRC±SD	0.45±1.49	0.35±1.63
ZV_D±SD	0.69±1.71	0.86±1.64
Z σV_D±SD	1.01±2.12	0.56±2.29
ZσlnC_L±SD	3.70±2.78	2.99±3.54

SA, severe asthma; BD, bronchodilator; ZFRC, calculated Z-score for functional residual capacity; ZV_D, calculated Z-score for dead space volume (end-inspiratory); ZσVD, calculated Z-score for SD for the standardised dead space; ZσlnC_L, calculated Z-score for SD for the natural logarithm for the standardised lung compliance. Values are means ± SD.

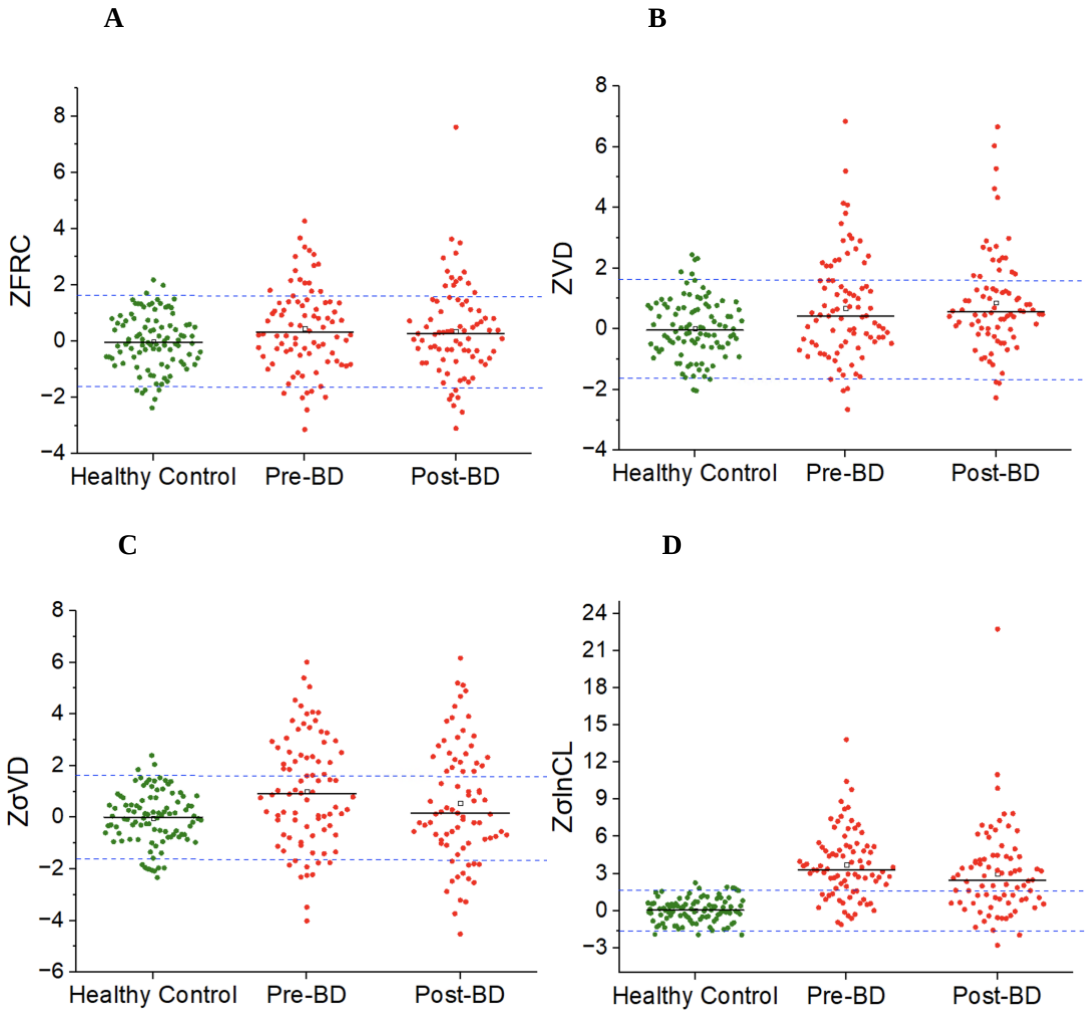


Figure 6.5. Calculated Z-scores for each CCP parameter in the whole severe asthma cohort. The graphs show the variation of these scores across the zero line. The dotted lines represent the 95th and fifth percentiles, which are equivalent to 1.645SD (ULN) and -1.645SD (LLN) respectively. The black lines show the medians. The healthy control data (in green) refer to the control cohort from Chapter 5; BD, bronchodilator; **A:** Z-scores of functional residual capacity (FRC); **B:** Z-scores of end-inspiratory dead space (VD); **C:** Z-scores of the average SD of the normal distribution for dead space across lung volume (σVD); **D:** Z-scores for the SD of log-normal distributions for alveolar compliance (σlnC_L).

Table 6.3. T-test analysis comparing the Z-scores for CCP parameters in the whole severe asthma cohort at baseline

Variables		**All-SA cohort**	
CCP		**Pre-BD**	**Post-BD**
ZFRC	*t*	2.8	1.9
	p	**0.007**	0.06
ZV_D	*t*	3.7	4.7
	p	**<0.001**	**<0.001**
$Z\sigma V_D$	*t*	4.4	2.2
	p	**<0.001**	**0.033**
$Z\sigma lnC_L$	*t*	12.2	7.5
	p	**<0.001**	**<0.001**

SA, severe asthma; BD, bronchodilator; ZFRC, calculated Z-score for functional residual capacity; ZV_D, calculated Z-score for dead space volume (end-inspiratory); $Z\sigma V_D$, calculated Z-score for SD for the standardised dead space; $Z\sigma lnC_L$, calculated Z-score for SD for the natural logarithm for the standardised lung compliance. *t*, T-test result. Significant *p* values are in bold.

Table 6.4. One-way-Chi-square analysis to study the Z-scores that were found to sit outside the normal range for CCP parameters in the whole severe asthma cohort

Variables		**All-SA cohort**	
CCP		**Pre-BD**	**Post-BD**
ZFRC	X^2	34.89	21.82
	p	**<0.001**	**<0.001**
ZV_D	X^2	54.89	60.36
	p	**<0.001**	**<0.001**
$Z\sigma V_D$	X^2	193.69	141.58
	p	**<0.001**	**<0.001**
$Z\sigma lnC_L$	X^2	866.52	493.88
	p	**<0.001**	**<0.001**

SA, severe asthma; BD, bronchodilator; ZFRC, calculated Z-score for functional residual capacity; ZV_D, calculated Z-score for dead space volume (end-inspiratory); $Z\sigma V_D$, calculated Z-score for SD for the standardised dead space; $Z\sigma lnC_L$, calculated Z-score for SD for the natural logarithm for the standardised lung compliance. X^2, chi-square test results. Significant *p* values are in bold.

6.3.1.2 Relationship among BEC and FeNO levels and ACQ-5 scores with CCP parameters

To investigate the links between baseline BEC and FeNO levels and ACQ-5 scores on baseline spirometry and CCP parameters, the previously described LME model (Model 6.1) was applied. The results are detailed in Table 6.5. Table 6.6 provides the same LME analysis but focuses specifically on the subset of patients with severe asthma who subsequently received biologics (n=67). Baseline FeNO levels were found not to be significantly correlated with any of the parameters. However, significant links were observed between ACQ-5 scores and FEV_1 % predicted and FVC % predicted ($p<0.002$ and $p<0.001$, respectively). For CCP parameters, there was a modest but significant link between BEC levels and σlnC_L ($p<0.05$), which indicated that a higher BEC was associated with a higher σlnC_L. No significant links were detected for the remaining parameters. When the same LME analysis was conducted on the subset of 67 severe asthma participants who underwent the biologics pathway, again a significant relationship was found between baseline BEC and σlnC_L ($p<0.001$, $F\text{-ratio}=14$). For all other variables, no significant links were detected.

Table 6.5. LME modelling: an exploration of the links between selected variables at baseline and spirometric and CCP parameters in all patients with severe asthma at baseline.

Variables		Pre- or post-BD	Eosinophils / $x10^9$ l^{-1}	FeNO / ppb	ACQ-5 score
Spirometry					
FEV_1 / % predicted	Coefficient±SE	6.5±0.7	-	-	-5.6±1.7
	F-ratio, p-value	82.8, **p<0.001**	[2.7], p=NS	[0.01], p=NS	10.9, **p<0.002**
FVC / % predicted	Coefficient±SE	5.5±0.9	-	-	-5.7±1.4
	F-ratio, p-value	32, **p<0.001**	[1.2], p=NS	[0.1], p=NS	14.9, **p<0.001**
FEV_1 /FVC	Coefficient±SE	-0.031±0.007	-	-	-
	F-ratio, p-value	18.1, **p<0.001**	[1.6], p=NS	[1.1], p=NS	[0.2], p=NS
CCP					
FRC / l	Coefficient±SE	-	-	-	-
	F-ratio, p-value	[0.1], p=NS	[0.8], p=NS	[0.9], p=NS	[1.9], p=NS
V_D / l	Coefficient±SE	-	-	-	-
	F-ratio, p-value	[0.0], p=NS	[0.1], p=NS	[0.04], p=NS	[0.0], p=NS
σV_D	Coefficient±SE	-0.028±0.009	-	-	-
	F-ratio, p-value	8.4, **p<0.01**	[1.4], p=NS	[0.0], p=NS	[0.7], p=NS
σlnC_L	Coefficient±SE	-0.08±0.01	0.15±0.07	-	-
	F-ratio, p-value	34.4, **p<0.001**	4.7, **p<0.05**	[0.1], p=NS	[0.0], p=NS

BD, bronchodilator; FeNO, fractional concentration of exhaled nitric oxide; ACQ-5, asthma control questionnaire-5; FEV_1, forced expiratory volume in 1s; FVC, forced vital capacity; FRC, functional residual capacity; VD, dead space volume (end-inspiratory); σVD, SD for the standardised dead space; σlnCL, SD for the natural logarithm for the standardised lung compliance. Square brackets around the F-ratio indicate that the variable was subsequently removed from the model. Values are means±standard error (SE).

Table 6.6. LME modelling: An exploration of the effect of selected variables on baseline spirometric and CCP parameters in the subset of patients with severe asthma who subsequently received biologics.

Variables		Pre- or post-BD	Eosinophils / $x10^9$ l^{-1}	FeNO / ppb	ACQ-5 score
Spirometry					
FEV_1 / % predicted	Coefficient±SE	6.2±0.8	-	-	-5.8±1.9
	F-ratio, p-value	56, **p<0.001**	[2.7], p=NS	[1.3], p=NS	8.6, **p<0.01**
FVC / % predicted	Coefficient±SE	5.0±1.0	-	-	-7.0±1.8
	F-ratio, p-value	22, **p<0.001**	[2.2], p=NS	[3.4], p=NS	17.4, **p<0.001**
FEV_1/FVC	Coefficient±SE	0.038±0.008	-	-	-
	F-ratio, p-value	22, **p<0.001**	[1.9], p=NS	[0.6], p=NS	[0.9], p=NS
CCP					
FRC / l	Coefficient±SE	-	-	-	-
	F-ratio, p-value	[1.2], p=NS	[0.5], p=NS	[0.6], p=NS	[1.2], p=NS
V_D / l	Coefficient±SE	-	-	-	-
	F-ratio, p-value	[0.45], p=NS	[0.28], p=NS	[0.20], p=NS	[0.23], p=NS
σV_D	Coefficient±SE	-0.028±0.011	-	-	-
	F-ratio, p-value	8.1, **p<0.02**	[2.8], p=NS	[0.0], p=NS	[2.2], p=NS
$\sigma \ln C_L$	Coefficient±SE	-0.08±0.01	0.21±0.05	-	-
	F-ratio, p-value	25, **p<0.001**	14, **p<0.001**	[0.0], p=NS	[0.4], p=NS

BD, bronchodilator; FeNO, fractional concentration of exhaled nitric oxide; ACQ-5, asthma control questionnaire-5; FEV_1, forced expiratory volume in 1s; FVC, forced vital capacity; FRC, functional residual capacity; VD, dead space volume (end-inspiratory); σVD, SD for the standardised dead space; σlnCL, SD for the natural logarithm for the standardised lung compliance. Square brackets around the F-ratio indicate variable was subsequently removed from the model. Values are means±standard error (SE).

6.3.1.3 Exacerbations in the year before starting biologics in participants who subsequently received biologics

Among the severe asthma patients who were prescribed biologics (n=67), in the year prior to the start of their biologic treatments, the number of exacerbations they experienced ranged from one to 12. Analysis of the frequency histogram (Figure 6.6) revealed a skewed distribution, which prompted the categorisation of patients into two groups: those who experienced a "standard" number of exacerbations ("standard exacerbators", ≤6 exacerbations per year) and those who experienced them frequently ("frequent exacerbators", >6 exacerbations per year). Comparative analysis (Table 6.7) showed that the frequent exacerbator

group had significantly higher BECs and ACQ-5 scores ($p<0.001$ and $p<0.05$, respectively) compared with the standard exacerbators.

Further comparison of spirometry and CCP values between these groups (Table 6.8) indicated that the frequent exacerbators had worse baseline FEV_1 % predicted and FVC % predicted scores ($p<0.01$ and $p<0.05$, respectively), as well as significantly higher baseline values for VD and σlnCL ($p<0.05$ and $p<0.001$, respectively) and significantly higher baseline ZVD and ZσlnCL ($p<0.001$ for both) compared to standard exacerbators prior to starting biologics. These findings suggest that frequent exacerbators exhibit more severe disease in the lungs, which is characterised by poorer lung function and greater inhomogeneity of ventilation, compared with standard exacerbators.

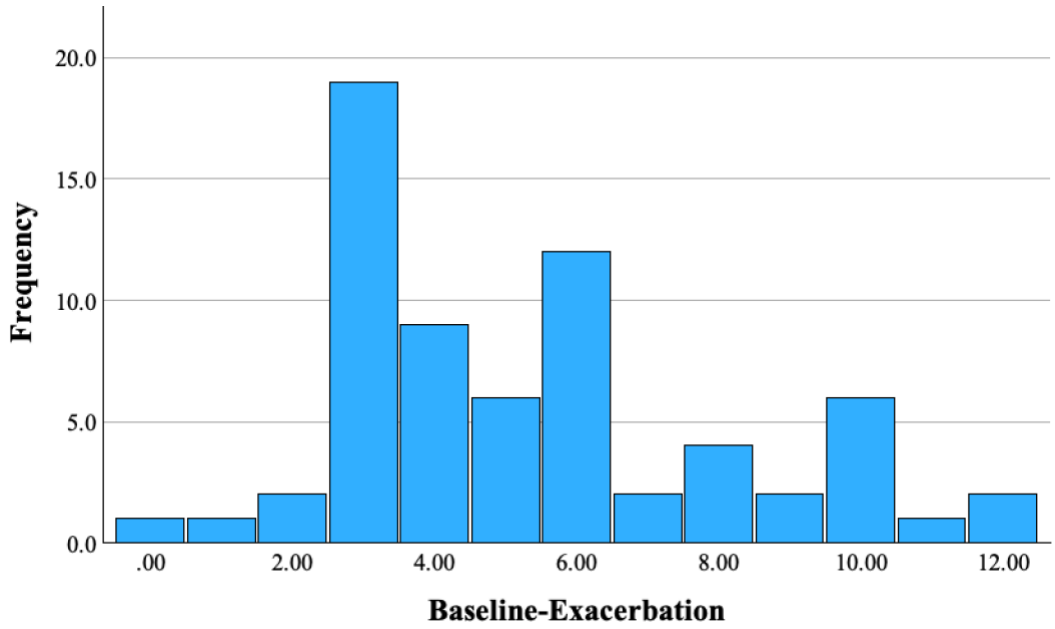


Figure 6.6. Exacerbation rates before biologics therapy. The mean exacerbation rate of the 67 patients was 5.4 and the SD was ±2.8.

Table 6.7. Comparison of characteristics between the patients who did and did not have particularly frequent exacerbations in the year prior to starting therapy with biologics

Characteristics	Standard exacerbator	Frequent exacerbator
Number of participants	50	17
Number of participants with one year follow-up visits	42	12
OCS (% of patients on maintenance)	22 (44)	3 (18)
Baseline BEC±SD / $x10^9$ l^{-1}	0.32±0.21	0.75±0.68***
Baseline FeNO±SD / ppb	46±47	75±68
Baseline ACQ-5 score±SD	2.2±1.2	3.0±1.1*

OCS, oral corticosteroids; ACQ-5, Asthma control questionnaire-5; BEC, blood eosinophil counts; FeNO, fractional concentration of exhaled nitric oxide. Statistical comparisons are for standard exacerbators vs. frequent exacerbators. Standard exacerbators are defined as those with ≤6 exacerbations per year, and frequent exacerbators are defined as those with >6 exacerbations per year. Values are means ± SD. *p<0.05, **p<0.01, ***p<0.001 (independent t-test).

Table 6.8. Comparison of spirometry and CCP parameters between the standard and frequent exacerbator groups of patients in the year prior to starting therapy with biologics.

Variables	Standard exacerbator		Frequent exacerbator	
Spirometry	**Pre-BD**	**Post-BD**	**Pre-BD**	**Post-BD**
Baseline FEV_1±SD / % predicted	78±21	85±19	62±20**	67±20**
Baseline FVC±SD / % predicted	95±20	101±18	84±20 *	87±17*
Baseline FEV_1/FVC±SD	0.66±0.11	0.69±0.12	0.59±0.13	0.63±0.14
CCP	**Pre-BD**	**Post-BD**	**Pre-BD**	**Post-BD**
Baseline FRC±SD / l	2.9±0.73	2.9±0.70	2.7±1.0	2.6±1
Baseline ZFRC±SD	0.29±1.48	0.15±1.34	0.96±1.97	0.76±1.74
Baseline V_D±SD / l	0.151±0.055	0.154±0.044	0.200±0.106*	0.177±0.081
Baseline ZV_D±SD	0.39±1.53	0.50±1.36	2.35±2.01***	1.88±1.95***
Baseline σV_D±SD	0.39±0.11	0.38±0.11	0.46±0.09*	0.43±0.09
Baseline ZσV_D±SD	0.89±2.26	0.65±2.10	1.96±1.88	1.30±1.92
Baseline σlnC_L±SD	0.79±0.18	0.73±0.20	1.0±0.24***	0.89±0.18*
Baseline ZσlnC_L±SD	3.05±2.43	2.38±2.56	6.17±3.17 ***	4.44±2.36*

BD, bronchodilator; FEV_1, forced expiratory volume in 1s; FVC, forced vital capacity; FRC, functional residual capacity; VD, dead space volume (end-inspiratory); σVD, SD for the standardised dead space; σlnCL, SD for the natural logarithm for the standardised lung compliance. Statistical comparisons are for standard exacerbators vs. frequent exacerbators (pre-BD data vs. pre-BD and post-BD data vs. post-BD). Standard exacerbators are defined as those with ≤6 exacerbations per year, and frequent exacerbators are defined as those with >6 exacerbations per year. Values are means±SD. *p<0.05, **p<0.01, *** p<0.001(independent t-test).

6.3.1.4 Relationship between spirometry and CCP parameters at baseline

Figures 6.7 and 6.8 illustrate the relationship between the baseline visit CCP parameters, FEV_1 % predicted and the FEV_1/FVC ratio for both pre- and post-BD data. The FEV_1 % predicted showed a strong correlation with both pre- and post-BD data for $\sigma lnCL$ and σVD *($p<0.0001$)*, and with only pre-BD data for VD *($p<0.0001$)*. Additionally, the FEV_1/FVC ratio demonstrated a high correlation with both pre- and post-BD data for all CCP parameters, with the strongest correlation observed for $\sigma lnCL$ *($p<0.0001$)*. These findings confirm that $\sigma lnCL$ and σVD are good markers of progressive lung function impairment in patients with asthma. Despite the clear correlation between these variables, substantial variation was observed around the regression lines, indicating that while they are highly correlated, they are not proxies for each other.

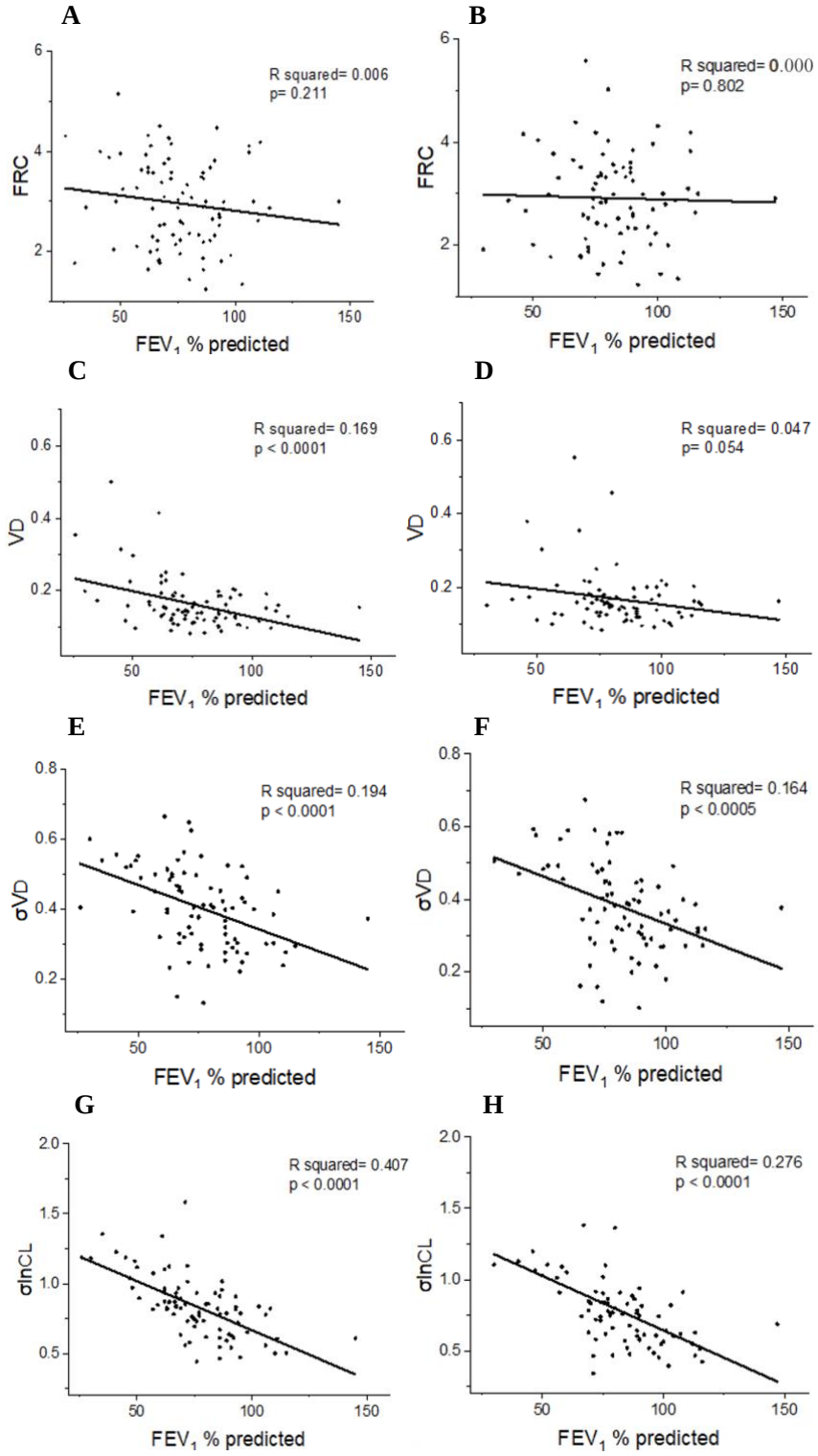


Figure 6.7. Relationship between forced expired volume in one second (FEV_1 % predicted) and CCP parameters pre- and post-BD. **A.** No correlation between FRC and FEV_1 % predicted pre-BD. **B.** No correlation between FRC and FEV_1 % predicted post-BD. **C.** Significant correlation between VD and FEV_1 % predicted pre-BD. **D.** No correlation between VD and FEV_1 % predicted post-BD. **E.** Significant correlation between σVD and FEV_1 % predicted pre-BD. **F.** Significant correlation between σVD and FEV_1 % predicted post-BD. **G.** Significant correlation between σlnCL and FEV_1 % predicted pre-BD. **H.** Significant correlation between σlnCL and FEV_1 % predicted post-BD. (Pearson correlations).

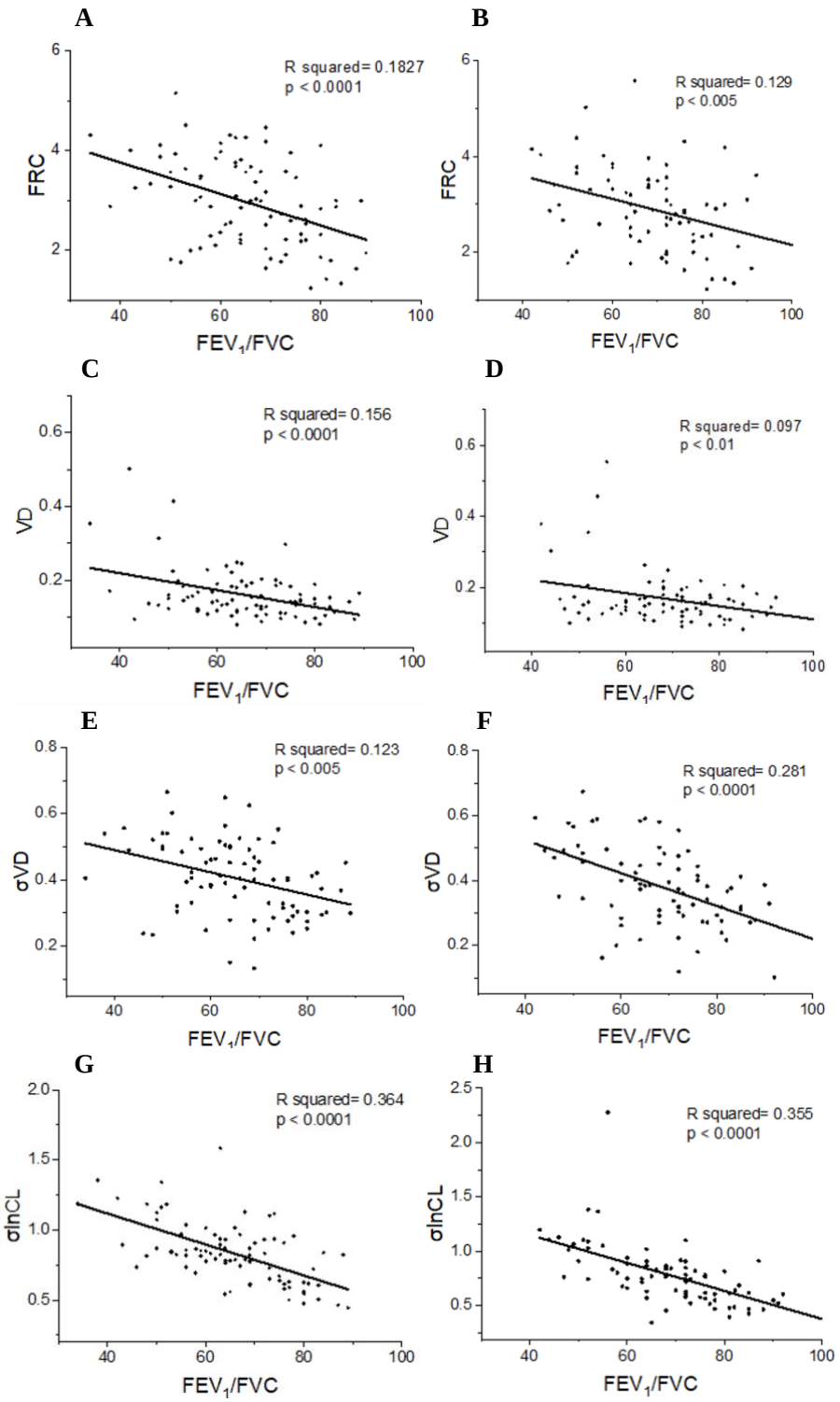


Figure 6.8. Relationship between FEV_1/FVC ratio and CCP parameters pre- and post-BD.
A**.** Significant correlation between FRC and FEV_1/FVC pre-BD. **B.** Significant correlation between FRC and FEV_1/FVC post-BD. **C.** Significant correlation between VD and FEV_1/FVC pre-BD. **D.** Significant correlation between VD and FEV_1/FVC post-BD. **E**. Significant correlation between σVD and FEV_1/FVC pre-BD. **F**. Significant correlation between σVD and FEV_1/FVC post-BD. **G.** Significant correlation between σlnCL and FEV_1/FVC pre-BD. **H.** Significant correlation between σlnCL and FEV_1/FVC post-BD (Pearson correlations).

6.3.1.5 Effect of BD on spirometry and CCP parameters

Table 6.9 presents the pre- and post-BD values for spirometry and CCP parameters at the baseline visit for the subset of patients who subsequently received biologics and for all 91 severe asthma participants. The results indicated that bronchodilation had a significant effect (increased) on all spirometric parameters including FEV_1 % predicted, FVC % predicted and FEV_1/FVC. Regarding CCP parameters, bronchodilation markedly improved (reduced) the inhomogeneity indices $\sigma lnCL$ and σVD (*p<0.001* for each). However, it did not have a significant impact on the anatomical dead space (VD) or FRC. Figure 6.9 shows the effect of the use of a BD on all spirometry and CCP parameters in the whole 91-member severe asthma cohort.

Table 6.9. Effects of bronchodilation on spirometric and CCP parameters in the whole severe asthma cohort and in the subset of patients with severe asthma who subsequently received biologics

Variables	**SA-biologics**		**All-SA cohort**	
Spirometry	**Pre-BD**	**Post-BD**	**Pre-BD**	**Post-BD**
FEV_1±SD / % predicted	74±21	80±21***	75±20	82±19***
FVC±SD / % predicted	92±20	97±19***	92±19	97±17***
FEV_1 /FVC (±SD)	0.64±0.11	0.68±0.13***	0.65±0.11	0.69±0.12***
CCP	**Pre-BD**	**Post-BD**	**Pre-BD**	**Post-BD**
FRC±SD / l	2.84±0.82	2.81±0.76	2.96±0.88	3.01±1.24
ZFRC±SD	0.49±1.62	0.42±1.76	0.45±1.49	0.35±1.63
V_D±SD / l	0.164±0.073	0.159±0.054	0.161±0.069	0.167±0.076
ZV_D±SD	0.84±1.86	0.91±1.77	0.69±1.71	0.86±1.64
σV_D±SD	0.41±0.11	0.39±0.11**	0.40±0.11	0.37±0.12***
Z σV_D±SD	1.07±2.13	0.73±2.13*	1.01±2.12	0.56±2.29***
σlnC_L±SD	0.85±0.22	0.77±0.20***	0.83±0.21	0.78±0.27***
$Z\sigma lnC_L$±SD	3.74±2.91	3.20±3.71***	3.70±2.78	2.99±3.54***

SA, severe asthma; SA-biologics, subset of SA patients who were prescribed biologics; BD, bronchodilator; FEV_1, forced expiratory volume in 1s; FVC, forced vital capacity; FRC, functional residual capacity; V_D, dead space volume (end-inspiratory); σVD, SD for the standardised dead space; σlnC_L, SD for the natural logarithm for the standardised lung compliance. Statistical comparisons are pre-BD data vs. post-BD data for each cohort. Values are means ± SD. **p<0.01, *** p<0.001 (paired t-test).

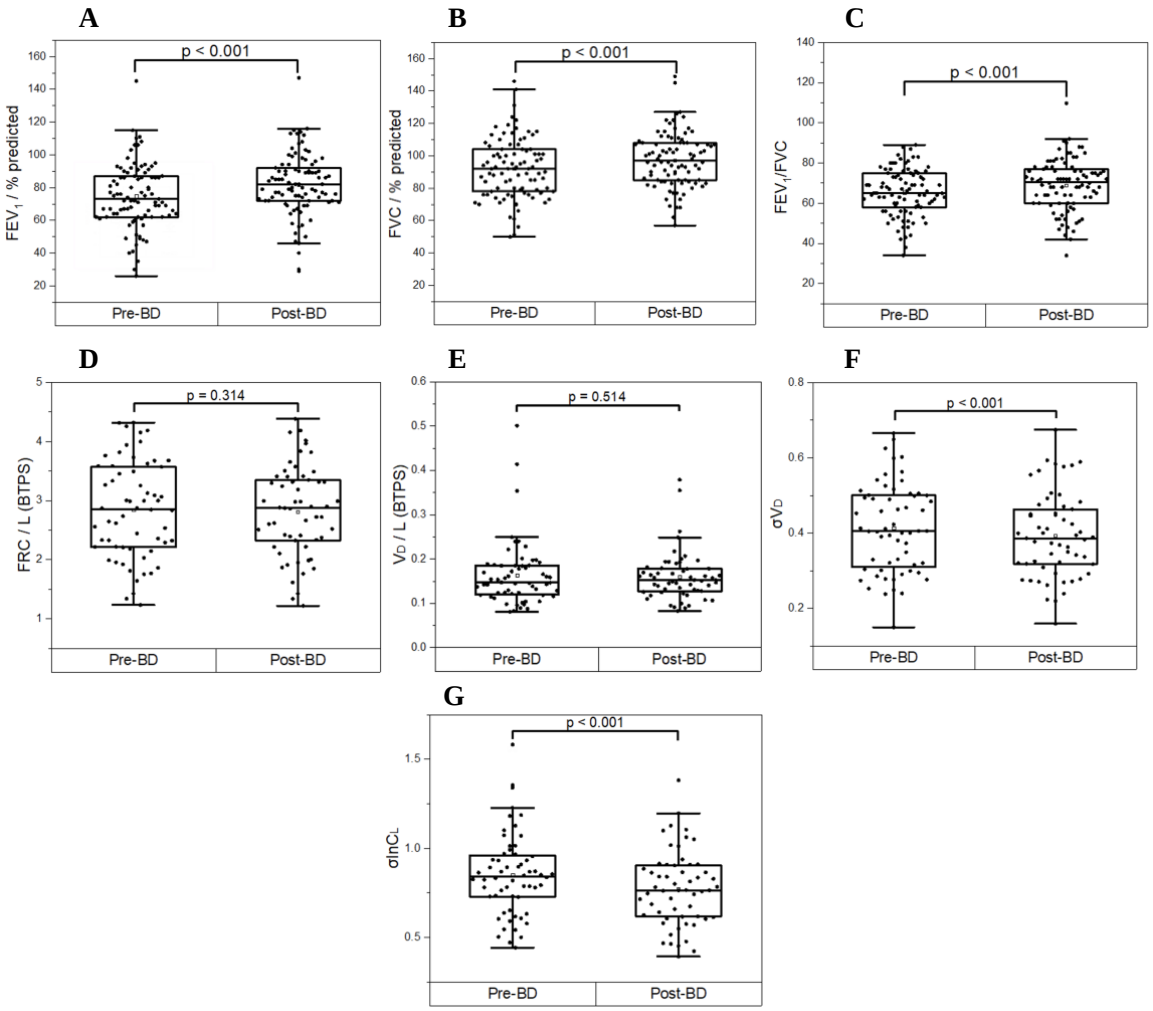


Figure 6.9. Effects of bronchodilation on spirometric and CCP parameters in the whole severe asthma cohort. **A.** Significant improvement in forced expired volume in one second (FEV_1 % predicted). **B.** Significant improvement in forced vital capacity (FVC % predicted). **C.** Significant improvement in FEV_1/FVC. **D.** No change in functional residual capacity (FRC). **E.** No change in dead space (end-inspiratory, V_D). **F.** Significant reduction (improvement) in SD of the standardised dead space. **G.** Significant reduction (improvement) in the natural logarithm of the standardised lung compliance ($\sigma \ln C_L$). For box and whisker plots, the median line is shown with the interquartile range as the box. The whiskers show the maximum and minimum values that still remain within 1.5 times the interquartile range beyond the box. Outliers are shown as points beyond the whisker plots.

6.3.2 Effects of biologic treatments three or four months after therapy (at the fourth injection)

Depending on the availability of the drugs and the clinician's decision, the 67 severe asthma patients who were prescribed biological therapy were assigned either mepolizumab or benralizumab during their baseline visit. Subsequently, they were scheduled for follow-up visits at their fourth biologic injection; the follow-up intervals were three months for those on mepolizumab and four months for those on benralizumab. However, due to the intervening COVID-19 pandemic, only 54 of the initial 67 patients were able to return for their scheduled second visits.

The impacts of the biologics on T2-high asthma biomarkers and symptoms are shown in Table 6.10, and the effect of the treatment on the spirometry and CCP parameters are shown in Table 6.11. Figure 6.10 illustrates the effect of the biological treatments on all variables. The administration of biologics resulted in significant reductions in BECs (*$p<0.001$, paired t-test*) and in the ACQ-5 scores (*$p<0.001$*, dependent *t-test*). It led to increased FEV_1 % predicted and FVC % predicted data (p*<0.005, paired t-test*). However, the pairwise t-test analysis did not show statistically significant effects on any CCP parameters.

Table 6.10. Effects of biologic therapy on symptoms and biomarker levels.

Variables	Before biologics	3–4 months post-biologics
BEC±SD / $x10^9$ l^{-1}(n=67, n=53)	0.43±0.42	0.04±0.05
Δ BEC±SD / $x10^9$ l^{-1}(n=53)		-0.40±0.45 ***
FeNO±SD / ppb (n=67, n=52)	53±54	51±41
Δ FeNO±SD / ppb (n=52)		2±36
ACQ-5 score±SD (n=65, n=43)	2.4±1.2	1.2±1.2
Δ ACQ-5 score±SD (n=42)		-0.86±1.13***

3/4 months, three months for those on mepolizumab and four months for those on benralizumab; Δ, change in parameter value between baseline and second visits (after fourth biologics injection); BD, bronchodilator; BEC, blood eosinophil count; FeNO, fractional concentration of exhaled nitric oxide; ACQ-5, asthma control questionnaire-5. Statistical comparisons are between data before biologics vs. three or four months post-biologics. Values are means ± SD. *** p<0.001 (paired t-test).

Table 6.11. Effects of biologic therapy on spirometry and CCP parameters.

Variables	**Before biologics**		**3–4 months post-biologics**	
Spirometry	**Pre-BD** n=67	**Post-BD** n=67	**Pre-BD** n=52	**Post-BD** n=51
FEV_1±SD / % predicted	74±22	80±21	80±24	86±21
Δ Pre-BD FEV_1±SD / % predicted			6±15 **	
Δ Post-BD FEV_1±SD / % predicted			5±13 **	
FVC±SD / % predicted	92±20	97±19	99±20	101±16
Δ Pre-BD FVC±SD / % predicted (n=52)			6.62±15.23 **	
Δ Post-BD FVC±SD / % predicted (n=51)			1.44±11.42	
FEV_1 /FVC (±SD)	0.64±0.12	0.68±0.13	0.64±0.12	68±0.12
Δ Pre-BD FEV_1 /FVC (±SD)			0.01±0.07 **	
Δ Post-BD FEV_1 /FVC (±SD)			0.02±0.07	
CCP	n=60	n=57	n=49	n=52
FRC±SD / l	2.84±0.82	2.81±0.76	3.01±0.84	2.93±0.79
ZFRC±SD	0.46±1.62	0.29±1.45	0.73±1.46	0.48±1.52
Δ Pre-BD FRC±SD / l (n=45)			-0.01±-0.40	
Δ Pre-BD ZFRC±SD (n=45)			-0.01±-0.79	
Δ Post-BD FRC±SD / l (n=45)			-0.02±0.44	
Δ Post-BD ZFRC±SD (n=45)			-0.05±-0.99	
V_D±SD / l	0.164±0.07	0.159±0.05	0.153±0.05	0.163±0.05
ZV_D±SD	0.88±1.85	0.81±1.60	0.50±1.60	0.84±1.50
Δ Pre-BD V_D±SD / l (n=45)			-0.01±-0.05	
Δ Pre-BD ZV_D±SD (n=45)			-0.29±1.39	
Δ Post-BD V_D ±SD / l (n=45)			0.0001±0.05	
Δ Post-BD ZV_D ±SD (n=45)			0.04±1.27	
σV_D±SD	0.41±0.11	0.39±0.11	0.40±0.11	0.37±0.11
ZσV_D ±SD	1.16±2.21	0.80±2.06	0.97±2.23	0.53±2.09
Δ Pre-BD σV_D±SD (n=45)			-0.02±0.13	
Δ Pre-BD ZσV_D ±SD (n=45)			-0.39±2.46	
Δ Post-BD σV_D±SD (n=45)			-0.02±0.10	
Δ Post-BD ZσV_D±SD (n=45)			-0.32±1.91	
σlnC_L±SD	0.85±0.22	0.77±0.20	0.83±0.20	0.76±0.19
ZσlnC_L±SD	3.83±2.94	2.85±2.65	3.49±2.62	2.63±2.48
Δ Pre-BD σlnC_L±SD (n=45)			-0.05±0.20	
Δ Pre-BD ZσlnC_L±SD (n=45)			-0.64±2.61	
Δ Post-BD σlnC_L±SD (n=45)			-0.04±0.17	
Δ Post-BD ZσlnC_L±SD (n=45)			-0.542.23	

3/4 months, three months for those on mepolizumab and four months for those on benralizumab; Δ, change in parameter value between baseline and follow-up visits (after fourth biologics injection); BD, bronchodilator; FEV_1, forced expiratory volume in 1s; FVC, forced vital capacity; Z-FRC, Z-score for functional residual capacity; Z-V_D, Z-score for dead space volume (end-inspiratory); Z-σV_D, Z-score for SD for the standardised dead space; Z-σlnC_L, Z-score for SD for the natural logarithm for the standardised lung compliance. Statistical comparisons are between data before biologics vs. three- or four-months post

biologics (pre-BD vs. pre-BD data and post-BD vs. post-BD data). Values are means±SD. *p<0.05, **p<0.01, ***p<0.001 (paired t-test).

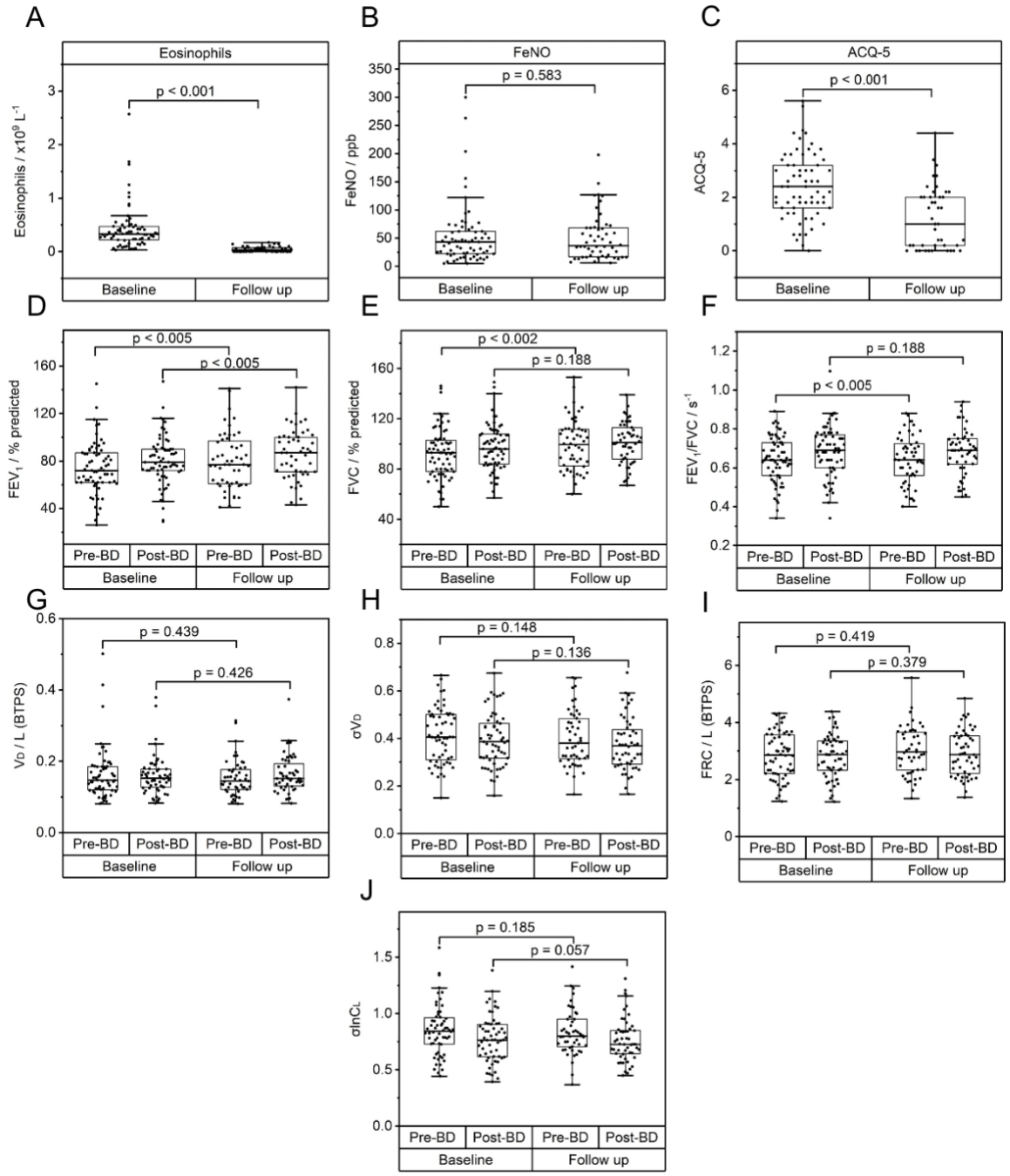


Figure 6.10. Response to biological therapy after three or four months of treatment. **A.** Significant reduction in BEC. **B.** No change in the fraction of nitric oxide in exhalate (FeNO). **C.** Significant reduction in score on asthma control questionnaire-5 (ACQ-5). **D.** Significant improvement of both pre- and post-bronchodilator (BD) forced expired volume in one second (FEV_1 % predicted). **E.** Significant improvement of pre-BD forced vital capacity (FVC % predicted) but not post-BD. **F.** Significant improvement of pre-BD FEV_1/FVC but not post-BD. **G.** No change in dead space (end-inspiratory, V_D). **H.** No change in SD of the standardised dead space (σV_D). **I.** No change in functional residual capacity (FRC). **J.** No change in SD of the natural logarithm of the standardised lung compliance ($\sigma \ln C_L$). For box and whisker plots, the median line is shown with the interquartile range as the box.

The whiskers show the maximum and minimum values that still remain within 1.5 times the interquartile range beyond the box. Outliers are shown as points beyond the whisker plots.

LME Model 6.2 was applied to investigate the effects of the biological therapy on spirometric and CCP parameters. This analysis incorporated pre- and post-BD values taken before and after biological treatment into a single model. It revealed not only that there were significant effects of the biological therapy on all spirometric parameters but also that there was a small but statistically significant effect of the therapy on $\sigma \ln C_L$ (Table 6.12). The type of biologic that was used (mepolizumab or benralizumab) did not significantly affect how the spirometric and CCP parameters changed after biologic administration.

Table 6.12. LME modelling: an exploration of the effects of biologic therapy on spirometric and CCP parameters in the subgroup of patients who had follow-up visits three or four months after starting biologic therapy.

Variables		Pre- or post-BD	Visit (before or after biologics)	Visit*type of biologics	Visit* pre- or post-BD
Spirometry					
FEV_1 / % predicted	Coefficient±SE	5.9±1.4	5.5±1.2	-	-
	F-ratio, p-value	27, **p<0.001**	20.4, **p<0.001**	[0.31], p=NS	[0.01], p=NS
FVC / % predicted	Coefficient±SE	3.2±1.1	4.0±1.2	-	-
	F-ratio, p-value	8.0, **p<0.01**	11.4, **p<0.001**	[0.9], p=NS	[3.0], p=NS
FEV_1/FVC	Coefficient±SE	-	2.4±1.1	-	-
	F-ratio, p-value	[0.01], p=NS	5.0, **p<0.05**	[1.5], p=NS	[0.2], p=NS
CCP					
FRC / l	Coefficient±SE	-0.07±0.03	-	-	-
	F-ratio, p-value	4, **p<0.05**	[0.0], p=NS	[0.5], p=NS	[0.2], p=NS
V_D / l	Coefficient±SE	-	-	-	-
	F-ratio, p-value	[0.4], p=NS	[0.6], p=NS	[1.1], p=NS	[1.8], p=NS
σV_D	Coefficient±SE	-0.02±0.01	-	-	-
	F-ratio, p-value	5.5, **p<0.05**	[2.3], p=NS	[1.0], p=NS	[0.0], p=NS
$\sigma \ln C_L$	Coefficient±SE	-0.07±0.01	-0.03±0.01	-	-
	F-ratio, p-value	20.6, **p<0.001**	4.6, **p<0.05**	[0.8], p=NS	[0.2], p=NS

BD, bronchodilator; FEV_1, forced expiratory volume in 1s; FVC, forced vital capacity; FRC, functional residual capacity; V_D, dead space volume (end-inspiratory); σV_D, SD for the standardised dead space; $\sigma \ln C_L$, SD for the natural logarithm for the standardised lung compliance. Square brackets around the F-ratio indicate variable was subsequently removed from the model. Values are means± standard error (SE).

As the administration of biological therapy led to significant changes in both the BEC and ACQ-5 data, it prompted the question of whether its impact on spirometric and CCP parameters was influenced by the magnitude of the effects observed on the BECs and ACQ-5 scores. To explore this, LME Model 6.1, incorporated the ACQ-5 score and the BEC and FeNO data, was applied, and the results are detailed in Table 6.13. This analysis revealed a significant effect of BEC on σlnCL (*F-ratio 49, p<0.001*) and σVD (*F-ratio 12.1, p<0.001*). As for spirometric parameters, both the BECs and ACQ-5 scores were found to exhibit significant effects on FEV_1 % predicted (*F-ratio 16, p<0.001,* and *F-ratio 17.2, p<0.001,* respectively) and on FVC % predicted (*F-ratio 6, p<0.02,* and *F-ratio 10.9, p<0.002,* respectively).

Table 6.13. LME modelling: an exploration of the effects of changes induced by biologic therapy on BECs, FeNO and ACQ-5 on spirometric and CCP parameters in the subgroup of patients who had follow-up visits three or four months after starting biologic therapy.

Variables		Pre- or post-BD	Eosinophils / $x10^9$ l^{-1}	FeNO / ppb	ACQ-5 score
Spirometry					
FEV_1 / % predicted	Coefficient±SE	5.9±1.0	-10.9±2.7	-	-3.48±0.84
	F-ratio, p-value	33.9, **p<0.001**	16, **p<0.001**	[1.3], p=NS	17.2, **p<0.001**
FVC / % predicted	Coefficient±SE	3.6±1.0	-6.9±2.8	0.06±0.02	-2.8±0.86
	F-ratio, p-value	11.1, **p<0.002**	6, **p<0.02**	5.6, **p<0.02**	10.9, **p<0.002**
FEV_1/FVC	Coefficient±SE	-	-	-	-
	F-ratio, p-value	[0.03], p=NS	[0.5], p=NS	[0.62], p=NS	[0.13], p=NS
CCP					
FRC / l	Coefficient±SE	-0.07±0.03	-	-	-
	F-ratio, p-value	4.2, **p<0.05**	[2.9], p=NS	[1.1], p=NS	[0.1], p=NS
VD / l	Coefficient±SE	-	-	-	-
	F-ratio, p-value	[0.01], p=NS	[2.4], p=NS	[0.08], p=NS	[0.9], p=NS
σVD	Coefficient±SE	-0.02±0.01	0.07±0.02	-	-
	F-ratio, p-value	4.8, **p<0.05**	12.1, **p<0.001**	[1.2], p=NS	[0.1], p=NS
σlnCL	Coefficient±SE	-0.07±0.01	0.21±0.03	-	-
	F-ratio, p-value	24.3, **p<0.001**	49, **p<0.001**	[1.6], p=NS	[1.7], p=NS

BD, bronchodilator; FEV_1, forced expiratory volume in 1s; FVC, forced vital capacity; FRC, functional residual capacity; VD, dead space volume (end-inspiratory); σVD, SD for the standardised dead space; σlnCL, SD for the natural logarithm for the standardised lung compliance. Square brackets around the F-ratio indicate variable was subsequently removed from the model. Values are means±standard error (SE).

Further examination of the post-BD data concerning the change in σlnCL with biologics indicated that these patients could be divided into two groups: σlnCL responders and σlnCL non-responders. This feature was not observed in the changes in FEV_1 % predicted (Figure 6.11). However, the AIC indicated that a bimodal distribution fitted the data significantly better than a unimodal distribution (*bimodal AIC=-216 vs. unimodal AIC=-144*). As a result, it was possible to classify the patients into σlnCL non-responders (those in whom σlnCL did not change after treatment with biologics) and σlnCL responders (those in whom σlnCL was significantly reduced by more than or equal to 0.03 after treatment with biologics). It is important to note that of the 54 participants who attended their follow-up visits, which were scheduled for three or four months after the first dose of biologics, only 45 participants had their post-BD data.

Table 6.14 presents a comparison of several variables between the two groups. The results revealed a significantly greater reduction in ACQ-5 scores after biologic therapy in the σlnCL responders when compared with the σlnCL non-responders ($p<0.05$) (Figure 6.12E). Tables 6.15 and 6.16 show a comparison of spirometric and CCP parameters between the two groups. The σlnCL responders demonstrated significantly higher increases in FEV_1 % predicted (Figure 6.12.A and B) and both pre- and post-BD ($p<0.001$ and $p<0.01$, respectively). Additionally, their FEV_1/FVC ratios post-BD significantly improved after biologic treatment, as illustrated in Figure 6.12.D, compared with the σlnCL non-responders.

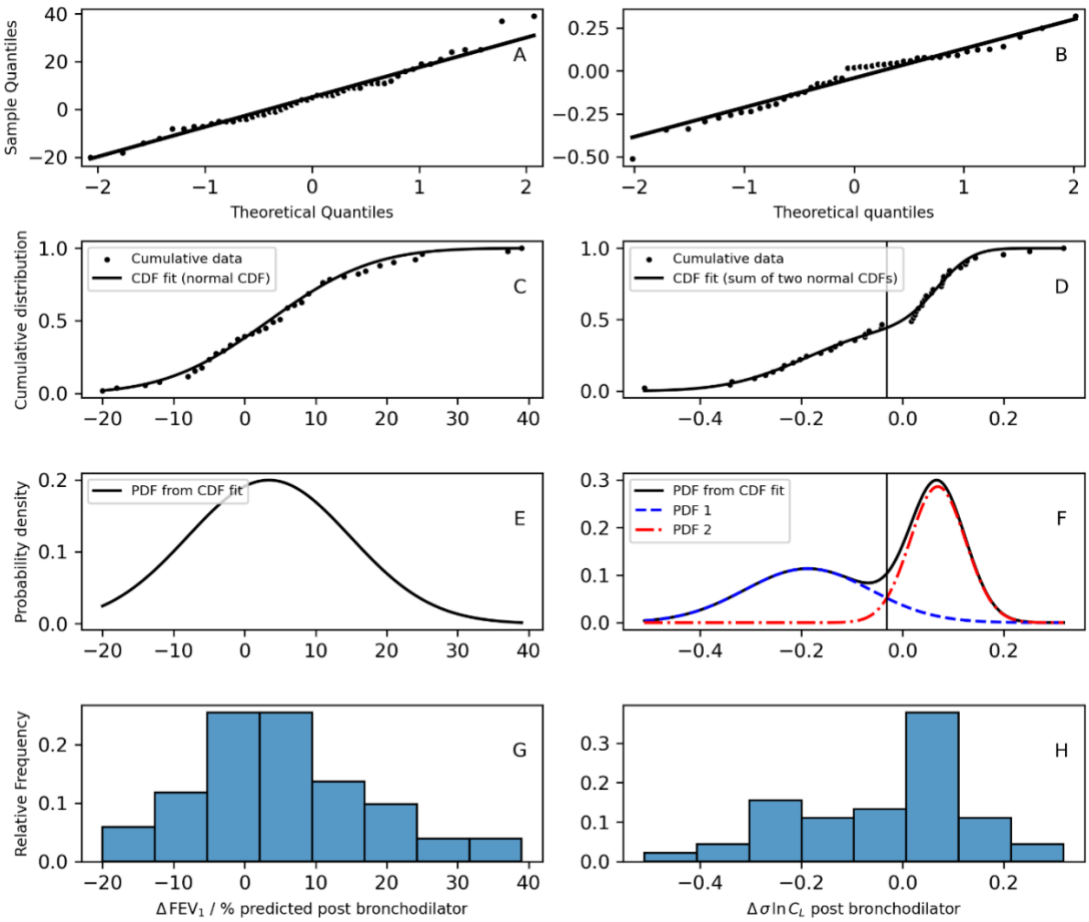


Figure 6.11. Effect of biologics on post-BD values of FEV_1 % predicted (left) and σlnCL (right). **A, B:** Q-Q plots. **C, D:** cumulative distributions, data and model fit. **E, F**: probability density functions, which illustrate underlying bimodal fit for σlnCL (D). **G, H**: sample histograms.

Table 6.14. Comparison of characteristics between the patients who did and did not show responses in post-BD σlnCL levels to therapy with biologics.

Characteristics	σlnCL non-responders	σlnCL responders	All
Number of participants	24 (53)	21 (47)	45
OCS (% of patients on maintenance)	11 (46)	8 (38)	19 (42)
Baseline exacerbations±SD	4.8±2.4	5±3	4.9±2.7
Exacerbations at one year±SD	0.46±0.72	0.29±0.85	0.38±0.78
Baseline BEC±SD / $x10^9$ l^{-1}	0.35±0.34	0.52±0.55	0.443±0.45
Follow-up BEC±SD / $x10^9$ l^{-1}	0.05±0.05	0.04±0.04	0.04±0.05
Δ BEC±SD / $x10^9$ l^{-1}	-0.31±0.32	-0.48±0.54	-0.39±0.44
Baseline FeNO±SD / ppb	46±41	41±28	44±35
Follow-up FeNO±SD / ppb	49±35	51±44	50±39
Δ FeNO±SD / ppb	3±27	9±36	6±31
Baseline ACQ-5 score±SD	2.1±1.2	2.5 ±1.3	2.2±1.2
Follow-up ACQ-5 score ±SD	1.4±1.1	0.8±0.9	1.1±1.0
Δ ACQ-5 score±SD	-0.49±0.86	-1.25±1.25*	-0.87±1.12

σlnCL, SD for the natural logarithm for the standardised lung compliance; OCS, oral corticosteroids; ACQ-5, asthma control questionnaire-5;BEC, blood eosinophil count; FeNO, fractional concentration of exhaled nitric oxide; Δ, change in parameter value between baseline and follow-up visits. Statistical comparisons are between σlnCL responder vs. -σlnCL non-responder. A σlnCL responder is defined as a patient who had a drop in their σlnCL statistic of ≥0.03 four months after commencing biologics therapy, while a σlnCL non-responder is a patient who did not experience such a drop. Values are means±SD. *p<0.05 (independent t-test).

Table 6.15. Comparison of variables from spirometry between the patients who did and did not show responses in post-BD σlnCL to therapy with biologics.

Variables	σlnCL-non-responders		σlnCL-responders		All	
Spirometry	**Pre-BD**	**Post-BD**	**Pre-BD**	**Post-BD**	**Pre-BD**	**Post-BD**
Baseline FEV_1±SD / % predicted	83±24	88±22	68±20*	74±21	76±22	82±22
Follow-up FEV_1±SD / % predicted	81±25	86±24	82±23	88±17	82±24	87±21
Δ FEV_1±SD / % predicted	-2±13	-2±9	15±15***	13±12***	6±16	5±13
Baseline FVC±SD / % predicted	100±19	103±20	89±19	97±18	95±20	100±19
Follow-up FVC±SD / % predicted	101±24	100±19	102±15	103±13	101±21	102±17
Δ FVC±SD / % predicted	1.3±13	-3±11	13±15*	5±11*	6.5±15.1	0.77±12
Baseline FEV_1 /FVC (±SD)	0.66±0.11	0.68±0.11	0.59±0.11	0.63±0.15	0.63±0.19	0.66±0.13
Follow-up FEV_1/FVC (±SD)	0.65±0.13	0.69±0.13	0.62±0.11	0.68±0.11	0.64±0.12	0.69±0.12
ΔFEV_1/FVC (±SD)	-0.01±0.05	0.01±0.04	0.03±0.09	0.06±0.07**	0.01±0.07	0.03±0.06

σlnCL, SD for the natural logarithm for the standardised lung compliance; BD, bronchodilator; FEV_1, forced expiratory volume in 1s; FVC, forced vital capacity. Statistical comparisons are of the σlnCL non-responders against the σlnCL responders (pre-BD vs. pre-BD data and post-BD vs. post-BD data). A σlnCL responder is defined as a patient who had a drop in their σlnCL of ≥0.03 four months after commencing biologics therapy, while a σlnCL non-responder is a patient who did not experience such a drop. Values are means±SD. *p<0.05, **p<0.01, *** p<0.001(independent t-test).

Table 6.16. Comparison of variables from CCP between the patients who did and did not show responses in post-BD σlnCL to therapy with biologics.

Variables	σlnCL-non-responders		σlnCL-responders		All	
CCP	**Pre-BD**	**Post-BD**	**Pre-BD**	**Post-BD**	**Pre-BD**	**Post-BD**
Baseline FRC±SD / l	2.9±0.70	2.8±0.65	3.1±0.86	3.1±0.83	3.01±0.79	2.96±0.74
Baseline ZFRC±SD	0.36±1.49	0.27±1.32	0.81±1.64	0.69±1.43	0.57±1.56	0.47±1.37
Follow-up FRC±SD / l	3.0±0.65	2.9±0.67	3.2±0.9	3.0±0.87	3.04±0.81	2.94±0.76
Follow-up ZFRC±SD	0.58±1.36	0.40±1.40	0.84±1.58	0.43±1.69	0.69±1.45	0.42±1.52
Δ FRC±SD / l	0.08±0.22	0.05±0.31	-0.07±0.57	-0.10±0.55	0.01±0.41	-0.02±0.44
Δ ZFRC±SD	0.24±0.54	0.14±0.69	-0.07±0.57	-0.10±0.55	0.06±0.79	-0.05±0.99
Baseline V_D±SD / l	0.144±0.044	0.153±0.042	0.185±0.100	0.167±0.071	0.163±0.078	0.159±0.057
Baseline ZV_D±SD	0.21±1.49	0.58±1.46	1.04±2.28	0.70±1.68	0.61±1.93	0.63±1.55
Follow-up V_D±SD / l	0.153±0.051	0.163±0.062	0.148±0.055	0.155±0.038	0.151±0.052	0.160±0.052
Follow-up ZV_D±SD	0.51±1.77	0.84±1.69	0.12±1.57	0.49±1.23	0.34±1.68	0.67±1.49
Δ V_D ±SD / l	0.01±0.03	0.01±0.04	-0.05±0.07**	-0.01±0.06	-0.01±0.05	0.0001±0.05
Δ ZV_D ±SD	0.25±0.91	0.26±1.0	-0.88±1.64 **	-0.21±1.51	-0.26±1.40	0.04±1.27
Baseline σV_D±SD	0.38±0.10	0.37±0.10	0.48±0.11**	0.42±0.12	0.42±0.11	0.40±0.12
Baseline ZσV_D	0.57±1.84	0.51±1.86	2.54±2.06**	1.47±2.33	1.51±2.16	0.96±2.12
Follow-up σV_D±SD	0.42±0.11	0.38±0.10	0.40±0.12	0.37±0.11	0.41±0.12	0.38±0.10
Follow-up ZσV_D	1.40±2.05	0.80±1.78	0.96±2.45	0.46±2.21	1.20±2.21	0.64±1.98
Δ σV_D±SD	0.03±0.12	0.03±0.10	-0.09±0.13**	-0.02±0.11	-0.02±0.14	-0.02±0.11
Δ ZσV_D	0.54±2.24	0.29±1.21	-1.57±2.35**	-1.01±2.33*	-0.41±2.50	-0.32±1.91
Baseline σlnCL±SD	0.74±0.16	0.70±0.17	0.98 ±0.24***	0.90±0.21***	0.86±0.23	0.80±0.21
Baseline ZσlnCL	2.40±2.01	1.89±2.16	5.55±3.33***	4.45±2.76***	3.90±3.12	3.08±2.75
Follow-up σlnCL±SD	0.84±0.21	0.79±0.19	0.81±0.20	0.71±0.20	0.83±0.21	0.76±0.20
Follow-up ZσlnCL	3.60±2.80	3.06±2.44	3.33±2.82	1.96±2.74	3.48±2.77	2.55±2.61

BD, bronchodilator; VD, dead space volume (end-inspiratory); FRC, functional residual capacity; σVD, SD for the standardised dead space; σlnCL, SD for the natural logarithm for the standardised lung compliance. Δ, change in parameter value between baseline and follow-up visits. Statistical comparisons are for the σlnCL non-responders against the σlnCL responders (pre-BD vs. pre-BD data and post-BD vs. post-BD data). A σlnCL responder is defined as a patient who had a drop in their σlnCL of ≥0.03 four months after commencing biologics therapy, while a σlnCL non-responder is a patient who did not experience such a drop. Values are means±SD. *p<0.05, **p<0.01, *** p<0.001(independent t-test).

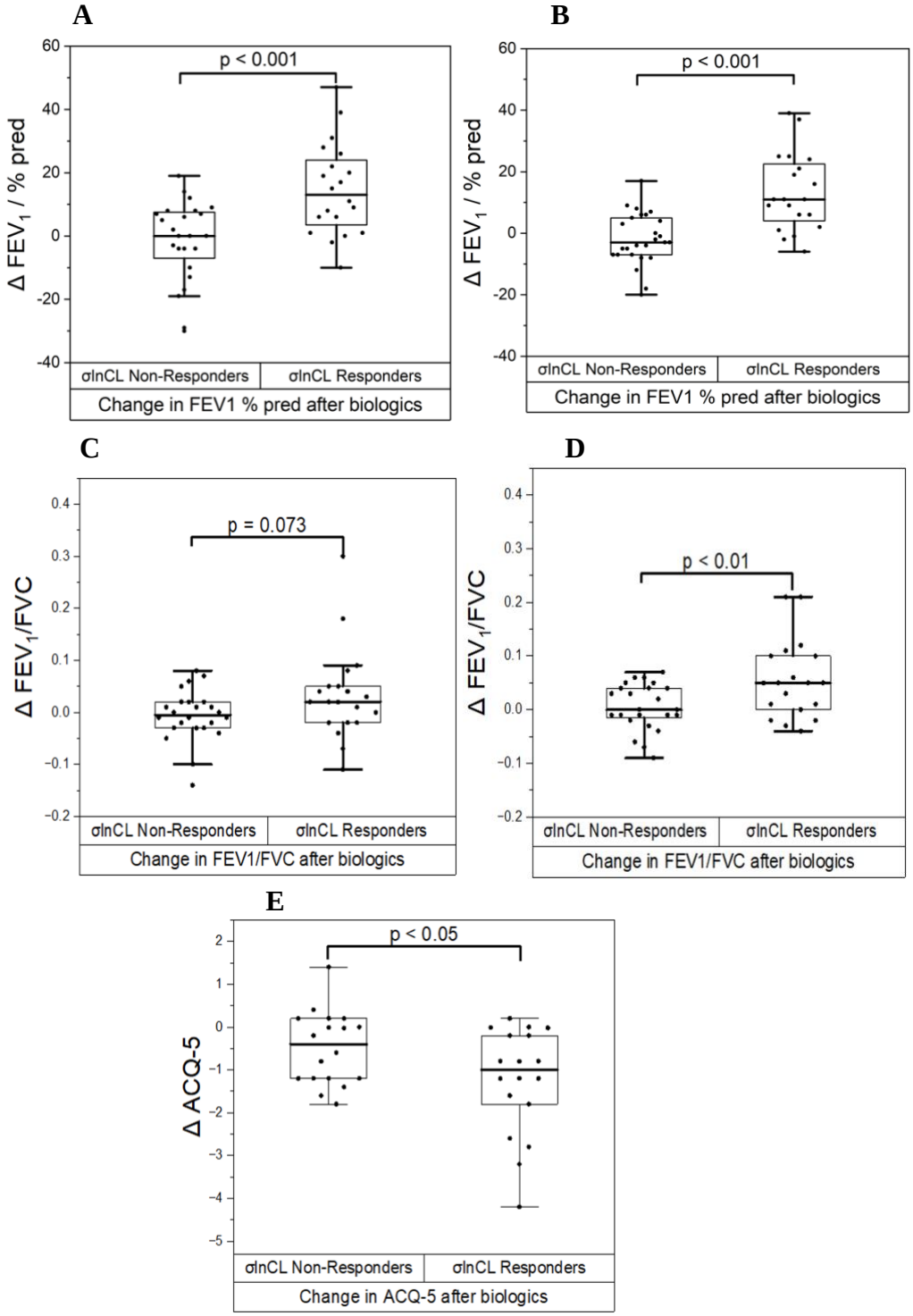


Figure 6.12. Comparison of the changes in FEV_1 % predicted, FEV_1/FVC ratio and ACQ-5 score between the patients who did and did not respond in terms of changes in σlnCL after they had started biologics. **A**: FEV_1 % predicted pre-BD results. **B**: FEV_1 % predicted post-BD results. **C**: FEV_1/FVC ratio pre-BD results. **D**: FEV_1/FVC post-BD results. **E**. ACQ-5 score. A σlnCL responder is defined as a patient who had a drop in their σlnCL of ≥0.03 four months after commencing biologics therapy, while a σlnCL non-responder is a patient who did not experience such a drop (independent t-test). For box and whisker plots, the median line is shown with the interquartile range as the box. The whiskers show the maximum and minimum values that still remain within 1.5 times the interquartile range beyond the box. Outliers are shown as points beyond the whisker plots.

6.3.3 Biologics one-year review

The study was not powered to examine clinical outcomes a year after the start of the biological treatments. Due to the COVID-19 pandemic, we were also unable to perform a one-year clinical assessment in terms of physiological measures. We proceeded to examine whether we could identify any predictors of the clinical response to biologic treatment assessed after one year by using the available data, such as exacerbation rate (Figure 6.13) and the patients' rate of use of maintenance OCS after one year of biological treatment.

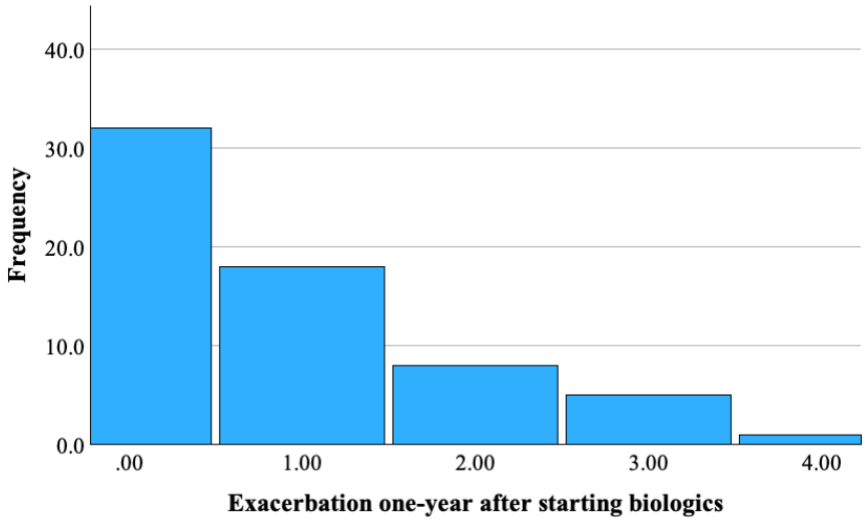


Figure 6.13. Exacerbation rates at the end of one year of biologic therapy. The mean exacerbation rate for the 67 patients was 0.8 and the SD was 1.1.

Consequently, I sought to identify patients who had achieved clinical remission (CR) after one year of biologics therapy versus those who did not. Patients were classified as having achieved CR if they met all the following conditions: zero exacerbations, zero maintenance use of OCS therapy for their asthma, an ACQ-5 score of less than 1.5, and a post-BD FEV_1% predicted of ≥80% or a change in pre-BD FEV_1 of >100ml [183]. For the FEV_1 criterion, data that were collected during the second visit (when patients received their fourth injections) were used. This was because some patients did not undergo spirometry at their one-year review

appointments, many of which were held online due to the COVID-19 pandemic. I then tested whether the proportions of patients in CR differed between σlnCL responders and σlnCL non-responders (Figure 6.11 classification). It was found that only three of 24 participants (12.5%) who were classified in the σlnCL non-responders group achieved CR, compared with eight of 21 participants (40%) in the σlnCL responders group, with a significant difference ($p<0.05$). This suggests that those with a prompt improvement in σlnCL values in response to biological treatment are more likely to achieve CR compared with those who show no change in σlnCL; members of the latter group are unlikely to achieve remission.

The analysis presented in Tables 6.17 and 6.18 underscores significant differences in clinical and lung function outcomes between patients who achieved CR and those who did not after the commencement of biological therapy. Baseline and follow-up ACQ-5 scores were significantly higher in the group that did not achieve CR, indicating poorer asthma control in these patients than in those who did achieve CR. Further spirometric and CCP comparisons revealed that the non-CR group had significantly lower follow-up FEV_1 % predicted values (three- or four-months post-biologic therapy), suggesting less improvement in lung function. These results are not surprising, given that one of the criteria for membership of the CR group was a post-BD FEV_1 % predicted of ≥80% or a change (improvement) in pre-BD FEV_1 of >100ml.

Patients who achieved CR exhibited a significantly greater reduction (improvement) in σlnCL after three or four months of biological treatment. This highlights that early improvement in σlnCL after the start of biological treatment might be a critical marker for the achievement of CR.

Table 6.17. Comparison of characteristics between the patients who did and did not achieve CR

Characteristics	Did not achieve CR	Achieved CR
Number of participants	39 (76.5)	12 (23.5)
OCS (% of patients on maintenance)	13 (33)	6 (50)
Baseline exacerbations±SD	5.6±2.99	4.17±3
Exacerbations at one year±SD	0.72±1.05	0 *
Baseline BEC±SD / $x10^9$ l^{-1}	0.48±0.51	0.33±0.14
Follow-up BEC±SD / $x10^9$ l^{-1}	0.04±0.05	0.04±0.05
Δ BEC±SD / $x10^9$ l^{-1}	-0.44±0.51	-0.29±0.15
Baseline FeNO±SD / ppb	51±49	40±34
Follow-up FeNO±SD / ppb	58±45	32±20
Δ FeNO±SD / ppb	5±41	-9±16
Baseline ACQ-5 score±SD	2.4±1.1	1.4 ±0.9 **
Follow-up ACQ-5 score ±SD	1.5±1.0	0.2±0.4 ***
Δ ACQ-5 score±SD	-0.80±1.23	-1.13±0.80

CR, clinical remission; σlnCL, SD for the natural logarithm for the standardised lung compliance; OCS, oral corticosteroids; ACQ-5, asthma control questionnaire-5; BEC, blood eosinophil counts; FeNO, fractional concentration of exhaled nitric oxide; Δ, change in parameter value between baseline and follow-up visits. Statistical comparisons are between the group of participants who achieved CR vs. those who did not achieve CR. CR is identified if the patient meets all of the following conditions: zero exacerbations, zero maintenance OCS therapy for their asthma, an ACQ-5 score of less than 1.5, and a post-BD FEV1% predicted of ≥80% or a change in pre-BD FEV_1 of >100ml. Non-CR is defined as not meeting any of these conditions. Values are means±SD. *p<0.05, **p<0.01, *** p<0.001 (independent t-test).

Table 6.18. Comparison of variables from spirometry and CCP between the patients who did and did not achieve CR.

Variables	Did not achieve CR		Achieved CR	
Spirometry	**Pre-BD**	**Post-BD**	**Pre-BD**	**Post-BD**
Baseline FEV_1±SD / % predicted	71±23	77±24	86±16	92±15
Follow-up FEV_1±SD / % predicted	74±22	81±21	96±21**	101±12**
Δ FEV_1±SD / % predicted	3±15	-4±13	10±11	9±10
Baseline FVC±SD / % predicted	92±21	97±20	100±18	106±13 *
Follow-up FVC±SD / % predicted	96±22	98±17	109±14	110±13
Δ FVC±SD / % predicted	5±16	0.84±12	10±11	3±10
Baseline FEV_1/FVC (±SD)	0.61±0.13	0.65±0.13	0.67±0.09	0.70±0.09
Follow-up FEV_1/FVC (±SD)	0.62±0.12	0.67±0.12	0.68±0.11	0.73±0.10
Δ FEV_1/FVC (±SD)	0.01±0.08	0.02±0.08	0.01±0.05	0.03±0.05
CCP	**Pre-BD**	**Post-BD**	**Pre-BD**	**Post-BD**
Baseline FRC±SD / l	3.0±0.79	3.0±0.69	2.84±0.88	2.87±0.93
Baseline ZFRC±SD	0.81±1.65	0.53±1.41	0.36±1.29	0.41±1.26
Follow-up FRC±SD / l	3.0±0.72	2.9±0.72	3.11±1.20	2.93±1.03
Follow-up ZFRC±SD	0.81±1.40	0.52±1.55	0.50±1.76	0.24±1.50
Δ FRC±SD / l	-0.06±0.33	0.06±0.42	0.17±0.58	-0.03±0.32
Δ FRC±SD	-0.06±0.33	-0.06±0.42	0.250.99	-0.12±0.74
Baseline V_D±SD / l	0.172±0.078	0.162±0.054	0.149±0.090	0.152±0.072
Baseline ZV_D±SD	0.97±1.94	0.70±1.56	0.23±2.04	0.49±1.65
Follow-up V_D±SD / l	0.155±0.052	0.166±0.056	0.148±0.048	0.150±0.027
Follow-up ZV_D±SD	0.56±1.68	0.92±1.64	0.20±1.40	0.53±1.03
Δ V_D ±SD / l	-0.02±0.05	0.00±0.04	-0.01±0.06	-0.01±0.07
Δ ZV_D ±SD	-0.44±1.45	-0.01±1.03	0.09±1.13	0.05±1.88
Baseline σV_D±SD	0.42±0.10	0.39±0.10	0.43±1.4	0.42±0.13
Baseline ZσV_D	1.53±2.0	0.97±1.89	1.48±2.73	1.33±2.55
Follow-up σV_D±SD	0.40±0.10	0.38±0.11	0.40±0.14	0.37±0.12
Follow-up ZσV_D	1.05±2.10	0.61±2.08	0.98±2.65	0.41±2.25
Δ σV_D±SD	-0.02±0.12	-0.02±0.08	-0.04±0.18	-0.02±0.15
Δ ZσV_D	-0.33±2.19	-0.17±1.82	-0.81±3.35	-0.99±2.08
Baseline σlnC_L±SD	0.87±0.23	0.79±0.21	0.87±0.22	0.84±0.22
Baseline ZσlnC_L	4.07±3.09	3.04±2.70	3.93±3.09	3.47±3.01
Follow-up σlnC_L±SD	0.85±0.18	0.79±0.18	0.78±0.24	0.70±0.22
Follow-up ZσlnC_L	3.77±2.38	2.98±2.23	2.74±3.32	1.77±3.01
Δ σlnC_L±SD	-0.3±0.21	-0.01±0.18	-0.12±0.17	-0.13±0.14 *
Δ ZσlnC_L	-0.34±2.72	-0.12±2.28	-1.58±2.20	-1.73±1.75 *

CR, clinical remission; FEV_1, forced expiratory volume in 1s; FVC, forced vital capacity; VD, dead space volume (end-inspiratory); FRC, functional residual capacity; σVD, SD for the standardised dead space; σlnCL, SD for the natural logarithm for the standardised lung compliance. Δ, change in parameter value between baseline and follow-up visits. Statistical comparisons are between the group of participants who achieved CR vs. those who did not achieve CR (pre-BD vs. pre-BD data and post-BD vs. post-BD data). CR is identified if the patient meets all the following conditions: zero exacerbations, zero maintenance OCS therapy for their asthma, an ACQ-5 score of less than 1.5, and a post-BD FEV_1% predicted of ≥80% or a change in pre-BD FEV_1 of >100ml. Non-CR is defined as not meeting any of these conditions. Values are means±SD. *p<0.05, **p<0.01 (independent t-test).

6.4 Discussion

6.4.1 Baseline data

6.4.1.1 Baseline CCP parameters compared with the normal ranges

The work that was performed for this thesis represents a pioneering effort to evaluate the CCP-derived indices of lung inhomogeneity in patients with severe T2-high asthma. Additionally, it was the first to calculate Z-scores successfully for the CCP parameters. This achievement enabled the differentiation of abnormal values. I had already completed the T2-high asthma project before I undertook the Z-score project (detailed in Chapter 5). However, I revisited the data to calculate Z-scores and then compared them with the findings of the control project outlined in Chapter 5.

The results indicate that a significant number of the severe asthmatics involved in this study had CCP parameter values outside the normal range, as shown in Figure 6.5. Yet some patients' values fell within the normal range. This finding is crucial because it highlights that the definition of severe asthma characterised by exacerbations, symptoms, and treatment requirements is not always directly related to objective measures of disease activity or physiological (lung function) abnormalities within the lung. Furthermore, the observation that some severe asthmatics exhibit normal CCP parameters despite the clinical severity of their disease challenges the traditional paradigms of asthma management. It suggests that severe asthma can manifest with varying degrees of physiological disruption and highlights the importance of comprehensive assessments that go beyond clinical symptoms and exacerbation history.

One key finding is the significantly elevated values of $\sigma lnCL$, an index of ventilation inhomogeneity, in this severe asthma patient group. The mean Z-score for $\sigma lnCL$ was 3.70 ± 2.78 pre-BD and 2.99 ± 3.54 post-BD. These figures indicate the occurrence of substantial

abnormalities in ventilation inhomogeneity, as reflected by σlnCL. These results are consistent with those reported by *Smith et al. (2020)* [140], reinforcing the robustness of these findings. *Smith et al. (2020)* conducted a pilot study of σlnCL in 17 patients with asthma and found higher σlnCL values in their asthma cohort compared to their age-matched control cohort [140]. In their study, they examined undifferentiated asthma patients (i.e., of varying severity and including type-2 low) and found elevated σlnCL compared to controls. In my cohort of severe T2-high asthma, I also found elevated σlnCL values, but they were significantly higher than those in Smith et al.'s study [140], likely because my cohort included only severe asthmatics.

This higher correlation underscores the use of σlnCL as a more accurate reflection of changes in the peripheral airways, making it a valuable tool for early intervention and management of asthma. This finding is particularly important because small-airway changes, which traditional spirometry measures might miss, often precede clinical symptoms and exacerbations. The high σlnCL values that were observed in this T2-high severe asthma cohort suggest significant ventilation inhomogeneity, which highlights the severe respiratory impairment that these patients face.

6.4.1.2 Relationship among BEC and FeNO levels and ACQ-5 scores with CCP parameters at baseline

In this study, LME modelling was employed to investigate the relationship between BEC and FeNO levels and ACQ-5 scores and spirometric and CCP measurements. The results revealed that σlnCL, a novel indicator of ventilation inhomogeneity, showed a significant association with levels of systemic eosinophilic inflammation, as determined by BEC, prior to the initiation of biologics. This association was significant across the entire asthma cohort ($p < 0.01$) and even more pronounced in the subset of patients who subsequently received biologics (with a *p-value* of < 0.001 and a large *F-ratio of 14*) (Tables 6.5 and 6.6). Conversely, FEV_1 % predicted demonstrated a moderate but significant correlation with symptoms, as

measured by the ACQ-5 score, but did not show a significant correlation with BEC. This differentiation suggests that while FEV_1 % predicted is a useful measure of symptom severity, σlnCL provides more specific insights into the underlying inflammation that drives severe asthma, particularly in patients who require biological therapy.

Recent findings have highlighted the importance of systemic eosinophilic inflammation as a predictor of treatment outcomes and exacerbations in asthma [56]. Elevated eosinophil levels are associated with increased disease burden, particularly in the peripheral lung, as reflected by the higher σlnCL values that were found in this study. This suggests that eosinophilic inflammation, which is a critical factor in asthma severity and control, contributes significantly to SAD. Given the critical role of SAD in asthma [184-186], it is essential to employ measures that are focused on these peripheral areas of the lungs in order to improve diagnosis and monitoring. In many cases, small airways are the sites of early pathological changes that can lead to obstructive lung conditions. The significant correlation that was found in this study between σlnCL and BEC, particularly in the subset of patients who qualified for biologics, underscores the relevance of σlnCL as a marker of ventilation inhomogeneity that is linked to systemic eosinophilic inflammation.

The findings from this study, in conjunction with other research that has employed similar technologies, underscore the potential of σlnCL as an effective marker in the identification of pulmonary pathological changes [155, 156]. The study by *Redmond et al.* (2024) highlighted the efficacy of σlnCL in the detection of early smoking-related changes in lung function in young, healthy smokers for whom conventional spirometry tests did not show up any significant abnormalities. This indicates that σlnCL can reveal subtle yet clinically relevant changes in lung function that traditional tests might miss [156]. Similarly, *Smith et al.* (2022) explored the utility of CCP in the quantification via σlnCL of lung inhomogeneity in COPD. Their study demonstrated that a focus on σlnCL enabled the detection of subtle lung

function changes, which are often not captured during the use of conventional spirometric measures. This makes σlnCL a potentially powerful tool for the early detection and monitoring of COPD progression [155].

Collectively, findings from this study suggest that increased levels of systemic eosinophilic inflammation are linked to a higher disease burden in the peripheral lung, which leads to elevated σlnCL values. This indicates that σlnCL is a valuable way to identify pathological changes in the lungs, particularly in the context of SAD. On the other hand, airflow limitation, as captured by FEV_1 % predicted measures, seems to be more closely tied to symptomatic presentation rather than the extent of eosinophilic inflammation. This distinction is important because it highlights the complementary roles of σlnCL and FEV_1 % predicted in understanding and managing asthma. The FEV_1 % predicted measure is useful to assess symptom severity, while σlnCL provides specific insights into the underlying inflammation that drives severe asthma, particularly in patients who require biologic therapy.

6.4.1.3 Exacerbations one year before starting biologics in participants who subsequently received biologics

The exacerbation rates that were experienced by the severe asthma patients were analysed before any of these patients began biological treatment, via the plotting of a frequency histogram. This exercise revealed two groups: standard exacerbators (≤6 exacerbations annually) and frequent exacerbators (>6 exacerbations annually). Frequent exacerbators had higher baseline BECs, ACQ-5 scores and FeNO levels both before and after the initiation of biological therapy. They also exhibited worse spirometry results *($p<0.01$)* and significantly higher σlnCL values *($p<0.001$)* before they started biological therapy compared with the standard exacerbators, and these differences persisted with treatment. This finding indicated greater lung disease burden.

6.4.1.4 Relationship between spirometric and CCP parameters at baseline

Regression analysis revealed a significant relationship between all CCP parameters, except for FRC and FEV_1 % predicted at baseline for both pre- and post-BD data. Notably, the correlation between σlnCL and FEV_1 % predicted was highly significant ($p<0.0001$) for both pre- and post-BD data. This suggests that σlnCL is a reliable marker od progressive disease severity. However, considerable variation around the regression lines (Figure 6.6.G and H) indicated that one variable could not act solely as a surrogate for the other. This significant correlation, coupled with the observed variability, suggests that although σlnCL and FEV_1 % predicted are related, they represent different aspects of lung function. The σlnCL parameter typically reflects conditions in the peripheral lung zones, particularly the small airways, whereas FEV_1 % predicted predominantly captures the influence of large airway dysfunction. Consequently, these parameters provide complementary insights into asthma pathophysiology; each highlights different aspects of the disease state. Furthermore, the study showed that this differentiation was consistent with the results from the LME Model 6.1, which investigated the effects of BEC, FeNO levels and ACQ-5 scores on spirometric and CCP measurements. It was revealed that σlnCL was highly correlated with BEC but not with symptoms, while FEV_1 % predicted showed the opposite pattern, being more closely related to symptoms as measured by the ACQ-5 score but not with BEC. This reinforces the hypothesis that σlnCL and FEV_1 % predicted are not proxies for each other but instead provide valuable, complementary information about the severity and nature of asthma.

Mingotti et al. (2020) evaluated the FEV_1/FVC ratio as a marker of poor clinical outcomes in asthmatic patients. Their study found that patients with FEV_1/FVC ratios in the lower-normal range experienced worse clinical outcomes than those with higher ratios. These outcomes were shown in terms of increased frequency of asthma symptoms, higher rates of exacerbations and greater reliance on medication. These patients did not exhibit obvious airway

obstruction based on traditional spirometric criteria (FEV_1 % predicted), but they showed significant clinical impairments. This finding underlined the clinical relevance of the lower limit of the normal FEV_1/FVC ratio [187]. Interestingly, all CCP parameters in this cohort were correlated highly with the FEV_1/FVC ratio (all with $p<0.01$); σlnC_L showed an especially strong correlation ($p<0.0001$) for both pre- and post-BD data.

The clear correlation between CCP parameters, FEV_1 % predicted and the FEV_1/FVC ratio highlights the comprehensive representation of lung pathology that is provided by the use of CCP, and this finding reinforces its value in asthma assessment and management. Spirometry measures airflow and is predominantly affected by changes in airway resistance. However, in the peripheral airways, where gas flow is slower, resistance does not significantly contribute to expiratory flow limitation during spirometry [188]. Although peripheral airways represent 95% of the total lung volume, they contribute only 10-20% to the total airway flow-resistive pressure loss in the lungs. Additionally, any heterogeneous changes in distal airway function may be obscured by increased flow in non-flow-limited areas [12, 189]. Consequently, spirometry primarily reflects the function of the larger airways and is relatively insensitive to detecting early impairment in the small airways making σlnC_L a metric of ventilation inhomogeneity a better index of small airways involvement.

6.4.1.5 Effect of BD on spirometric and CCP parameters

Use of the BD (Salbutamol) during the baseline visits of all the severe asthma patients (n=91) significantly improved all their spirometric parameters, σlnC_L and σV_D after its application ($p<0.001$). Salbutamol's primary mechanism of action is bronchodilation, which is achieved through the activation of beta-2-adrenergic receptors. This activation stimulates the production of adenylate cyclase, which in turn activates protein kinase A, causing the airway smooth muscle to relax [190]. Additionally, it has been demonstrated to enhance water clearance from the alveoli [191, 192].

The observed changes in spirometric parameters (FEV_1 % predicted, FVC % predicted and FEV_1/FVC) after BD administration can be attributed to the relaxation of smooth muscle in the larger airways, which results in reduced airway resistance. The changes in $\sigma lnCL$ and σVD post-BD application might be linked to the hyper-reactivity of smooth muscle in the small airways (peripheral lung zones). Use of the BD decreases airway resistance, and this leads to faster inflation of less ventilated lung areas and therefore more even lung inflation and reduced variation in local lung compliance (which decreases $\sigma lnCL$). Additionally, the reduction in levels of lung oedema through increased water clearance in the peripheral lung may have also affected the distribution of ventilation.

6.4.2 Effects of biologic treatments three or four months after therapy (at the fourth injection)

The main objective of this part of the project was to examine the effects of biological therapy (at the fourth injection) on lung inhomogeneity and function. This timing was aligned with each patient's clinical care pathway at the clinic. It enabled us to investigate the potential for an "early treatment response signal" in terms of measures of disease activity within the lung.

After three or four months of biological treatment, through the application of paired comparisons between before and after biologics treatment data, significant reductions in BECs were observed *($p<0.001$)* but no effect on FeNO level was found. This outcome (a drop in BEC) is consistent with previous studies on biologics (mainly mepolizumab and benralizumab) [56, 62, 193, 194]. Both these drugs reduce the sizes of the systemic pools of available effector cells and circulating IL-5, and this action leads ultimately to a decrease in BEC [56, 62, 193, 194]. The findings also indicated a statistically significant and clinically meaningful improvement in asthma symptoms, evidenced by a mean change in ACQ-5 score of -0.86 *($p<0.001$*, Figure 6.9C).

The LME modelling demonstrated that the type of biologic used was not significant in these findings. However, the analysis, which included both pre- and post-BD values before and after biological treatment, revealed a small but significant effect of the biological therapy on σlnCL. This suggests that the targeting of eosinophilic inflammation with biological therapy leads to early improvements in lung disease activity, as measured by physiological assessments such as FEV_1 % predicted and σlnCL. These results highlight the efficacy of biological treatments in the reduction of eosinophilic inflammation and the improvement of lung function and asthma control. The consistent drop in BEC underscores the targeted action of these therapies, while the improvement in ACQ-5 scores, spirometric measures and σlnCL confirms their clinical benefits.

The results in this thesis align with those reported by *Farah et al. (2019)*, who observed significant improvements in spirometric and multiple-breath washout indices, such as LCI and S_{acin} (discussed in more detail in Chapter 2), after one month of mepolizumab treatment in a prospective cohort of 20 adults ($p<0.04$). These improvements were sustained at 26 weeks, suggesting that the targeting of eosinophilic inflammation systemically with biologics can impact small airways more effectively than the use of inhaled therapies [195]. *Farah et al. (2019)* proposed that changes in the peripheral airway compartment might contribute to the observed improvements in FEV_1 and highlighted that changes in multiple-breath washout indices correlated with alterations in symptoms (ACQ-5), which was not the case for spirometric changes [195]. They demonstrated that treatment with mepolizumab led to significant improvements in S_{acin}, which reflected improvements in ventilation homogeneity at the acinar level and small-airway function. The reduction in S_{acin} was associated with decreased eosinophilic inflammation, highlighting the potential of S_{acin} as a sensitive marker for monitoring the efficacy of biological treatments in severe asthma [195]. This relationship was similar to that found in this cohort of T2-high asthma patients, in which σlnCL measurements,

a CCP marker of ventilation inhomogeneity, were highly correlated with BEC both at baseline and after biological treatment.

Indeed, further analysis revealed that, with regard to σlnC_L, any impact of the biological therapy was primarily and significantly associated with the extent of eosinophilic inflammation and the treatment response in terms of BEC; no other independent variables demonstrated significant effects. This provides additional support for the idea that reductions in systemic eosinophilic inflammation are linked to changes in inflammatory disease burden in the peripheral regions of the lung (as reflected by σlnC_L). The study by *Gonem et al.* (2015) further supports the significance of small-airway dysfunction in asthma [117]. Through the use of inert gas washout and hyperpolarised helium-3 MRI, they provided detailed insights into the small-airway function and ventilation distribution within the lungs of asthmatic patients. Their findings revealed significant acinar airspace involvement, which was characterised by increased ventilation heterogeneity and identifiable ventilation defects. This indicates that small-airway dysfunction plays a critical role in asthma pathophysiology, even in patients with normal spirometric values. Moreover, the degree of acinar involvement that they found was strongly correlated with clinical measures of asthma severity, such as symptom scores and exacerbation frequency [117]. Overall, the findings from *Farah et al.* (2019), *Gonem et al.* (2015) [117, 195] and my work described here underscore the critical role of small-airway function in asthma. They highlight the need for comprehensive assessment methods, including advanced measures such as S_{acin} and $\sigma lnCL$, to provide a detailed understanding of asthma pathophysiology and treatment response. These measures can significantly enhance rates of early detection, the efficacy of targeted treatment, and overall management of severe asthma, ultimately improving patient outcomes.

In my analysis with the application of the LME model, the impact of biologics on FEV_1% predicted was associated with both the reduction in BEC and the degree of symptom

improvement (ACQ-5). Conversely, the effects on σlnCL were predominantly linked to changes in BEC. This difference underscores the complementary nature of these measurements: while FEV_1 % predicted is related to symptom improvements, σlnCL is a sensitive marker of ventilation heterogeneity and small-airway function.

A thorough analysis of the post-BD change in σlnCL with biological therapy showed clearly that there were two distinct patient groups: σlnCL non-Responders and σlnCL Responders. However, this distinction was not evident during consideration of the change in FEV_1 % predicted, which followed a unimodal distribution. This distinction revealed that when biologics caused a significant change in disease activity within the lung, as measured by σlnCL, patients experienced improvements in both symptoms and overall lung function, as assessed by spirometry (Figure 6.11). From this dichotomization, it became apparent that fully optimized standard therapy (e.g., through GINA steps) still leaves a subset of patients with ongoing, inadequately treated inflammation within the lungs (as evidenced by the worse baseline lung function of σlnCL Responders), which can be modified with biologics. Furthermore, the changes in lung disease activity induced by biologics appeared largely independent of their effect on reducing the frequency of T2-driven exacerbations, which, in nearly all patients, was achieved through the suppression of BEC.

This finding raised the possibility that CCP assessment and stratification of patients as Responders or Non-Responders based on σlnCL could serve as an "early response signal," potentially predicting the longer-term clinical response to biologic therapy. Indeed, the results suggested that patients with an early improvement in σlnCL were more likely to experience clinical remission after one year of biologic therapy compared to those with no change in σlnCL. However, larger studies are needed to more robustly validate this observation.

6.4.3 Biologics one-year review

The management of T2-high asthma has been transformed due to the emergence of biological treatments. The positive impact of these biologics in terms of reducing exacerbation rates, minimising the use of OCSs, and improving functional and clinical outcomes has fundamentally altered the approach to severe asthma treatment. Consequently, some experts are focused not only on the effective improvement of the management of asthma but also on the possibility of achieving remission in severe asthma [196, 197]. The treatment response of the 67 patients in this study who had received biologic therapy for one year was analysed through the use of their clinical data and a comparison of their use of OCSs and the numbers of exacerbations they experienced per year before and after the initiation of biologics [193, 198]. Evidence of treatment response was observed in all patients except one. Hence, the vast majority of patients in this cohort responded positively to biologics. Therefore, it was not feasible to discern predictors that distinguished responders from non-responders in terms of this classification. Each patient had fewer exacerbations in the year after they had started biologics compared with the year before. Other data, such as spirometry results and ACQ-5 scores, were excluded from the responder definition due to the absence of a complete dataset at one year. The only non-responder patient in this cohort exhibited a very high baseline exacerbation rate of 10 per year, along with an elevated measurement of BEC ($1.68 \times 10^{9}l^{-1}$), a significantly high FeNO level (204ppb) and an ACQ-5 score of 4.5. Consequently, clinicians considered a switch of medication for this patient from mepolizumab to dupilumab.

This project was not designed to identify CR in asthma patients who had undertaken biological therapy. However, I leveraged the available data from the one-year review and clinical data from the three or four-month review post-biologics to achieve this. CR in asthma is defined by the absence of significant symptoms and the need for rescue medication, maintained over a specified period during treatment. In this context, patients were classified as

achieving CR if they met all the following criteria: zero exacerbations, zero requirement for maintenance OCS therapy, an ACQ-5 score of less than 1.5, and a post-BD FEV_1 % predicted of ≥80% or a change in pre-BD FEV_1 of >100ml [183]. The analysis revealed that CCP assessment and stratification of patients into σlnCL responders versus σlnCL non-responders three to four months after the start of biologics could serve as an "early response signal" that might be useful to predict their longer-term clinical response to biological therapy. Indeed, our findings indicate that patients who showed early improvement in σlnCL were more likely to achieve CR one year after starting biological treatment, in contrast to those whose σlnCL measures remained unchanged.

6.5 Research limitations

According to NICE guidelines, patients in the UK who are prescribed biologics (such as benralizumab and mepolizumab) must meet specific criteria related to biomarker levels and histories of exacerbations [61, 68]. As a result, the majority of patients in this cohort had severe, long-standing asthma with significant airway remodeling and permanent lung damage. This makes it difficult to include treatment-naïve patients in the study, which limits the ability to fully assess the utility of CCP in asthma and its role in evaluating treatment response. The inclusion of patients who had already undergone various treatments introduces challenges such as confounding effects from prior therapies, inconsistent baseline characteristics, and potentially biased treatment responses. These factors complicate the interpretation of results and may have impacted the assessment of the true efficacy of biologic therapies.

Additionally, the findings may have reduced generalizability to newly diagnosed or treatment-naïve patients, further limiting the applicability of the research. Future studies could address this by including treatment-naïve patients from primary care settings or those with recently diagnosed asthma. Novel indices of ventilation inhomogeneity or small-airway

dysfunction, like those provided by CCP, are likely to be more useful for patients with milder, earlier-stage disease, as opposed to those with severe, long-standing asthma [119, 155].

Another limitation was the high rate of treatment response to biologics that was observed. This strong response may not reflect the response rates seen in randomised controlled trials (RCTs) of biologics. Incorporation of an RCT design into such research projects would substantially help to establish causality, reduce bias, and ensure precise and reliable outcome measurements. An RCT would provide a robust framework for the evaluation of treatment impacts.

Furthermore, in this study, data were missing at the one-year review, including spirometric and CCP measures and ACQ-5 scores. This was due to the COVID-19 pandemic, which necessitated the conduct virtually of all non-clinically essential visits. This missing data may have affected the study's findings and the robustness of the conclusions that have been drawn. Addressing these limitations in future studies will help to provide a clearer understanding of the efficacy and impact of CCP in T2-high asthma.

6.6 Conclusion

In summary, the key finding of this study is that the novel measure of ventilation inhomogeneity, $\sigma lnCL$, derived from the CCP, was most strongly associated with systemic eosinophilic inflammation, both in terms of baseline values and changes induced by biologic treatment, in patients with severe T-2 high asthma. Additionally, an early response in $\sigma lnCL$ to biologics was shown to identify patients more likely to experience improvements in symptoms, lung function, and potentially achieve long-term remission. $\sigma lnCL$ also exhibited notable correlations with traditional spirometric parameters, particularly FEV_1 %predicted and the FEV_1/FVC ratio.

Chapter 7. The long-term effect of COVID-19 on respiratory physiology

7.1 Introduction

When this work started, COVID-19 was a newly emerging disease, and not much was known about its impact on respiratory physiology. Early research during the pandemic indicated that infection with the virus that causes COVID-19 could lead to lasting health issues, as discussed in Chapter 2. The primary objective of this project was to investigate the long-term consequences and abnormalities in pulmonary physiology among patients in the recovery phase after hospitalisation with COVID-19. The hypothesis was that CCP lung inhomogeneity measures could be used to detect differences in lung physiology in patients who had had COVID-19. Specifically, the aim was to assess whether CCP could be used to identify parameters that were associated with severe COVID-19 disease, even after patients had recovered.

Initially, this work was published in conjunction with another post-COVID-19 study that utilised the same technical advance (CCP) in an additional patient cohort [139]. This publication predated the investigation of normal values, which was discussed in Chapter 5 of this thesis. In this chapter, I present exclusively my cohort. I begin with results that have been published but with a more detailed analysis to showcase the clinical lung function and CCP parameters across the various groups in this cohort. Subsequently, I employ the outcomes from Chapter 5 regarding Z-scores to interpret the findings. This work aimed to test whether physiological differences could be detected in these patients through the use of CCP and the application of Z-scores rather than normal values.

7.2 Methods

7.2.1 Participants

7.2.1.1 Identification of participants

This was a prospective, observational, clinical physiology study that was designed to align with the Oxford University Hospital (OUH) clinical pathway. It was aimed to follow-up patients who were recovering from COVID-19, which had caused them to require hospitalisation. The study involved the recruitment of participants who were attending the respiratory clinic at the OUH as part of their follow-up pathway as they recovered from COVID-19.

Prior to their clinical visits, patients were sent research information sheets. During their clinic appointments, the clinician or nurse in charge of their care asked if they were interested in participating in the research. If they expressed interest, as the primary researcher, I explained the study in detail, reviewed the information sheet with them and obtained informed consent. Informed consent was obtained from all participants before their inclusion in the study. The study adhered to the principles outlined in the Declaration of Helsinki and Good Clinical Practice guidelines. If it was convenient for the patient, the CCP breathing test was performed at the time of their medical appointment. Otherwise, a separate research visit was scheduled at the patient's earliest convenience.

Participants were studied under ethical approval reference 20/NW/0235 as part of the capturing multi-organ effects of COVID-19 (CMORE) lung physiology study. The work presented in this chapter was conducted within the framework of this study but focused on the post-COVID-19 effects on respiratory physiology. The CMORE- lung physiology study aimed to investigate whether there were long-lasting abnormalities in the respiratory and pulmonary vascular physiology of patients recovering from COVID-19 [199]. The work I present in this

chapter was part of the physiological studies that were conducted under the CMORE lung physiology study.

The patients' dates of admission to the hospital with COVID-19 ranged from March 2020 to February 2021. Participants were studied at two time points: their first clinic visit, which occurred three-to-six months after their hospital discharge; and their second visit, which took place 12 months after their discharge. During these visits, comprehensive physiological assessments were conducted, and these included the CCP breathing test (Figure 7.1).

7.2.1.2 Inclusion criteria

Participants were required to fulfil the following requirements.

- Male or female aged 18 years or over.
- Willing and able to provide informed consent to participate in the study.
- Recovering from acute COVID-19 (that required hospitalisation), with the acute illness confirmed by a positive polymerase chain reaction swab for the COVID-19 infection agent, severe acute respiratory syndrome coronavirus-2 (SARS-CoV-2) and a confident clinical diagnosis made by the attending clinician based on symptoms, blood tests and/or radiological findings.
- Have been discharged from hospital, where they had been admitted due to COVID-19 infection, three-to-six months previously.

7.2.1.3 Exclusion criteria

- Inability to tolerate mouthpiece/nose clip
- Major abdominal surgery in the previous three weeks
- Pregnancy
- Significant cardiac disease

- Current exacerbation of respiratory disease

7.2.2 Study protocol

Figure 7.1 illustrates all the tests that were conducted at each visit. Tests shown in grey are those performed as part of the CMORE lung physiology study but are not presented in this thesis.

At their baseline visit (three-to-six months post-hospital discharge) all the participants underwent:

1. a lung inhomogeneity measurement (discussed in detail in Chapter 4 of this thesis);
2. spirometry (FEV_1, FVC and FEV_1/FVC ratio) (discussed in Chapter 2 of this thesis);
3. measurement of their lung diffusing capacity/gas transfer factors (DLCO, KCO and VA) (discussed in Chapter 2 of this thesis); and
4. CT thorax scans (CTPA plus HRCT).

At the follow-up visit (12 months after hospital discharge), the participants underwent lung inhomogeneity measurements only.

The study cohort was divided into three groups based on their COVID-19 severity and respiratory support.

- Group 1 comprised patients who had required hospitalisation but had received only basic treatment or simple supplemental O_2. These patients met the World Health Organisation (WHO) severity classification of 4 for hospitalised patients who required only basic therapy and 5 for those who required O_2 therapy [200].
- Group 2 consisted of patients who had been admitted to the respiratory high-dependency unit and treated with non-invasive respiratory support through the use of

high-flow nasal cannulas (HFNCs) or continuous positive airway pressure (CPAP). The condition of these patients corresponded to the WHO severity scale of 6 [200].

- Group 3 comprised patients who had been hospitalised in the intensive-care unit (ICU) and treated via invasive mechanical ventilation (IMV). These patients' conditions corresponded to the WHO severity scales 7 to 9 [200].

The WHO severity classification ranges from 0 to 10 (in which 0 signifies non-infected and 10 indicates very severe COVID-19 infection leading to death) [200]. In this cohort, the severity of COVID-19 infection ranged from WHO classifications 4 to 9. Figure 7.2, taken from the publications of the WHO working group on the clinical characterisation and management of COVID-19 infection, illustrates the organisation's classification of COVID-19 severity [200].

The study cohort was also stratified into three categories based on radiological pathophysiological changes:

1. the normal category: this group exhibited radiological findings within the normal range, which indicated the absence of significant pathological changes;
2. the "ground glass" category: this group displayed radiological evidence of "ground glass" opacities, which suggested certain pulmonary pathophysiological changes; and
3. the "ground glass and fibrotic" category: members of this group demonstrated both ground glass opacities and fibrotic changes on radiological assessment. The presence of fibrotic changes suggested a more advanced and potentially irreversible stage of lung pathology that was characterised by the development of fibrous tissue.

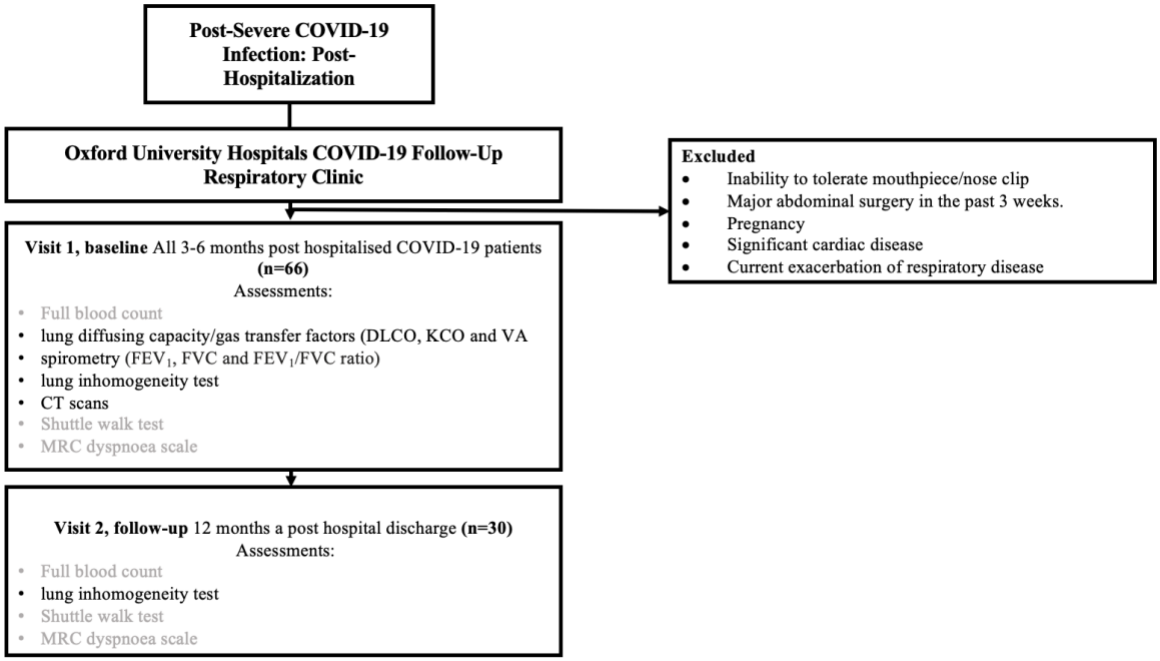


Figure 7.1. Flow diagram shows the clinical care pathway followed by the study participants within the OUH COVID-19 follow-up respiratory clinic. Physiological tests that were performed as part of the CMORE lung physiology study but were not included in this project are shown in grey text.

Patient State	Descriptor	Score
Uninfected	Uninfected; no viral RNA detected	0
Ambulatory mild disease	Asymptomatic; viral RNA detected	1
	Symptomatic; independent	2
	Symptomatic; assistance needed	3
Hospitalised: moderate disease	Hospitalised; no oxygen therapy*	4
	Hospitalised; oxygen by mask or nasal prongs	5
Hospitalised: severe diseases	Hospitalised; oxygen by NIV or high flow	6
	Intubation and mechanical ventilation, pO_2/FiO_2 ≥150 or SpO_2/FiO_2 ≥200	7
	Mechanical ventilation pO_2/FIO_2 <150 (SpO_2/FiO_2 <200) or vasopressors	8
	Mechanical ventilation pO_2/FiO_2 <150 and vasopressors, dialysis, or ECMO	9
Dead	Dead	10

Figure 7.2. WHO COVID-19 clinical progression or severity scale, indicating severity levels from 0 to 10. RNA, ribonucleic acid; NIV, non-invasive ventilation; FiO_2, fraction of inspired O_2; pO_2, partial pressure of O_2; SpO_2, O_2 saturation as measured by pulse oximetry; ECMO, extracorporeal membrane oxygenation [200].

7.2.3 Statistical analysis

Most statistical tests were conducted through the use of SPSS [157] and the results were assumed to be statistically significant at $p<0.05$. To assess the impact of various factors on lung function and CCP variables, I employed either linear regression or LME regression, depending on whether there were repeated observations for one individual [181]. To compare two measurements, a paired *t-test* was employed. To compare the means of three groups, a one-way analysis of variance *(ANOVA)* was used. To assess the significance of associations between two categorical variables, a *chi-square* test was utilised. Correlation coefficients (*Spearman*) were used as appropriate.

7.2.3.1 Analysis conducted on the data via linear regression

The principles used to guide the construction of the LME models are listed below:

- The dependent parameters were derived from lung function and CCP parameters. The lung function parameters were: FEV_1% predicted, FVC% predicted, FEV_1/FVC, DLCOc% predicted, KCOc% predicted, and VA% predicted. The CCP parameters were: VD, VA, FRC% predicted σVD and σlnCL.
- The participant characteristics that were included were: sex, log(age), log(height), log(BMI) and smoking history, measured in terms of pack-years. Characteristics were excluded if they had already been controlled for within the dependent variable. For instance, age, height and sex were omitted when the dependent variable was FRC% predicted, as these variables already influenced the predicted FRC value.
- COVID-19 severity (Group 1, 2 or 3).
- Period (log(days)) since discharge from the hospital. The interaction between this variable and COVID-19 severity was accounted for in the model for those dependent

variables for which measurements were made more than once for any individual. This analysis was restricted to those participants for whom there were data from both visits.

- The participant number was included as a random effect when there was more than one value for a dependent variable per participant.

In a stepwise manner, non-significant factors and covariates that were associated with participant characteristics and periods since discharge were progressively removed, starting with the least significant. The process continued until only the significant terms, along with COVID-19 severity, remained. This process facilitated the evaluation of the significance of the COVID-19 severity factors.

To appraise the significance of the radiological findings, a comparable analysis was carried out in which COVID-19 severity was substituted with a radiology score. This score comprised three levels that corresponded with the three radiological categories listed in section 7.2.2: 1, normal CT; 2, ground glass opacities observed on CT without any indication of fibrosis; and 3, one or more features of fibrosis evident on CT. Several different models were used based on the specific analysis requirements (mentioned below).

The first LME model was designed to study the effect of COVID-19 severity on lung function and CCP parameters. The LME model for variable *x* was written as follows:

$$x \sim IsFemale + log(age) + log(height) + log(BMI) + pack\text{-}years + COVID\text{-}severity + log(days) + COVID\text{-}severity * log(days) + (1|participant\ ID) \quad \text{(Model 7.1)}$$

The second LME model was designed to study the significance of the radiological findings regarding lung function and CCP parameters. The LME model for variable *x* was written as follows:

x~IsFemale+log(age)+log(height)+log(BMI)+pack-years+CT-score+log(days)+

*CT-score*log(days)+(1|participant ID)* (Model 7.2)

7.2.3.2 Analysis conducted on Z-scores for CCP parameters

Z-scores were calculated as described in Chapter 5. The ULN was taken as 1.645, and the LLN as -1.645; these values defined the upper and lower 5% for the normal distribution. *Student t-tests* were conducted to assess whether or not the overall Z-scores of the CCP parameters within the different severity groups were significantly different from zero. *Chi-square* tests were used to determine whether the numbers of abnormal Z-scores within the different COVID severity levels were significantly greater than those that would have been expected by chance. In cases in which the numbers in the contingency table were small, or in cases in which the expected values were not integers, the probabilities were estimated by simulation (100,000 simulations were used).

7.3 Results

Sixty-six participants from various COVID-19 severity groups were recruited for the study. All participants underwent the CCP measurement protocol, but six were unable to complete the breathing test and in five cases the model failed to fit the data due to a leak in the equipment during the experimental measurement. Unfortunately, only 30 of the initial 66 participants returned for their second visits. During these follow-up visits, it was found that the model successfully fitted 28 of the datasets, with two failures.

Table 7.1 presents a summary of participants' characteristics by disease severity for both the initial and follow-up visits. The participants were well-matched across different disease severities in terms of age and height. However, consideration of the initial visit participants' characteristics (three-to-six months post-hospital discharge) showed that weight and BMI increased with disease severity, although only the association between severity and BMI reached statistical significance ($p<0.05$). At the follow-up visits (12 months post-hospital discharge), there were no statistically significant differences in participant characteristics across the COVID-19 severity groups, except for height. Participants in the higher severity group (severity level 3) were shorter than the others. This may have been because most of the participants who returned for their follow-up visits in this severity group were female. Figure 7.3A illustrates the number of participants in each COVID-19 severity group.

Table 7.2 summarises the participants' characteristics by radiological pathological changes for the initial visit only, as follow-up images were not available. There were no statistically significant differences in participant characteristics across the radiological scores. Figure 7.3B displays the number of participants in each radiological score group.

A *chi-square* test was conducted to assess the association between COVID-19 severity and CT scores. The value of the *chi-square* statistic was *25.761* with four degrees of freedom

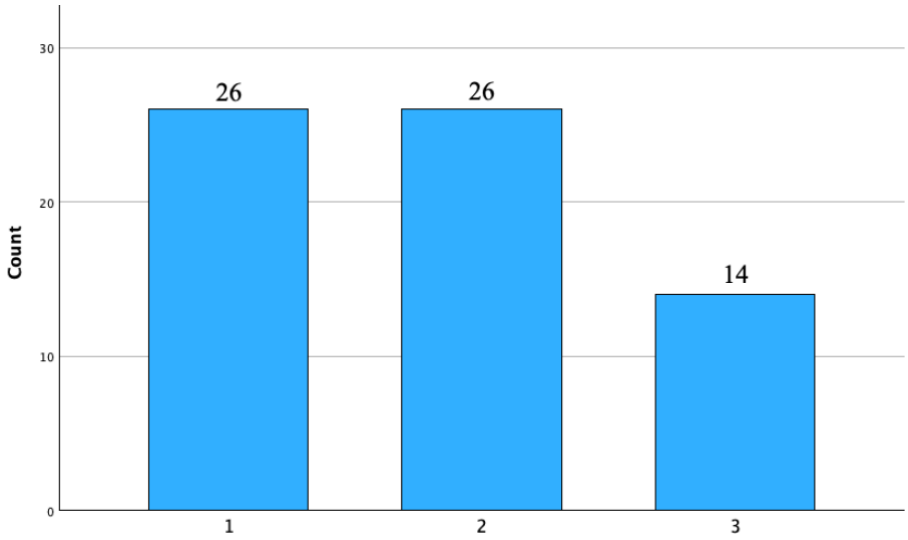
(*df*) and a *p-value<0.001*, which indicated a statistically significant association between COVID-19 severity and CT scores.

Table 7.1. Participant characteristics by disease severity

Variables	Basic/O_2 Severity (1)	HFNC/CPAP Severity (2)	IMV Severity (3)	Overall Severity (1-3)
WHO severity	4-5	6	7-9	4-9
Numbers of participants				
First visit	26	26	14	66
Second visit	11	16	3	30
Number of females (/ %)				
First visit	8 (31)	4 (15)	4 (28)	16 (24)
Second visit	1 (9)	1 (6)	2 (67)	4 (13)
Age±SD / yr				
First visit	60±9	59±9	61± 9	60±9
Second visit	59±6	59±11	60±9	59±9
Height±SD / m				
First visit	1.74± 0.11	1.73±0.08	1.69 ±0.11	1.72±0.10
Second visit	1.80±0.09	1.75±0.07	1.55 ±0.07***	1.75±0.10
Weight±SD / kg				
First visit	87±17	97±23	97±28	93±22
Second visit	100±15	96±23	95±40	98±22
BMI±SD / $kg.m^{-2}$				
First visit	28±5	32±7	33±9 *****	31±7
Second visit	31±5	31±7	39±14	32±7
Smoking / %				
First visit	9 (35)	11 (42)	7 (50)	27 (39)
Second visit	5 (45)	6 (37)	1 (33)	12 (40)
Pack-Years				
First visit	8±14	7±13	9±13	8±13
Second visit	10±14	6±13	0.33±0.57	7±13

WHO, World Health Organisation; Basic/O_2, standard hospital care with or without simple O_2 therapy; HFNC/ CPAP, high-flow nasal cannula or continuous positive airway pressure; IMV, invasive mechanical ventilation; BMI, body mass index. Values are means±SD. *p<0.05, ***p<0.001 *one-way ANOVA.*

A



B

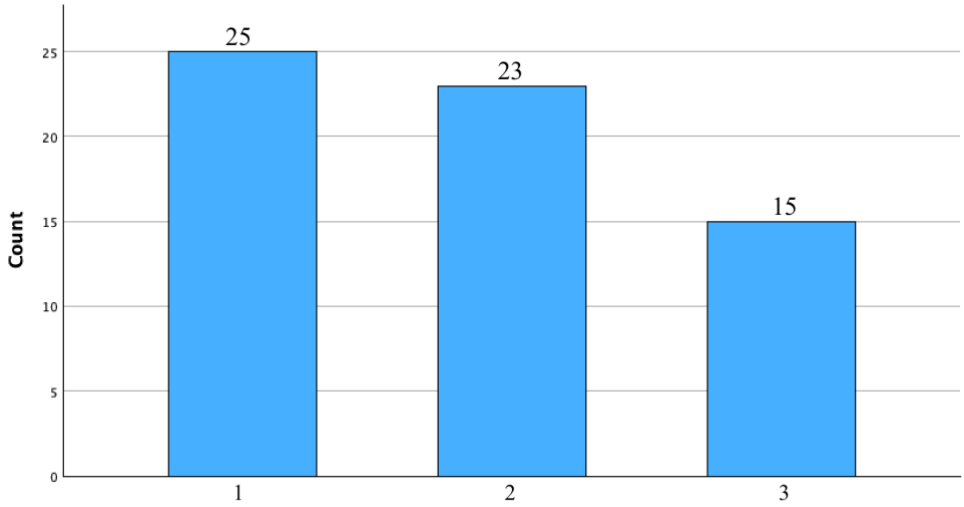


Figure 7.3. Histograms show the number of patients who were categorised into each group at the initial visit (three-to-six months post hospital discharge). **A)** Categorised according to the COVID-19 severity groups: 1-**Basic/O_2**: study participants who had been admitted to hospital during acute infection with COVID-19 but required only basic treatment or were placed on O_2 therapy; 2-**HFNC/CPAP:** participants who had been admitted to hospital during acute infection with COVID-19 and were supplied with HFNCs or CPAP; and 3-**IMV (severe):** participants who had been admitted to the ICU and placed on IMV. **B)** Categorised according to radiological pathophysiological changes: 1-**Normal**: radiological findings within the normal range, which indicated the absence of significant pathological changes; 2-**Ground glass**: radiological evidence of ground glass opacities, which suggested certain pulmonary pathophysiological changes; 3-**Ground glass and fibrotic changes**: both ground glass opacities and fibrotic changes on radiological assessment. The presence of fibrotic changes suggested a more advanced and potentially irreversible stage of lung pathology that was characterised by the development of fibrous tissue. Three of the 66 participants did not have baseline radiology.

Table 7.2. Participant characteristics by radiological pathological changes

Variables	Normal (1)	Ground glass (2)	Ground glass and fibrotic (3)	Overall Severity (1-3)
Numbers of participants	25	23	15	63
Number of females (/ %)	4 (16)	7 (30)	3 (20)	14 (22)
Age±SD / yr	57±10	61±8	63± 8	60±9
Height±SD / m	1.73± 0.09	1.72±0.11	1.75 ±0.11	1.73±0.10
Weight±SD / kg	90±19	98±27	91±23	93±22
BMI±SD / $kg.m^{-2}$	30±5	33±8	30±7	31±7
Smoking / %	8 (32)	9 (39)	9 (60)	26 (41)
Pack-Years	6.5±13	7.2±13	10.3±13	8±13

1-Normal: radiological findings within the normal range, which indicated the absence of significant pathological changes; 2-Ground glass: radiological evidence of ground glass opacities, which suggested certain pulmonary pathophysiological changes; 3-Ground glass and fibrotic changes: both ground glass opacities and fibrotic changes on radiological assessment. The presence of fibrotic changes suggested a more advanced and potentially irreversible stage of lung pathology that was characterised by the development of fibrous tissue. Three of the 66 participants did not have baseline radiology. BMI, body mass index. Values are means±SD.

7.3.1 Clinical lung function parameters 3 to 6 months post-hospital discharge

For clinical lung function only data from the initial visit (3-6 months post-hospital discharge) were available.

7.3.1.1 Clinical lung function parameters across COVID-19 severity groups

Figure 7.4 shows the clinical lung function parameters, which were recorded at the first visit, three-to-six months after hospital discharge. These parameters were measured only at the first visit. An overview of these parameters for this cohort across the different severity groups (1, 2 and 3) is provided in Table 7.3. Table 7.4 presents the outcomes of the LME modelling (Model 7.1). The results from the LME analysis are presented for various clinical lung function parameters and predictors: COVID-19 severity (1, 2 or 3), height, BMI, pack-years and sex.

The intercept for FEV_1 % predicted was significant ($p < 0.001$). This essentially has no physiological meaning because it simply reflects the choices made for the scaling of the predictors. Here, for example, in the regressor log(BMI), if BMI happened to be measured in grams/m^2 instead of in kg/m^2, then the intercept would be entirely different. Therefore, the significance or otherwise of the values for the intercept in the regression analyses of this chapter will not be considered further. The coefficients for COVID-19 severity showed no significant difference between the Severity 1 group and the two more severe groups, which suggested that severity alone may not have influenced the FEV_1 % predicted factor in a statistically significant manner. A significant negative association was found between BMI and FEV_1 % predicted ($p=0.003$), which implied that higher BMI was associated with poorer lung function.

Similar to FEV_1, changes in FVC % predicted were not significantly different across the COVID-19 severity groups. However, BMI showed a significant negative effect on FVC % predicted ($p=0.005$); this finding aligned with the known impact of higher BMI on lung volume reduction.

For the ratio of FEV_1 to FVC there were no significant differences for Severity 2 and Severity 3 compared to Severity 1, although there was a trend towards a decrease in the ratio for the more severe groups.

DLCOc% predicted started high (for the Severity 1 group, which is taken as the baseline group) but showed a noticeable decline in the most severe COVID-19 group (Severity 3) (*p=0.146*). This finding suggested that there was a notable impact of severe COVID-19 on gas exchange capabilities.

No significant differences were observed across the severity groups for KCOc % predicted, but a significant positive relationship was found between BMI and KCOc % predicted (*p=0.017*). This latter finding indicated an increased transfer coefficient per unit volume in participants with higher BMI.

Alveolar volume % predicted began high for the baseline Severity 1 group but showed a decreasing trend in the more severe COVID-19 groups, with a greater reduction in Severity 3, although this fall did not reach statistical significance (*p=0.093*). This highlights that the lung volume available for gas exchange was reduced in more severe cases.

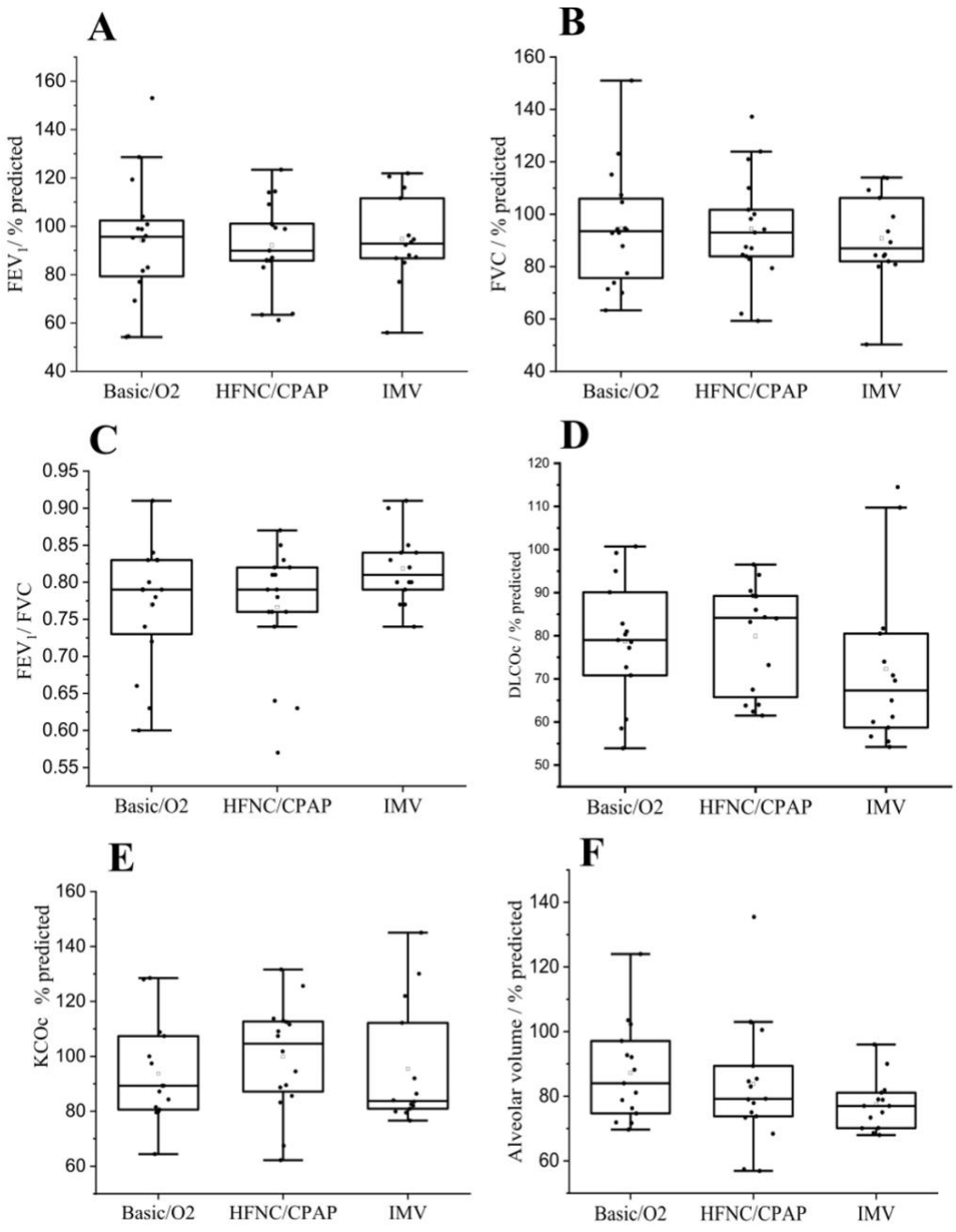


Figure 7.4. Lung function parameters across different COVID-19 severity groups. **A.** There was no significant difference in forced expiratory volume in 1s (FEV_1) % predicted across the severity groups. **B.** There was no significant difference in forced vital capacity (FVC) % predicted across the severity groups. **C.** The FEV_1/FVC ratio showed a trend toward lower ratios in the most severe group, but this trend did not reach statistical significance. **D.** The diffusing capacity of the lung for CO corrected for haemoglobin (DLCOc) was found to be lower in the Severity 3 (most severe) group. **E.** No significant difference in CO transfer coefficient for the lung corrected for haemoglobin (KCOc) was noted across the COVID-19 severity groups. **F.** Alveolar volume was found to be lower in the COVID-19 Severity 3 group. Severity group 1: Basic/O_2, standard hospital care with or without simple O_2 therapy; Severity group 2: HFNC/CPAP, high-flow nasal cannula or continuous positive airway pressure; Severity group 3: IMV, invasive mechanical ventilation. For box and whisker plots, the median line is shown with the interquartile range as the box. The whiskers show the maximum and minimum values that still remain within 1.5 times the interquartile range beyond the box. Outliers are shown as points beyond the whisker plots.

Table 7.3. Clinical lung function and radiology three-to-six months after hospital discharge across COVID-19 severity groups

Variables	Basic/O_2 Severity (1)	HFNC/CPAP Severity (2)	IMV Severity (3)	Overall Severity (1-2)
WHO severity	4-5	6	7-9	4-9
Days since hospital discharge±SD	154±66	162±49	157±37	158±54
Spirometry	(n=16)	(n=17)	(n=14)	(n=47)
FEV_1±SD / % predicted	94±26	92±18	95±18	94±20
FVC±SD / % predicted	95±22	94±20	90±17	93±20
(FEV_1 /FVC) ±SD	0.76±0.08	0.76±0.08	0.81±0.04	0.78±0.07
Gas transfer	(n=15)	(n=17)	(n=14)	(n=46)
$DLCO_C$±SD / % predicted	77±14	79±13	69±16	75±15
KCO_C±SD / % predicted	92±20	99±18	92±19	94±19
Alveolar volume ±SD / % predicted	87±15	84±19	77±8	83±15
Images				
Ground glass changes on CT±SD (/ %)	11 (42)	13 (50)	14 (100)	38 (58)
Fibrotic changes on CT±SD (/ %)	1 (4)	4 (15)	10 (71)	15 (23)

WHO, World Health Organisation; Basic/O_2, standard hospital care with or without simple O_2 therapy; HFNC/CPAP, high-flow nasal cannula or continuous positive airway pressure; IMV, invasive mechanical ventilation; FEV_1, forced expiratory volume in 1s; FVC, forced vital capacity; DLCOc, diffusing capacity of the lung for CO corrected for haemoglobin; KCOc, CO transfer coefficient for the lung corrected for haemoglobin; CT, computed tomography. Values are means±SD.

Table 7.4. Regression coefficients for COVID-19 severity and significant participant characteristics regarding clinical lung function parameters, taken from LME modelling.

Predictors	*Est.*	*SE*	*df*	*p*
FEV_1±SD / % predicted				
Intercept	224.365	43.160	43	**<0.001**
Severity 1	0	0	-	**-**
Severity 2	1.576	6.771	43	0.817
Severity 3	5.367	7.177	43	0.459
Log(BMI)	-38.839	12.363	43	**0.003**
FVC±SD / % predicted				
Intercept	213.734	42.151	43	**<0.001**
Severity 1	0	0	-	-
Severity 2	3.237	6.613	43	0.627
Severity 3	0.664	7.009	43	0.925
Log(BMI)	-35.570	12.074	43	**0.005**
(FEV_1 /FVC) ±SD				
Intercept	0.769	0.047	44	**<0.001**
Severity 1	0	0	-	**-**
Severity 2	-0.003	0.026	44	0.910
Severity 3	0.049	0.027	44	0.074
$DLCO_C$±SD / % predicted				
Intercept	77.300	9.322	43	**<0.001**
Severity 1	0	0	-	-
Severity 2	1.431	5.168	43	0.783
Severity 3	-8.031	5.421	43	0.146
KCO_C±SD / % predicted				
Intercept	-5.227	40.683	42	0.898
Severity 1	0	0	-	-
Severity 2	3.158	6.467	42	0.628
Severity 3	-4.491	6.850	42	0.516
Log(BMI)	29.238	11.718	42	**0.017**
Alveolar volume ±SD / % predicted				
Intercept	87.207	9.622	43	**<0.001**
Severity 1	0	0	-	-
Severity 2	-3.368	5.335	43	0.531
Severity 3	-9.626	5.596	43	0.093

Est, estimate; *SE*, standard error; *df*, degrees of freedom; *p*, probability value; FEV_1, forced expiratory volume in 1s; FVC, forced vital capacity; DLCOc, diffusing capacity of the lung for CO corrected for haemoglobin; KCOc, CO transfer coefficient for the lung corrected for haemoglobin. Significant *p*-values are in bold. Severity 1 is the Basic/O_2 group; Severity 2 is the HFNC/CPAP group; Severity 3 is the IMV group. For the baseline categorical variable, Severity 1 was set as 0 and – as it is redundant.

7.3.1.2 Clinical lung function parameters across different CT-scores

Only CT scans that had been taken at the initial visit (three-to-six months after hospital discharge) were available. Of the 66 participants, 63 had CT scans at their initial visits. Figure 7.5 shows the first visit clinical lung function parameters across the different CT scores. An overview of these parameters for this cohort across the CT scores CT-1 to CT-3 (which corresponded with Severity groups 1 to 3) is provided in Table 7.5. Table 7.6 presents the outcomes of the LME modelling (Model 7.2). The results from the LME analysis are presented for various clinical lung function parameters with the predictors of COVID-19 severity (CT-1, CT-2, CT-3), height, BMI, pack-years and sex.

The baseline FEV_1 % predicted was high. However, a reduction was noted as radiological severity increased from CT-1 to CT-3, although these changes were not statistically significant (*p=0.672* for CT-3). Notably, a significant negative correlation was observed with BMI (*p=0.004*), which indicated that increased BMI was associated with decreased FEV_1 % predicted, as in the analysis of severity.

Similar to FEV_1, initial FVC % predicted (CT-1) started high but the reductions in FVC % predicted across the more severe CT categories (CT-2 and CT-3) were not statistically significant (*p=0.365* and *p=0.271*, respectively). Again, higher BMIs showed a significant negative impact (*p=0.005*).

The ratio of FEV_1 to FVC was stable across the CT categories, with no significant changes observed.

DLCOc % predicted was significantly impacted by the severity of the radiological findings. The CT-3 group in particular, which represented the most severe disease category, showed a notable decrease (*p=0.038*), which indicated significant impairment of gas exchange in this group.

For KCOc % predicted, no significant differences were found across the COVID-19 severity groups. However, BMI showed a significant positive association with KCOc % predicted (*p=0.016*), suggesting that higher BMI was associated with higher KCOc values.

Alveolar volume % predicted started high at baseline (CT-1) and showed a significant decrease in the CT-3 category (*p=0.020*). This finding suggested that more severe radiological damage was associated with reduced lung volumes that were available for gas exchange.

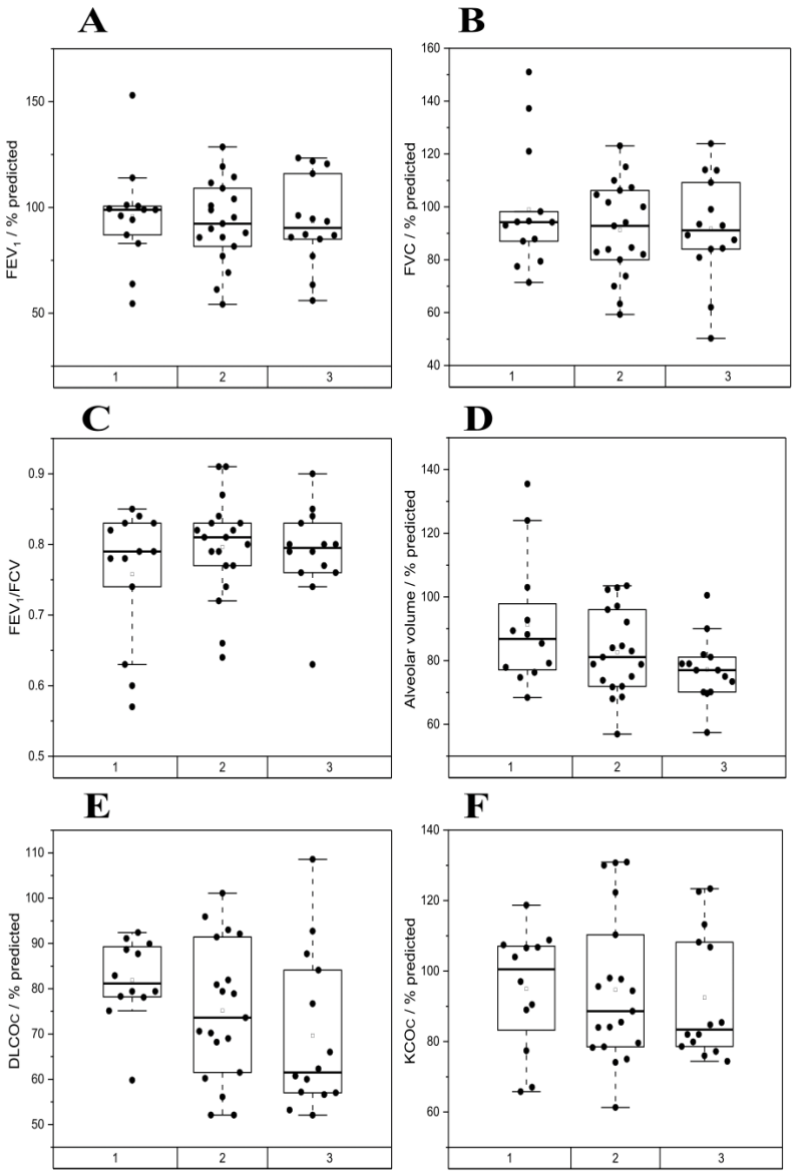


Figure 7.5. Lung function parameters across different CT scores at the first visit, which occurred between three and six months after hospital discharge. **A.** Forced expiratory volume in 1s (FEV_1) % predicted was found to be lower as the CT score increased. **B.** The average forced vital capacity (FVC) % predicted across more severe disease categories (CT-2 and CT-3) were not statistically significant. **C.** FEV_1/FVC was stable across the CT categories, with no significant changes observed. **D.** Alveolar volume started high at baseline but showed a significant decrease in the CT-3 group (most lung damage). **E.** The diffusing capacity of the lung for CO corrected for haemoglobin (DLCOc) was found to be lower in the CT-3 category (most lung damage). **F.** No significant difference in CO transfer coefficient for the lung corrected for haemoglobin (KCOc) was noted across the CT scores. 1-Normal: radiological findings within the normal range, which indicated the absence of significant pathological changes; 2-Ground glass: radiological evidence of ground glass opacities, which suggested certain pulmonary pathophysiological changes; 3-Ground glass and fibrotic changes: both ground glass opacities and fibrotic changes on radiological assessment. For box and whisker plots, the median line is shown with the interquartile range as the box. The whiskers show the maximum and minimum values that still remain within 1.5 times the interquartile range beyond the box. Outliers are shown as points beyond the whisker plots.

Table 7.5. Clinical lung function between three and six months after hospital discharge across different CT scores.

Variables	Normal (1)	Ground glass (2)	Ground glass and fibrotic (3)	Overall Severity (1-3)
Days since hospital discharge±SD	165±51	158±67	153±37	160±54
Spirometry	(n=13)	(n=19)	(n=14)	(n=46)
FEV_1±SD / % predicted	96±24	93±19	93±21	94±21
FVC±SD / % predicted	99±23	91±18	92±21	94±21
(FEV_1 /FVC) ±SD	0.76±0.09	0.80±0.07	0.79±0.06	0.78±0.07
Gas transfer	(n=12)	(n=19)	(n=14)	(n=45)
$DLCO_C$±SD / % predicted	82±9	75±15	70±17 *****	75±15
KCO_C±SD / % predicted	95±17	95±21	92±18	94±19
Alveolar volume±SD / % predicted	91±20	83±13	77±10 *****	83±15

1-Normal: radiological findings within the normal range, which indicated the absence of significant pathological changes; 2-Ground glass: radiological evidence of ground glass opacities, which suggested certain pulmonary pathophysiological changes; 3-Ground glass and fibrotic changes: both ground glass opacities and fibrotic changes on radiological assessment. FEV_1 forced expiratory volume in 1s; FVC forced vital capacity; DLCOc, diffusing capacity of the lung for CO corrected for haemoglobin; KCOc, CO transfer coefficient for the lung corrected for haemoglobin. Three of the 66 participants did not have an initial visit to radiology. Values are means±SD. $^{*}p < 0.05$. Linear Mix effect Modelling (LME) table 7.6.

Table 7.6. Regression coefficients for CT scores and significant participant characteristics against clinical lung function parameters from the LME modelling.

Predictors	*Est.*	*SE*	*df*	*p*
FEV_1±SD / % predicted				
Intercept	223.864	43.683	42	**<0.001**
CT-1	0	0	-	-
CT-2	-1.105	6.989	42	0.875
CT-3	-3.184	7.462	42	0.672
Log(BMI)	-37.562	12.267	42	**0.004**
FVC±SD / % predicted				
Intercept	218.622	41.970	42	**<0.001**
CT-1	0	0	-	-
CT-2	-6.150	6.751	42	0.365
CT-3	-8.005	7.170	42	0.271
Log(BMI)	-35.076	11.786	42	**0.005**
FEV_1 /FVC±SD				
Intercept	0.758	0.049	43	**<0.001**
CT-1	0	0	-	-
CT-2	0.039	0.027	43	0.167
CT-3	0.032	0.029	43	0.278
$DLCO_C$±SD / % predicted				
Intercept	81.894	9.494	42	**<0.001**
CT-1	0	0	-	-
CT-2	-6.725	5.369	42	0.217
CT-3	-12.263	5.729	42	**0.038**
KCO_C±SD / % predicted				
Intercept	-3.243	40.926	41	0.937
CT-1	0	0	-	-
CT-2	-1.960	6.697	41	0.771
CT-3	-2.285	7.108	41	0.749
Log(BMI)	28.913	11.545	41	**0.016**
Alveolar volume ±SD / % predicted				
Intercept	91.223	9.580	42	**<0.001**
CT-1	0	0	-	-
CT-2	-8.582	5.418	42	0.121
CT-3	-13.991	5.780	42	**0.020**

Est, estimate; *SE*, standard error; *df*, degrees of freedom; *p*, probability value; FEV_1, forced expiratory volume in 1s; FVC, forced vital capacity; DLCOc, diffusing capacity of the lung for CO corrected for haemoglobin; KCOc, CO transfer coefficient for the lung corrected for haemoglobin; Significant *p*-values are in bold. CT-1, Normal: radiological findings within the normal range, which indicated the absence of significant pathological changes; CT-2, Ground glass: radiological evidence of ground glass opacities which suggested certain pulmonary pathophysiological changes; CT-3, Ground glass and fibrotic changes: both ground glass opacities and fibrotic changes on radiological assessment. For the baseline categorical variable, CT-1 was set as 0 and – as it is redundant.

7.3.2 CCP parameters 3 to 6 months and 12-months post-hospital discharge

For CCP parameters, data from the initial visit (between three- and six-months post hospital discharge) and the follow-up visit (12 months post hospital discharge) were available. A comparison between the two visits is discussed in more detail separately in section 7.3.2.3.

7.3.2.1 CCP parameters across COVID-19 severity groups

Figure 7.6 shows the CCP parameters at the first visit. An overview of these CCP parameters for this cohort across the different severity groups is provided in Table 7.7, and Table 7.8 presents the outcomes of the LME modelling (Model 7.1). The results from the LME analysis are presented for various CCP parameters with the predictors of COVID-19 severity (1, 2 and 3), height, BMI, days since discharge, pack-years and sex.

A significant increase in V_D was observed in the most severe COVID-19 group compared with the baseline Severity 1 ($p=0.002$). This finding indicated that patients who had faced more severe COVID-19 had greater increases in dead space. Height showed a strong positive association with V_D ($p<0.001$), which reflected expected physiological variations in lung volume with body size.

V_A did not show significant differences across the COVID-19 severity levels; there was a slight but not significant ($p=0.377$) decrease in V_A for the most severe cases (Severity 3). A significant positive correlation was found between height and VA ($p<0.001$) while BMI was negatively associated with VA ($p=0.004$); these findings indicated that, as with lung volume, alveolar volume was greater in taller people, and that higher BMI was associated with reduced alveolar volume, possibly due to mechanical compression and reduced chest wall compliance.

FRC % predicted started high in the baseline Severity 1 and showed a significant decline in more severe cases ($p=0.018$ for Severity 3), which suggested that severe COVID-19

negatively affected lung capacity. BMI also showed a significant negative association with FRC % predicted (*p<0.001*). Pack-years of smoking showed a marginal impact on FRC (*p=0.016*), indicating the adverse effects of long-term smoking on lung function.

For σVD, no significant changes were observed across the different severity groups. Females exhibited a higher σVD (*p= 0.001*).

σlnCL showed no significant changes with increasing COVID-19 severity; a modest but insignificant increase was observed with Severity 3 (*p=0.101*). Gender differences were also noted, with females showing slightly higher σlnCL (*p = 0.037*).

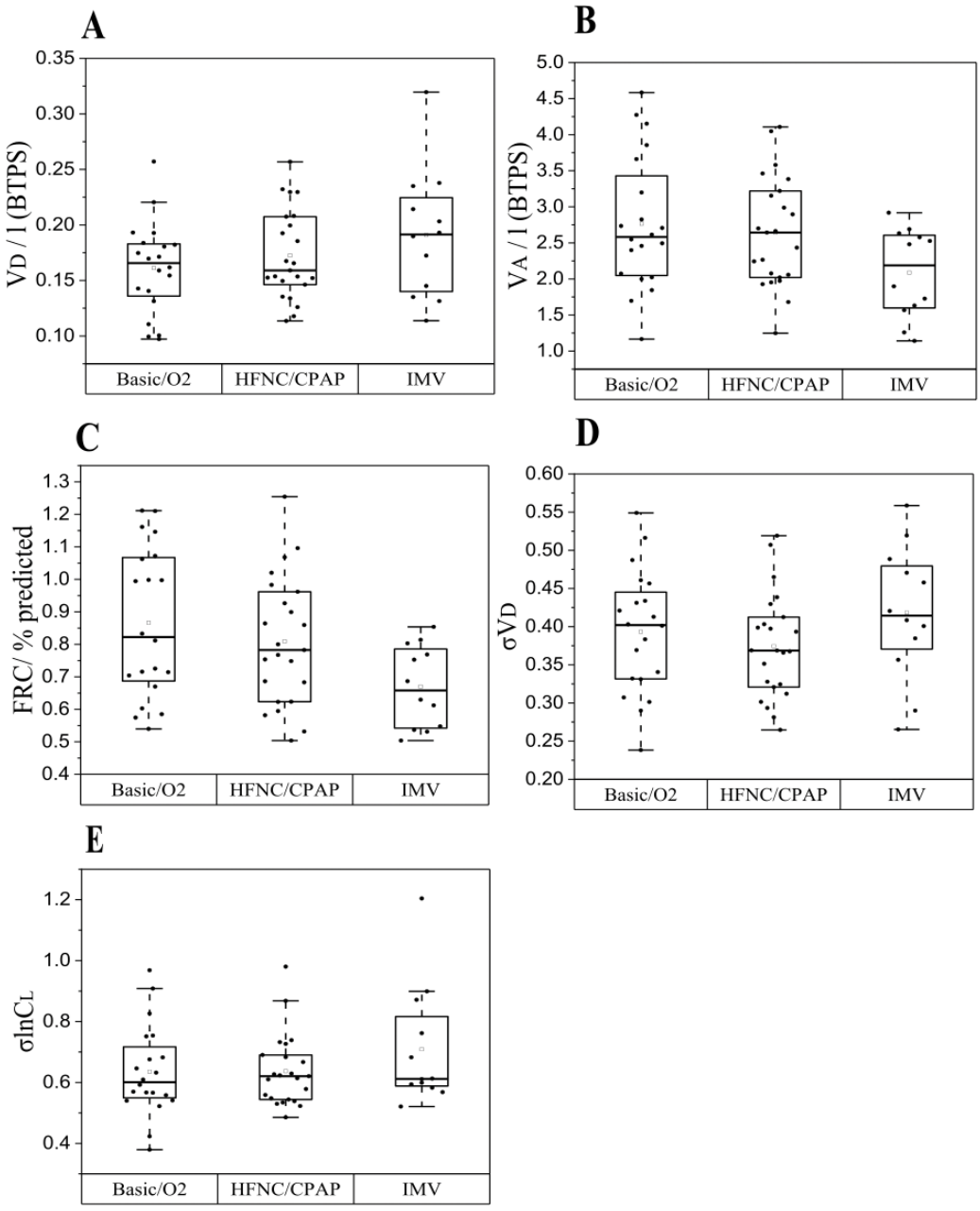


Figure 7.6. CCP parameters across different COVID-19 severity groups at the first visit, which took place three-to-six months after hospital discharge. **A.** End-inspiratory dead space (VD) was significantly larger in the most severely affected group. **B.** Alveolar volume (VA) appeared to decrease as severity increased but this did not reach statistical significance. **C.** Functional residual capacity % predicted (FRC% predicted) was significantly lower in the most severe group). **D.** The average of the SD of the normal distribution for dead space across lung volume (σVD) remained unchanged across the severity groups. **E.** The SD of log-normal distributions for alveolar compliance (σlnCL) showed no significant changes with increasing COVID-19 severity, but a modest increase was observed with Severity 3. Basic/O_2, standard hospital care with or without simple O_2 therapy; HFNC/CPAP, high-flow nasal cannula or continuous positive airway pressure; IMV, invasive mechanical ventilation. For box and whisker plots, the median line is shown with the interquartile range as the box. The whiskers show the maximum and minimum values that still remain within 1.5 times the interquartile range beyond the box. Outliers are shown as points beyond the whisker plots.

Table 7.7. CCP parameters between three and six months after hospital discharge across different COVID-19 severities.

Variables	Basic/O_2 Severity (1)	HFNC/CPAP Severity (2)	IMV Severity (3)	Overall Severity (1-2)
WHO severity	4-5 n=20	6 n=23	7-9 n=12	4-9 n=55
V_D±SD / l	0.161±0.041	0.172±0.040	0.190±0.058 **	0.172±0.045
V_A±SD / l	2.76±0.92	2.64±0.76	2.08±0.61	2.56±0.52
FRC±SD / % predicted	0.86±0.23	0.81±0.19	0.67±0.13 *	0.79±0.20
σV_D	0.39±0.08	0.37±0.07	0.42±0.09	0.39±0.07
σlnC_L	0.64±0.15	0.64±0.12	0.70±0.19	0.65±0.15

WHO, World Health Organisation; Basic/O_2, standard hospital care with or without simple O_2 therapy; HFNC/CPAP, high-flow nasal cannula or continuous positive airway pressure; IMV, invasive mechanical ventilation; V_D, dead space at end-inspiration; V_A, alveolar volume at FRC; FRC, functional residual capacity; σV_D, the SD of the normal distribution for (normalised) dead space across lung volume; σlnC_L, the SD of log-normal distributions for (normalised) alveolar compliance. BTPS, body temperature (37°C), ambient pressure and gas saturated with water vapour. Values are means±SD. *, p<0.05; **, p<0.005, Linear Mix effect Modelling (LME) table 7.8.

Table 7.8. Regression coefficients for COVID-19 severity and significant participant characteristics regarding CCP parameters from LME modelling.

Predictors	*Est.*	*SE*	*df*	*p*
V_D / l (BTPS)				
Intercept	-0.087	0.048	77.385	0.071
Severity 1	0	0	-	-
Severity 2	0.010	0.009	68.651	0.300
Severity 3	0.041	0.012	58.773	**0.002**
Log(Height)	0.448	0.076	53.012	**<0.001**
V_A±SD / l				
Intercept	2.617	1.725	50	0.136
Severity 1	0	0	-	-
Severity 2	0.029	0.180	50	0.872
Severity 3	-0.203	0.228	50	0.377
Log(Height)	8.007	1.349	50	**<0.001**
Log(BMI)	-1.279	0.426	50	**0.004**
FRC /% predicted				
Intercept	2.376	0.389	67.680	**<0.001**
Severity 1	0	0	-	**-**
Severity 2	-0.055	0.043	76.809	0.207
Severity 3	-0.149	0.061	59.393	**0.018**
Log(BMI)	-0.450	0.111	60.083	**<0.001**
Pack-years	0.004	0.002	54.167	**0.016**
σV_D				
Intercept	0.370	0.045	51	**<0.001**
Severity 1	0	0	-	**-**
Severity 2	-0.005	0.022	51	0.804
Severity 3	0.029	0.026	51	0.265
Sex-0	0	0	-	-
Sex-1	0.079	0.023	51	**0.001**
σlnC_L				
Intercept	0.614	0.085	79	**<0.001**
Severity 1	0	0	-	**-**
Severity 2	0.006	0.038	72.265	0.870
Severity 3	0.083	0.050	57.413	0.101
Sex-0	0	0	-	-
Sex-1	0.099	0.046	53.925	**0.037**

Est, estimate; *SE*, standard error; *df*, degrees of freedom; *p*, probability value; V_D, dead space at end-inspiration; V_A, alveolar volume at FRC; FRC, functional residual capacity; σV_D, the SD of the normal distribution for (normalised) dead space across lung volume; σlnC_L, the SD of log-normal distributions for (normalised) alveolar compliance; BTPS, body temperature (37°C), ambient pressure and gas saturated with water vapour; BMI, body mass index; Sex-0, male; Sex-1, female; Severity 1 is Basic/O_2 group; Severity 2 is HFNC/CPAP group; Severity 3 is IMV group; Log(days), days since hospital discharge. Significant *p*-values are in bold. For baseline categorical variables, Severity 1 and Sex-0 were set as 0 and – as it is redundant.

7.3.2.2 CCP parameters across different CT-scores

Figure 7.7 showcases the clinical lung function parameters across the different CT scores at the first visit. An overview of the first visit CCP parameters for this cohort across the different CT scores (CT-1 to CT-3) is provided in Table 7.9. Table 7.10 presents the outcomes of the LME modelling (Model 7.2). The results from the LME analysis are presented for various CCP parameters with the predictors of COVID-19 severity (CT-1, CT-2, CT-3), height, BMI, days since discharge, pack-years and sex.

For V_D, the analysis showed a significant increase ($p=0.012$) in the CT-3 group, which comprised patients with severe lung damage that was shown by the presence of both ground glass opacities and fibrotic changes. Height was strongly correlated with V_D, which suggested that taller individuals have larger dead space volumes ($p<0.001$).

Changes in V_A across different CT categories were not statistically significant, although there was a trend towards reduced V_A in the most severe CT-3 group ($p = 0.412$). Both height and BMI significantly influenced V_A, with height positively affecting V_A ($p < 0.001$) and BMI negatively affecting it ($p < 0.001$), highlighting the impact of body composition on lung volumes.

FRC % predicted started high at baseline (CT-1) with a minor non-significant reduction in the CT-2 and CT-3 groups. BMI negatively impacted FRC % predicted significantly ($p<0.001$), and smoking history (pack-years) was associated with a slight decrease in FRC ($p=0.022$).

The σV_D showed no significant changes across the CT categories. However, gender showed an impact where females exhibited a higher σV_D ($p = 0.002$).

$\sigma \ln CL$ showed minor changes across the CT categories, although these were not statistically significant.

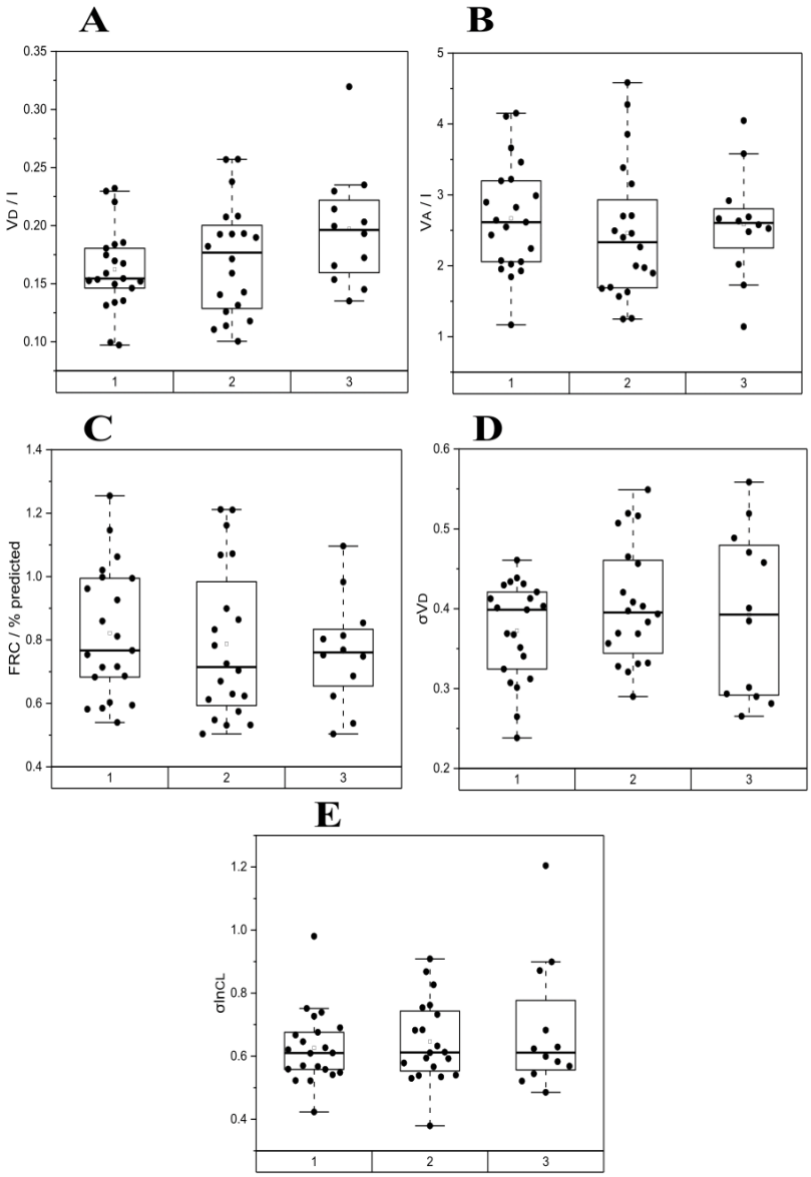


Figure 7.7. CCP parameters across different CT scores at the first visit. **A.** End-inspiratory dead space (VD) was significantly larger in the CT-3 group (most lung damage). **B.** Alveolar volume (VA) seemed to be lower as severity increased but this did not reach statistical significance. **C.** Functional residual capacity % predicted (FRC% predicted) seemed to be reduced as severity increased but this did not reach statistical significance. **D.** The average SD of the normal distribution for dead space across lung volume (σVD) was unchanged across the severity groups**. E.** The SD of log-normal distributions for alveolar compliance (σlnCL) was unchanged across the severity groups. 1-Normal: radiological findings within the normal range, which indicated the absence of significant pathological changes; 2-Ground glass: radiological evidence of ground glass opacities, which suggested certain pulmonary pathophysiological changes; 3-Ground glass and fibrotic changes: both ground glass opacities and fibrotic changes on radiological assessment. For box and whisker plots, the median line is shown with the interquartile range as the box. The whiskers show the maximum and minimum values that still remain within 1.5 times the interquartile range beyond the box. Outliers are shown as points beyond the whisker plots.

Table 7.9. CCP parameters between three and six months after hospital discharge across different CT scores.

Variable	Normal (1) n=21	Ground glass (2) n=20	Ground glass and fibrotic (3) n=12	Overall Severity (1-3) n=53
V_D±SD / l	0.162±0.036	0.171±0.048	0.197±0.050 *	0.173±0.045
V_A±SD / l	2.67±0.78	2.46±0.96	2.58±0.76	0.57±0.84
FRC±SD / % predicted	0.82±0.20	0.79±0.24	0.76±0.169	0.79±0.21
σV_D	0.37±0.06	0.41±0.07	0.39±0.10	0.39±0.07
$\sigma \ln C_L$	0.63±0.11	0.65±0.13	0.68±0.21	0.65±0.14

1-Normal: radiological findings within the normal range, which indicated the absence of significant pathological changes; 2-Ground glass: radiological evidence of ground glass opacities, which suggested certain pulmonary pathophysiological changes; 3-Ground glass and fibrotic changes: both ground glass opacities and fibrotic changes on radiological assessment; V_D, dead space at end-inspiration; V_A, alveolar volume at FRC; FRC, functional residual capacity; σV_D, the SD of the normal distribution for (normalised) dead space across lung volume; $\sigma \ln C_L$, the SD of log-normal distributions for (normalised) alveolar compliance; BTPS, body temperature (37°C), ambient pressure and gas saturated with water vapour. Values are means±SD. *, $p<0.05$. Linear Mix effect Modelling (LME) table 7.10.

Table 7.10. Regression coefficients for CT scores and significant participant characteristics regarding the CCP parameters from the LME modelling.

Predictors	*Est.*	*SE*	*df*	*p*
V_D / l (BTPS)				
Intercept	-0.042	0.049	71.300	0.396
CT-1	0	0	-	-
CT-2	0.014	0.011	49.606	0.198
CT-3	0.033	0.013	51.156	**0.012**
Log(Height)	0.366	0.079	49.376	**<0.001**
V_A±SD / l				
Intercept	3.179	1.577	62.216	**0.048**
CT-1	0	0	-	-
CT-2	0.019	0.175	50.572	0.914
CT-3	-0.172	0.208	51.131	0.412
Log(Height)	8.814	1.312	50.688	**<0.001**
Log(BMI)	-1.566	0.372	58.799	**<0.001**
FRC /% predicted				
Intercept	2.628	0.401	66.087	**<0.001**
CT-1	0	0	-	-
CT-2	-0.015	0.053	51.280	0.784
CT-3	-0.077	0.064	51.849	0.236
Log(BMI)	-0.533	0.113	57.677	**<0.001**
Pack-years	0.005	0.002	51.841	**0.022**
σV_D				
Intercept	0.360	0.045	49	**<0.001**
CT-1	0	0	-	-
CT-2	0.020	0.023	49	0.379
CT-3	0.025	0.026	49	0.330
Sex-0	0	0	-	-
Sex-1	0.085	0.026	49	**0.002**
σlnC_L				
Intercept	0.630	0.089	78	**<0.001**
CT-1	0	0	-	-
CT-2	0.022	0.044	51.891	0.621
CT-3	0.051	0.052	53.067	0.337

Est, estimate; *SE*, standard error; *df*, degrees of freedom; *p*, probability value; V_D, dead space at end-inspiration; V_A, alveolar volume at FRC; FRC, functional residual capacity; σV_D, the SD of the normal distribution for (normalised) dead space across lung volume; σlnC_L, the SD of log-normal distributions for (normalised) alveolar compliance; BTPS, body temperature (37°C), ambient pressure and gas saturated with water vapour; BMI, body mass index; Sex-0, male;Sex-1, female; CT-1, Normal: radiological findings within the normal range, which indicated the absence of significant pathological changes; CT-2, Ground glass: radiological evidence of ground glass opacities, which suggested certain pulmonary pathophysiological changes; CT-3, Ground glass and fibrotic changes: both ground glass opacities and fibrotic changes on radiological assessment. Significant *p*-values are in bold. For baseline categorical variables, CT-1 and Sex-0 were set as 0 and – as it is redundant.

7.3.2.3 CCP parameters at the initial vs. follow-up visits

At the follow-up visit (12 months after hospital discharge), only the CCP breathing test was conducted. Of the initial 66 participants, 30 returned for their follow-up assessments. Analysis of the five CCP parameters revealed that only σV_D exhibited a significant difference after the condition/treatment compared with before, with a *p-value* of *0.002* (Table 7.11). The remaining parameters did not show significant changes, which indicated that the passage of time had not had a significant impact on these measures.

Table 7.11. CCP parameters at three-to-six months and 12 months after hospital discharge.

Variable	**Visit 1 (3-6 months post-hospital discharge)** n=55	**Visit 2 (12 months post-hospital discharge)** n=28
V_D±SD / l	0.172±0.045	0.171±0.035
V_A±SD / l	2.56±0.52	2.75±0.94
FRC±SD / % predicted	0.79±0.20	0.83±0.21
σV_D	0.39±0.07	0.35±0.06 **
$\sigma \ln C_L$	0.65±0.15	0.64±0.14

V_D, dead space at end-inspiration; V_A, alveolar volume at FRC; FRC, functional residual capacity; σV_D, the SD of the normal distribution for (normalised) dead space across lung volume; $\sigma \ln C_L$, the SD of log-normal distributions for (normalised) alveolar compliance. Values are means±SD. ** $p<0.005$ (paired t-test).

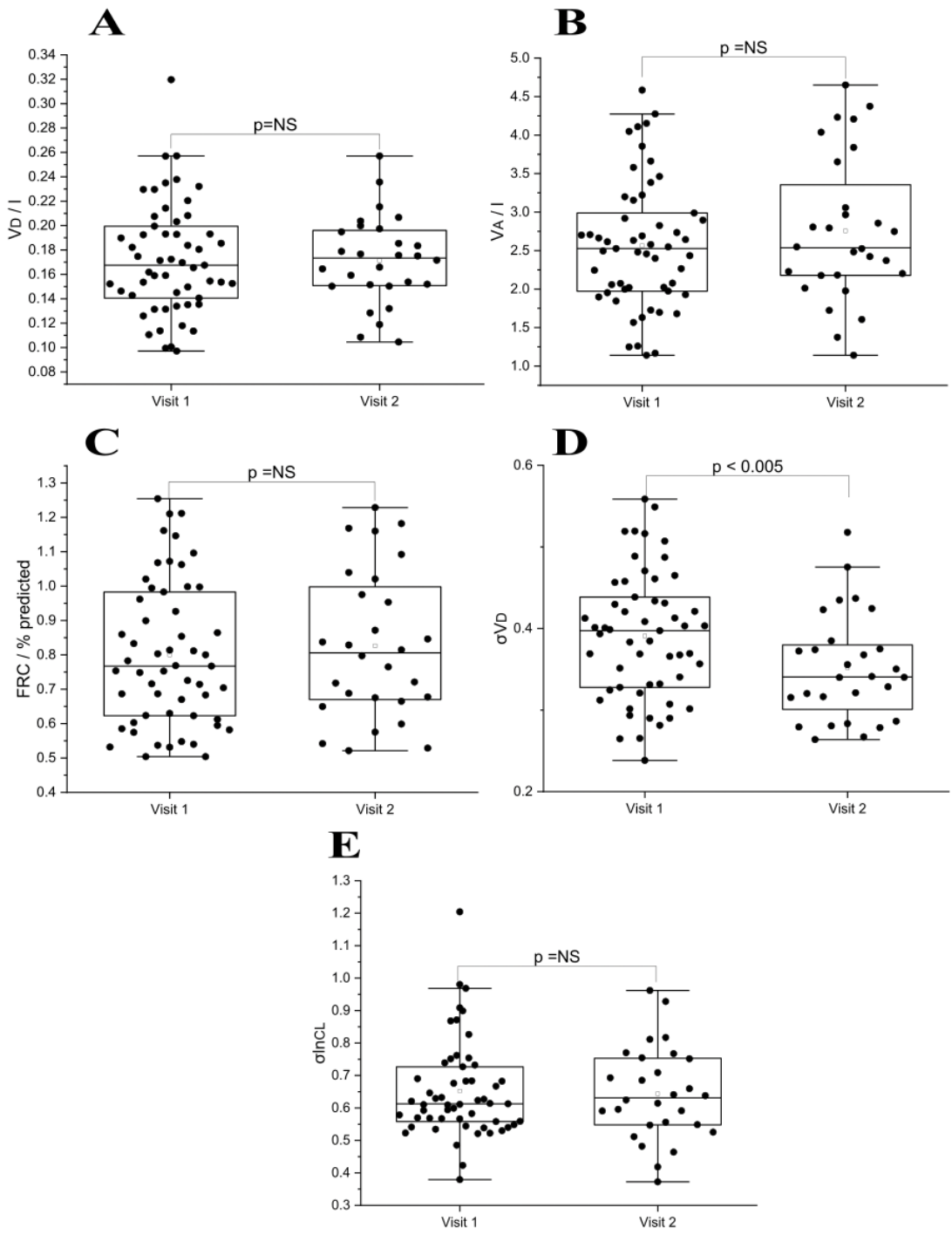


Figure 7.8. CCP parameters at the initial and follow-up visits. **A.** There was no significant difference in end-inspiratory dead space (VD) between visits. **B.** There was no significant difference in alveolar volume (VA) between visits. **C.** There was no significant difference in the functional residual capacity % predicted (FRC% predicted) between visits. **D.** There was a significant reduction in the SD of the normal distribution for dead space across lung volume (σVD) between visits. **E.** The SD of log-normal distributions for alveolar compliance (σlnCL) was unchanged across severity groups. Visit 1: initial visit three-to-six months post hospital discharge. Visit 2: follow-up visit 12 months post hospital discharge. For box and whisker plots, the median line is shown with the interquartile range as the box. The whiskers show the maximum and minimum values that still remain within 1.5 times the interquartile range beyond the box. Outliers are shown as points beyond the whisker plots.

7.3.3 Relationship between CCP and clinical lung function parameters at the initial visit

The correlation analysis among the traditional clinical lung function and CCP parameters, which is shown in Table 7.12 and Figures 7.9, 7.10 and 7.11, showcases only the significant correlations.

FEV_1 % predicted was significantly positively correlated with the CCP alveolar volume (VA) (*r=0.530, p<0.001*) (Figure 7.9A) and with FRC % predicted (*r=0.399, p=0.013*) (Figure 7.10A). These findings suggest that higher forced expiratory volume in one second is associated with greater lung volumes. However, its correlations with VD, σVD and σlnCL were weak and not statistically significant.

FVC % predicted demonstrated very strong positive correlations with VA (*r=0.727, p<0.001*) (Figure 7.9B) and with FRC % predicted (*r=0.616, p<0.001*) (Figure 7.10B). Its correlations with VD, σVD and σlnCL were weak and not statistically significant.

The FEV_1/FVC ratio had significant negative correlations with both VA (*r=-0.430, p=0.007*) (Figure 7.9C) and with FRC % predicted (*r=-0.430, p=0.007*) (Figure 7.10C). These findings indicate that a higher ratio is associated with smaller lung volumes. The correlations with VD, σVD and σlnCL were weak and not statistically significant.

DLCOc % predicted exhibited moderate positive correlations with VD (*r=0.337, p=0.041*) (Figure 7.11) and with VA (*r=0.382, p=0.019*) (Figure 7.9D), suggesting that higher diffusion capacity of the lung for carbon monoxide is associated with larger lung volumes. Its correlations with FRC % predicted, σVD and σlnCL were weak and not statistically significant.

KCOc % predicted showed a weak negative correlation with VA (*r=-0.282, p=0.091*) and a significant negative correlation with FRC % predicted (*r=-0.395, p=0.016*) (Figure 7.10D). These findings indicate that larger lung volumes are associated with a lower carbon monoxide transfer coefficient. Its correlations with VD, σVD and σlnCL were weak and not statistically significant.

Alveolar volume % predicted showed very strong positive correlations with both FRC % predicted (*r=0.771, p<0.001*) (Figure 7.10E) and with V_A (measured through the use of CCP) (r=*0.777, p<0.001*) (Figure 7.9E). These findings highlight the strong relationship between these measures of lung volume. Its correlations with V_D, σV_D and σlnCL were weak and not statistically significant.

Table 7.12. Correlation analysis among clinical lung function and CCP parameters in the post-COVID-19 cohort at their first visit

Variables		VD / l (BTPS)	VA / l	FRC /% predicted	σVD	σlnCL
FEV_1 / % predicted	Pearson Correlation	.120	.530	.399	-.113	-.279
	p	.472	**<.001**	**.013**	.499	.090
FVC/ % predicted	Pearson Correlation	.074	.727	.616	-.065	-.131
	p	.658	**<.001**	**<.001**	.697	.434
FEV_1 /FVC	Pearson Correlation	.030	-.430	-.430	-.038	-.175
	p	.856	**.007**	**.007**	.823	.294
$DLCO_C$ / % predicted	Pearson Correlation	.337	.382	.256	.024	.158
	p	**.041**	**.019**	.126	.887	.351
KCO_C/ % predicted	Pearson Correlation	.243	-.282	-.395	-.067	.055
	p	.147	.091	**.016**	.696	.747
Alveolar volume / % predicted	Pearson Correlation	.075	.777	.771	.084	.133
	p	.657	**<.001**	**<.001**	.619	.434

V_D, End-inspiratory dead space; V_A, alveolar volume at FRC; FRC, functional residual capacity; σV_D, the SD of the normal distribution for (normalised) dead space across lung volume; σlnCL, the SD of log-normal distributions for (normalised) alveolar compliance; BTPS, body temperature (37°C), ambient pressure and gas saturated with water vapour; FEV_1, forced expiratory volume in 1s; FVC, forced vital capacity; DLCOc, diffusion capacity of the lung for CO corrected for haemoglobin; KCOc, CO transfer coefficient for the lung corrected for haemoglobin. Significant *p*-values are in bold.

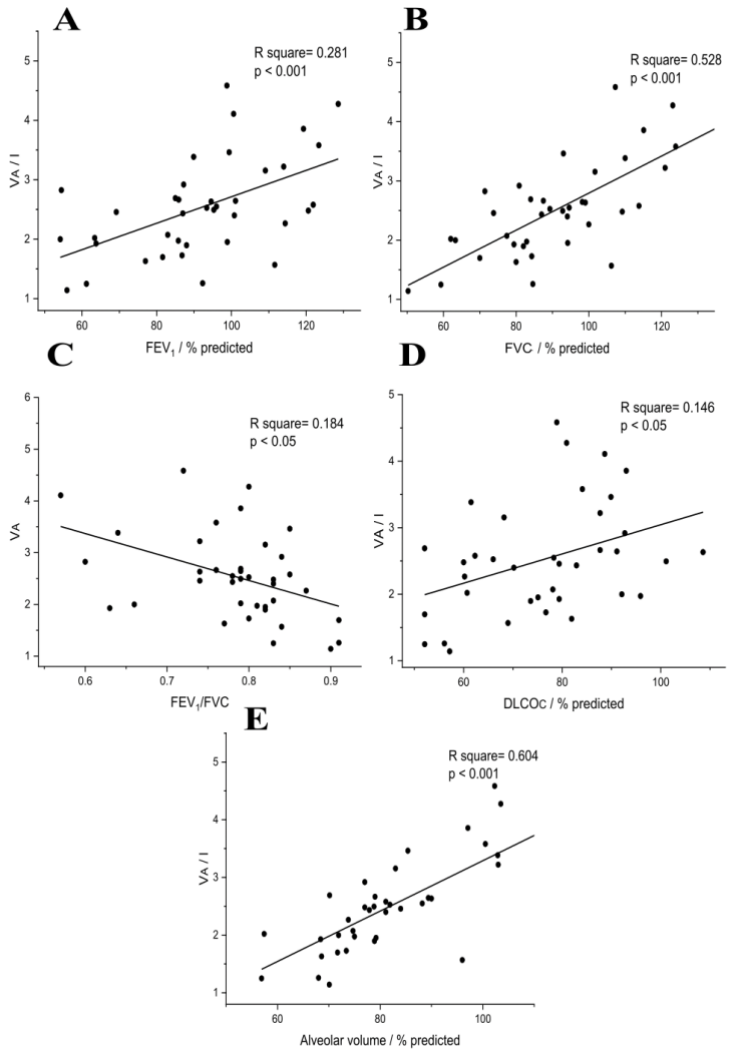


Figure 7.9. Relationship between alveolar volume (VA) measured by CCP and clinical lung function. **A.** A significant correlation between VA and forced expiratory volume in 1s (FEV_1) % predicted. **B.** A significant correlation between VA and forced vital capacity (FVC) % predicted. **C.** A significant correlation between VA and diffusion capacity of the lung for CO corrected for haemoglobin (DLCOc) % predicted. **D**. A significant negative correlation between VA and FEV_1/FVC. **E**.A significant correlation between VA and alveolar volume % predicted, measured by conventional lung function.

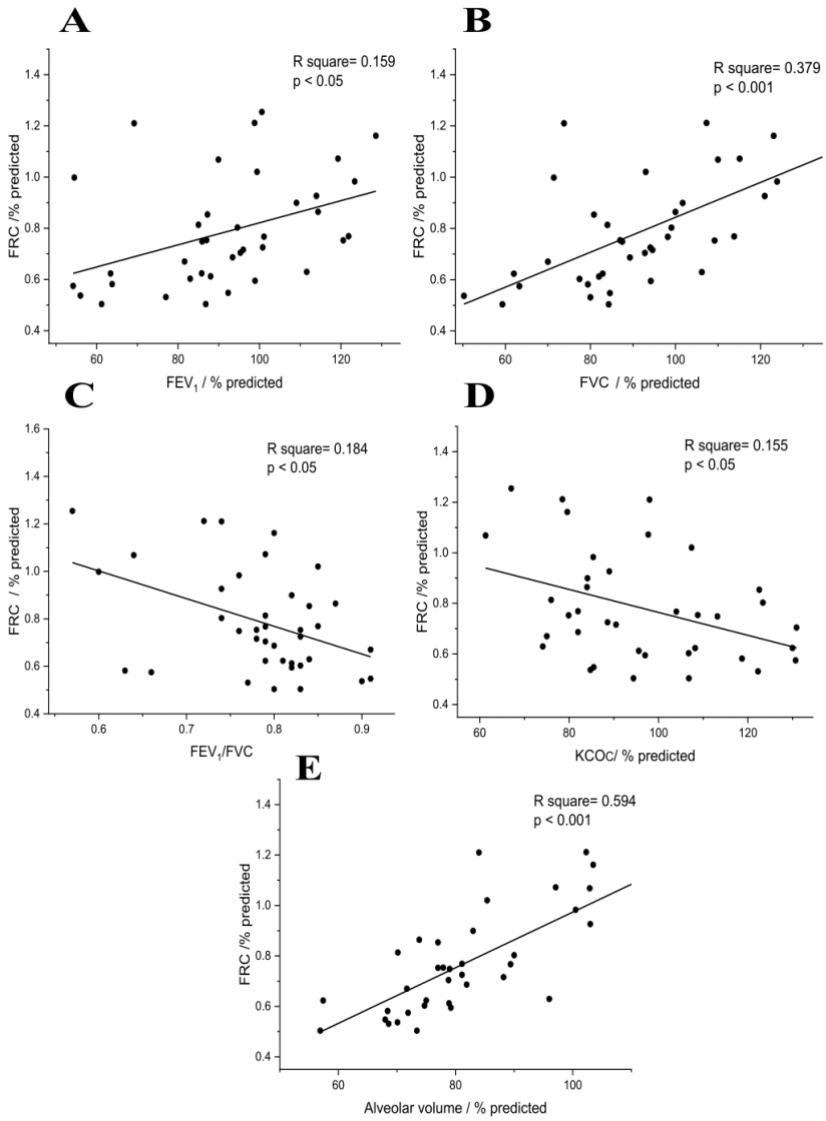


Figure 7.10. Relationship between functional residual capacity (FRC) % predicted measured by CCP and clinical lung function. **A.** A significant correlation between FRC and forced expiratory volume in 1s (FEV_1) % predicted. **B.** A significant correlation between FRC and forced vital capacity (FVC) % predicted. **C.** A significant negative correlation between FRC and FEV_1/FVC. **D**. A significant negative correlation between FRC and CO transfer coefficient for the lung corrected for haemoglobin (KCOc). **E**. A significant correlation between FRC and alveolar volume % predicted, as measured by conventional lung function.

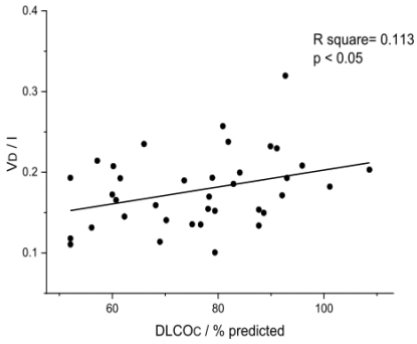


Figure 7.11. Relationship between end-inspiratory dead space (VD) measured by CCP and diffusion capacity of the lung for CO corrected for haemoglobin (DLCOc). The graph shows a significant positive correlation between VD and DLCOc.

7.3.4 Analysis of CCP parameters through the use of Z-scores

7.3.4.1 Z-scores across COVID-19 severity groups

Table 7.13 presents Z-scores that were calculated for each lung inhomogeneity parameter that was measured at the initial and follow-up visits within this cohort across the COVID-19 severity groups. The calculation took into consideration the participants' ages, heights, BMIs and sexes, based on the prediction equation that was developed for the study described in Chapter 5. Significant differences were observed in ZVD between the severity groups; in particular, it was significantly higher in the Severity-3 group (IMV), both at the initial and second visits. The parameters ZFRC, ZσVD and ZσlnCL did not show significant changes across the severity groups. However, ZFRC tended to decrease with increasing severity at both visits, whereas ZσlnCL showed a trend towards increasing scores with greater severity in both initial and follow-up assessments. Figure 7.13 shows the calculated Z-scores for each lung inhomogeneity parameter within this cohort across COVID-19 severities, compared with the healthy control cohort that was discussed in Chapter 5.

A *Student's t-test* was employed to compare the CCP parameter Z-scores with zero (Table 7.14). The results revealed distinctive patterns across the severity groups. Specifically,

ZVD exhibited statistical significance in the Severity 2 (HFNC/CPAP) group (*p=0.003*) and more prominently in the Severity 3 (IMV) group (*p=0.002*), but it did not differ significantly from zero in the Severity 1 (basic/O_2 therapy) group. On the other hand, ZFRC did not show a significant difference from zero in any severity group. ZσVD displayed significant differences from zero in both the basic/O_2 and IMV groups, but not in the HFNC/CPAP group. In contrast, ZσlnCL showed significant differences from zero in all severity groups (Severity 1, *p=0.018; Severity 2, p=0.003; and Severity 3, p=0.028*).

Additionally, a *chi-square* (X^2) goodness-of-fit test was conducted to examine whether the numbers of abnormal Z-scores for each CCP parameter within the COVID-19 severity levels differed significantly from the numbers of observations that would be expected to arise through chance (Table 7.15). For VD, for the basic/O_2 therapy group there was no excess of abnormal values. However, for the other two severity groups, there were significantly more individuals with high values for ZVD than would be expected by chance (*p<0.001*). For ZσVD and ZσlnCL, there were more abnormally high values than would be expected to occur by chance in all groups. For ZFRC, there were more abnormally low values than would be expected to occur by chance.

able 7.13. Calculated Z-scores for each CCP parameter three-to-six months and 12 months after hospital discharge across different COVID-19 severity groups.

Variables	Basic/O_2 Severity (1)	HFNC/CPAP Severity (2)	IMV Severity (3)	Overall Severity (1-2)
WHO severity	4-5	6	7-9	4-9
ZVD±SD / l				
First visit (n=20, n=23,n=12,and n=55)	0.514±1.002	0.910±1.159	2.165±1.737 **	1.040±1.380
Second visit (n=10, n=15,n=3,and n=28)	0.762±1.034	0.288±1.027	2.892±1.284 **	0.736±1.286
ZFRC±SD / % predicted				
First visit (n=20, n=23,n=12,and n=55)	-0.552±1.49	-0.454±1.346	-0.890±1.373	-0.585±1.389
Second visit (n=10, n=15,n=3,and n=28)	0.237±0.961	-0.667±1.091	-0.981±1.617	-0.375±1.159
ZσVD				
First visit (n=20,n=23,n=12,and n=55)	0.576±1.521	0.194±1.334	0.631±1.785	0.428±1.493
Second visit (n=10, n=15,n=3,and n=28)	0.145±1.397	-0.077±1.596	0.106±1.253	0.021±1.449
ZσlnCL				
First visit (n=20,n=23,n=12,and n=55)	1.050±1.517	0.892±1.159	1.8175±2.010	1.151±1.520
Second visit (n=10, n=15,n=3,and n=28)	0.969±1.652	0.797±1.574	3.589±2.966	1.157±1.894

WHO, World Health Organisation; Basic/O_2, standard hospital care with or without simple O_2 therapy; HFNC/CPAP, high-flow nasal cannula or continuous positive airway pressure; IMV, invasive mechanical ventilation; VD, dead space at end-inspiration; VA, alveolar volume at FRC; FRC, functional residual capacity; σVD, the SD of the normal distribution for (normalised) dead space across lung volume; σlnCL, the SD of log-normal distributions for (normalised) alveolar compliance; BTPS, body temperature (37°C), ambient pressure and gas saturated with water vapour. Values are means±SD. **, p<0.005; *one-way ANOVA*.

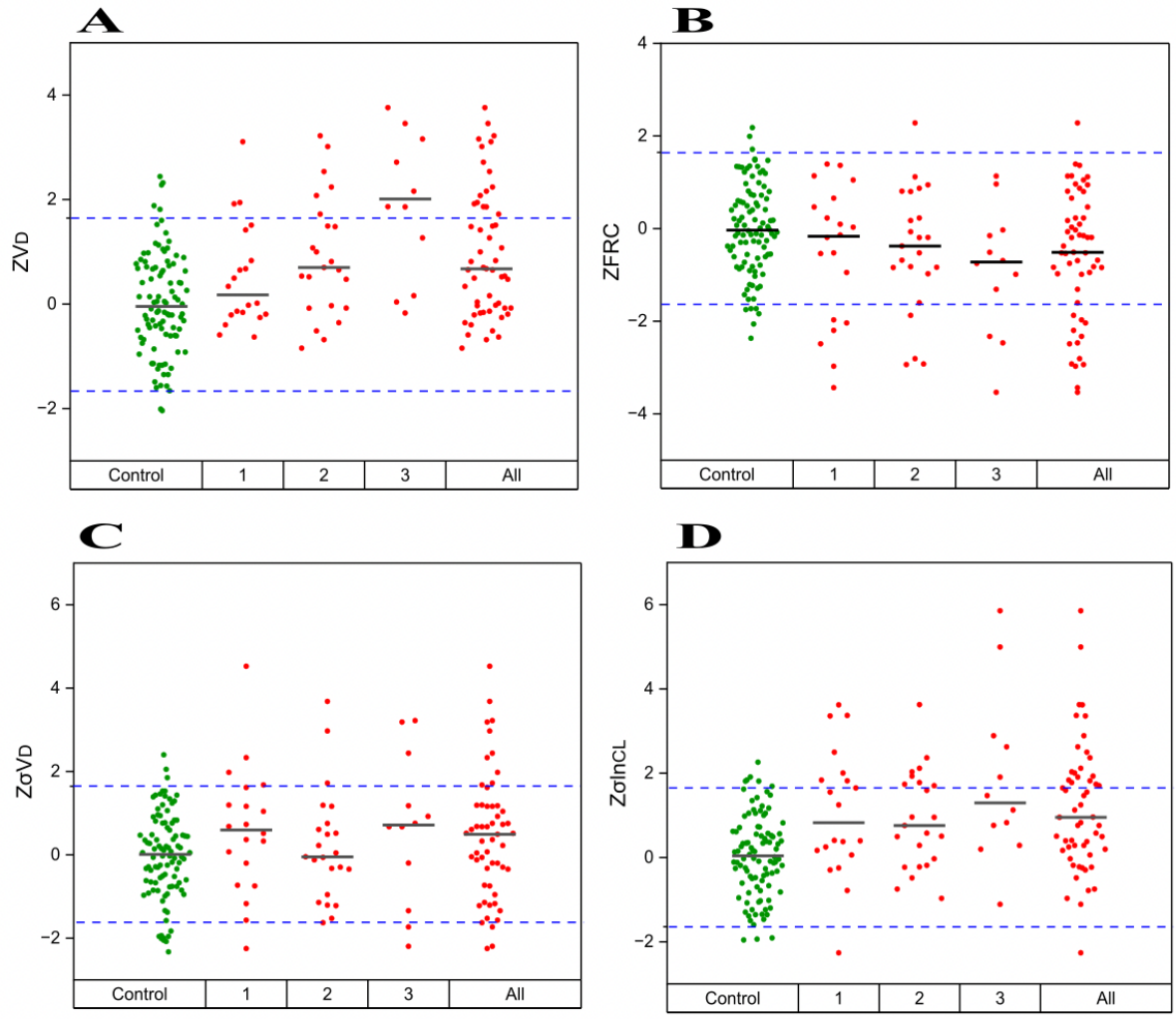


Figure 7.13. Calculated Z-scores for CCP parameters (three-to-six months after hospital discharge) across different COVID-19 severity groups. The graphs show the variation of these scores across the zero-line. The dotted lines represent the 95th and fifth percentiles, which are equivalent to 1.645 and -1.645 respectively. The black lines show the medians. Control (in green) refers to the healthy control cohort from Chapter 5. Severity 1, Basic/O_2, standard hospital care with or without simple O_2 therapy; Severity 2, HFNC/CPAP, high-flow nasal cannula or continuous positive airway pressure; Severity 3, IMV, invasive mechanical ventilation. **A**. Z-scores of end-inspiratory dead space (VD); **B**. Z-scores of functional residual capacity (FRC); **C**. Z-scores for the SD of log-normal distributions for alveolar compliance (σlnCL); **D**. Z-scores of the average SD of the normal distribution for dead space across lung volume (σVD).

Table 7.14. T-test analysis to compare with zero the Z-scores for CCP parameters at the initial visit across different COVID-19 severity groups.

Variables	Basic/O_2 Severity (1) n=20	HFNC/CPAP Severity (2) n=23	IMV Severity (3) n=12	Overall Severity (1-2) n=55
WHO severity	4-5	6	7-9	4-9
ZVD				
t	1.7	3.3	3.9	4.9
p	0.100	**0.003**	**0.002**	**<0.001**
ZFRC				
t	-1.1	-0.7	-1.4	-1.8
p	0.279	0.487	0.178	0.073
ZσVD				
t	2.9	1.9	2.3	4.2
p	**0.008**	0.061	**0.044**	**<0.001**
ZσlnCL				
t	2.6	3.3	2.5	4.8
p	**0.018**	**0.003**	**0.028**	**<0.001**

WHO, World Health Organisation; Basic/O_2, standard hospital care with or without simple O_2 therapy; HFNC/CPAP, high-flow nasal cannula or continuous positive airway pressure; IMV, invasive mechanical ventilation; VD, dead space at end-inspiration; VA, alveolar volume at FRC; FRC, functional residual capacity; σVD, the SD of the normal distribution for (normalised) dead space across lung volume; σlnCL, the SD of log-normal distributions for (normalised) alveolar compliance; *t*, *T-test* result. Significant *p*-values are in bold.

Table 7.15. Chi-square analysis to study the Z-scores for CCP parameters at the initial visit across different COVID-19 severity groups that sat outside the normal range.

Variables	Basic/O_2 Severity (1) n=20	HFNC/CPAP Severity (2) n=23	IMV Severity (3) n=12	Overall Severity (1-2) n=55
WHO severity	4-5	6	7-9	4-9
ZVD				
X^2	0.26	17.32	61.07	44.23
p	0.620	**<0.001**	**<0.001**	**<0.001**
ZFRC				
X^2	21.31	5.05	6.33	36.38
p	**<0.001**	**0.025**	**0.019**	**<0.001**
ZσVD				
X^2	6.57	5.05	14.75	29.30
p	**0.015**	**0.025**	**0.002**	**<0.001**
ZσlnCL				
X^2	12.89	26.19	26.68	72.36
p	**0.002**	**<0.001**	**<0.001**	**<0.001**

WHO, World Health Organisation; Basic/O_2, standard hospital care with or without simple O_2 therapy; HFNC/CPAP, high-flow nasal cannula or continuous positive airway pressure; IMV, invasive mechanical ventilation; VD, dead space at end-inspiration; VA, alveolar volume at FRC; FRC, functional residual capacity; σVD, the SD of the normal distribution for (normalised) dead space across lung volume; σlnCL, the SD of log-normal distributions for (normalised) alveolar compliance; X^2, *chi-square* test results. Significant *p*-values are in bold.

7.3.4.2 Z-scores across different CT-scores

Table 7.16 presents the Z-scores that were calculated for the initial and follow-up visits for each lung inhomogeneity parameter within this cohort across the different CT scores. There were no statistically significant differences in the CCP parameter Z-scores across the different CT scores at either visit. Figure 7.14 shows the calculated Z-scores for each lung inhomogeneity parameter within this cohort across the different CT scores, compared with the data for the healthy control cohort that was discussed in Chapter 5.

A Student t-test was employed to compare the CCP parameter Z-scores with zero across different CT scores (Table 7.17). The aim through the performance of this analysis was to evaluate the differences in lung inhomogeneity parameters across varying degrees of lung pathology that were visualised in CT scans. The results revealed distinctive patterns across severity groups. Specifically, ZVD indicated statistically significant differences across all CT scores when compared to zero. The normal group (CT-1) had a *t-value* of *2.7* with a *p-value* of *0.014*, which suggested mild deviations from zero. In the more severe categories, the ground glass group (CT-2) and the ground glass with fibrotic changes group (CT-3) showed higher deviations, with *p-values* of *<0.001* and *0.024* respectively, which indicated that dead space had increased in these conditions. In terms of ZFRC, there was a significant decrease as the severity increased and it was particularly notable in the most severe CT category (CT-3). This change indicated that the lung volume available for gas exchange was reduced. The variability in ZσVD was less significant, although a slight increase was observed in the ground glass group. ZσlnCL exhibited statistically significant differences across all CT scores when compared to zero, which suggested that lung compliance altered with disease progression.

Additionally, a *chi-square* (X^2) goodness-of-fit test was conducted (Table 7.18) to examine the Z-scores for various CCP parameters at the initial visit across the three different CT scores. For the ZVD parameter, the *chi-square* (X^2) statistics and *p-values* revealed

significant differences in all groups. In the Normal (CT-1) group, X^2 was *8.72* with a *p-value* of *0.018.* The ground glass group (CT-2) showed a highly significant difference with X^2 of *37.89* and a *p-value* of *<0.001,* while the ground glass with fibrotic changes (CT-3) group also demonstrated a significant difference with X^2 of *33.96* and a *p-value* of *<0.001*. The combined analysis across all CT scores showed a strong association between ZVD scores and the severity of radiological findings, with an overall X^2 of *70.79* and a *p-value* of *<0.001*.

For the ZFRC parameter, significant differences were observed across all groups. The Normal group had an X^2 of *16.64* with a *p-value* of *0.003*, the ground glass group had an X^2 of *9.47* with a *p-value* of *0.015,* and the ground glass with fibrotic changes group had an X^2 of *20.28* with a *p-value* of *0.002*. The overall severity analysis showed an X^2 of *42.55* with a *p-value* of *<0.001,* which indicated a significant association between ZFRC scores and the severity of the CT scores.

The ZσVD parameter revealed mixed results. In the Normal group, no significant difference was observed, with an X^2 of *0.90* and a *p-value* of *0.625*. However, in the ground glass group, the X^2 was *9.47* with a *p-value* of *0.015,* and in the ground glass with fibrotic changes group, the X^2 was *10.10* with a *p-value* of *0.019.* Both of these latter results indicated significant differences. The overall analysis showed a significant association, with an X^2 of *16.01* and a *p-value* of *0.001*.

The ZσlnCL parameter showed highly significant differences across all groups. In the Normal group, the X^2 was *35.49* with a *p-value* of *<0.001,* the ground glass group had an X^2 of *51.57* with a *p-value* of *<0.001,* and the ground glass with fibrotic changes group had an X^2 of *20.28* with a *p-value* of *0.002*. The overall analysis demonstrated a strong association between ZσlnCL scores and the severity of the radiological findings, with an X^2 of *106.18* and *a p-value* of *<0.001*.

Table 7.16. Calculated Z-scores for each CCP parameter three-to-six months and 12 months after hospital discharge across different CT scores

Variables	Normal (1)	Ground glass (2)	Ground glass and fibrotic (3)	Overall Severity (1-3)
ZV_D±SD / l				
First visit (n=21, n=20,n=12,and n=53)	0.664±1.135	1.188±1.293	1.419±1.887	1.033±1.399
Second visit (n=10, n=14,n=4,and n=28)	0.186±1.084	0.948±1.084	1.371±1.124	0.736±1.286
ZFRC±SD / % predicted				
First visit (n=21, n=20,n=12,and n=53)	-0.337±1.623	-0.638±1.313	-0.996±1.158	-0.600±1.411
Second visit (n=10, n=14,n=4,and n=28)	-0.194±1.156	-0.536±1.302	-0.264±0.707	-0.375±1.159
$Z\sigma V_D$				
First visit (n=21, n=20,n=12,and n=53)	0.107±1.192	0.726±1.616	0.451±1.817	0.418±1.508
Second visit (n=10, n=14,n=4,and n=28)	-0.350±1.112	0.037±1.244	0.896±2.647	0.021±1.449
$Z\sigma \ln C_L$				
First visit (n=21, n=20,n=12,and n=53)	1.047±1.123	0.999±1.464	1.420±2.182	1.113±1.518
Second visit (n=10, n=14,n=4,and n=28)	1.228±1.322	1.085±1.775	1.234±3.655	1.157±1.894

1-Normal: radiological findings within the normal range, which indicated the absence of significant pathological changes. 2-Ground glass: radiological evidence of ground glass opacities, which suggested certain pulmonary pathophysiological changes. 3-Ground glass and fibrotic changes: both ground glass opacities and fibrotic changes on radiological assessment. V_D, dead space at end-inspiration; V_A, alveolar volume at FRC; FRC, functional residual capacity; σV_D, the SD of the normal distribution for (normalised) dead space across lung volume; $\sigma \ln C_L$, the SD of log-normal distributions for (normalised) alveolar compliance; BTPS, body temperature (37°C), ambient pressure and gas saturated with water vapour. Values are means±SD. *one-way ANOVA*.

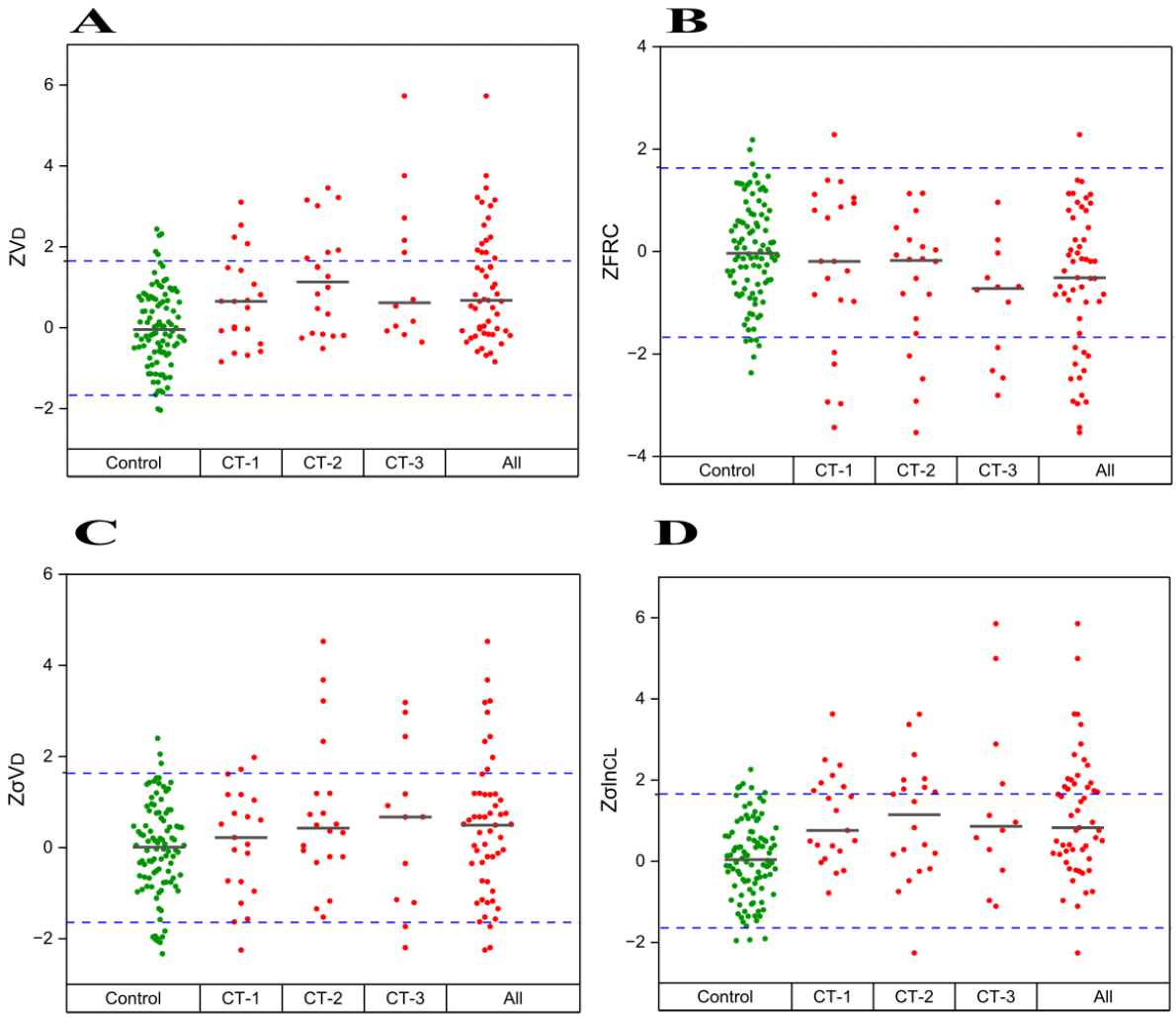


Figure 7.14. Calculated Z-scores for CCP parameters across different CT scores. The graphs show the variation of these scores across the zero-line. The dotted lines represent the 95th and fifth percentiles, which are equivalent to 1.645 and -1.645 respectively. The black lines show the median. Control (in green) refers to the healthy control cohort from Chapter 5; CT-1, radiological findings within the normal range, which indicated the absence of significant pathological changes; CT-2, radiological evidence of ground glass opacities, which suggested certain pulmonary pathophysiological changes; CT-3, both ground glass opacities and fibrotic changes on radiological assessment. **A**.Z-scores of end-inspiratory dead space (VD); **B**. Z-scores of functional residual capacity (FRC); **C**. Z-scores of the average SD of the normal distribution for dead space across lung volume (σVD); **D**. Z-scores for the SD of log-normal distributions for alveolar compliance (σlnCL).

Table 7.17. T-test analysis compares against zero the Z-scores for CCP parameters at the initial visit across different CT scores.

Variables	Normal (1) n=21	Ground glass (2) n=20	Ground glass and fibrotic (3) n=12	Overall Severity (1-3) n=53
ZV$_D$				
t	2.7	4.1	2.6	5.6
p	**0.014**	**<0.001**	**0.024**	**<0.001**
ZFRC				
t	-0.9	-2.2	-2.9	-3.1
p	0.352	**0.043**	**0.013**	**0.003**
ZσV$_D$				
t	0.4	2.0	0.9	2.1
p	0.685	0.059	0.408	**0.038**
ZσlnC$_L$				
t	4.3	3.1	2.3	5.6
p	**<0.001**	**0.007**	**0.046**	**<0.001**

1-Normal: radiological findings within the normal range, which indicated the absence of significant pathological changes; 2-Ground glass: radiological evidence of ground glass opacities, which suggested certain pulmonary pathophysiological changes; 3-Ground glass and fibrotic changes: both ground glass opacities and fibrotic changes on radiological assessment. V$_D$, dead space at end-inspiration; V$_A$, alveolar volume at FRC; FRC, functional residual capacity; σV$_D$, the SD of the normal distribution for (normalised) dead space across lung volume; σlnC$_L$, the SD of log-normal distributions for (normalised) alveolar compliance; *t*, *T-test* result. Significant *p*-values are in bold.

Table 7.18. Chi-square analysis to compare against zero Z-scores for CCP parameters at the initial visit across different CT scores.

Variables	Normal (1) n=21	Ground glass (2) n=20	Ground glass and fibrotic (3) n=12	Overall Severity (1-3) n=53
ZV$_D$				
X^2	8.72	37.89	33.96	70.79
p	**0.018**	**<0.001**	**<0.001**	**<0.001**
ZFRC				
X^2	16.64	9.47	20.28	42.55
p	**0.003**	**0.015**	**0.002**	**<0.001**
ZσV$_D$				
X^2	0.90	9.47	10.10	16.01
p	0.625	**0.015**	**0.019**	**0.001**
ZσlnC$_L$				
X^2	35.49	51.57	20.28	106.18
p	**<0.001**	**<0.001**	**0.002**	**<0.001**

1-Normal: radiological findings within the normal range, which indicated the absence of significant pathological changes; 2-Ground glass: radiological evidence of ground glass opacities, which suggested certain pulmonary pathophysiological changes; 3-Ground glass and fibrotic changes: both ground glass opacities and fibrotic changes on radiological assessment. V$_D$, dead space at end-inspiration; V$_A$, alveolar volume at FRC; FRC, functional residual capacity; σV$_D$, the SD of the normal distribution for (normalised) dead space across lung volume; σlnC$_L$, the SD of log-normal distributions for (normalised) alveolar compliance; X^2, *chi-square* test results. Significant *p*-values are in bold.

7.4 Discussion

The findings from this study provide insights into the long-term effect of COVID-19 on pulmonary function and the relationship between disease severity and such function. The study cohort was well-matched across different disease severities in terms of age and height, and this matching ensured that the observed differences in outcomes were probably due to disease severity rather than demographic confounders (Tables 7.1 and 7.2). At the initial visit (three-to-six months post-hospital discharge), it was noted that disease severity increased with weight and BMI; with BMI, it reached statistical significance ($p<0.05$). This finding is in line with those of previous studies that have reported a correlation between higher BMI and severe outcomes in COVID-19 patients [201, 202]. The increased BMI in more severe cases may reflect pre-existing conditions that predispose individuals to severe COVID-19. At the follow-up visit (12 months after hospital discharge), the differences in participant characteristics across severity groups were less pronounced, with only height showing a statistically significant difference. The shorter mean stature observed in the higher severity group (severity 3) might be due to the higher proportion of female participants in this group who attended their follow-ups.

The study also explored the relationship at the initial visit between pathological changes observed through radiology and patient characteristics. The lack of statistically significant differences in participant characteristics across radiological scores suggests that factors such as age, height, weight and BMI do not significantly influence the radiological severity of lung involvement in COVID-19. This is consistent with findings from other studies that have shown the radiological severity of COVID-19 pneumonia to be driven primarily by the viral load and host immune response rather than demographic factors [203-205]. The significant association between COVID-19 severity and CT scores (*chi-square statistic=25.761, df=4, p-value<0.001*) underscores the critical role of radiological imaging in the assessment of disease

severity. Higher CT scores, which indicated more extensive lung involvement (ground glass and fibrotic changes), were associated with greater clinical severity of COVID-19.

7.4.1 Clinical lung function parameters three-to-six months after hospital discharge

The results of the analysis of the cohort in this study align well with the British Thoracic Society guidelines, which advocate the evaluation of PFTs three months after hospital discharge [206]. Notably, the average period for this cohort that had passed since discharge exceeded three months, and therefore a suitable timeline was provided for the assessment of long-term pulmonary recovery. Unfortunately, due to time constraints and the challenges of conducting research during the pandemic, only lung function tests from the initial visit (three-to-six months post-hospital discharge) were available. It was difficult to obtain a complete set of lung function tests at the 12-month follow-up, as only essential lung function tests were being conducted at that time.

Research on lung function recovery after COVID-19 infection has shown variable results [199, 207-209]. Some individuals experience gradual improvements in their lung function, and this is substantiated by studies that have documented recovery in terms of parameters such as FVC and DLCO more than a year after infection [207-209]. A specific longitudinal study [208] noted progressive improvement across multiple assessment periods three, six, nine and 12 months after discharge. This progression is particularly notable in patients who had severe impairments initially, which suggests that many individuals who are afflicted with severe forms of the disease can follow a slow but continuous recovery pattern [208].

Through the employment of the LME model (Model 7.1), this study offers insights into the association between COVID-19 severity and various lung function parameters, while the impact of the individuals' physical characteristics and pack-years of smoking are taken into

account. Unfortunately, pre-existing comorbidities such as hypertension, diabetes, high cholesterol levels, and histories of respiratory, cardiac, or kidney disease were not explored. Studies have shown that the most common comorbidity of COVID-19 is hypertension, followed by diabetes, high BMI and cardiovascular disease [81, 82]. In a nationwide, multicentre study, 50% of the patients were found to have hypertension as a comorbidity, which was statistically significant when compared with the control group ($p=0.007$). Histories of respiratory disease were also statistically significant when compared with the control group ($p<0.05$) [199].

The average spirometry test results (FEV_1 % predicted, FVC % predicted) across the severity groups were within the normal range [91, 210]. The findings from the initial visit indicated that severity alone did not influence either FEV_1 % predicted or FVC % predicted in a statistically significant manner. BMI emerged as a significant predictor that was negatively associated with both FEV_1 % predicted and FVC % predicted. This finding underscores the role of obesity in influencing lung function decline and aligns with published research that has linked higher BMI to poorer FEV_1 % predicted and FVC % predicted actors [211]. The FEV_1/FVC ratio also showed no significant differences between the severity groups. However, there was a trend towards an increase in the ratio in the most severely affected group (IMV group, Severity 3), which may have indicated potentially restrictive lung damage in the more severe COVID-19 cases. This restrictive pattern is typically characterised by a decrease in lung volumes, which can be a consequence of fibrotic changes or other forms of lung injury. These results correlate with a larger multicentre study that included some of the data from this project [199]. The CMORE/PHOSP-COVID collaborative study was a nationwide effort that included a large, diverse cohort of patients who had been hospitalised due to COVID-19. Participants were recruited from multiple centres across the UK in order to ensure that the sample was representative of the population. The study noted trends towards decreased FEV_1/FVC ratios

in patients with more severe COVID-19, which indicated a restrictive pattern of lung damage [199].

The results from the DLCOc% predicted measurements in this study align with those from other literature [88, 199, 209, 212-219]. They reflect an overall reduction in diffusion capacity across various severities of COVID-19. DLCO is a critical measure that is used to assess the efficiency of gas exchange across the alveolar-capillary membrane. In the context of COVID-19, DLCO has emerged as a particularly sensitive indicator of lung damage, even in patients who may otherwise show normal spirometry results, such as the patients in this cohort. While the mean DLCOc% predicted did not differ statistically across the COVID-19 severity groups, its average was notably below 80% suggesting a compromised lung function (diffusing capacity) in this cohort, as outlined in Table 7.3. This finding suggests a trend towards greater impairment in more severely affected individuals. Low DLCO values are generally associated with later stages of the recovery process and indicate possible persistent damage or recovery challenges [210, 212].

DLCO is derived from two main components. The first is KCO, which represents the capacity to diffuse CO per unit of alveolar volume under standardised conditions during a breath hold at total lung capacity (TLC). The second primary measure is the alveolar volume, which is an estimate of TLC that is obtained through a single-breath measure. In this study, as in several others [210, 212, 213, 216, 220, 221], a decrease in alveolar volume % predicted was observed rather than a decline in KCO. Specifically, the more severe group (HFNC/CPAP, Severity 2) demonstrated a decreasing trend, with a greater reduction in the Severity 3 group (IMV). This damage could stem from the COVID-19 infection itself or the impact of IMV, which had been used as a therapeutic intervention. Subsequent studies that involved the monitoring of patients recovering from SARS revealed that compromised lung function might persist for months or even years [220, 221].

Radiological assessments indicated the presence of ground glass opacity in more than 50% of this cohort. This finding was consistent with others in the literature; other studies have commonly reported ground glass opacity as the most frequent CT-observed abnormality in survivors of severe COVID-19 [209, 212-214]. Additionally, 71% of the IMV group exhibited evidence of fibrotic changes in their CT images. An intriguing yet unanswered question is whether these changes resulted directly from COVID-19 pneumonia infection or whether they emerged as barotrauma or volutrauma as a consequence of IMV. The LME model (Model 7.2) incorporated radiology scores and various lung function parameters with consideration of individual characteristics and smoking history. It was found that when this model was used for the analysis, the data that were categorised by radiology score at the initial visit and those categorised by COVID-19 severity produced similar patterns in spirometric parameters such as FEV_1 % predicted and FVC % predicted. Both FEV_1 % predicted and FVC % predicted remained within the normal range and did not show statistically significant differences across the CT scores. Interestingly, a reduction was noted as radiological severity increased from CT-1 to CT-3, although it was not statistically significant.

The presence of ground glass and fibrotic changes (CT-3) correlated with a decline in DLCO % predicted. This result highlighted impaired gas exchange efficiency. A significant association was evident between the alveolar volume % predicted and the presence of fibrosis in radiological images. There was a noticeable decrease in accessible alveolar volume (available for gas exchange), which corresponded with the presence of fibrosis in the radiological image. However, the KCO % predicted did not exhibit similar impacts based on the radiological score in this model.

Recent advances in imaging techniques, such as hyperpolarised xenon MRI, have revealed persistent abnormalities in lung function that correlate with reductions in DLCO [88, 222]. *Grist et al. (2022)* and *Matheson et al. (2022)* utilised hyperpolarised xenon MRI to study

lung abnormalities in patients with long COVID. Their studies revealed a reduction in the ratio of xenon that dissolved in red blood cells relative to that in tissue/plasma. This finding correlated closely with reduced DLCO. These imaging studies suggest that the observed reductions in DLCO may be related to microvascular changes and the loss of small blood vessels in the lung, possibly as a result of COVID-19-associated pulmonary vascular endotheliitis and microthrombi.

Moreover, residual ground glass opacities that have been observed in follow-up CT scans have been correlated with reduced DLCO, as shown *by Frija-Masson et al. (2021)* [216]. These findings suggest that the structural changes in lung parenchyma, which persist months after the initial infection, probably contribute to impaired gas exchange and sustained reductions in DLCO. Another hypothesis is that COVID-19-related pulmonary vascular endotheliitis and microthrombi may contribute to long-term vascular and parenchymal damage, which results in a sustained reduction in DLCO. In this context, the inability to perform comprehensive follow-up lung function tests 12 months after discharge may have limited the full assessment of long-term pulmonary outcomes in our cohort. However, the observed trends in lung function impairment at the initial follow-up are consistent with those reported in other studies, suggesting that a similar pattern of persistent lung dysfunction may be present in our cohort.

7.4.2 CCP parameters three-to-six months and 12-months after hospital discharge

The same approach was used with the CCP parameters to assess the impact of COVID-19 severity, taking into account physiological metrics, smoking history, and in this case, days since hospital discharge. This adjustment was necessary because some participants had two CCP measurements: one taken during their initial visit and another at their follow-up visit. The analysis was conducted through the use of the Model 7.1 LME model.

The analysis of CCP parameters further delineated the impact of COVID-19 severity on functional lung volumes. Participants who were classified as part of the most severe group (IMV, Severity 3) had significantly greater amounts of anatomical dead space (VD) (*p=0.002*). This finding suggests that changes in pathological pulmonary volume escalate with disease severity. The increased VD indicates that a significant portion of inhaled air is lost in the dead space and does not contribute to gas exchange. This finding suggests persistent ventilation-perfusion mismatch and reduced lung volumes available for effective ventilation. This suggests a persistent ventilation-perfusion mismatch and reduced lung volumes available for effective ventilation. It remains unclear whether this increase in VD is due to the effects of COVID-19 itself or the mechanical ventilation.

Previous studies have noted that the amount of dead space increases with height [175]. Given these results and those of the work I performed on the normal cohort through the use of the same technology (as explained in Chapter 5), it is evident that VD is strongly correlated with height. This correlation reflects the physiological correlation between body size and lung volume. Therefore, height was introduced as a covariate in the LME model. Despite the significance of this term (Table 7.8), it did not negate the strong association between COVID-19 severity and increased VD. However, the lack of significant changes in the number of days since hospital discharge suggests that time since discharge by itself does not markedly influence dead space volume, implying that this may not be something that can be recovered.

Alveolar volume did not show statistically significant differences across different COVID-19 severity levels, but there was a trend toward lower VA in the most severe cases (IMV, Severity 3). As in the case of VD, VA showed a substantial positive association with height (*p<0.001*) that was consistent with the expected physiological relationship between taller stature and larger lung capacities [171]. The negative correlation with BMI with a significant *p-value* (*0.004*) supports published literature, which states that higher BMIs are

associated with reduced lung volumes, probably due to the mechanical effects of adipose tissue on diaphragm movement and lung expansion [168].

Estimates for FRC were derived from the CCP by combining the alveolar volume and dead space at end-expiration. FRC was then normalised by predicted values based on each participant's age, height and sex, and the results were expressed as % predicted. Notably, the predictive equations lacked a BMI term. Since it has been observed that there is a substantial variation of FRC with BMI [168], a log(BMI) term was introduced as a covariate in the LME model. Despite the significance of this term (Table 7.8), it did not eliminate the significant association that was found between COVID-19 severity and reduced FRC. Figure 7.6.C demonstrates the severity-related reductions. Smoking history was incorporated into all LME models to account for its effects on lung function and CCP parameters. Smoking history did not significantly influence most parameters across severity and CT-scoring groups, except for FRC measured by the CCP. Pack-years of smoking history positively influenced FRC, but this did not eliminate the significant association between COVID-19 severity and FRC reduction (Tables 7.8 and 7.10). Additionally, animal studies have demonstrated that prolonged smoke exposure leads to physiological and morphological changes, including alveolar enlargement and destruction, which are consistent with emphysema [223, 224].

When the results were combined from the low measurement of FRC via CCP and the low alveolar volume measurement from the single-breath DLCO washout, it became apparent that these measurements might be attributable to various factors. One possibility was that hospital admission for COVID-19 pneumonia was linked to lower lung volumes/ loss of lung parenchyma. This may have reflected the loss of alveolar units, which could have occurred due to reduced alveolar expansion (or atelectasis) or alveolar destruction due to COVID-19 illness itself. Another possibility is that individuals with smaller lungs may have faced an increased risk that they would develop severe COVID-19 pneumonia requiring hospitalisation. It is a

challenge to distinguish between these two possibilities, and this emphasises the difficulties in interpretation when pre-infection measurements are lacking as control values.

Finally, although the average $\sigma lnCL$ and σV_D were highest in the IMV group (Severity 3), surprisingly, they did not show significant differences across the severity groups. This may have reflected the absence of a control group of people who had no prior infection with COVID-19, and this absence of data motivated the work I described in Chapter 5.

The analysis across different CT scores in this cohort (through the use of Model 7.2) yielded results that were consistent with those observed in CCP parameters across COVID-19 severity groups. Notably, patients with more severe radiological findings (CT-3) exhibited significantly higher V_D, as shown in Table 7.9. This finding aligned with the LME outcomes (Table 7.10), in which V_D was markedly higher in the CT-3 group compared with CT-1, suggesting that severe COVID-19 negatively impacts lung structure and function. Height consistently showed a positive correlation with both V_D and V_A, indicating a link between larger body size and increased lung volumes, which is a well-documented and expected physiological phenomenon. Conversely, BMI was found to impact V_A and FRC negatively; this finding underscored the detrimental effects of greater body mass on lung volume and capacity.

CCP parameters were analysed separately at two different time points, three-to-six months and 12 months after hospital discharge. At the 12-month follow-up visit, at which only the CCP breathing test was conducted, a significant finding was observed regarding the parameter σV_D, which exhibited a notable difference between the two time points ($p=0.002$). This suggests that changes in the distribution of ventilation within the lungs may evolve, and this may reflect ongoing recovery or persistent alterations in lung mechanics. The lack of significant changes in the other CCP parameters between the two visits indicates that for most aspects of lung function measured by CCP, the condition of the participants remained relatively

stable between three-to-six months and 12 months after discharge. This stability might imply that the majority of recovery in these parameters occurs within the first few months after the infection, with little additional improvement or deterioration thereafter. Alternatively, it might suggest that the persistent alterations in lung function that have been established by three-to-six months after discharge remain unresolved even after a year. The significant change in σV_D could indicate underlying physiological processes that continue to adjust long after the initial recovery period, perhaps related to the redistribution of airflow or ongoing reparative processes within the lung tissue. Given that σV_D represents the variability of dead space across different lung volumes, this finding might reflect a normalisation process or ongoing dysfunction in certain regions of the lungs. However, the small sample size at the 12-month mark (with only 30 of the original 66 participants returning for follow-up) presents a limitation. This attrition could introduce bias, particularly if the participants who did not return had different recovery trajectories compared with those who did. As such, while these findings are informative, they should be interpreted with caution.

7.4.3 Relationship between CCP and clinical lung function parameters at the initial visit

The correlation analysis between traditional clinical lung function and CCP parameters, as detailed in Table 7.12 and Figures 7.9, 7.10 and 7.11, revealed significant relationships among these metrics. FEV_1 % predicted showed a significant positive correlation with V_A and FRC % predicted. This correlation indicated that higher forced expiratory volumes are associated with greater lung volumes. FVC % predicted showed even stronger correlations with V_A and FRC % predicted, reinforcing the association between lung volume and forced vital capacity. In contrast, the correlations between FEV_1 % predicted and CCP parameters such as V_D, σV_D and $\sigma \ln C_L$ were weak and not statistically significant. The FEV_1/FVC ratio demonstrated significant negative correlations with VA and FRC % predicted, suggesting that

a higher FEV_1/FVC ratio is associated with smaller lung volumes. This inverse relationship emphasises the complex interplay between lung volume and airflow limitation, in which a higher ratio might indicate restrictive patterns of lung disease.

Alveolar volume % predicted exhibited very strong positive correlations with both FRC % predicted and V_A, which indicated a robust relationship between different measures of lung volume. The consistent correlations between V_A and other lung volume parameters underscore their importance in the assessment of overall lung function.

DLCOc % predicted showed moderate positive correlations with V_D and V_A. This finding suggests that a greater diffusion capacity of the lung for carbon monoxide is associated with larger lungs, due to their greater surface area. Conversely, KCOc % predicted was significantly negatively correlated with FRC % predicted. This finding highlights that larger lungs are associated with lower carbon monoxide transfer efficiency.

The observed variability and lack of significant correlations between some CCP parameters (σV_D, $\sigma lnCL$) and traditional lung function measures suggest that these variables represent different aspects of lung physiology. For instance, $\sigma lnCL$ is often related to conditions in the peripheral lung zones, particularly small airways, whereas traditional spirometric measures such as FEV_1 % predicted and FVC % predicted to capture the influence of large airway dysfunction (discussed in Chapter 6) [155, 156]. In conditions like asthma (seen in Chapter 6), where airway dysfunction is present, $\sigma lnCL$ correlates strongly with spirometric measures like FEV_1 and FEV_1/FVC. However, in post-COVID-19 patients, the pathology is not primarily related to airway or small-airway dysfunction. Instead, the lasting damage from COVID-19 tends to involve the destruction of lung parenchyma and reduced lung volume, which are not adequately captured by small-airway measures like $\sigma lnCL$. This differentiation is crucial, as it indicates that these parameters provide complementary insights into lung function and that each highlights separate aspects of pulmonary health and disease.

7.4.4 Analysis through the use of Z-scores

This thesis represents a pioneering effort to calculate Z-scores for the CCP parameters with allowance for the differentiation of abnormal values. Before I initiated the Z-score project (detailed in Chapter 5), I completed the CMORE lung physiology project. However, I revisited the data to calculate Z-scores, which could then be compared with those calculated in the control project outlined in Chapter 5. Notably, this project lacked a control group, and although initial and follow-up visits were conducted, there were no baseline lung function data for the cohort prior to their severe COVID-19 infections.

The analysis of CCP parameters through the use of Z-scores provides important insights into the pulmonary impact of COVID-19 across varying severity levels. Significant differences were observed in Z_{VD} between severity groups, particularly in the IMV group, for which Z_{VD} was notably higher at both the initial and follow-up visits than it was for the other groups. This suggests a persistent alteration in dead space ventilation, which may reflect more severe lung injury in these patients. Other CCP parameters, such as Z_{FRC}, $Z_{\sigma VD}$, and $Z_{\sigma \ln CL}$, showed trends but did not reach statistical significance across severity levels. This finding indicates that although lung volume and compliance may be affected by COVID-19, the degree of impact varies.

The *Student t-test* results further highlighted these trends; Z_{VD} was found to be significantly different from zero in the more severe groups (HFNC/CPAP and IMV), a finding which underscored the role of ventilatory inefficiency in severe COVID-19 cases. Interestingly, $Z_{\sigma \ln CL}$ also showed significant differences from zero across all severity groups, indicating that lung compliance alterations are a common feature in COVID-19 survivors, regardless of the initial severity.

The *chi-square* goodness-of-fit test reinforced these findings. It revealed that abnormal Z-scores for Z_{VD}, $Z_{\sigma VD}$-, and $Z_{\sigma \ln CL}$ occurred more frequently in higher severity groups than

would be expected by chance, particularly in the IMV group. This pattern suggests a correlation between increased disease severity and the extent of lung inhomogeneity, which may relate to the long-term respiratory consequences of severe COVID-19.

When these findings were compared with the CT scores, ZVD again emerged as a significant marker, as higher scores were correlated with more severe radiological findings. The ZFRC parameter showed a significant decrease with increasing CT severity (CT-3, ground glass and fibrotic changes), which was consistent with reduced availability of lung volume for gas exchange in more severe cases. These results emphasise the relationship between radiological severity and functional impairment.

Overall, the Z-score analysis across both clinical severity and radiological findings underscored the multifaceted impact of COVID-19 on lung function, particularly in patients with severe disease. The persistence of abnormal Z-scores at follow-up highlighted the need for ongoing monitoring and targeted interventions to address the long-term respiratory sequelae of COVID-19.

7.5 Research limitations

This study provides important insights into the long-term pulmonary effects of COVID-19, particularly in relation to disease severity and lung function. However, several limitations should be acknowledged. The absence of a control group and baseline lung function data before infection limits the interpretation of the results. Additionally, the lack of symptom scores and exercise testing means that the full spectrum of functional impairments may not have been captured. The limited follow-up data, with only 30 participants returning 12 months after their discharge from the hospital, could also have led to underestimations of the true extent of recovery or persistent dysfunction.

7.6 Conclusion

One key advantage of this study was its novel approach in using Z-scores for CCP parameters, combined with radiological findings, to provide a more detailed understanding of the multifaceted impact of COVID-19 on lung function. The use of Z-scores enabled the assessment of whether CCP parameters were within normal ranges, and the use of Student t-tests and chi-square tests revealed significant differences and an excess of abnormal values in certain groups. This was particularly helpful especially in the absence of a control group in the study. The regression analysis further highlighted that the primary lasting physiological abnormalities in the most severe cases (IMV group and CT scores with fibrotic changes) were associated with decreases in FRC and increases in V_D. These findings contribute significantly to current knowledge regarding the long-term consequences of COVID-19, and their implications emphasise the need for continued monitoring and the development of tailored interventions for those affected.

Chapter 8. Conclusion and future research direction

The hypothesis of the research that was performed for this thesis is that CCP can serve as a sensitive and complementary technique to traditional lung function measures in the assessment and tracking of specific lung pathophysiological changes. The experimental work described in the various chapters of this thesis has demonstrated that, like any promising new technique, CCP presents both strengths and challenges. This thesis provides insights into the use of CCP in clinical practice, particularly through the establishment of normal values for CCP parameters, demonstration of its utility in T2-high asthma, and evaluation of the long-term respiratory effects of COVID-19.

The introduction and examination of the ventilation inhomogeneity metric, $\sigma lnCL$, which was derived from CCP, in T2-high asthma is a key contribution. This parameter has been shown to correlate with systemic inflammation in asthma and offers a potential predictive marker for treatment response. The findings also underscore the importance of CCP as a tool that not only complements but also enhances existing methodologies such as spirometry and LCI, as it offers a more nuanced and comprehensive assessment of pulmonary function. CCP shows potential in specific contexts in which it can be used to provide pathophysiological insights. For instance, in severe T2-high asthma, the $\sigma lnCL$ metric might serve as an early predictive marker to identify patients who are more likely to benefit from biological therapies, and thereby it could contribute to more personalised and effective treatment strategies than are available now. Similarly, CCP has proved valuable in the identification of pathological alterations in lung function among COVID-19 survivors (through the use of V_D, FRC, and

considerably through σlnCL). These findings suggest that it has broader applicability in the monitoring of long-term respiratory conditions.

Despite its strengths, CCP has limitations. One major weakness is its complexity and the need for sophisticated equipment and expertise to administer it, which could limit its accessibility in some clinical settings. Additionally, CCP's sensitivity, particularly in the detection of subtle pulmonary changes, requires further validation. The technique lacks the extensive clinical validation and widespread acceptance that LCI enjoys. A promising aspect of CCP is the potential to combine its use with other measurement techniques, such as oscillometry and LCI, to enable clinicians to leverage the strengths of all techniques, which could lead to more accurate disease monitoring and better patient outcomes.

8.1 Chapter 5: Determination of normal values for CCP parameters

The primary goal of the work described in Chapter 6 was to establish standardised normal values for CCP parameters through the analysis of a comprehensive dataset taken from healthy control participants. Despite the challenges posed by the COVID-19 pandemic, which significantly impacted the original research plan of this thesis, I successfully obtained data from 98 healthy volunteers, who represented a wide range of demographics. This dataset was instrumental in the development of a regression model that was used to predict normal CCP values based on variables such as age, height, BMI and gender. The observed behaviour of the regression models, which aligned with patterns that had been documented in published literature, validated the potential of CCP as a valuable tool by which to assess lung function.

A key strength of this research was its methodological rigour, which was shown particularly in the careful selection of healthy volunteers and the consistency with which the breathing test protocol using the MFS was applied. The development and validation of a regression model based on comprehensive demographic data also strengthened the study, as it

provided a reliable tool for the assessment of CCP parameters across different populations. Moreover, the ability of the researcher to adapt the research focus in response to the COVID-19 pandemic demonstrated flexibility and resilience, directing this project to contribute valuable insights into post-COVID-19 lung physiology. The inclusion of both young and mature healthy controls enhanced the generalisability of the findings, as it offered a broad reference range for future clinical applications of CCP.

However, the research had limitations. The most significant was the relatively small size of the healthy volunteer sample, which constrained the ability to employ a non-parametric model and necessitated the use of a normal distribution assumption in the regression analysis. This limitation may have introduced some bias, which may have affected the accuracy of the predicted normal values for CCP parameters. Additionally, the absence of participants under the age of 18 years limited the ability fully to explore age-dependent trends in CCP lung inhomogeneity parameters. Another key limitation of this study is the lack of diversity within the cohort, as the majority of participants were white Caucasians and predominantly residents of Oxford with a semi-active lifestyle. This homogeneity may limit the generalizability of the findings to more diverse populations with different ethnic backgrounds, geographical locations, or varying activity levels.

8.2 Chapter 6: The use of CCP to monitor the effect of therapeutic interventions in T2-high asthma

The work has provided significant awareness of the utility of CCP in the management of severe T2-high asthma. The evaluation of the correlations between CCP-derived parameters, such as the ventilation inhomogeneity metric σ_{lnCL} and other disease markers such as inflammatory biomarkers, symptoms, and traditional lung function measures, has highlighted the potential of CCP as a complementary tool for use to assess and track specific lung

pathophysiological changes in asthma. An important finding was the correlation between σlnCL and BEC, both at baseline and after biological therapy. This correlation underscores the complexity of severe T2-high asthma and the need to use multifaceted approaches to assess disease status and treatment response. The usefulness of σlnCL to dichotomise patients into σlnCL responders and non-responders to biological therapy shows its potential predictive role. Improvements were observed in FEV_1% predicted and ACQ-5 scores among σlnCL responders, despite their worse baseline lung function compared with non-responders. These observations suggest that σlnCL could serve as an early predictive marker and contribute to a personalised and effective treatment strategy for severe asthma.

This project's strengths lay in its integration of CCP with established clinical markers of asthma to provide a comprehensive assessment of lung function. Additionally, the study's standardised protocol, which included both pre- and post-bronchodilator CCP and spirometric measurements, complete blood counts, ACQ-5 assessments and FeNO measurements, ensured that consistent and reliable data were collected.

However, this project had limitations that should be addressed in future research. One major limitation was that all participants in the study showed substantial improvement when they were treated with biologics. Although clearly good news, it meant that the generalisability of the findings was limited due to this homogeneous response. The across-the-board improvement could be attributable to the fact that most of the patients had severe, chronic disease that was characterised by significant airway remodelling and permanent lung damage. The lack of patients with mild disease meant that the potential of CCP could not be explored in less severe or earlier stages of T2-high asthma, in which the impact of therapeutic interventions might be different.

Future research should be focused on expanding the study population to include a broader range of T2-high asthma patients, particularly those in the early stages of the disease.

This would enable a more comprehensive evaluation of CCP parameters as early indicators of treatment response. Longitudinal studies should also be conducted to validate the utility of σlnCL in the tracking of disease progression and predictions of long-term outcomes. Furthermore, integration of CCP with other emerging diagnostic tools could enhance its sensitivity and specificity, and therefore provide a more holistic assessment of lung function in asthma patients.

8.3 Chapter 7: Use of CCP to evaluate the long-term effect of COVID-19 on respiratory physiology

The redirection of research due to the COVID-19 pandemic led to a smooth transition in the experimental endeavours that are outlined in this thesis and enabled a valuable contribution to the study of COVID-19's long-term effects on respiratory function. Survivors of severe COVID-19 were recruited to the capturing multi-organ effects of COVID-19 lung physiology study, and participants in that project were recruited to this research, which enabled the alignment of this work with that of the clinical respiratory pathway clinic at OUH.

The findings from this project revealed that COVID-19 was associated with pathological alterations in specific lung model parameters, particularly those related to volumes (VD and FRC) and pulmonary inhomogeneity (σlnCL and σVD). After COVID-19 infection, people exhibited elevated VD and decreased FRC levels, with more severe effects observed in individuals who had survived a more severe disease. The proposed mechanism suggests that these changes are due to the loss of alveoli and destruction of the alveolar-capillary membranes in specific lung regions, while other areas remain relatively unaffected and maintain normal function.

This research's strength lies in its timely and relevant focus on understanding the long-term pulmonary impacts of COVID-19, a critical area of study given the ongoing effects of the pandemic. The use of CCP to assess lung inhomogeneity provides a novel way to evaluate the lingering effects of SARS-CoV-2 on lung physiology and to gain insights that traditional lung function tests may not capture. The study's comprehensive design, which included a broad range of tests and follow-up imaging, ensured that participants' respiratory health was thoroughly assessed.

However, the lack of symptom scores, exercise tests, and MRI images for comparison with other physiological measures was a limitation. Additionally, the non-incorporation of comorbidities as a confounding factor may have affected the results, and the low number of patients who returned for their follow-up visits further limited the findings.

Future research should focus on investigating whether the observed CCP parameters correlate with or predict clinical symptoms and long-term morbidity in COVID-19 survivors. Comparisons between CCP findings, cardiopulmonary exercise testing, and changes in perceived levels of breathlessness over time could provide valuable knowledge regarding the clinical relevance of these alterations. Additionally, exploration of whether similar pathological responses occur in patients with other forms of viral pneumonia would broaden the applicability of these findings and enhance our understanding of respiratory disease progression post-infection.

8.4 Future research direction

The research presented in this thesis has laid a strong foundation for the use of CCP as a complementary tool in lung function assessment. The findings demonstrate the potential use of CCP to provide valuable perceptions of lung pathophysiological changes, which could serve

as sensitive additions to traditional lung function measures. However, like any promising new technique, CCP presents both strengths and challenges that must be addressed in future research.

Several key research directions could build on the findings of this thesis. First, to enhance the robustness of the regression model, studies should be designed to recruit a larger and more diverse cohort of healthy volunteers, including participants under the age of 18 years. This expansion would enable more comprehensive data analysis and improve the generalisability of CCP's standard values across different populations.

Second, researchers should focus on applying the established normal values and regression models to longitudinal studies of patients with conditions such as severe asthma and post-COVID-19 lung disease. This approach would help validate CCP's utility in tracking disease progression and monitoring treatment responses over time, and such validation would provide further evidence of CCP's clinical relevance.

Third, to maximise the potential of CCP, its integration with other diagnostic tools, such as oscillometry and LCI, should be explored. Combining these techniques could enhance the sensitivity and specificity of lung disease diagnostics, which would lead to more accurate assessments and better patient outcomes.

Finally, there is a need for large-scale clinical trials to validate the use of CCP in routine clinical practice. These trials should be designed to demonstrate the technique's effectiveness in improving patient outcomes, particularly in the early detection and monitoring of lung diseases.

In conclusion, although this thesis has demonstrated the promise of CCP as a valuable tool in respiratory medicine, its continued refinement, validation and integration into clinical practice are essential to realise its potential fully. Continued exploration and validation of CCP

across diverse populations will be essential to establish its broad applicability and clinical utility in respiratory medicine.

Bibliography

1. Momtazmanesh, S., et al., *Global burden of chronic respiratory diseases and risk factors, 2013;2019: an update from the Global Burden of Disease Study 2019.* eClinicalMedicine.
2. The Lancet Respiratory, M., *Rates of lung disease in Europe: an uncomfortable equilibrium.* The Lancet Respiratory Medicine, 2013. **1**(8): p. 585.
3. O'Neill, S., et al., *The cost of treating severe refractory asthma in the UK: an economic analysis from the British Thoracic Society Difficult Asthma Registry.* Thorax, 2015. **70**(4): p. 376-378.
4. Organization, W.H., *WHO Coronavirus Disease (COVID-19) Dashboard*. 2023.
5. Fabbri, L., et al., *Parenchymal lung abnormalities following hospitalisation for COVID-19 and viral pneumonitis: a systematic review and meta-analysis.* Thorax, 2022: p. thoraxjnl-2021-218275.
6. Petousi, N., et al., *Measuring lung function in airways diseases: current and emerging techniques.* Thorax, 2019. **74**(8): p. 797-805.
7. Gustafsson, P.M., et al., *Multiple-breath inert gas washout and spirometry versus structural lung disease in cystic fibrosis.* Thorax, 2008. **63**(2): p. 129-34.
8. Sanders, D.B., et al., *Chest computed tomography scores of severity are associated with future lung disease progression in children with cystic fibrosis.* Am J Respir Crit Care Med, 2011. **184**(7): p. 816-21.
9. Subbarao, P., et al., *Multiple-Breath Washout as a Lung Function Test in Cystic Fibrosis. A Cystic Fibrosis Foundation Workshop Report.* Ann Am Thorac Soc, 2015. **12**(6): p. 932-9.
10. Goldman, M.D., C. Saadeh, and D. Ross, *Clinical applications of forced oscillation to assess peripheral airway function.* Respir Physiol Neurobiol, 2005. **148**(1-2): p. 179-94.
11. Oostveen, E., et al., *The forced oscillation technique in clinical practice: methodology, recommendations and future developments.* Eur Respir J, 2003. **22**(6): p. 1026-41.
12. Robinson, P.D., M.D. Goldman, and P.M. Gustafsson, *Inert gas washout: theoretical background and clinical utility in respiratory disease.* Respiration, 2009. **78**(3): p. 339-55.
13. Horsley, A.R., et al., *Lung clearance index is a sensitive, repeatable and practical measure of airways disease in adults with cystic fibrosis.* Thorax, 2008. **63**(2): p. 135-40.
14. Robinson, P.D., et al., *Consensus statement for inert gas washout measurement using multiple- and single- breath tests.* European Respiratory Journal, 2013. **41**(3): p. 507.
15. Elborn, J.S., *Cystic fibrosis.* The Lancet, 2016. **388**(10059): p. 2519-2531.
16. Aurora, P., et al., *Multiple-breath washout as a marker of lung disease in preschool children with cystic fibrosis.* Am J Respir Crit Care Med, 2005. **171**(3): p. 249-56.
17. Stanojevic, S., et al., *Progression of Lung Disease in Preschool Patients with Cystic Fibrosis.* Am J Respir Crit Care Med, 2017. **195**(9): p. 1216-1225.
18. Davies, J., et al., *Assessment of clinical response to ivacaftor with lung clearance index in cystic fibrosis patients with a G551D-CFTR mutation and preserved*

spirometry: a randomised controlled trial. Lancet Respir Med, 2013. **1**(8): p. 630-638.
19. Summermatter, S., et al., *Impact of Software Settings on Multiple-Breath Washout Outcomes.* PLoS One, 2015. **10**(7): p. e0132250.
20. Anagnostopoulou, P., et al., *False normal Lung Clearance Index in infants with cystic fibrosis due to software algorithms.* Pediatr Pulmonol, 2015. **50**(10): p. 970-7.
21. Yammine, S., et al., *Impact of different breathing protocols on multiple-breath washout outcomes in children.* Journal of Cystic Fibrosis, 2014. **13**(2): p. 190-197.
22. Ratjen, F., et al., *Effect of changes in tidal volume on multiple breath washout outcomes.* PLoS One, 2019. **14**(7): p. e0219309.
23. John B. West, A.M.L., *Respiratory Physiology: The Essentials.* 11 ed.: Wolters Kluwer.
24. Ochs, M., et al., *The number of alveoli in the human lung.* Am J Respir Crit Care Med, 2004. **169**(1): p. 120-4.
25. Levitzky, M.G., *Pulmonary Physiology*. 6th ed. 2002: McGraw-Hill Medical Publishing.
26. Asthma, G.I.f., *Global Strategy for Asthma Management and Prevention, 2020*. 2020.
27. Pembrey, L., et al., *Understanding asthma phenotypes: the World Asthma Phenotypes (WASP) international collaboration.* ERJ Open Research, 2018. **4**(3): p. 00013-2018.
28. Asthma, G.I.f., *Global Strategy for Asthma Management and Prevention*. 2023.
29. Network, T.G.A., *The Global Asthma Report 2018*. 2018, Global Asthma Network: Auckland, New Zealand.
30. *Global, regional, and national incidence, prevalence, and years lived with disability for 328 diseases and injuries for 195 countries, 1990-2016: a systematic analysis for the Global Burden of Disease Study 2016.* Lancet, 2017. **390**(10100): p. 1211-1259.
31. K-C, B., *History of Allergy. Chem Immunol Allergy*. Vol. 100. 2014.
32. Sakula, A., *Sir John Floyer's A Treatise of the Asthma (1698).* Thorax, 1984. **39**(4): p. 248-254.
33. Osler, S.W., *the principles and practice of medicine.* 1894, New York: Appleton.
34. McFadden, E.R., Jr., *A century of asthma.* Am J Respir Crit Care Med, 2004. **170**(3): p. 215-21.
35. Pavord, I.D., et al., *After asthma: redefining airways diseases.* The Lancet, 2018. **391**(10118): p. 350-400.
36. *SIGN158 British guideline on the management of asthma A national clinical guideline*, in *British Thoracic Society* 2019.
37. Crapo, R.O., et al., *Guidelines for methacholine and exercise challenge testing-1999. This official statement of the American Thoracic Society was adopted by the ATS Board of Directors, July 1999.* Am J Respir Crit Care Med, 2000. **161**(1): p. 309-29.
38. Corren, J., *Asthma phenotypes and endotypes: an evolving paradigm for classification.* Discov Med, 2013. **15**(83): p. 243-9.
39. Kuruvilla, M.E., F.E. Lee, and G.B. Lee, *Understanding Asthma Phenotypes, Endotypes, and Mechanisms of Disease.* Clin Rev Allergy Immunol, 2019. **56**(2): p. 219-233.
40. Haldar, P., et al., *Cluster analysis and clinical asthma phenotypes.* Am J Respir Crit Care Med, 2008. **178**(3): p. 218-224.
41. Gibeon, D., et al., *Obesity-Associated Severe Asthma Represents a Distinct Clinical Phenotype: Analysis of the British Thoracic Society Difficult Asthma Registry Patient Cohort According to BMI.* Chest, 2013. **143**(2): p. 406-414.

42. Hekking, P.-P.W. and E.H. Bel, *Developing and Emerging Clinical Asthma Phenotypes.* The Journal of Allergy and Clinical Immunology: In Practice, 2014. **2**(6): p. 671-680.
43. Van Veen, I.H., et al., *Airway inflammation in obese and nonobese patients with difficult-to-treat asthma.* Allergy, 2008. **63**(5): p. 570-574.
44. Habib, N., M.A. Pasha, and D.D. Tang, *Current Understanding of Asthma Pathogenesis and Biomarkers.* Cells, 2022. **11**(17).
45. Douwes, J., et al., *Non-eosinophilic asthma: importance and possible mechanisms.* Thorax, 2002. **57**(7): p. 643-648.
46. Robinson, D., et al., *Revisiting Type 2-high and Type 2-low airway inflammation in asthma: current knowledge and therapeutic implications.* Clinical & Experimental Allergy, 2017. **47**(2): p. 161-175.
47. Pène, J., et al., *Chronically Inflamed Human Tissues Are Infiltrated by Highly Differentiated Th17 Lymphocytes.* The Journal of Immunology, 2008. **180**(11): p. 7423.
48. Fitzpatrick, A.M., et al., *T2-"Low" Asthma: Overview and Management Strategies.* J Allergy Clin Immunol Pract, 2020. **8**(2): p. 452-463.
49. Dougherty, R.H., et al., *Accumulation of intraepithelial mast cells with a unique protease phenotype in T(H)2-high asthma.* J Allergy Clin Immunol, 2010. **125**(5): p. 1046-1053.e8.
50. Fahy, J.V., *Type 2 inflammation in asthma — present in most, absent in many.* Nature Reviews Immunology, 2015. **15**(1): p. 57-65.
51. Brusselle, G.G., T. Maes, and K.R. Bracke, *Eosinophils in the Spotlight: Eosinophilic airway inflammation in nonallergic asthma.* Nature Medicine, 2013. **19**(8): p. 977-979.
52. Molfino, N.A., et al., *Molecular and clinical rationale for therapeutic targeting of interleukin-5 and its receptor.* Clinical & Experimental Allergy, 2012. **42**(5): p. 712-737.
53. Eckl-Dorna, J., et al., *Tracing IgE-Producing Cells in Allergic Patients.* Cells, 2019. **8**(9): p. 994.
54. Dweik, R.A., et al., *An official ATS clinical practice guideline: interpretation of exhaled nitric oxide levels (FENO) for clinical applications.* Am J Respir Crit Care Med, 2011. **184**(5): p. 602-15.
55. Wadsworth, S., D. Sin, and D. Dorscheid, *Clinical update on the use of biomarkers of airway inflammation in the management of asthma.* Journal of asthma and allergy, 2011. **4**: p. 77-86.
56. Couillard, S., et al., *Sub-stratification of type-2 high airway disease for therapeutic decision-making: A 'bomb' (blood eosinophils) meets 'magnet' (FeNO) framework.* Respirology, 2022. **27**(8): p. 573-577.
57. Couillard, S., et al., *Sub-stratification of type-2 high airway disease for therapeutic decision-making: A 'bomb' (blood eosinophils) meets 'magnet' (FeNO) framework.* Respirology, 2022. **27**(8): p. 573-577.
58. Dragonieri, S. and G.E. Carpagnano, *Biological therapy for severe asthma.* Asthma Res Pract, 2021. **7**(1): p. 12.
59. Normansell, R., et al., *Omalizumab for asthma in adults and children.* Cochrane Database Syst Rev, 2014(1): p. Cd003559.
60. Ortega, H.G., et al., *Mepolizumab Treatment in Patients with Severe Eosinophilic Asthma.* New England Journal of Medicine, 2014. **371**(13): p. 1198-1207.
61. NICE, *Mepolizumab for treating severe eosinophilic asthma*. 2021.

62. Hilvering, B., L. Xue, and I.D. Pavord, *Evidence for the efficacy and safety of anti-interleukin-5 treatment in the management of refractory eosinophilic asthma.* Ther Adv Respir Dis, 2015. **9**(4): p. 135-45.
63. Pavord, I.D., et al., *Mepolizumab for severe eosinophilic asthma (DREAM): a multicentre, double-blind, placebo-controlled trial.* The Lancet, 2012. **380**(9842): p. 651-659.
64. Pavord, I.D., et al., *Mepolizumab for Eosinophilic Chronic Obstructive Pulmonary Disease.* New England Journal of Medicine, 2017. **377**(17): p. 1613-1629.
65. Castro, M., et al., *Dupilumab Efficacy and Safety in Moderate-to-Severe Uncontrolled Asthma.* New England Journal of Medicine, 2018. **378**(26): p. 2486-2496.
66. Castro, M., et al., *Reslizumab for inadequately controlled asthma with elevated blood eosinophil counts: results from two multicentre, parallel, double-blind, randomised, placebo-controlled, phase 3 trials.* The Lancet Respiratory Medicine, 2015. **3**(5): p. 355-366.
67. Haldar, P., et al., *Mepolizumab and Exacerbations of Refractory Eosinophilic Asthma.* New England Journal of Medicine, 2009. **360**(10): p. 973-984.
68. NICE, *Benralizumab for treating severe eosinophilic asthma*. 2019.
69. Rabe, K.F., et al., *Efficacy and Safety of Dupilumab in Glucocorticoid-Dependent Severe Asthma.* New England Journal of Medicine, 2018. **378**(26): p. 2475-2485.
70. Menzies-Gow, A., et al., *Tezepelumab in Adults and Adolescents with Severe, Uncontrolled Asthma.* New England Journal of Medicine, 2021. **384**(19): p. 1800-1809.
71. Zhu, N., et al., *A Novel Coronavirus from Patients with Pneumonia in China, 2019.* N Engl J Med, 2020. **382**(8): p. 727-733.
72. Chilamakuri, R. and S. Agarwal, *COVID-19: Characteristics and Therapeutics.* Cells, 2021. **10**(2): p. 206.
73. Zhou, P., et al., *A pneumonia outbreak associated with a new coronavirus of probable bat origin.* Nature, 2020. **579**.
74. Bourgonje, A.R., et al., *Angiotensin-converting enzyme 2 (ACE2), SARS-CoV-2 and the pathophysiology of coronavirus disease 2019 (COVID-19).* J Pathol, 2020. **251**(3): p. 228-248.
75. *A minimal common outcome measure set for COVID-19 clinical research.* Lancet Infect Dis, 2020. **20**(8): p. e192-e197.
76. World Health, O., *Laboratory testing for coronavirus disease 2019 (COVID-19) in suspected human cases: interim guidance, 2 March 2020*. 2020, World Health Organization: Geneva.
77. Xie, X., et al., *Chest CT for Typical Coronavirus Disease 2019 (COVID-19) Pneumonia: Relationship to Negative RT-PCR Testing.* Radiology, 2020. **296**(2): p. E41-E45.
78. Polak, S.B., et al., *A systematic review of pathological findings in COVID-19: a pathophysiological timeline and possible mechanisms of disease progression.* Modern Pathology, 2020. **33**(11): p. 2128-2138.
79. Ackermann, M., et al., *Pulmonary Vascular Endothelialitis, Thrombosis, and Angiogenesis in Covid-19.* New England Journal of Medicine, 2020. **383**(2): p. 120-128.
80. Chen, N., et al., *Epidemiological and clinical characteristics of 99 cases of 2019 novel coronavirus pneumonia in Wuhan, China: a descriptive study.* The Lancet, 2020. **395**(10223): p. 507-513.

81. Zhou, F., et al., *Clinical course and risk factors for mortality of adult inpatients with COVID-19 in Wuhan, China: a retrospective cohort study.* The Lancet, 2020. **395**(10229): p. 1054-1062.
82. Zhang, J.J.Y., et al., *Risk Factors for Severe Disease and Efficacy of Treatment in Patients Infected With COVID-19: A Systematic Review, Meta-Analysis, and Meta-Regression Analysis.* Clin Infect Dis, 2020. **71**(16): p. 2199-2206.
83. Oronsky, B., et al., *A Review of Persistent Post-COVID Syndrome (PPCS).* Clin Rev Allergy Immunol, 2023. **64**(1): p. 66-74.
84. Zhao, Y.-m., et al., *Follow-up study of the pulmonary function and related physiological characteristics of COVID-19 survivors three months after recovery.* EClinicalMedicine, 2020. **25**.
85. Sanchez-Ramirez, D.C., et al., *Long-Term Impact of COVID-19: A Systematic Review of the Literature and Meta-Analysis.* Biomedicines, 2021. **9**(8): p. 900.
86. Stewart, I., et al., *Residual Lung Abnormalities after COVID-19 Hospitalization: Interim Analysis of the UKILD Post–COVID-19 Study.* American Journal of Respiratory and Critical Care Medicine, 2022. **207**(6): p. 693-703.
87. Yu, M., et al., *Prediction of the Development of Pulmonary Fibrosis Using Serial Thin-Section CT and Clinical Features in Patients Discharged after Treatment for COVID-19 Pneumonia.* Korean J Radiol, 2020. **21**(6): p. 746-755.
88. Grist, J.T., et al., *Lung Abnormalities Detected with Hyperpolarized 129Xe MRI in Patients with Long COVID.* Radiology, 2022. **305**(3): p. 709-717.
89. Gold, W. and L. Koth, *Pulmonary Function Testing.* Murray and Nadel's Textbook of Respiratory Medicine, 2016: p. 3.
90. Ranu, H., M. Wilde, and B. Madden, *Pulmonary function tests.* The Ulster medical journal, 2011. **80**(2): p. 84-90.
91. Sim, Y.S., et al., *Spirometry and Bronchodilator Test.* Tuberc Respir Dis (Seoul), 2017. **80**(2): p. 105-112.
92. Brody, A.S., et al., *High-resolution computed tomography in young patients with cystic fibrosis: Distribution of abnormalities and correlation with pulmonary function tests.* The Journal of Pediatrics, 2004. **145**(1): p. 32-38.
93. Lehtimäki, L., et al., *Peripheral inflammation in patients with asthmatic symptoms but normal lung function.* J Asthma, 2005. **42**(7): p. 605-9.
94. *British Thoracic Society,A Guide to Performing Quality Assured Diagnostic Spirometry.* 2013; Available from: https://www.brit-thoracic.org.uk/media/70454/spirometry_e-guide_2013.pdf
95. Sylvester, K.P., et al., *ARTP statement on pulmonary function testing 2020.* BMJ Open Respiratory Research, 2020. **7**(1): p. e000575.
96. Hill S, M.M., *Improving the quality of diagnostic spirometry in adults: the National Register of certified professionals and operators.* 2016.
97. Woolnough, S., *Diagnosing the problem: Right test, right time* Asthma + Lung UK, 2023.
98. Ward, H., B.G. Cooper, and M.R. Miller, *Improved Criterion for Assessing Lung Function Reversibility.* Chest, 2015. **148**(4): p. 877-886.
99. Davis, B.E., C.M. Blais, and D.W. Cockcroft, *Methacholine challenge testing: comparative pharmacology.* J Asthma Allergy, 2018. **11**: p. 89-99.
100. Stanojevic, S., et al., *ERS/ATS technical standard on interpretive strategies for routine lung function tests.* European Respiratory Journal, 2022. **60**(1): p. 2101499.
101. Criée, C.P., et al., *Body plethysmography--its principles and clinical use.* Respir Med, 2011. **105**(7): p. 959-71.

102. Goldman, M.D., C. Saadeh, and D. Ross, *Clinical applications of forced oscillation to assess peripheral airway function.* Respiratory Physiology & Neurobiology, 2005. **148**(1): p. 179-194.
103. Oostveen, E., et al., *The forced oscillation technique in clinical practice: methodology, recommendations and future developments.* European Respiratory Journal, 2003. **22**(6): p. 1026.
104. Mountain, J.E., et al., *Potential for noninvasive assessment of lung inhomogeneity using highly precise, highly time-resolved measurements of gas exchange.* Journal of applied physiology (Bethesda, Md. : 1985), 2018. **124**(3): p. 615-631.
105. Rodríguez-Roisin, R., et al., *Ventilation-perfusion imbalance and chronic obstructive pulmonary disease staging severity.* J Appl Physiol (1985), 2009. **106**(6): p. 1902-8.
106. Paul, D.R., et al., *Consensus statement for inert gas washout measurement using multiple- and single- breath tests.* European Respiratory Journal, 2013. **41**(3): p. 507.
107. Wagner, P.D., *The multiple inert gas elimination technique (MIGET).* Intensive Care Medicine, 2008. **34**(6): p. 994-1001.
108. Wagner, P.D., et al., *Ventilation-perfusion inequality in chronic obstructive pulmonary disease.* J Clin Invest, 1977. **59**(2): p. 203-16.
109. Wagner, P.D., et al., *Ventilation-perfusion inequality in asymptomatic asthma.* Am Rev Respir Dis, 1978. **118**(3): p. 511-24.
110. Fowler, W.S., E.R. Cornish, Jr., and S.S. Kety, *Lung function studies. VIII. Analysis of alveolar ventilation by pulmonary N2 clearance curves.* J Clin Invest, 1952. **31**(1): p. 40-50.
111. Jensen, R., et al., *A Systematic Approach to Multiple Breath Nitrogen Washout Test Quality.* PLoS One, 2016. **11**(6): p. e0157523.
112. Nuttall, A.G.L., et al., *Lung clearance index: assessment and utility in children with asthma.* European Respiratory Review, 2019. **28**(154): p. 190046.
113. Gustafsson, P.M., *Peripheral airway involvement in CF and asthma compared by inert gas washout.* Pediatr Pulmonol, 2007. **42**(2): p. 168-76.
114. Zwitserloot, A., et al., *Clinical application of inert gas Multiple Breath Washout in children and adolescents with asthma.* Respir Med, 2014. **108**(9): p. 1254-9.
115. Svenningsen, S., et al., *Is ventilation heterogeneity related to asthma control?* European Respiratory Journal, 2016. **48**(2): p. 370.
116. Farah, C.S., et al., *Ventilation heterogeneity predicts asthma control in adults following inhaled corticosteroid dose titration.* Journal of Allergy and Clinical Immunology, 2012. **130**(1): p. 61-68.
117. Gonem, S., et al., *Characterization of acinar airspace involvement in asthmatic patients by using inert gas washout and hyperpolarized ³helium magnetic resonance.* Journal of Allergy and Clinical Immunology, 2016. **137**(2): p. 417-425.
118. Horsley, A., *Lung clearance index in the assessment of airways disease.* Respir Med, 2009. **103**(6): p. 793-9.
119. Sandhu, D., et al., *Computed cardiopulmonography and the idealized lung clearance index, iLCI2.5, in early-stage cystic fibrosis.* Journal of Applied Physiology, 2023. **135**(1): p. 205-216.
120. Ament, S.J., et al., *PET lung ventilation/perfusion imaging using (68)Ga aerosol (Galligas) and (68)Ga-labeled macroaggregated albumin.* Recent Results Cancer Res, 2013. **194**: p. 395-423.
121. Musch, G., et al., *Topographical distribution of pulmonary perfusion and ventilation, assessed by PET in supine and prone humans.* J Appl Physiol (1985), 2002. **93**(5): p. 1841-51.

122. Richard, J.C., et al., *Quantitative assessment of regional alveolar ventilation and gas volume using 13N-N2 washout and PET.* J Nucl Med, 2005. **46**(8): p. 1375-83.
123. Treppo, S., S.M. Mijailovich, and J.G. Venegas, *Contributions of pulmonary perfusion and ventilation to heterogeneity in V(A)/Q measured by PET.* J Appl Physiol (1985), 1997. **82**(4): p. 1163-76.
124. Ebner, L., et al., *The role of hyperpolarized (129)xenon in MR imaging of pulmonary function.* Eur J Radiol, 2017. **86**: p. 343-352.
125. Fain, S.B., et al., *Functional lung imaging using hyperpolarized gas MRI.* J Magn Reson Imaging, 2007. **25**(5): p. 910-23.
126. Mugler, J.P., 3rd and T.A. Altes, *Hyperpolarized 129Xe MRI of the human lung.* J Magn Reson Imaging, 2013. **37**(2): p. 313-31.
127. Altes, T.A., et al., *Hyperpolarized 3He MR lung ventilation imaging in asthmatics: preliminary findings.* J Magn Reson Imaging, 2001. **13**(3): p. 378-84.
128. Aysola, R., et al., *Demonstration of the heterogeneous distribution of asthma in the lungs using CT and hyperpolarized helium-3 MRI.* J Magn Reson Imaging, 2010. **32**(6): p. 1379-87.
129. Ciaffoni, L., et al., *In-airway molecular flow sensing: A new technology for continuous, noninvasive monitoring of oxygen consumption in critical care.* Science Advances, 2016. **2**(8): p. e1600560.
130. Jaffe, M.B. *Mainstream or Sidestream Capnography ?* 2002.
131. Downard, K., *Mass spectrometry : a foundation course*. 2004: Royal Society of Chemistry, Cambridge, 2004.
132. Buszewski, B., et al., *Human exhaled air analytics: biomarkers of diseases.* Biomedical Chromatography, 2007. **21**(6): p. 553-566.
133. Andrew M. Ellis, C.A.M., *Proton Transfer Reaction Mass Spectrometry: Principles and Applications*. 2014: Wiley.
134. Covington, J.A., et al., *The application of FAIMS gas analysis in medical diagnostics.* Analyst, 2015. **140**(20): p. 6775-6781.
135. Baum, M.M., et al., *Validation of a new spectrometer for noninvasive measurement of cardiac output.* Review of Scientific Instruments, 2004. **75**(7): p. 2290-2299.
136. Berden, G., R. Peeters, and G. Meijer, *Cavity ring-down spectroscopy: Experimental schemes and applications.* International Reviews in Physical Chemistry, 2000. **19**(4): p. 565-607.
137. Cummings, B., et al., *Laser-based absorption spectroscopy as a technique for rapid in-line analysis of respired gas concentrations of O2 and CO2.* J Appl Physiol (1985), 2011. **111**(1): p. 303-7.
138. N.Smith, *Monitoring Heart and Lung Function Using In-line Laser Spectroscopy.* PhD thesis ,University of Oxford, 2019.
139. Magor-Elliott, S.R.M., et al., *Altered lung physiology in two cohorts after COVID-19 infection as assessed by computed cardiopulmonography.* J Appl Physiol (1985), 2022. **133**(5): p. 1175-1191.
140. Smith, N.M.J., et al., *Novel measure of lung function for assessing disease activity in asthma.* BMJ Open Respiratory Research, 2020. **7**(1): p. e000531.
141. Douglas, C.G., *A method for determining the total respiratory exchange in man.* J Physiol, 1911. **42**: p. 17-18.
142. Stuart-Andrews, C., et al., *Continuous indirect calorimetry--a laboratory simulation of a new method for non-invasive metabolic monitoring of patients under anaesthesia or in critical care.* Physiol Meas, 2006. **27**(2): p. 155-64.
143. Walsh, T.S., *Recent advances in gas exchange measurement in intensive care patients.* BJA: British Journal of Anaesthesia, 2003. **91**(1): p. 120-131.

144. West, J.B., *Ventilation/blood flow and gas exchange*. 5th ed.: Blackwell Scientific Publications.
145. Mountain, J.E., *The Lognormal Lung: Quantifying Inhomogeneity of Ventilation* PhD thesis ,University of Oxford, 2016.
146. Fowler, W.S., *Lung function studies; the respiratory dead space.* Am J Physiol, 1948. **154**(3): p. 405-16.
147. O'Neill, D.P. and P.A. Robbins, *A mechanistic physicochemical model of carbon dioxide transport in blood.* Journal of Applied Physiology, 2017. **122**(2): p. 283-295.
148. Magor-Elliott, S.R.M., et al., *A dynamic model of the body gas stores for carbon dioxide, oxygen, and inert gases that incorporates circulatory transport delays to and from the lung.* J Appl Physiol (1985), 2021. **130**(5): p. 1383-1397.
149. Snyder WSC, C.M., Nasset ES, Karhausen LR, Parry-Howells G, Tipton IH., *Report on the Task Group on Reference Man*. 1975: ICRP Publication 23.Pergamon Press, Oxford.
150. *Basic anatomical and physiological data for use in radiological protection: reference values. A report of age- and gender-related differences in the anatomical and physiological characteristics of reference individuals. ICRP Publication 89.* Ann ICRP, 2002. **32**(3-4): p. 5-265.
151. Brown, R.P., et al., *Physiological parameter values for physiologically based pharmacokinetic models.* Toxicol Ind Health, 1997. **13**(4): p. 407-84.
152. Wyler, F., et al., *Correction of sensor crosstalk error in Exhalyzer D multiple-breath washout device significantly impacts outcomes in children with cystic fibrosis.* Journal of Applied Physiology, 2021. **131**(3): p. 1148-1156.
153. Horsley, A. and C. Darquenne, *Better late than never: correcting the error in the Exhalyzer nitrogen washout system.* J Appl Physiol (1985), 2021. **131**(4): p. 1286-1287.
154. Wojsyk-Banaszak, I., et al., *How Does the Corrected Exhalyzer Software Change the Predictive Value of LCI in Pulmonary Exacerbations in Children with Cystic Fibrosis?* Diagnostics (Basel), 2023. **13**(14).
155. Smith, N.M.J., et al., *The Lognormal Lung: A new approach to quantifying lung inhomogeneity in COPD.* Front Physiol, 2022. **13**: p. 1032126.
156. Redmond, J.L., et al., *Computed Cardiopulmonography for the Detection of Early Smoking-Related Changes in the Lungs of Young Individuals Who Smoke.* CHEST, 2024. **165**(5): p. 1107-1110.
157. Statistics, B.S. IBM Corporation and its licensors 1989, 2021.Version 28.
158. Hope, T.M.H., *Chapter 4 - Linear regression*, in *Machine Learning*, A. Mechelli and S. Vieira, Editors. 2020, Academic Press. p. 67-81.
159. Gareth James, D.W., Trevor Hastie, Robert Tibshirani, *An Introduction to Statistical Learning*. 2013: Springer New York, NY.
160. Mishra, P., et al., *Descriptive statistics and normality tests for statistical data.* Ann Card Anaesth, 2019. **22**(1): p. 67-72.
161. Rosopa, P.J., M.M. Schaffer, and A.N. Schroeder, *Managing heteroscedasticity in general linear models.* Psychological Methods, 2013. **18**(3): p. 335-351.
162. Quanjer, P.H., et al., *Multi-ethnic reference values for spirometry for the 3-95-yr age range: the global lung function 2012 equations.* Eur Respir J, 2012. **40**(6): p. 1324-43.
163. Laszlo, G., *Standardisation of lung function testing: helpful guidance from the ATS/ERS Task Force.* Thorax, 2006. **61**(9): p. 744-6.

164. Kanis, J.A., *Assessment of fracture risk and its application to screening for postmenopausal osteoporosis: synopsis of a WHO report. WHO Study Group.* Osteoporos Int, 1994. **4**(6): p. 368-81.
165. Kanis, J.A. and C.C. Glüer, *An update on the diagnosis and assessment of osteoporosis with densitometry. Committee of Scientific Advisors, International Osteoporosis Foundation.* Osteoporos Int, 2000. **11**(3): p. 192-202.
166. Hall, G.L., et al., *Official ERS technical standard: Global Lung Function Initiative reference values for static lung volumes in individuals of European ancestry.* Eur Respir J, 2021. **57**(3).
167. Salome, C.M., G.G. King, and N. Berend, *Physiology of obesity and effects on lung function.* J Appl Physiol (1985), 2010. **108**(1): p. 206-11.
168. Jones, R.L. and M.-M.U. Nzekwu, *The Effects of Body Mass Index on Lung Volumes.* Chest, 2006. **130**(3): p. 827-833.
169. Brandsma, C.-A., et al., *Lung ageing and COPD: is there a role for ageing in abnormal tissue repair?* European Respiratory Review, 2017. **26**(146): p. 170073.
170. Sharma, G. and J. Goodwin, *Effect of aging on respiratory system physiology and immunology.* Clin Interv Aging, 2006. **1**(3): p. 253-60.
171. Cook, C.D. and J.F. Hamann, *Relation of lung volumes to height in healthy persons between the ages of 5 and 38 years.* J Pediatr, 1961. **59**: p. 710-4.
172. Steier, J., et al., *Observational study of the effect of obesity on lung volumes.* Thorax, 2014. **69**(8): p. 752-9.
173. Dixon, A.E. and U. Peters, *The effect of obesity on lung function.* Expert Rev Respir Med, 2018. **12**(9): p. 755-767.
174. LoMauro, A. and A. Aliverti, *Sex differences in respiratory function.* Breathe (Sheff), 2018. **14**(2): p. 131-140.
175. Tusman, G., et al., *Reference values for volumetric capnography-derived non-invasive parameters in healthy individuals.* J Clin Monit Comput, 2013. **27**(3): p. 281-8.
176. Sheel, A.W., P.B. Dominelli, and Y. Molgat-Seon, *Revisiting dysanapsis: sex-based differences in airways and the mechanics of breathing during exercise.* Experimental Physiology, 2016. **101**(2): p. 213-218.
177. Juniper, E.F., et al., *Development and validation of a questionnaire to measure asthma control.* Eur Respir J, 1999. **14**(4): p. 902-7.
178. Juniper, E.F., et al., *Measuring asthma control. Clinic questionnaire or daily diary?* Am J Respir Crit Care Med, 2000. **162**(4 Pt 1): p. 1330-4.
179. Juniper, E.F., et al., *Measurement properties and interpretation of three shortened versions of the asthma control questionnaire.* Respir Med, 2005. **99**(5): p. 553-8.
180. Henderson, J., et al., *Asthma control in general practice -- GP and patient perspectives compared.* Aust Fam Physician, 2013. **42**(10): p. 740-3.
181. SPSS, *Linear Mixed-Effects Modeling in SPSS: An Introduction to the MIXED Procedure*.
182. Akaike, H., *A new look at the statistical model identification.* IEEE Transactions on Automatic Control, 1974. **19**(6): p. 716-723.
183. Blaiss, M., et al., *Consensus of an American College of Allergy, Asthma, and Immunology, American Academy of Allergy, Asthma, and Immunology, and American Thoracic Society workgroup on definition of clinical remission in asthma on treatment.* Ann Allergy Asthma Immunol, 2023. **131**(6): p. 782-785.
184. Usmani, O.S., et al., *The prevalence of small airways disease in adult asthma: A systematic literature review.* Respir Med, 2016. **116**: p. 19-27.

185. Kraft, M., et al., *The role of small airway dysfunction in asthma control and exacerbations: a longitudinal, observational analysis using data from the ATLANTIS study.* Lancet Respir Med, 2022. **10**(7): p. 661-668.
186. Lipworth, B., A. Manoharan, and W. Anderson, *Unlocking the quiet zone: the small airway asthma phenotype.* The Lancet Respiratory Medicine, 2014. **2**(6): p. 497-506.
187. Mingotti, C., et al., *Evaluating the FEV1/FVC ratio in the lower range of normality as a marker of worse clinical outcomes in asthmatic subjects without airway obstruction.* Respiratory Medicine, 2020. **162**: p. 105880.
188. Macklem, P.T. and J. Mead, *Resistance of central and peripheral airways measured by a retrograde catheter.* J Appl Physiol, 1967. **22**(3): p. 395-401.
189. McNamara, J.J., et al., *Heterogeneous lung emptying during forced expiration.* J Appl Physiol (1985), 1987. **63**(4): p. 1648-57.
190. Morgan, S.J., et al., *β-Agonist-mediated relaxation of airway smooth muscle is protein kinase A-dependent.* J Biol Chem, 2014. **289**(33): p. 23065-23074.
191. Licker, M., et al., *Aerosolized salbutamol accelerates the resolution of pulmonary edema after lung resection.* Chest, 2008. **133**(4): p. 845-52.
192. Sakuma, T., et al., *Beta-adrenergic agonist stimulated alveolar fluid clearance in ex vivo human and rat lungs.* Am J Respir Crit Care Med, 1997. **155**(2): p. 506-12.
193. Harvey, E.S., et al., *Mepolizumab effectiveness and identification of super-responders in severe asthma.* European Respiratory Journal, 2020. **55**(5): p. 1902420.
194. Tan, L.D., et al., *Benralizumab: a unique IL-5 inhibitor for severe asthma.* J Asthma Allergy, 2016. **9**: p. 71-81.
195. Farah, C.S., et al., *Mepolizumab improves small airway function in severe eosinophilic asthma.* Respiratory Medicine, 2019. **148**: p. 49-53.
196. Menzies-Gow, A., et al., *An expert consensus framework for asthma remission as a treatment goal.* J Allergy Clin Immunol, 2020. **145**(3): p. 757-765.
197. Portacci, A., S. Dragonieri, and G.E. Carpagnano, *Super-Responders to Biologic Treatment in Type 2-High Severe Asthma: Passing Fad or a Meaningful Phenotype?* J Allergy Clin Immunol Pract, 2023. **11**(5): p. 1417-1420.
198. Kavanagh, J.E., et al., *Real-World Effectiveness and the Characteristics of a "Super-Responder" to Mepolizumab in Severe Eosinophilic Asthma.* Chest, 2020. **158**(2): p. 491-500.
199. *Multiorgan MRI findings after hospitalisation with COVID-19 in the UK (C-MORE): a prospective, multicentre, observational cohort study.* Lancet Respir Med, 2023. **11**(11): p. 1003-1019.
200. Marshall, J.C., et al., *A minimal common outcome measure set for COVID-19 clinical research.* The Lancet Infectious Diseases, 2020. **20**(8): p. e192-e197.
201. Simonnet, A., et al., *High Prevalence of Obesity in Severe Acute Respiratory Syndrome Coronavirus-2 (SARS-CoV-2) Requiring Invasive Mechanical Ventilation.* Obesity (Silver Spring), 2020. **28**(7): p. 1195-1199.
202. Finer, N., S.P. Garnett, and J.M. Bruun, *COVID-19 and obesity.* Clin Obes, 2020. **10**(3): p. e12365.
203. Sun, Z., et al., *A systematic review of chest imaging findings in COVID-19.* Quantitative Imaging in Medicine and Surgery, 2020. **10**(5): p. 1058-1079.
204. Wang, Y., et al., *Temporal Changes of CT Findings in 90 Patients with COVID-19 Pneumonia: A Longitudinal Study.* Radiology, 2020. **296**(2): p. E55-E64.
205. Pan, F., et al., *Time course of lung changes at chest CT during recovery from coronavirus disease 2019 (COVID-19).* Radiology, 2020. **295**(3): p. 715-721.
206. BTS, *British Thoracic Society Guidance on Respiratory Follow Up of Patients with a Clinico- Radiological Diagnosis of COVID-19 Pneumonia.* 2020.

207. Martino, G.P., et al., *6 and 12 month outcomes in patients following COVID-19-related hospitalization: a prospective monocentric study.* Intern Emerg Med, 2022. **17**(6): p. 1641-1649.
208. Wu, X., et al., *3-month, 6-month, 9-month, and 12-month respiratory outcomes in patients following COVID-19-related hospitalisation: a prospective study.* Lancet Respir Med, 2021. **9**(7): p. 747-754.
209. Steinbeis, F., et al., *Severity of respiratory failure and computed chest tomography in acute COVID-19 correlates with pulmonary function and respiratory symptoms after infection with SARS-CoV-2: An observational longitudinal study over 12 months.* Respir Med, 2022. **191**: p. 106709.
210. Pellegrino, R., et al., *Interpretative strategies for lung function tests.* European Respiratory Journal, 2005. **26**(5): p. 948.
211. Schachter, L.M., et al., *Obesity is a risk for asthma and wheeze but not airway hyperresponsiveness.* Thorax, 2001. **56**(1): p. 4-8.
212. Zhao, Y.M., et al., *Follow-up study of the pulmonary function and related physiological characteristics of COVID-19 survivors three months after recovery.* EClinicalMedicine, 2020. **25**: p. 100463.
213. Sanchez-Ramirez, D.C., et al., *Long-Term Impact of COVID-19: A Systematic Review of the Literature and Meta-Analysis.* Biomedicines, 2021. **9**(8).
214. Faverio, P., et al., *One-year pulmonary impairment after severe COVID-19: a prospective, multicenter follow-up study.* Respiratory Research, 2022. **23**(1): p. 65.
215. Stockley, J.A., et al., *Lung function and breathing patterns in hospitalised COVID-19 survivors: a review of post-COVID-19 Clinics.* Respir Res, 2021. **22**(1): p. 255.
216. Frija-Masson, J., et al., *Residual ground glass opacities three months after Covid-19 pneumonia correlate to alteration of respiratory function: The post Covid M3 study.* Respir Med, 2021. **184**: p. 106435.
217. Wang, T., et al., *Comorbidities and multi-organ injuries in the treatment of COVID-19.* Lancet, 2020. **395**(10228): p. e52.
218. Stockley, J.A., et al., *Lung function and breathing patterns in hospitalised COVID-19 survivors: a review of post-COVID-19 Clinics.* Respiratory Research, 2021. **22**(1): p. 255.
219. Fortini, A., et al., *One-year evolution of DLCO changes and respiratory symptoms in patients with post COVID-19 respiratory syndrome.* Infection, 2022. **50**(2): p. 513-517.
220. Hui, D.S., et al., *The 1-Year Impact of Severe Acute Respiratory Syndrome on Pulmonary Function, Exercise Capacity, and Quality of Life in a Cohort of Survivors.* Chest, 2005. **128**(4): p. 2247-2261.
221. NGAI, J.C., et al., *The long-term impact of severe acute respiratory syndrome on pulmonary function, exercise capacity and health status.* Respirology, 2010. **15**(3): p. 543-550.
222. Matheson, A.M., et al., *Persistent 129Xe MRI Pulmonary and CT Vascular Abnormalities in Symptomatic Individuals with Post-acute COVID-19 Syndrome.* Radiology, 2022. **305**(2): p. 466-476.
223. Cendon, S.P., et al., *Pulmonary emphysema induced by passive smoking: an experimental study in rats.* Brazilian Journal of Medical and Biological Research, 1997. **30**.
224. Wright, J.L. and A. Churg, *Cigarette smoke causes physiologic and morphologic changes of emphysema in the guinea pig.* Am Rev Respir Dis, 1990. **142**(6 Pt 1): p. 1422-8.